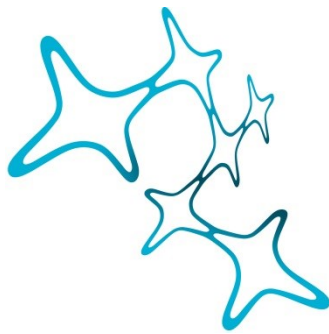

LIPID METABOLISM IN
REMYELINATION: DOES A HIDDEN
DIALOGUE EXIST BETWEEN THE
CENTRAL NERVOUS SYSTEM AND THE
PERIPHERY?

Garyfallia Gouna



Graduate School of
Systemic Neurosciences

LMU Munich



Dissertation der Graduate School of Systemic Neurosciences der
Ludwig-Maximilians-Universität München

21st of November, 2023

Supervisor

Prof. Dr. Mikael Simons

Institute of Neuronal Cell Biology (TUM-NCB)

Technical University Munich

Institute for Stroke and Dementia Research (ISD)

German Center for Neurodegenerative Diseases (DZNE)

First Reviewer: Prof. Dr. Mikael Simons

Second Reviewer: Prof. Dr. Lena Burbulla

External Reviewer: Dr. Sarah Jaekel

Date of Submission: 21st of November, 2023

Date of Defense: 26th of February, 2024

TABLE OF CONTENTS

Abstract.....	3
Introduction	5
1. Demyelinating diseases: the process of remyelination and the contribution of glial cells in the central nervous system.....	5
2. Lipid metabolism and remyelination: is it the key to an effective repair mechanism?.....	8
2.1 Cholesterol in central nervous system.....	8
2.2 Lipid droplets in central nervous system	10
2.3 Interplay of lipids between central nervous system and periphery: adipose tissue - brain axis.....	12
3. Hypothesis and aims	13
Project 1: Trem2-dependent lipid droplet biogenesis in phagocytes is required for remyelination.	14
Project 2: The “lipodystrophy” brain exhibits enhanced remyelination in a UCP1-independent manner.	31
Discussion and future outlook.....	72
1. Why remyelination fails?.....	72
2. Lipid metabolism and remyelination.....	73
3. Limitations and Future perspectives	78
References.....	82
List of Figures	90
Introduction	90
Project 1: Trem2-dependent lipid droplet biogenesis in phagocytes is required for remyelination.....	90
Project 2: The “lipodystrophy” brain exhibits enhanced remyelination in a UCP1-independent manner.....	90
Discussion	91
List of Tables	91
Project 2: The “lipodystrophy” brain exhibits enhanced remyelination in a UCP1-independent manner.....	91
List of abbreviations	92
List of publications	99
Copyright of figures taken from publications	100
Acknowledgements.....	126
Author contributions.....	129
Curriculum Vitae	131

ABSTRACT

Inflammatory demyelinating disorders of the central nervous system (CNS) manifest through the pivotal features of myelin disruption and imbalanced inflammation. Within this category, multiple sclerosis (MS) emerges as a major member, distinguished by the formation of demyelinated lesions induced by inflammation. In response to demyelinating stimuli, the CNS initiates a regenerative process known as remyelination, wherein the active participation of glial cells serves to resolve inflammation and promote repair. However, during the progressive phase of MS, remyelination fails, leading to the exacerbation of disease symptoms.

The objective of remyelination is to reinstate the integrity of disrupted myelin sheaths, which predominantly consist of lipids. Lipid metabolism in the CNS is of paramount importance as it fulfills crucial functions in structural support, signaling, and energy storage. Lipids hold a central role in remyelination as the phagocytosis of myelin debris, followed by the intracellular process and extracellular efflux of debris lipid components contribute to a successful lesion repair. Simultaneously, the upregulation of *de novo* lipid biosynthesis, such as cholesterol, also facilitates the regenerative response. Whereas the significance of lipid metabolism in remyelination has only recently begun to be elucidated, the majority of research in this field focuses on local processes within the CNS. New studies indicate that aberrant systemic metabolism, as observed in conditions like obesity, influences the process of remyelination. Nevertheless, the mechanisms through which peripheral lipid metabolism impacts lesion recovery and the inflammatory capacity remain poorly understood. Thus, in this thesis, I aimed to bridge the existing knowledge gap by exploring, in two distinct projects, how lipid metabolism in both the CNS and the periphery influences the regenerative capacity upon acute demyelination.

In *Project 1*, I investigated the role of lipid storage in microglia/macrophages (phagocytes) and its influence on the process of remyelination. I discovered that the conversion of free cholesterol into cholesterol esters and the subsequent formation of lipid droplets (LD) in phagocytes are essential prerequisites for the process of remyelination. When phagocytes fail to generate LD, the resolution of inflammation is impaired and ultimately remyelination proves unsuccessful. I also found that mice lacking the triggering receptor expressed on myeloid cells 2 (TREM2) fail to produce LD due to their incapability to adapt to surplus cholesterol exposure, consequently leading to the development of endoplasmic reticulum (ER) stress. Mitigating ER stress in TREM2-deficient mice restores LD formation and the inflammation is resolved. Thus, I concluded that the biogenesis of LD in response of acute demyelinating injury constitutes a protective mechanism crucial for the remyelination process.

In *Project 2*, I explored the role of dysregulated peripheral lipid metabolism on the remyelination response. Utilizing a murine model that recapitulates the phenotype of

lipodystrophy, I discovered that, after acute CNS demyelinating stimuli, lesion repair is promoted, while the inflammation is resolved. Metabolomic analysis revealed increased levels of branched-chain amino acids (BCAAs) and numerous phosphatidylcholine (PCs) species with polyunsaturated long-chain fatty acids (LCFAs) in the plasma of lipodystrophic mice. Successive proteomic analysis indicated a metabolic activation of brown adipose tissue (BAT) via stimulated thermogenesis. The activation of thermogenesis via the uncoupling protein 1 (UCP1)-dependent pathway, however, did not result in enhanced lesion repair. Therefore, I concluded, that, upon demyelinating injury, lipodystrophic mice exhibit enhanced remyelination and resolution of inflammation, mediated in a UCP1-independent way.

In a nutshell, both projects of my thesis aimed to examine the role of lipid metabolism in the context of remyelination, in an effort to gain a deeper understanding of the molecular mechanisms that govern the regenerative process, in order to promote efficient treatment strategies. Undoubtedly, lipids stand at the core of this intricate process, urging further appreciation and investigation into their crucial significance.

INTRODUCTION

1. Demyelinating diseases: the process of remyelination and the contribution of glial cells in the central nervous system

Inflammatory demyelinating diseases are a major source of neuroinflammation and nerve damage in the central nervous system (CNS) of affected young adults. Among these diseases, multiple sclerosis (MS) is the most prevalent, and its global prevalence has shown a remarkable increase of over 10% in recent years across Western Europe and North America^{1,2}. Recent evidence highlights the increased economic burden of MS in Europe and the United States, underscoring the significance of understanding the pathology of the disease^{3,4}. MS is classified into four phenotypes: clinically isolated syndrome (CIS), relapsing-remitting MS (RRMS), primary-progressive MS (PPMS), and secondary progressive MS (SPMS). These phenotypes are characterized by two key aspects: disease activity, which includes relapses or new manifestations on magnetic resonance imaging (MRI), and disability progression. These classifications and descriptors are commonly employed in clinical trials for patient selection and treatment allocation⁵.

The hallmark of MS pathology and other inflammatory demyelinating diseases is the disruption of myelin sheaths resulting from compromised immune regulation, in a process known as demyelination. Demyelination is characterized by the destruction of myelin integrity, increased inflammation, and reduced axonal stability. Physiologically in the CNS, myelin sheaths are produced by mature oligodendrocytes (mOLGs) and protect neurons by enabling metabolic support and fast transmission of electrical signals along the axon. In demyelination, myelin sheaths are entirely lost, while axons remain intact. However, chronic demyelinating injury can potentially trigger subsequent axonal damage, given that axons can remain in a chronically demyelinated state^{6,7}. Within this state, glial cells play a central role, facilitating repair mechanisms referred to as remyelination. In the 1980s, pioneering studies provided the initial evidence that remyelination is an effective repair mechanism. These studies revealed that remyelination rescues electrical conduction along the nerve axon and involves the generation of mOLGs by adult oligodendrocyte precursor cells OPCs (aOPCs) to remyelinate axons^{8,9}. In another groundbreaking study from the same era, oligodendrocytes were established as the primary drivers of remyelination. This research illustrated that the transplantation of oligodendrocytes into mouse models devoid of native myelin facilitated the production of new myelin sheaths¹⁰. Nowadays, the fundamental stages of remyelination have been thoroughly established (Fig. 1)⁷.

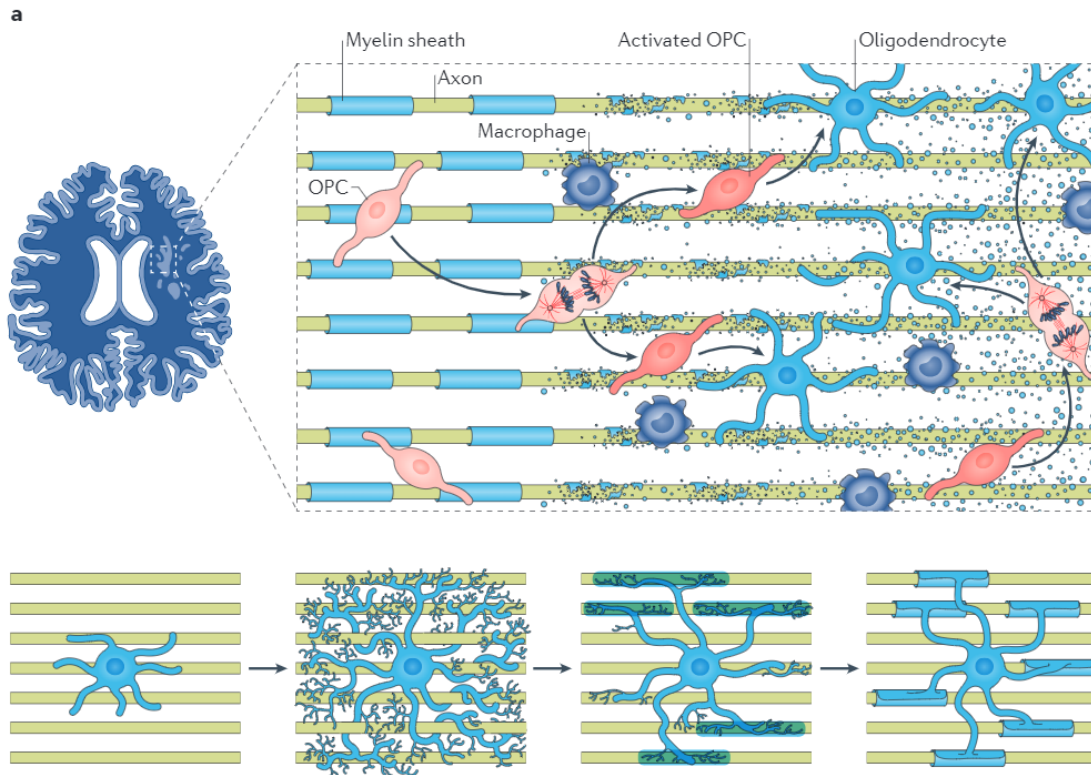


Figure 1 The remyelination process orchestrates the response of oligodendrocytes and microglia/macrophages towards regeneration. In the upper panel, a demyelinating lesion in a coronal section of human brain affected by MS is illustrated. After damage to myelinated regions in the CNS, the process of remyelination begins with the activation of oligodendrocyte precursor cells (OPCs), which then proliferate and differentiate into new mOLGs (signified by a color change from light red to blue). Following activation, OPCs surrounding the lesion can migrate within the lesion, where in combination with the pre-existing OPCs, collectively support the regenerative response. Of note, microglia/macrophages (here noted as macrophages) are observed in the lesion, playing crucial roles in myelin debris phagocytosis and promoting lesion recovery. Subsequent to the differentiation of oligodendrocytes, the progression of myelin formation unfolds in three distinct steps, as elucidated in the lower part of the panel: new mOLGs form numerous processes and express myelin proteins, such as myelin basic protein (MBP), followed by the primary envelopment of the axon through an extension of myelin membrane. Ultimately, mOLGs create compacted, multilayered myelin sheaths via continuous membrane elaboration and cytoplasm extrusion, which wrap the axons further. Data source: Reproduced with permission from Springer Nature; Franklin and ffrench-Constant, Regenerating CNS myelin - from mechanisms to experimental medicines., *Nat. Rev. Neurosci.*, Volume 18, 756, 2017, Springer Nature⁷.

In the process of remyelination, the synchronized response of oligodendrocytes, microglia, and astrocytes places glial cells at the core of this regenerative mechanism. Initially, oligodendrocyte precursor cells (OPCs) get activated. Upon activation, OPCs within the lesion area proliferate, whereas OPCs in the vicinity of the lesion migrate into the damaged area and proliferate, populating the lesion. Eventually OPCs in the damaged area differentiate into mature oligodendrocytes (mOLGs), which generate new myelin sheaths. Synthesis of new myelin occurs in three distinct steps; first, myelin proteins such as the structural myelin basic protein (MBP) are expressed in extended mOLGs processes towards the naked axons.

Second, mOLGs initiate axonal wrapping by the extension of the myelin membrane, which ultimately acquires multiple layers, forming the new compacted myelin sheaths around the axons at the last step (Fig. 1, lower panel)⁷. During demyelination, some “old” mOLGs survive the damage and can participate in the regenerative response¹¹. Crucially, a recent study has revealed that newly formed mOLGs derived from recruited OPCs play a primary role in remyelination, whereas the “old” mOLGs that have survived contribute only minimally to the process in cortex¹².

Apart from oligodendrocytes, microglia exert several functions in the regenerative response. Upon demyelination, microglia become activated and are recruited to the lesion site. In this area, they engage in the phagocytosis of myelin debris, so as to eliminate myelin components that may hinder the process of remyelination¹³. The clearance of damaged myelin is mediated by several microglia receptors, including the triggering receptor expressed on myeloid cells 2 (TREM2). Consequently, microglia secrete proregenerative components, such as activin A and insulin-like growth factor 1 (IGF1), and modulate the extracellular matrix with the assistance matrix metalloproteinases (MMPs). Thus, microglia functions in demyelinating injury synergistically facilitate the recruitment of OPCs and their differentiation into mOLGs, promoting regeneration¹⁴. Upon injury, microglial population exhibits heterogeneity among different brain regions, which appears in their transcriptomic profile. Interestingly, the subpopulation of disease-associated microglia (DAM) is upregulated in diseases such as Alzheimer’s disease (AD) and motor neuron disorders. Nonetheless, DAM cluster is further linked to regeneration and wound healing, highlighting the phagocytic nature of microglia^{14,15}. In the context of DAM microglia, *Trem2* emerges as one of the most significantly enriched genes. TREM2 stimulates apolipoprotein E (*ApoE*) signaling in microglia and mediates the phagocytosis of damaged neurons in neurodegeneration MS models and AD¹⁶. Microglia recruitment in the demyelinating area can also be mediated by astrocytes¹⁷. Astrocytes can exert both beneficial and detrimental roles in remyelination, which highly depend on the remyelination stage and their interplay with other cells¹⁸.

Remyelinated axons can easily be distinguished from undamaged axons in tissue, since remyelinated myelin sheaths appear thinner and shorter¹⁹. Even though, myelin remains fully functional and provides metabolic support to the axons²⁰. Myelin composition has been extensively researched in the context of developmental myelination. Myelin is distinctive for its high lipid content (70-85%) and low protein content (15-30%), unlike other biological membranes, which typically maintain an equal lipid-to-protein ratio (50-50%)²¹. In the context of remyelination, lipids assume a central role in many aspects. Microglia/macrophages phagocytose damaged lipids within myelin debris, and mOLGs synthesize newly formed lipids within the new myelin sheaths. Apart from lipids contribution in the structure of myelin *per se*, lipid metabolism also regulates the local and peripheral immune and inflammatory response, upon demyelinating injury²²⁻²⁴. While remyelination is a natural adaptive response to CNS tissue injury, aimed at tissue remodeling, it frequently proves to be

unsuccessful, especially in progressive MS^{25,26}. Therefore, it becomes evident that exploring the role of lipid metabolism in promoting the regenerative response after demyelination is of great importance.

2. Lipid metabolism and remyelination: is it the key to an effective repair mechanism?

Lipids comprise a wide array of molecules that participate in essential biological processes both in CNS and periphery. Lipids play three primary roles; they participate in the structural composition of all biological cell membranes, function as energy storage depots and metabolic substrates and regulate intracellular and intercellular signaling pathways in health and disease^{27,28}. In the CNS, the multifaceted role of lipids is of paramount importance, as they constitute the primary structural component of myelin²¹. Physiologically, myelin sheaths consist of 40% phospholipids, 40% cholesterol and 20% glycosphingolipids²⁹. While these lipids have received increased attention in developmental CNS research³⁰⁻³², the scientific exploration of lipid metabolism in CNS injury regeneration is also notable. When considering MS, numerous studies offer evidence for the involvement of lipid metabolism not only in the disease's pathogenesis but also as potential markers for diagnosis and treatment²⁴, with special attention given to cholesterol.

2.1 Cholesterol in central nervous system

Cholesterol is primarily synthesized *de novo* in the CNS, as the blood brain barrier (BBB) anatomically limits the entry of cholesterol from the periphery. Cholesterol, despite being a fundamental structural element in all biological membranes, such as cell plasma membranes, is predominantly found within myelin sheaths in the CNS³³⁻³⁵. In myelination during development, oligodendrocytes are the primary cells responsible for synthesizing cholesterol in adequate quantities³⁶. Nevertheless, astrocytes also have the capacity to synthesize cholesterol and provide supplementation to oligodendrocytes through lipoprotein particles containing ApoE. In adulthood, the primary role of cholesterol synthesis shifts to astrocytes, which supply cholesterol to neurons and other glial cells under healthy conditions^{33,37,38}. Consequently, it is apparent that cholesterol plays a fundamental role in maintaining the health and functionality of myelin, achieved through the combination of *de novo* synthesis within glial cells and "lipid recycling" via lipoprotein particles between glial cells.

In remyelination, both *de novo* synthesis and "lipid recycling" processes occur, with the specific mechanisms depending on the characteristics and chronicity of

demyelinating lesions. In an *ex vivo* model of demyelination, a recent study showed that astrocytes mediate cholesterol export to oligodendrocytes, regulating their survival and enhancing the regeneration capacity³⁹. In acute demyelinating lesions following cuprizone administration *in vivo*, it has been suggested that oligodendrocytes rely on supplementation of lipids from the “lipid recycling” process for remyelination from CNS microglia/macrophages (phagocytes)⁴⁰. Simultaneously, the transcriptional profile of cholesterol synthesis genes is suppressed in most CNS cells, but not in CNS phagocytes. CNS phagocytes require the activation of both sterol synthesis and cholesterol efflux pathways (ATP-binding cassette transporters ABCA1 and ABCG1) for an effective remyelination capacity⁴⁰. In contrast, within chronic demyelinating lesions upon cuprizone (copper chelator compound⁴⁰) treatment, the “lipid recycling” mechanisms are compromised, prompting neurons and oligodendrocytes to endogenously synthesize cholesterol for remyelination, at least as a partial rescue mechanism. In this state, CNS phagocytes acquire a foamy morphology, which may indicate a defective liver X receptor (LXR) signaling, thus dampening cholesterol efflux^{33,40,41}. Hence, CNS phagocytes function as central regulators in the process of remyelination in both acute and chronic demyelination *in vivo*.

In demyelinating lesions, CNS phagocytes adopt a foamy phenotype, often referred to as “foam cells”. Foam cells resemble the lipid laden macrophages observed in atherosclerosis⁴² and follow a polarizing triphasic motif upon demyelinating stimuli (Fig. 2)⁴³. In the initial phase of acute demyelination (Phase I), phagocytes engulf damaged myelin debris, acquiring a pro-inflammatory phenotype while suppressing anti-inflammatory components⁴⁴⁻⁴⁶. In Phase II, phagocytes catabolize myelin debris into lipid mediators, which in turn activate peroxisome proliferator-activated receptor (PPAR) and LXR signaling pathways^{47,48}. It is known that cholesterol endogenously activates LXR signaling⁴⁹. The activation of PPAR and LXR pathways suppress the expression of pro-inflammatory molecules in phagocytes, suggesting that myelin intracellular processing in phagocytes promotes anti-inflammation⁴³. In conditions like aging, our group has shown that foamy phagocytes fail to effectively efflux cholesterol and accumulate cholesterol crystals in lysosomes, which in turn provoke lysosomal disruption and activation of NLRP3 inflammasome⁵⁰. These studies suggest that foam cells actively contribute to the regeneration process in demyelinating conditions. The characteristic of foam cells is the intracellular accumulation of lipid droplets (LD)⁴³.

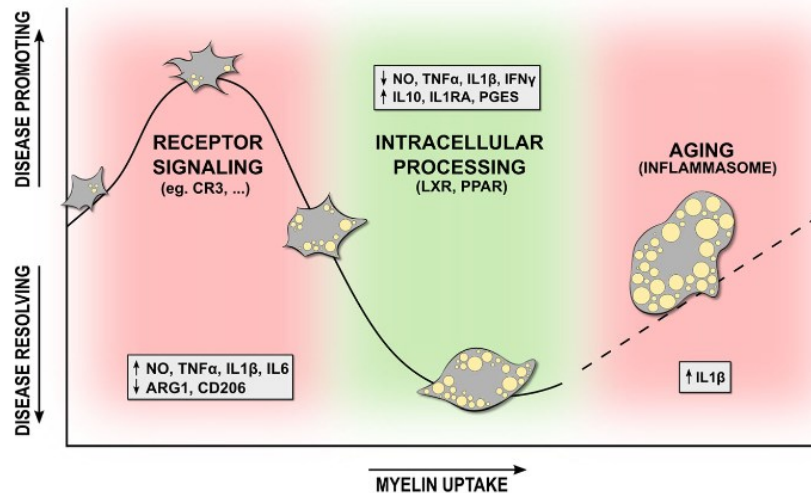


Figure 2 Foam cells in remyelination respond in three phases. Phase I: the initial phagocytosis of myelin triggers a disease-inducing phenotype in phagocytes, which release increased levels of pro-inflammatory mediators and less anti-inflammatory factors. This phenotype is promoted due to the swift activation signaling pathways following the engagement of the complement receptor 3 (CR3). In this phase levels of nitric oxide (NO), tumor necrosis factor alpha (TNF- α), interleukin 1 beta (IL1 β) and interleukin 6 (IL-6) are upregulated, while levels of arginase 1 (ARG1) and mannose receptor (CD206) are downregulated. Phase II: over time, phagocytosed myelin is processed, leading to the generation of specific lipid metabolites. These lipids activate anti-inflammatory nuclear receptors liver X receptor (LXR) and peroxisome proliferator-activated receptor (PPAR). In the second phase, the levels of pro-inflammatory mediators as NO, TNF- α , IL1 β and interferon gamma (IFN γ) are decreased, whereas levels of interleukin 10 (IL10), interleukin-1 receptor antagonist (IL1RA) and prostaglandin E synthase (PGES) are increased. Phase III: as aging progresses, phagocytes are unable to effectively process myelin debris and efflux the substantial amounts of cholesterol rich components. Hence, cholesterol crystals are accumulating with consequent activation of NOD-, LRR- and pyrin domain-containing protein 3 (NLRP3) inflammasome. In this phase, the levels of IL1 β are elevated. Data source: Reproduced with permission (open source) from Grajchen et al., The physiology of foamy phagocytes in multiple sclerosis., *Acta Neuropathol. Commun.*, page 7, 2018, 6:124⁴³.

2.2 Lipid droplets in central nervous system

For an extended period, LDs were primarily regarded as inert lipid reservoirs, with no recognized metabolic roles. Nowadays, LDs are recognized as multifaceted dynamic organelles with several metabolic functions due to their unique spherical structure and composition^{51,52}. The structure of LD is characterized of a phospholipid monolayer, which surrounds a hydrophobic core composed of triglycerides (TGs) and cholesterol esters⁵³. The phospholipid monolayer is decorated with several proteins (LD proteome), providing a structural support and a platform for many metabolic processes, such as lipophagy^{54,55}. LD biogenesis is taking place at the ER, where LDs bud either toward the cytoplasm or the inner luminal space of ER and into the

nucleus^{56,57}. In the periphery, LDs function in multiple levels; they provide substrates to meet energy metabolism demands and support the formation of cell membranes⁵⁸, while they regulate inflammatory responses and insulin signaling⁵⁹. LDs have been extensively researched in peripheral health and pathological conditions, and their presence in the CNS has garnered increased attention in recent years⁶⁰⁻⁶².

Several studies have suggested the mechanisms of LD formation in the brain in pathology (Fig. 3)⁶¹. Briefly, extracellular material such as, lipoprotein particles⁶³, apoptotic cells¹⁶, myelin debris⁵⁰, lipids released from neuronal activity⁶⁴ or even synaptic elements, are phagocytosed and directed to lysosomes. Intracellularly, the physiological process of autophagy can also supply lysosomes with lipid components under starvation conditions⁶⁵. Lysosomes process the lipid material and converts it into free fatty acids (FFAs) and free cholesterol, which both in this state are toxic for the cell. Thereby, physiologically, both FFAs and cholesterol are used for the composition of TGs and cholesterol esters, which are incorporated into the hydrophobic core of LDs at the ER site, in an effort to alleviate lipid toxicity in the cell⁶¹. Nonetheless, research has demonstrated that elevated LD accumulation can also be triggered by *de novo* lipid biosynthesis resulting from increased reactive oxygen species (ROS) generated by oxidative stress or mitochondrial dysfunction⁶⁶. LDs have been detected in various cell types within the CNS, particularly in the presence of neurodegenerative conditions such as Alzheimer's and Creutzfeldt-Jakob disease, as well as in the context of aging⁶². In the context of demyelination, LDs have been observed primarily in CNS phagocytes, as a result of myelin debris uptake⁶¹. Thus, it becomes evident that brain lipid metabolism is of crucial importance in both homeostasis and under regenerative response. While the brain has a substantial lipid composition, it is the second most enriched tissue, with adipose tissue serving as the primary lipid storage organ and one of the metabolic centers in the body^{61,67}.

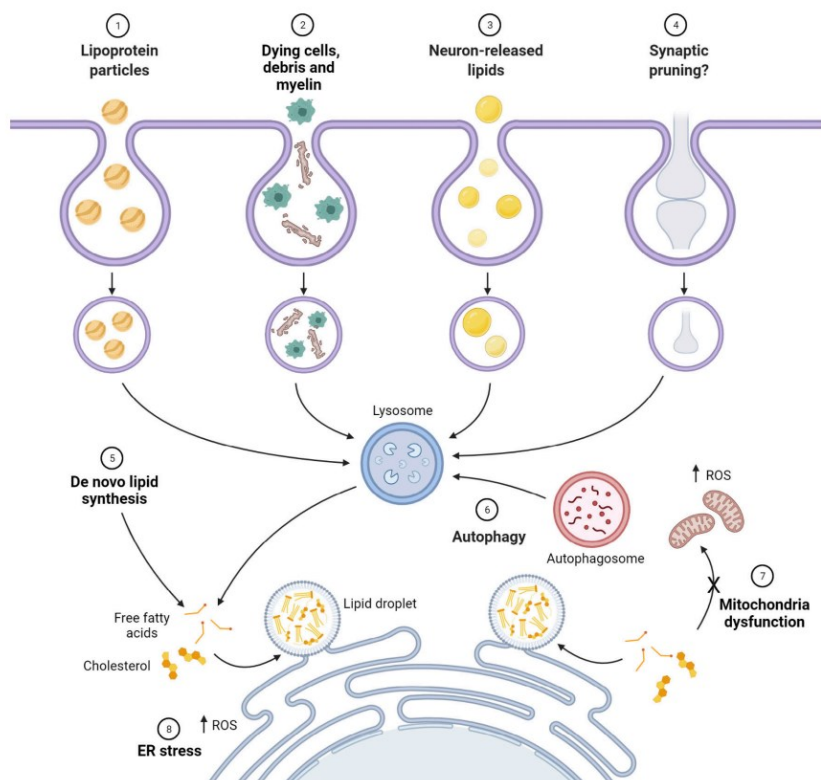


Figure 3 What triggers lipid droplet (LD) formation in the CNS? A schematic illustration outlining the confirmed and proposed mechanisms of LD biogenesis in neural cells of CNS. For a detailed description, see text. ROS: reactive oxygen species. Data source: Used with permission of Rockefeller University Press from Lipid droplets in the nervous system, Ralhan et al., *J. Cell. Biol.* 2021 Vol. 220 No. 7 e202102136⁶¹, year of copyright 2023; permission conveyed through Copyright Clearance Center, Inc.

2.3 Interplay of lipids between central nervous system and periphery: adipose tissue - brain axis

Adipose tissue serves as a central regulator of systemic metabolism within the body, functioning as both a storage site for lipids and a mediator of lipid distribution. It regulates lipid mobilization through the processes of lipogenesis and lipolysis. In lipogenesis, FFAs are utilized for the biosynthesis of TGs, while in lipolysis, they are released to interact with peripheral organs. Additionally, adipose tissue operates as an endocrine organ, producing several secreted factors known as adipokines, which regulate immune responses and facilitate communication with other organs in the body, including the brain^{27,68}. The adipose tissue-brain axis comprises two communication pathways. The first pathway involves the signaling from adipose tissue to the brain through secreted factors like the adipokine leptin, which activates the hypothalamus and governs metabolism and appetite. The second pathway relies on sympathetic and sensory innervation connecting adipose tissue with the CNS^{69,70}.

Adipose tissue is the organ most significantly affected in obesity and, a growing body of literature indicates that obesity exacerbates the pathophysiology of MS. Obesity promotes adipose tissue hypertrophy and activation of peripheral immune response, establishing a chronic inflammatory environment. In this microenvironment, lipolysis in adipose tissue is elevated, which in turn increases saturated fatty acids to promote further the activation of the immune system and the NLRP3 inflammasome cascade. Obesity also triggers the secretion of various pro- and anti-inflammatory adipokines, all of which have been correlated to the MS pathology⁷¹. Thereby, it becomes apparent that the dysregulation of peripheral lipid metabolism can influence the regenerative response in MS pathophysiology.

3. Hypothesis and aims

In this thesis I investigated how lipid metabolism regulates the process of regeneration upon acute demyelinating injury. We addressed lipid metabolism in two anatomic distinct body regions. In *Project 1*, I focused on the CNS and how disruption of lipid metabolism affects phagocyte response and remyelination. Our hypothesis postulated that the dysregulation of cholesterol metabolism and disruption of lipid sensor receptors in CNS phagocytes will adversely impact the remyelination process. In *Project 2*, I shifted my focus to peripheral lipid metabolism and its role in the regenerative response. Here, we hypothesized that complete ablation of normal lipid storage in adipose tissue in periphery will affect the remyelination process in acute injury. Both approaches aimed to provide a deeper understanding of the significance of lipid metabolism for normal brain functions, including remyelination, both within the brain and in the periphery.

PROJECT 1: Trem2-dependent lipid droplet biogenesis in phagocytes is required for remyelination.

The current chapter includes the research article “Trem2-dependent lipid droplet biogenesis in phagocytes is required for remyelination.” This article, which has been already published, reports the importance of lipid droplets in remyelination upon acute CNS injury.









More specifically, my research in project 1 focused on lipid storage in microglia/macrophages and its impact on remyelination. I observed that mice lacking TREM2 are unable to generate LD due to their inability to adapt to excess cholesterol exposure, resulting in ER stress. By promoting ER stress alleviation in TREM2-deficient mice, LD formation is restored, and inflammation resolves. This emphasizes the importance of LD biogenesis in protecting against acute demyelinating injury and promoting remyelination. Furthermore, I discovered that the conversion of free cholesterol to cholesterol esters and the subsequent formation of LD in phagocytes are necessary molecular mechanisms for successful remyelination. Without LD formation, the resolution of inflammation is hindered, leading to unsuccessful remyelination.

The author of this thesis is the first author of this article. For details regarding author contributions, please refer to the “Author Contributions” part of this thesis.

Used with permission of Rockefeller University Press, from TREM2-dependent lipid droplet biogenesis in phagocytes is required for remyelination, Gouna et al., J. Exp. Med. 2021 Vol. 218 No. 10 e20210227 year of copyright 2023; permission conveyed through Copyright Clearance Center, Inc.

BRIEF DEFINITIVE REPORT

TREM2-dependent lipid droplet biogenesis in phagocytes is required for remyelination

Garyfallia Gouna^{1,2} , Christian Klose³ , Mar Bosch-Queralt^{1,2} , Lu Liu⁴ , Ozgun Gokce^{4,5} , Martina Schifferer^{2,5} , Ludovico Cantuti-Castelvetri^{1,2*} , and Mikael Simons^{1,2,5*} 

Upon demyelinating injury, microglia orchestrate a regenerative response that promotes myelin repair, thereby restoring rapid signal propagation and protecting axons from further damage. Whereas the essential phagocytic function of microglia for remyelination is well known, the underlying metabolic pathways required for myelin debris clearance are poorly understood. Here, we show that cholesterol esterification in male mouse microglia/macrophages is a necessary adaptive response to myelin debris uptake and required for the generation of lipid droplets upon demyelinating injury. When lipid droplet biogenesis is defective, innate immune cells do not resolve, and the regenerative response fails. We found that triggering receptor expressed on myeloid cells 2 (TREM2)-deficient mice are unable to adapt to excess cholesterol exposure, form fewer lipid droplets, and build up endoplasmic reticulum (ER) stress. Alleviating ER stress in TREM2-deficient mice restores lipid droplet biogenesis and resolves the innate immune response. Thus, we conclude that TREM2-dependent formation of lipid droplets constitute a protective response required for remyelination to occur.

Introduction

Tissue injury is followed by a repair process, which attempts to reestablish tissue structure and function, but within the central nervous system (CNS), persistent and sometimes even progressive neurological deficits remain (Franklin and Ffrench-Constant, 2017). Remyelination is an example of a regenerative process that can occur in diseases such as multiple sclerosis but often fails during the progressive phase of the disease (Dendrou et al., 2015; Reich et al., 2018). Identifying the mechanisms that determine the outcome of lesions is therefore an important goal for the design of regenerative medicines (Plemel et al., 2017). Microglia are a prime therapeutic target because they represent a key cellular component of the regenerative response, which occurs in distinct phases, starting with microglia activation, followed by phenotype adaptation, and ending with the resolution of the response (Cunha et al., 2020; Miron et al., 2013). We know very little about the underlying checkpoints that drive the sequence of these regenerative responses. A key function of microglia is to clear cellular debris, a process that is necessary to pave the way for the regenerative response and for inflammation resolution (Kotter et al., 2006; Lampron et al., 2015; Lloyd and Miron, 2019). In demyelinating lesions, myelin debris

clearance poses a challenge to microglia, as myelin is lipid-rich and consists of large amounts of cholesterol, which cannot be degraded and therefore requires mechanisms for storage and efflux (Cantuti-Castelvetri et al., 2018; Bogie et al., 2020; Berghoff et al., 2021; Bosch-Queralt et al., 2021). We have previously shown that the cholesterol efflux pathway is insufficiently activated in phagocytes within demyelinating lesions of aged mice (Cantuti-Castelvetri et al., 2018). We found that cholesterol-rich myelin debris can overwhelm the efflux capacity of phagocytes, resulting in the accumulation of foamy microglia with large amounts of lipid droplets and cholesterol crystals in lesions. Here, we aim to identify the molecules that control lipid metabolism in microglia in demyelinating lesions. Triggering receptor expressed on myeloid cells 2 (TREM2), an immunoglobulin superfamily cell surface receptor that is specifically expressed in microglia in the CNS, is one key signaling pathway for microglia activation (Deczkowska et al., 2018; Lewcock et al., 2020). Upon activation by lipid ligands, TREM2 signals through its associated immunoreceptor tyrosine-based activation motif (ITAM)-containing adapter protein TYRO protein tyrosine kinase-binding protein (DAP12) to modulate

¹Institute of Neuronal Cell Biology, Technical University Munich, Munich, Germany; ²German Center for Neurodegenerative Diseases, Munich, Germany; ³Lipotype GmbH, Dresden, Germany; ⁴Institute for Stroke and Dementia Research, University Hospital of Munich, Ludwig Maximilian University of Munich, Munich, Germany; ⁵Munich Cluster of Systems Neurology (SyNergy), Munich, Germany.

*L. Cantuti-Castelvetri and M. Simons contributed equally to this paper; Correspondence to Mikael Simons: mikael.simons@dzne.de; Ludovico Cantuti-Castelvetri: ludovico.cantuti-castelvetri@dzne.de.

© 2021 Gouna et al. This article is distributed under the terms of an Attribution-Noncommercial-Share Alike-No Mirror Sites license for the first six months after the publication date (see <http://www.rupress.org/terms/>). After six months it is available under a Creative Commons License (Attribution-Noncommercial-Share Alike 4.0 International license, as described at <https://creativecommons.org/licenses/by-nc-sa/4.0/>).

proliferation, immune responses, phagocytic capacity, and lipid metabolism. Previous work has shown that TREM2-null microglia fail to acquire an activated transcriptional signature upon various neuropathological insults in mice, resulting in defects in debris clearance (Cantoni et al., 2015; Poliani et al., 2015). However, there remains an incomplete understanding of TREM2-dependent lipid processing after tissue injury. To address this question, we use a toxin-based model in which we locally inject the toxin into the CNS of mice to induce injury to myelin. As expected, lesion recovery was impaired, but surprisingly, TREM2-deficient mice failed to develop foamy microglia with lipid droplets in lesions. Lipid droplets arise at the ER through localized lipogenesis (Walther et al., 2017), but TREM2-deficient microglia developed ER stress, and alleviating this response restored lipid droplet formation. One of the characteristics of lipid droplets is their capacity to buffer excess lipids, but they have also been associated with cellular damage pathways. To determine the role of lipid droplet formation in remyelination, we used mice deficient in acyl-CoA:cholesterol acyltransferase (ACAT; *soat1/Acat*), which is required for the esterification of cellular cholesterol with fatty acids. Upon demyelinating injury, ACAT-deficient mice failed to develop lipid droplet-loaded foamy microglia and showed a marked impairment of lesion recovery. Thus, our data provide evidence that TREM2-dependent formation of lipid droplets represents a protective response required for remyelination to occur.

Results and discussion

TREM2 is required for lipid droplet biogenesis and remyelination

To elucidate the role of TREM2 in myelin clearance, we employed a toxin-based model of demyelination in which lysolecithin (LLC) creates a demyelinated lesion within 4 d postinjection (dpi), followed by lesion repair. Using transmission electron microscopy (TEM), we first quantified remyelination in WT and TREM2-deficient mice (TREM2 KO) in 21-dpi lesions and observed fewer myelinated axons and higher g-ratios (the ratio of the inner axonal diameter to the total outer diameter) in TREM2 KO lesions (Fig. 1, A–C). Furthermore, using antibodies against adenomatous polyposis coli (APC; clone CC1), fewer oligodendrocytes were detected in 21-dpi lesions of TREM2 KO mice compared with control, indicating defective lesion repair in TREM2 KO animals (Fig. S1, A and B) as previously described (Cantoni et al., 2015; Poliani et al., 2015). TEM analyses revealed a marked accumulation of myelin debris with honeycomb-like appearance in 21-dpi TREM2 KO lesions (Fig. S1, C and D). Further characterization of the lesions showed that TREM2 KO and WT 4-dpi lesions were of similar size but with a lower number of allograft inflammatory factor 1 (IBA1⁺) cells in TREM2 KO (Fig. S1, E and F; and Fig. 2, A and B). Microglia/macrophages assessed at additional time points revealed that IBA1⁺ cell density decreased in WT lesions with time but not in TREM2 KO lesions, pointing to impaired innate immune cell resolution in TREM2 KO mice (Fig. 2, A and B). We found no significant differences in the percentage of galectin-3 (Igals3 or MAC2) MAC2⁺/IBA1⁺ cells, in the number of CD11b⁺CD45^{hi} cells and in the density of glial fibrillary acidic protein (GFAP⁺) astrocytes in lesions (Fig. S1, G–J).

To determine the underlying mechanism of defective innate immune cell resolution, we focused on the formation of foamy microglia, which form between 14 and 21 dpi in parallel with the regenerative response. Surprisingly, significantly fewer foamy microglia, characterized by numerous lipid droplets, were observed within TREM2 KO lesions (Fig. 1, A and D). As cholesterol-rich myelin fragments are degraded in the lysosomal system, free cholesterol is released and esterified for storage in lipid droplets. The lack of lipid droplets could be explained by a delay in lipid droplet formation. However, our TEM analysis showed that foamy phagocytes were absent in TREM2 KO, even in lesions at 62 dpi (Fig. 1, A and D). The lack of foamy microglia in TREM2 KO was confirmed by immunohistochemistry (IHC) using antibodies against perilipin 2 (PLIN2), a structural component of lipid droplets, and IBA1. In line with our ultrastructural analysis, the number of IBA1⁺PLIN2⁺ cells increased in WT lesions at 21 and 62 dpi but not in TREM2 KO lesions (Fig. 2, A and C). In addition, IHC analysis for TREM2 revealed that 70% of PLIN2⁺IBA1⁺ cells also colabeled for TREM2 (Fig. 2 D).

We have previously shown that myelin debris overloading of microglia can result in the transition of cholesterol into its crystalline form, which triggers lysosomal rupture and inflammasome stimulation (Cantuti-Castelvetri et al., 2018). However, by combining laser reflection and fluorescence confocal microscopy (reflection microscopy), we found that IBA1⁺ cells contained fewer cholesterol crystals in lesions of TREM2 KO compared with WT mice, indicating that cholesterol crystals cannot account for the poor lesion regeneration of TREM2 KO mice (Fig. 2 E).

To determine whether the deficiency of TREM2 leads to defective lipid droplet formation, postnatal and adult microglia were isolated and cultured with myelin debris for 8 or 24 h. Immunofluorescence analyses using antibodies against PLIN2 showed that lipid droplets accumulated in myelin-treated WT microglia at 8 h and to an even a greater extent at 24 h. In contrast, the number of lipid droplets formed by TREM2 KO cells was significantly lower and never reached the levels of WT microglia (Fig. 3, A–C). To provide further evidence for defective lipid droplet biogenesis in TREM2 KO microglia, we performed Western blot experiments and found that myelin debris treatment triggered the expression of PLIN2 in WT but not TREM2 KO microglia (Fig. 3, D and E). Furthermore, RT-PCR for *soat1/Acat*, the enzyme responsible for cholesterol esterification, mice showed a twofold increase in WT but not TREM2 KO microglia (Fig. 3 F). To explore further the impaired biogenesis of lipid droplets in TREM2 KO microglia, we performed an untargeted lipidomic analysis on myelin debris-treated microglia (Fig. 3 G). As expected, myelin debris treatment induced cholesterol accumulation in both WT and TREM2 KO microglia. However, cholesterol was mostly esterified in WT microglia, while a larger fraction remained as free cholesterol in TREM2 KO cells. Interestingly, myelin treatment induced a distinct lipid profile in TREM2 KO cells characterized by the deficiency of lysophosphatidylcholine (LPC), lysophosphatidylserine (LPS), and lysophosphatidylethanolamine (LPE). Furthermore, triglycerides, another major component of lipid droplets, were generated to a lesser extent in TREM2 KO compared with WT microglia. TREM2 KO microglia accumulated a larger amount

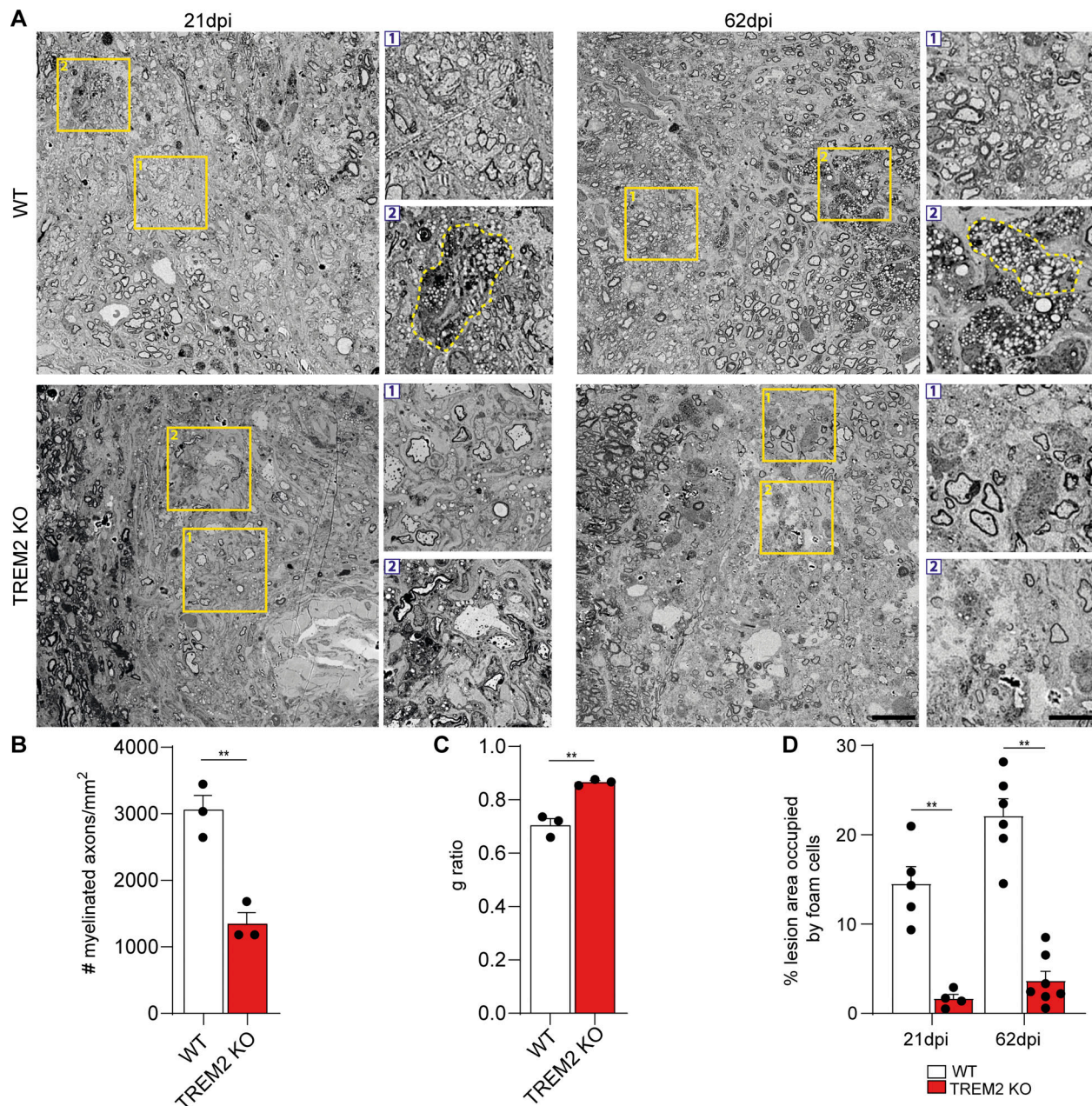


Figure 1. TREM2 is required for lipid droplet biogenesis and remyelination. (A) Scanning electron microscopic images of 21- and 62-dpi lesions from WT and TREM2 KO mice. Zoomed-in images are provided by areas marked by yellow boxes. Box 1 highlights remyelination and box 2 highlights foam cells (yellow dashed lines) in WT lesions. Poor remyelination and absence of foam cells are shown by boxes 1 and 2 in TREM2 KO lesions. (B and C) Quantification of the density of myelinated axons and g-ratio of 21-dpi lesions of WT and TREM2 KO mice. (D) Quantification of the percent area of the lesion occupied by foam cells in 21-dpi lesions of WT and TREM2 KO mice. Scale bars, 10 μ m for the large image and 2 μ m for the zoomed-in image. *n* = 3–4 animals per condition for A–C; *n* = 4–7 lesions per condition for D. For the g-ratio analysis, a minimum of 250 axons per condition were analyzed. *, *P* < 0.05; **, *P* < 0.01.

of phosphatidic acid, a precursor in the formation of triacylglycerols (TAGs) and phospholipids. Together, our results show that TREM2 is required for the synthesis of cholesterol esters and TAGs for lipid droplet biogenesis after myelin debris uptake.

Cholesterol esterification is necessary for remyelination

To determine whether the impaired cholesterol esterification could represent one reason for poor remyelination, we induced

LLC lesions in ACAT KO mice. Electron microscopic analysis of 21-dpi lesions confirmed that no lipid droplets were formed in ACAT KO animals, proving that esterification of cellular cholesterol with fatty acids is required for lipid droplet formation in phagocytes after demyelinating injury (Fig. 4, A and B; and Fig. S2 A). Analysis of semithin sections and TEM images showed that remyelination was remarkably poor in ACAT KO lesions (Fig. 4, A and C; and Fig. S2, A and B). IHC analysis of microglia showed a significant increase in the number of IBA1⁺ cells in

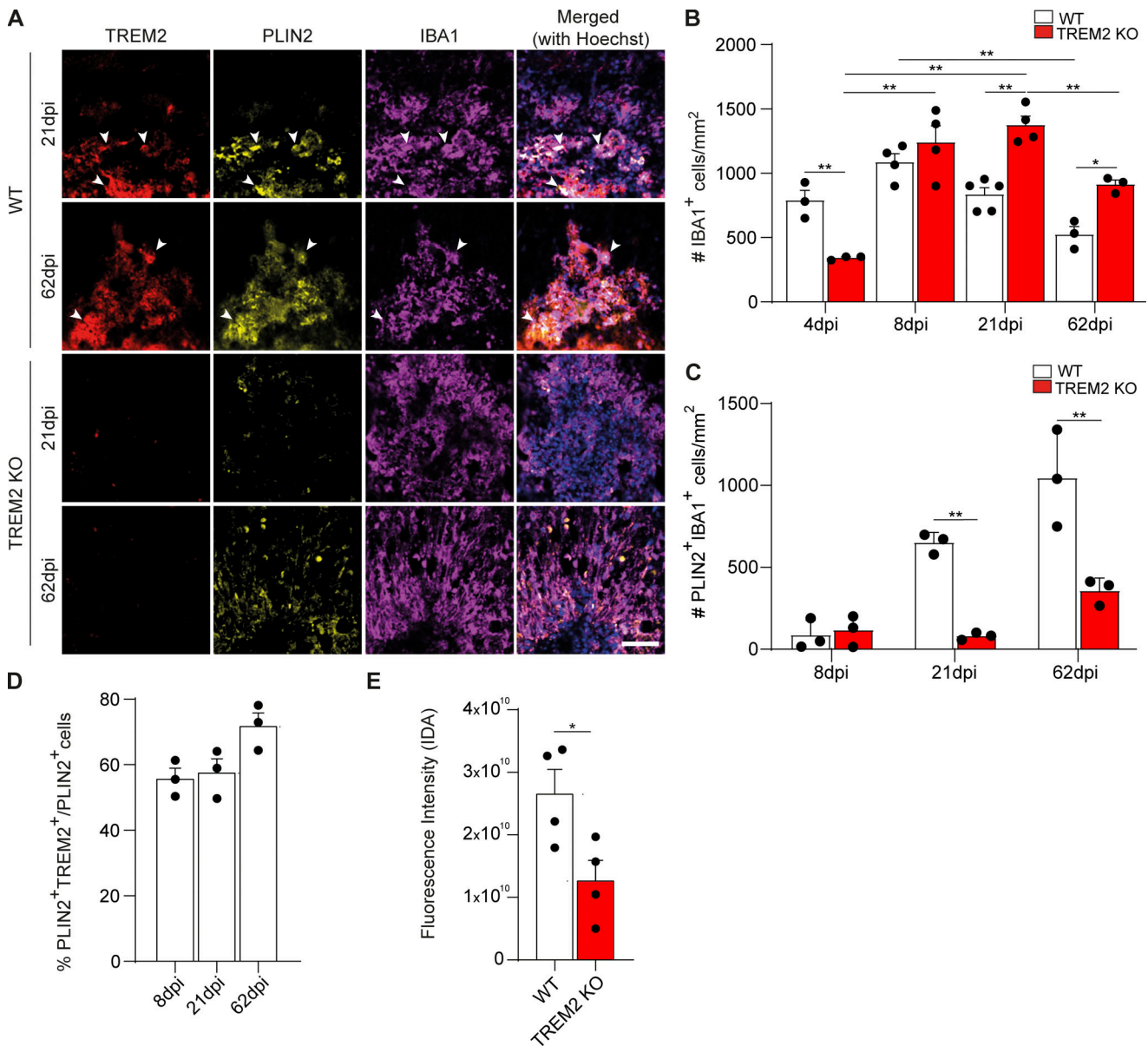


Figure 2. TREM2 is required for innate immune cell resolution and foam cell formation. (A) Confocal images of 21- and 62-dpi lesions from WT and TREM2 KO mice after staining for TREM2 (red), PLIN2 (yellow), and IBA1 (magenta), showing the colocalization of PLIN2 and TREM2 (arrowheads mark triple-positive cells). Scale bar, 50 μ m. (B) Quantification of the density of IBA1⁺ cells at 4, 8, 21, and 62 dpi. (C) The density of PLIN2⁺ IBA1⁺ microglia (cells per mm²) was quantified for WT and TREM2 KO. (D) Quantification of the percentage of PLIN2⁺ IBA1⁺ cells, which are also positive for TREM2, in 21-dpi WT lesions. (E) Quantification of cholesterol crystal fluorescence by reflection confocal microscopy in WT and TREM2 KO lesions at 21 dpi. *n* = 3–5 animals per condition for A–D; *n* = 4 lesions per condition for E. Data represent mean \pm SEM. For B and C, P values were calculated using two-way ANOVA (A) with Šidák post hoc correction. For D, P values were calculated using one-way ANOVA. For E, P values were calculated using two-tailed unpaired t test. *, *P* < 0.05; **, *P* < 0.01. IDA, integrated density area.

lesions at 21 dpi (Fig. 4, D and E). While the number of GFAP⁺ astrocytes were unaltered, there was a slight reduction in the percentage of MAC2⁺/IBA1⁺ cells in ACAT KO lesions at 4 dpi (Fig. S2, C and D). The exacerbated innate immune inflammation at 21 dpi could not be explained by a defect in myelin degradation, as the percentage of myelin-loaded microglia (labeled with the lipid dye fluoromyelin [FM] and the lysosome-associated membrane glycoprotein 1 [LAMP1]) was not different in lesions of WT and ACAT KO mice (Fig. 4 F). Similar to TREM2 KO lesions, using reflection microscopy and TEM, we detected

fewer cholesterol crystals in microglia of ACAT KO lesions compared with WT (Fig. S2 E). Reflection microscopy of myelin-treated microglia confirmed that cholesterol crystals formed both in lysosomes and on lipid droplets (Fig. S2, F–H). Therefore, the phase transition of cholesterol into its crystalline form can likely initiate in lipid droplets. Indeed, occasionally very large crystals (>15 μ m) were observed in the lesions by TEM (Fig. S2 I). Thus, our data show that the ability to esterify cholesterol is a key adaptive function of microglia and a necessary response for regeneration to occur.

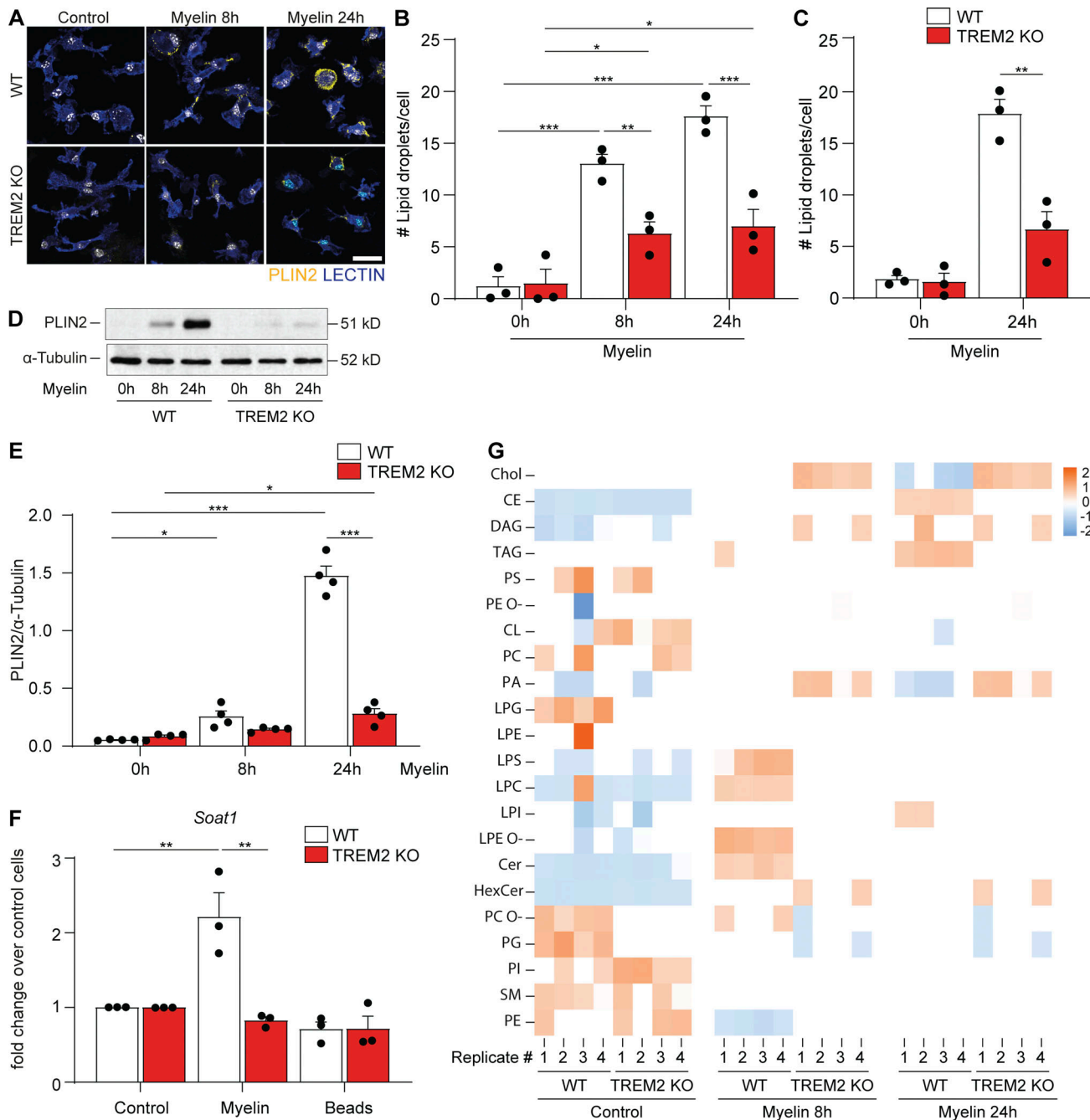


Figure 3. Cholesterol esterification and lipid droplet formation are defective in myelin-treated TREM2 KO microglia. (A) Confocal images of WT and TREM2 KO microglia of the control condition (0 h) or treated with myelin for 8 and 24 h and stained for PLIN2, isolectin (lectin), and Hoechst. Scale bar, 25 μ m. **(B and C)** Quantification of the number of lipid droplets per cell in postnatal (B) and adult (C) microglia. **(D and E)** Western blots and quantification for PLIN2 and α -tubulin in WT and TREM2 KO cells in serum-free media 8 h and 24 h after myelin treatment. The intensity of the band of PLIN2 was normalized to α -tubulin. **(F)** Real-time PCR for ACAT (*Soat1*) in WT and TREM2 KO cells in serum-free media 24 h after myelin treatment and 24 h after exposure to beads. Data are expressed as fold change over the untreated cells. **(G)** Untargeted lipidomics analysis of WT and TREM2 KO cells cultured in serum-free media or with myelin for 8 or 24 h. $n = 3$ biological replicates per condition for A–C, and F; $n = 4$ biological replicates for D and E; $n = 4$ biological replicates for F. The results are representative of three independent experiments. For the lipidomics analysis, each replicate was from a different animal. Data represent as mean \pm SEM. P values were calculated using two-way ANOVA (A) with Šidák post hoc correction. *, $P < 0.05$; **, $P < 0.01$; ***, $P < 0.001$. CE, cholesterol ester; Chol, cholesterol.

ER stress and protein synthesis defects in demyelinating lesions of TREM2-deficient mice

As cholesterol esterification and TAG biosynthesis take place in the ER, we speculated that activation of ER stress could

represent the underlying reason for impaired lipid droplet formation in TREM2 KO microglia. Myelin debris uptake might lead to cholesterol overload in the ER, which is known to trigger the activation of the eukaryotic translation initiation factor 2- α

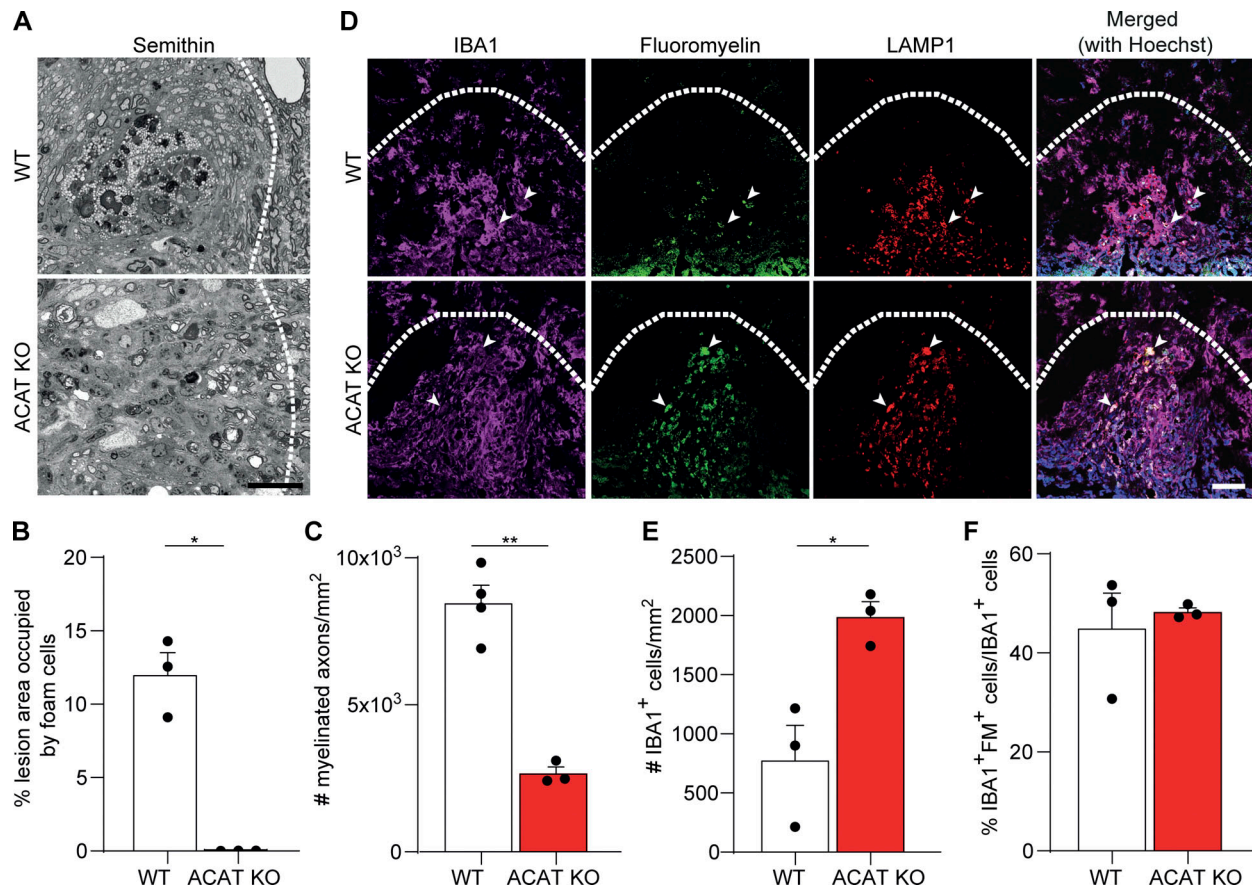


Figure 4. Cholesterol esterification is necessary for remyelination. (A) Representative images of azure blue staining of semithin sections from 21-dpi lesions from WT and ACAT KO mice. (B and C) The quantification of foam cells (B) and remyelinated axons (C). (D–F) Confocal images (D) and quantification (E) of 21-dpi lesions showing increased density of inflammatory cells (IBA1⁺, magenta) in ACAT KO mice compared with the WT control. The number of phagocytes with undigested myelin (arrowheads in D labeled with IBA1, magenta; FM, green; and LAMP1, red) was similar between WT and ACAT KO animals; quantification shown in F. Scale bars, 15 μ m in A and 50 μ m in D. $n = 3–4$ mice per condition for all the experiments. Data represent mean \pm SEM. P values were calculated using two-tailed unpaired *t* test. *, $P < 0.05$; **, $P < 0.01$.

kinase 3, which phosphorylates and inactivates eukaryotic translation initiation factor 2 α (eIF2 α), attenuating protein translation. Indeed, IHC analyses of microglia in demyelinating lesions revealed an increase in the number of IBA1⁺ cells immunopositive for phosphorylated eIF2 α (p-eIF2 α) in TREM2 KO compared with WT lesions (Fig. 5, A and B). To determine the rate of protein translation, lesioned WT and TREM2 KO animals were injected with O-propargyl-puromycin (OP puro), which is incorporated into nascent polypeptide chains. TREM2 KO lesions showed a significant decrease in the number of OP puro⁺IBA1⁺ cells (Fig. 5, C and D), indicating a low rate of protein synthesis in TREM2 KO microglia. We hypothesized that myelin debris uptake-induced cellular stress might be the reason for defective protein translation in TREM2 KO microglia. To explore this possibility, we treated primary microglia with myelin debris and quantified the incorporation of OP puro. A strong increase in OP puro incorporation was observed after myelin treatment in both WT and TREM2 KO microglia (Fig. S3, A and B). However, the incorporation rapidly declined in TREM2 KO but not WT cells after 24 h of treatment, suggesting active suppression of protein synthesis in the absence of TREM2. In addition, we observed by Western blot analysis increased levels of p-eIF2 α in

myelin-treated TREM2 KO compared with WT microglia, further supporting our conclusion that ER stress may turn off protein translation (Fig. S3, C and D). Furthermore, the levels of active, phospho-Jun N-terminal kinase (p-JNK) was also increased in TREM2 KO microglia, which is known to contribute to the phosphorylation and inactivation of eIF2 α (Fig. S3, C and E).

Our data support the hypothesis that myelin debris uptake in TREM2 KO microglia results in ER stress and suppression of protein translation, which possibly impairs lipid droplet biogenesis. Thus, we tested whether mitigation of ER stress is able to improve lipid droplet biogenesis in TREM2 KO mice. We applied 4-phenyl butyric acid (PBA), a widely used small-molecule chaperone known to reduce ER stress (Ozcan et al., 2006), and found that pretreatment of microglia with PBA restored the formation of lipid droplets in TREM2 KO microglia after myelin treatment (Fig. S3, F and G). In addition, when TREM2 KO mice were treated with a daily injection of PBA, we observed an increase in lipid droplet formation in IBA⁺ cells in lesions at 21 dpi (Fig. 5, E and F). There was also a significant decrease of IBA1⁺ cells in TREM2 KO lesions at 21 dpi, providing evidence for a beneficial effect of PBA in inflammation resolution in lesions (Fig. 5, G and H). The amount of myelin debris (labeled with FM) in the lysosomes of microglia

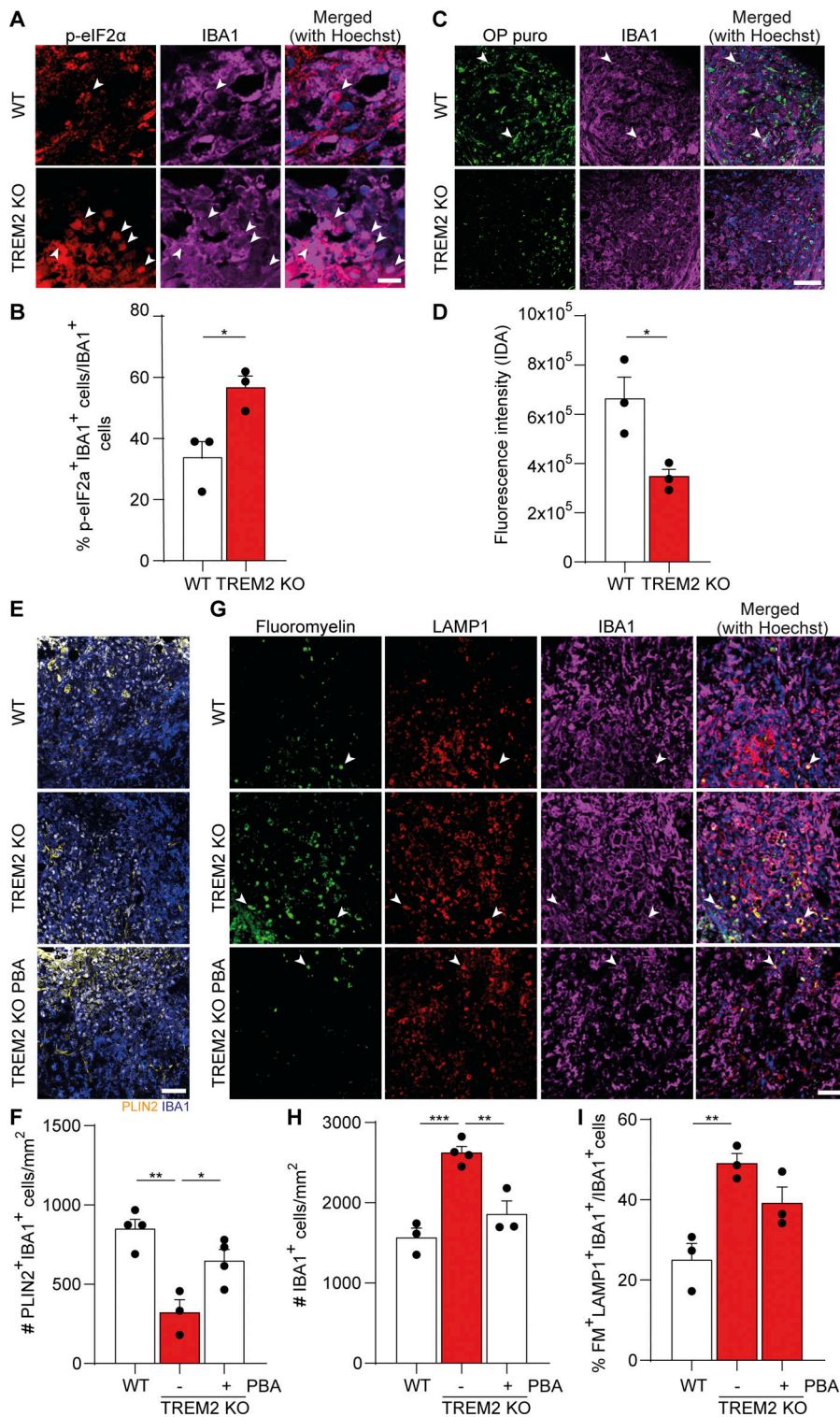


Figure 5. ER stress and protein synthesis defects in TREM2 KO demyelinating lesions. (A and B) Confocal images (A) and relative quantification (B) of 21-dpi lesions from WT and TREM2 KO mice after staining for p-eIF2α (red), IBA1 (magenta), and Hoechst (blue). **(C)** Confocal images of 21-dpi lesions from WT and TREM2 KO mice injected with OP puro (green) 1 h before perfusion and stained for IBA1 (magenta). **(D)** The rate of incorporation was quantified by measuring the integrated density area (IDA) of OP puro within the IBA1⁺ cells within the lesion borders. **(E)** Confocal images and quantification of 21-dpi lesions from WT and TREM2 KO and TREM2 KO mice treated with daily injection of 100 mg/kg PBA stained for PLIN2 (yellow), IBA1 (blue), and Hoechst (white). **(F)** Quantification of the density of PLIN2⁺IBA1⁺ cells. **(G)** Representative confocal images from WT, TREM2 KO, and PBA-treated TREM2 KO mice, stained for FM (green), LAMP1 (red), IBA1 (magenta), and Hoechst (blue); arrowheads mark the colocalization of the markers. **(H)** Quantification of the total number of IBA1⁺ microglia per mm² of lesion. **(I)** Percentage of FM⁺LAMP1⁺IBA1⁺ cells over the total number of IBA1⁺ cells within the lesion boundaries. Scale bars, 10 μm in A and 50 μm in C, E, and G. For all the experiments, n = 3–4 animals per condition. Data represent mean ± SEM. P values were calculated using two-tailed unpaired t test for B and D and one-way ANOVA followed by Tukey’s post hoc test for F, H, and I. *, P < 0.05; **, P < 0.01; ***, P < 0.001.

(labeled for LAMP1) did not differ in lesions of TREM2 KO mice (Fig. 5, G and I). Taken together, these results show that lipid-induced ER stress contributes to impaired lipid droplet formation in TREM2 KO mice.

General discussion and conclusions

Demyelinating injury is followed by phagocytosis of cholesterol-rich myelin debris by microglia/macrophages. While lysosomal

enzymes are responsible for the degradation of most myelin components, cholesterol cannot be degraded and is therefore transferred from late endosomes to the ER. Because the ER has an extremely low cholesterol carrying capacity, there are adaptive mechanisms that protect phagocytes from the toxic effect of free cholesterol (Moore and Tabas, 2011). One protective factor is the liver X receptor (LXR), which regulates the transcription of cholesterol export genes (Evans and

Mangelsdorf, 2014). Another is ACAT, which detoxifies cholesterol by forming cholesterol esters for storage in lipid droplets (Moore and Tabas, 2011). Here, we show that cholesterol esterification is necessary for phagocytes to adapt to excess cholesterol arising from phagocytosis of myelin debris in demyelinating lesions. When this buffering mechanism is defective, phagocytes do not resolve from demyelinating lesions, and the regenerative response fails. We found that TREM2-deficient mice are unable to elicit the adaptive response to excess cholesterol exposure. The reason could be that TREM2-dependent gene expression is necessary to trigger the generation of enzymes required for lipid droplet formation. Because TREM2-deficient phagocytes are able to internalize myelin debris but fail to mount the necessary metabolic responses to the internalized cargo, they become exposed to the toxicity of free cholesterol that builds up with time. Consequently, cholesterol-induced cellular stress develops. Previous studies have shown that cholesterol loading of macrophages activates the unfolded protein response pathway (Feng et al., 2003), and in accordance with these studies, we observed evidence of ER stress in myelin debris-loaded TREM2-deficient phagocytes. Transient protein synthesis inhibition is an important protective mechanism used by cells during ER stress (Xu et al., 2005; Lin and Popko, 2009); however, in the context of myelin debris clearance, such a response could be deleterious as it also blocks the synthesis of lipid metabolism genes. Our lipidomic analysis reveals that TREM2-deficient phagocytes not only fail to generate cholesterol esters but also are deficient in TAG generation. The accumulation of phosphatidic acid in TREM2-deficient phagocytes points to decreased activity of lipin phosphatidic acid phosphatase, which catalyzes the conversion of phosphatidic acid to diacylglycerol (DAG; Carman and Han, 2019). Lipin is unique among biosynthetic enzymes in TAG generation as its enzyme activity is regulated by its transition between the ER and the cytosol, a process under the control of mammalian target of rapamycin-mediated phosphorylation of lipin. Intriguingly, a previous study provided evidence of defective mammalian target of rapamycin signaling in TREM2-deficient microglia (Ulland et al., 2017), providing a possible link of how TREM2 may control TAG generation.

While we highlight a role of lipid droplets in buffering cholesterol-mediated toxicity, it is increasingly becoming clear that lipid droplets also provide protective functions against other forms of lipotoxicity. For example, elevated reactive oxygen species induces the formation of lipid droplets, which sequester polyunsaturated fatty acids, protecting them from oxidative damage (Ioannou et al., 2019). In another context, lipid droplets do not appear to be protective but, instead, are harmful in their role of mediating neuronal damage together with reactive oxygen species generated by defective mitochondria or inflammatory signals (Liu et al., 2015). It is interesting to compare our results with a recent study performed in a model of chronic demyelination, which shows that TREM2-deficient mice accumulate oxidized and nonoxidized cholesterol ester (Nugent et al., 2020). Whereas our results show that TREM2 function is required for the formation of cholesterol esters and lipid droplets, Nugent et al. (2020) came to a different conclusion.

The reasons for these discrepancies are not clear, but one possibility is that TREM2 has additional functions in models of chronic injury in which the generation of reactive oxygen species plays a more important role. Our experiments using ACAT-deficient mice show that remyelination fails when microglia/macrophages are unable to transition into foamy phagocytes. These results imply that the generation of lipid droplets represents an adaptive response required for efficient lesion recovery after acute demyelination. Such foamy phagocytes filled with lipid droplets accumulate in the resolution phase of lesions in aged mice, a condition associated with poor remyelination (Cantuti-Castelvetri et al., 2018; Grajchen et al., 2018). Although these findings superficially appear to contradict each other, it is important to recall that there are two major pathways to prevent the accumulation of free cholesterol in cells. In aging, the underlying deficit is the insufficient activation of LXR, a pathway required to induce the expression of genes involved in cholesterol efflux, such as the plasma membrane cholesterol transporters and apolipoprotein E (Cantuti-Castelvetri et al., 2018). Consequently, excessive amounts of cholesterol-rich myelin debris accumulate in phagocytes, resulting in increased formation of lipid droplets and the transition of cholesterol into crystals. This is in contrast to TREM2 deficiency, which is associated with impaired formation of lipid droplets followed by the exhaustion of phagocyte buffering capacity and stress pathway activation. It is interesting to note that cholesterol crystals were detected both on lipid droplets and in lysosomes. Whereas the overall number of crystals declines, crystals associated with lysosomes still form in TREM2-deficient microglia. Currently, we do not know which of the two types of crystals plays a pathogenic role, but it is tempting to speculate that crystals formed in lysosomes that can cause lysosomal rupture and inflammasome activation are more damaging.

In summary, the results presented here add to a developing picture of how phagocytes function in clearing excess cholesterol that is building up in lesions after a demyelinating insult. It appears that both cholesterol efflux and esterification are essential and that the activation of both pathways is required to promote the resolution of innate immune inflammation and to support remyelination.

Materials and methods

Mice, cell lines, and antibodies

Mice

WT C57BL/6 mice were purchased from Janvier Labs, kept in groups of three in Greenline IVC GM500 plastic cages, and housed in a temperature-controlled environment ($21 \pm 2^\circ\text{C}$) on a 12-h light/dark cycle with food and water available ad libitum in the animal facility in German Center for Neurodegenerative Diseases. *Trem2*^{-/-} mice were established in the C57BL/6 background. SOAT1 KO mice were purchased from The Jackson Laboratory and were backcrossed once in the C57BL/6 background (#002896). All mice used for our experiments were male. All experiments were approved by the institutional animal use and care committee. For the in vivo treatment, 50 mg/kg PBA was administered i.p. every day, starting the day of the LLC injection.

Cell line

L929 cells were grown in DMEM supplemented by 10% FCS, L-glutamine, and antibiotics. For maintenance, these cells were resuspended in freezing media containing 50% FCS and 10% DMSO at concentrations of 5×10^6 to 1×10^7 cells/ml. Aliquots in 1.5-ml cryotubes were frozen slowly at $1^\circ\text{C}/\text{min}$ by placing tubes in a Nalgene cryo freezing container in a -80°C freezer and then transferring to liquid nitrogen storage.

Primary antibodies

Rabbit IBA1 (234 004, 1:500 for IHC; Synaptic Systems), PLIN2 (GP40, 1:500 for histology, 1:3,000 for Western blotting; PROGEN), p-eIF2 α (ab32157, 1:200 for staining, 1:2,000 for Western blotting; Abcam), total eIF2 α (2103, 1:2,000 for Western blotting; Cell Signaling Technology), JNK1+JNK2 (p-T183+Y185, ab4821, 1:1,000 for Western blotting; Abcam), JNK1+JNK2 (ab112501, 1:1,000 for Western blotting; Abcam), LAMP1 (sc-19992, 1:100 for histology; Santa Cruz Biotechnology), TREM2 (AF1729, 1:200 for histology; R&D Systems), α -tubulin clone B-5-1-2 (T5168; Sigma-Aldrich); GAPDH (ab9484, 1:5,000 for Western blotting; Abcam), GFAP (173004, 1:500; Synaptic Systems), MAC2 (125402, 1:250; BioLegend), APC (OP80, 1:100; Merck Calbiochem), and oligodendrocyte transcription factor 2 (OLIG2; ab9610, 1:200; Millipore).

Secondary antibodies

Alexa Fluor 488-, 647-, and 555-conjugated antibodies (Invitrogen) were used.

Other reagents

FM green fluorescent myelin stain from Invitrogen (Cat. F34651), Hoechst 33342 from Sigma (Bisbenzimidazole Hoechst 33342, B2261), and isolectin from Vector Laboratories (DL-1208). L- α -LPC from egg yolk was from Sigma (L4129).

Kits

The Click-iT Cell Reaction Buffer Kit was used (C10269; Thermo Fisher Scientific).

IHC

Animals were anesthetized by 10 mg/ml ketamine and 1 mg/ml xylazine solution i.p. perfused transcardially with 4% paraformaldehyde (PFA). Postfixation of spinal cords was done in 4% PFA overnight. The brain tissue was further cryoprotected in 30% sucrose in PBS for 24 h. After freezing the tissue on dry ice using Tissue-Tek O.C.T., 16- μm coronal sections were cut by a Leica CM 1900 cryostat. The sections were rinsed with $1\times$ PBS containing 0.2% Tween 20 and permeabilized in 0.5% Triton X-100 for 10–30 min depending on primary antibody. For the TREM2 staining, antigen retrieval was performed for 10 min at 120°C in the autoclave in sodium citrate buffer (10 mM, pH 6). Blocking solution (1% FBS, 1% fish gelatin, and 1% bovine calf serum in PBS) was added for 1 h at room temperature to block endogenous mouse tissue immunoglobulins. Primary antibodies, diluted in 10% blocking solution, were added and incubated overnight at 4°C . On the following day, sections were incubated with secondary antibodies, diluted in 10% blocking

solution, for 1 h at room temperature. The sections were washed with PBS followed by incubation in secondary antibody for 1 h at room temperature. Sections were then washed, stained with 2 $\mu\text{g}/\text{ml}$ Hoechst 33342, and mounted with fluorescence mounting medium (81381; Sigma-Aldrich). For the protein synthesis analysis, cells were incubated with 10 μM OP puro (HY-15680; MedChemExpress) for 60 min. The cells were then fixed in 4% PFA. The cells were permeabilized in 0.1% Triton X-100 for 3 min, washed, and processed with the Click-iT Cell Reaction Buffer Kit (C10269; Thermo Fisher Scientific) according to the manufacturer's instructions. Briefly, the cells were incubated for 30 min with a solution of reaction buffer, CuSO_4 , buffer additive, and 5 μM Alexa Fluor 488 Azide (A10266; Thermo Fisher Scientific). The cells were then washed and stained with isolectin. For the in vivo study, LLC lesions were induced as described above. 1 h before the perfusion, the animals were anaesthetized with medetomidine-midazolam-fentanyl (MMF), and a solution of 10 μM OP puro was administered via i.p. injection. The lesions were sectioned and stained with the Click-iT Cell Reaction Buffer Kit and for conventional histology. The cells were imaged with a Leica SP5 confocal microscope with a 63 \times objective. For reflection microscopy, 14- μm sections were stained with DyLight 594-conjugated GSL I-B4 isolectin (DL1207; Vector Laboratories) and DAPI. The sections were then imaged with a Leica SP5 AOBS confocal microscope according to the manufacturer's instructions. For the quantification of the crystals, at least two random 100 \times pictures per lesion were taken to calculate the integrated density area. For the quantification of the lesion area, the surface of demyelination shown by negative FM staining was measured in serial sections of a lesion, which were separated by a known distance. According to the truncated cone model, lesion volume was calculated in IPython. The code is available at https://github.com/lenkavaculciakova/lesion_volume.

TEM

Mouse spinal cords were fixed in 2.5% glutaraldehyde and 4% PFA in 0.1 M sodium cacodylate buffer at pH 7.4 after deep anesthesia (isoflurane) perfusion. Spinal cords were vibratome sectioned and immersion fixed in the same buffer for 24 h at 4°C . After tissue trimming and washes in 0.1 M sodium cacodylate buffer, postfixation in reduced osmium (2% osmium, 2.5% potassium ferrocyanide in 0.1 M cacodylate buffer) was followed by en bloc uranyl acetate (1% aqueous uranyl acetate) contrasting, graded dehydration in ethanol, and embedding in epon resin (Serva). After ultrathin sectioning, the grids (Leica UC7 Ultramicrotome) were contrasted by 1% uranyl acetate and lead citrate (Ultrastain; Leica). Semithin sections were contrasted by an equimolar mixture containing 1% methylene blue (Carl Roth GmbH & Co. Kg) in 100 ml sodium tetraborate and 1% (1 g) azure blue (Carl Roth) in 100 ml water. Images were acquired with a JEOL JEM 1400plus TEM equipped with a Ruby 8 megapixel CCD camera. For each analysis, randomly selected regions in three to five different animals were imaged. Data analysis was performed using ImageJ 1.41 software (<https://imagej.net/Fiji>). The g-ratios were measured with ImageJ on transverse electron micrographs at 8,000 \times magnification. The perimeters of each axon and the myelin sheath were measured with the freehand

tool by tracing the outer surfaces of each structure. The g-ratio was calculated as the diameter of the axon over the diameter of its myelin.

Myelin isolation and purification

Myelin was isolated from 8-wk-old C57BL/6 mouse brains by sequential centrifugation on discontinuous sucrose gradient according to a protocol previously described (Norton and Poduslo, 1973), with some modifications. The ultracentrifugation was done using an SW41 Ti rotor. The brain tissues were homogenized with a Dounce homogenizer in a solution containing 10 mM Hepes, 5 mM EDTA, and 0.32 M sucrose. The homogenized tissue was layered on Hepes/EDTA buffer containing 0.85 M sucrose and centrifuged at 24,600 rpm for 30 min with low deceleration and acceleration. The crude myelin fraction was removed from the interface, resuspended in ice-cold distilled water, and centrifuged at 9,500 rpm for 15 min. The hypo-osmotic shock was applied to the pellet two more times. The pellet from the last step was dissolved in Hepes/EDTA buffer containing 0.3 M sucrose and placed over the 0.85 M sucrose; all the centrifugation steps and hypo-osmotic shocks were repeated as before. Eventually, the purified myelin pellet was resuspended in 1 ml PBS and stored at -20°C .

Microglia treatment

Microglia were isolated from C57BL/6, P6-P8 WT mice by MACS technology. Brain tissue was dissociated using a Papain-based Neural Tissue Dissociation Kit (Miltenyi Biotec). Briefly, brain tissue was removed, cut into small pieces, and dissociated by enzymatic digestion provided in the kit. The tissue suspension was applied to a 70- μm cell strainer and washed twice with DMEM containing 1 mM sodium pyruvate. The final pellet was resuspended in 10 vol of DMEM containing 10% FCS, 1 mM sodium pyruvate, and 1% antibiotics (DMEM/FCS) plus 1 vol CD11b microbeads (130-093-634; Miltenyi Biotec) and incubated at 4°C for 15 min. After washing with DMEM/FCS, the pellet was resuspended in 500 μl of the same medium and applied to a MACS column in the magnetic field after washing three times; the CD11b⁺ cells (microglia) were flushed out of the column and centrifuged at 400 $\times g$ for 10 min at 4°C . Isolated microglia were plated on 8-mm coverslips at 7×10^4 cell/ml and incubated until confluent. Myelin was sonicated in an ultrasound water bath for 5 min. Primary microglia cultures were treated with 8 μg myelin and incubated for 2–24 h. The cells were then fixed with 4% PFA and stained for PLIN2, DyLight 694-labeled tomato lectin, and 2 $\mu\text{g}/\text{ml}$ Hoechst 33342. The cells were imaged on a Leica SP5 confocal microscope with a 63 \times objective.

LLC-induced demyelination

Stereotactic injection of LLC in the spinal cord was performed in WT C57BL/6, SOAT1, and TREM2 mice that were 9–15 wk old. 1% LLC was prepared by dissolving L- α -LPC from egg yolk (L4129; Sigma) in PBS, pH 7.4 (10010056; Gibco). 3% Monastral Blue was prepared by dissolving Copper(II) phthalocyanine-tetrasulfonic acid tetrasodium salt (274011; Sigma-Aldrich) in Milli-Q water, and the solution was sterilized by filtration through a 0.45- μm filter and autoclaving. Prior to injection, 1 μl 3% Monastral Blue

was mixed with 25 μl 1% LLC. Glass Capillaries for Nanoliter 2010 (504949 or 4878; World Precision Instruments) were pulled using the P-1000 Next Generation Micropipette Puller (Sutter Instrument). The program had the following parameters: heat, 530; pull, 0; velocity 60; time, 250; pressure, 500; ramp, 520; microinjection-BF100.50.10; tip, <1 μm ; taper, 6–8 mm; R, ~ 40 –80 M Ω ; heat = ramp; FB255B; and 2.5-mm box. Before surgery, the animals were anesthetized by MMF i.p. (0.5 mg/kg body weight medetomidine, 5.0 mg/kg midazolam, and 0.05 mg/kg fentanyl). The anesthetized animals were kept on a heating pad at 37°C , and the anesthetic depth was monitored by checking the reflex between the toes and the corneal reflex. The surgery and intraspinal injection of LLC was conducted using the Digital Mouse Stereotaxic Frame and Nanoliter 2010 injector with MICRO4 controller (World Precision Instruments) as previously described (Cantuti-Castelvetri et al., 2018). After the spinal cord was exposed, the capillary was positioned 0.55 mm lateral to the dorsal artery and lowered 1.20 mm into the tissue. At each injection site, 1 μl of 1% LLC containing 0.12% Monastral Blue was injected at a speed of 350 nl/min. 1 min after the end of the delivery, the capillary was retracted. After injection, the wound was sutured. After the operation, the animals were injected with 250 μl of 0.9% NaCl (normal saline solution) to compensate for the loss of blood and with the analgesic buprenorphine at a dose of 0.1 mg/kg. When MMF was used for anesthesia, 2.5 mg/kg atipamezole, 0.5 mg/kg flumazenil, and 1.2 mg/kg naloxone i.p. was administered to antagonize the anesthesia and awaken the animal. The animals were administered buprenorphine s.c. for 2 days after surgery.

Gene expression analysis

For the isolation of RNA, primary microglia were treated with myelin or Fluoresbrite beads. At the end of the treatment, the cells were collected in Buffer RLT, and the RNA was isolated with RNeasy (74104; Qiagen). The RNA was retrotranscribed to cDNA with the Superscript III kit (18080051; Thermo Fisher Scientific). For quantitative PCR, the cDNA was quantified with the Power SYBR Green PCR Master Mix (4367659; Thermo Fisher Scientific) on an Applied Biosystems 7500 Fast Cycler according to the PCR mix data sheet. The relative quantification of each gene was performed with the $\Delta\Delta\text{Ct}$ method: Each gene was quantified, and its expression was normalized to the housekeeper gene cytochrome C1 (CYC1). The primers used for the analysis were SOAT1, forward 5'-TGCTGACGCTCTTCTGTGTC-3'; SOAT1 reverse WT, 5'-GAGCTGTTGGGGAGTAGGTG-3'; SOAT1 reverse mutant, 5'-CCTTCTATCGCCTTCTTGACG-3'; CYC1 forward, 5'-ATGGGAGA TGTTTCATGCGG-3'; and CYC1 reverse, 5'-CTGAGGTCAGGGGT AAAGC-3'.

Flow cytometry

The mice were anesthetized and perfused with cold PBS. Each brain was removed, and the lesions were microdissected individually under a dissection microscope. Dissociation of single cells was performed by using gentleMACS Dissociator with the Papain-based Neural Tissue Dissociation Kit (Miltenyi Biotec). Cell pellets were blocked with mouse FcR-blocking reagent (1:100, CD16/CD32 monoclonal antibody; eBioscience) and

stained for 15 min using 7-AAD (25 µg/ml; Thermo Fisher Scientific) and the antibodies against CD45 (1:200, eFluor450, 30-F11; eBioscience) and CD11b (1:200, PE/Cy7, M1/70; eBioscience) followed by washing with PBS. FACS analysis was performed with flow cytometry (SH800; Sony). Flow cytometry data were analyzed using FlowJo v10.

Western blotting

Following separation with SDS-PAGE, the proteins were transferred from the gel onto the nitrocellulose membrane using the Mini Trans-Blot Module. The gel sandwich in blotting cassette was placed in the tank of the module containing transfer buffer (0.25 M Tris base, 1.92 M glycine, 20% methanol) with 100 V for 1 h. The membrane was washed in PBS with 0.1% Tween 20 (PBST) for 10 min, immersed in 3% BSA in PBST as a blocking solution for 30 min at room temperature, and then incubated with primary antibody in PBST at 4°C overnight. After washing, it was incubated with HRP-conjugated secondary antibody in PBST for 1 h at room temperature. Then targeted protein was detected with enhanced chemiluminescence method using Luminol enhancer and peroxide solutions (Pierce/Thermo Fisher Scientific) and visualized with an Odyssey Fc imager from LI-COR.

Image processing and analysis

Images were acquired via a Leica TCS SP5 confocal microscope and processed and analyzed with Imaris (64×, version 9.2.0) and ImageJ 1.41 image processing software.

Lipid extraction for mass spectrometry lipidomics

Mass spectrometry (MS)-based lipid analysis was performed by Lipotype GmbH as described elsewhere (Fitzner et al., 2020). Lipids were extracted using a two-step chloroform/methanol procedure (Ejsing et al., 2009). Samples were spiked with internal lipid standard mixture containing cardiolipin (CL) 16:1/15:0/15:0/15:0, ceramide (Cer) 18:1;2/17:0, DAG 17:0/17:0, hexosylceramide (HexCer) 18:1;2/12:0, lysophosphatidate (LPA) 17:0, LPC 12:0, LPE 17:1, lysophosphatidylglycerol (LPG) 17:1, lysophosphatidylinositol (LPI) 17:1, LPS 17:1, phosphatidate (PA) 17:0/17:0, phosphatidylcholine (PC) 17:0/17:0, phosphatidylethanolamine (PE) 17:0/17:0, phosphatidylglycerol (PG) 17:0/17:0, phosphatidylinositol (PI) 16:0/16:0, phosphatidylserine (PS) 17:0/17:0, cholesterol ester 20:0, sphingomyelin (SM) 18:1;2/12:0;0, TAG 17:0/17:0/17:0, and cholesterol D6. After extraction, the organic phase was transferred to an infusion plate and dried in a speed vacuum concentrator. First-step dry extract was resuspended in 7.5 mM ammonium acetate in chloroform:methanol:propanol (1:2:4 vol:vol:vol), and second-step dry extract was resuspended in 33% ethanol solution of methylamine:chloroform:methanol (0.003:5:1 vol:vol:vol). All liquid-handling steps were performed using Hamilton Robotics STARlet robotic platform with the Anti Droplet Control feature for organic solvents pipetting.

MS data acquisition and analysis

Samples were analyzed by direct infusion on a Q Exactive Mass Spectrometer (Thermo Fisher Scientific) equipped with a TriVersa NanoMate ion source (Advion Biosciences). Samples were analyzed in both positive and negative ion modes with a

resolution of $R_{m/z} = 200$ of 280,000 for MS and $R_{m/z} = 200$ of 17,500 for tandem MS experiments in a single acquisition. Tandem MS was triggered by an inclusion list encompassing corresponding MS mass ranges scanned in one-dimensional increments. Both MS and tandem MS data were combined to monitor cholesterol ester, DAG, and TAG ions as ammonium adducts; PC and PC O- as acetate adducts; and CL, PA, PE, PE O-, PG, PI, and PS as deprotonated anions. MS only was used to monitor LPA, LPE, LPE O-, LPI, and LPS as deprotonated anions; Cer, HexCer, SM, LPC, and LPC O- as acetate adducts, and cholesterol as ammonium adduct of an acetylated derivative. Data were analyzed with in-house-developed lipid identification software based on LipidXplorer (Herzog et al., 2011). Data postprocessing and normalization were performed using an in-house-developed data management system. Only lipid identifications with a signal-to-noise ratio >5 and a signal intensity fivefold higher than in corresponding blank samples were considered for further data analysis.

Statistics

Statistical analysis was performed with GraphPad Prism (GraphPad Software Inc.). The number of animals and cultures used for the experiments are indicated in the bars graphs of the figures or in the figure legends. No statistical methods were used to predetermine sample sizes, but our sample sizes are similar to those generally employed in the field. Data distribution was assumed to be normal, but this was not formally tested. To compare two groups, two-tailed unpaired Student's *t* test was applied. One-way ANOVA followed by Tukey's post hoc test was performed for comparison of more than two groups. To compare the interactions between different animal or cell lines, two-way ANOVA followed by Tukey's post hoc test was used. A *P* value of <0.05 was considered significant in all tests. All values are represented as mean ± SEM.

Online supplemental material

Fig. S1 depicts how myelin clearance and remyelination is impaired in TREM2 KO lesions. Fig. S2 displays how inflammation, remyelination, and cholesterol crystal formation is affected by the defective cholesterol esterification in the ACAT KO mouse model. Fig. S3 shows that in TREM2 KO microglia, ER stress is caused by myelin phagocytosis.

Acknowledgments

We thank Dr. Sabina Tahirovic, Agata Rhomberg, Georg Kisslinger, Kerstin Karg, and Lina Dinkel of the German Center for Neurodegenerative Diseases for their technical assistance.

The work was supported by grants from the German Research Foundation (SPP2191, TRR 128-2, Project ID 408885537-TRR 274, Synergy Excellence Cluster, EXC2145, Projekt ID390857198), the Human Frontier Science Program, the European Research Council (Consolidator Grant to M. Simons), and the Dr. Miriam and Sheldon G. Adelson Medical Research Foundation.

Author contributions: L. Cantuti-Castelvetri and M. Simons conceived the project and designed experiments. L. Cantuti-Castelvetri, G. Gouna, M. Bosch-Queralt, M. Schifferer, C. Klose,

O. Gokce, and L. Liu carried out experiments and analyzed the data. L. Cantuti-Castelvetri and G. Gouna visualized the data. L. Cantuti-Castelvetri and M. Simons wrote the manuscript. L. Cantuti-Castelvetri and M. Simons supervised the project.

Disclosures: C. Klose reported being a shareholder and employee at Lipotype GmbH. No other disclosures were reported.

Submitted: 28 January 2021

Revised: 21 June 2021

Accepted: 29 July 2021

References

Berghoff, S.A., L. Spieth, T. Sun, L. Hosang, L. Schlaphoff, C. Depp, T. Düking, J. Winchenbach, J. Neuber, D. Ewers, et al. 2021. Microglia facilitate repair of demyelinated lesions via post-squalene sterol synthesis. *Nat. Neurosci.* 24:47–60. <https://doi.org/10.1038/s41593-020-00757-6>

Bogie, J.F.J., E. Grajchen, E. Wouters, A.G. Corrales, T. Dierckx, S. Vanherle, J. Mailleux, P. Gervois, E. Wolfs, J. Dehairs, et al. 2020. Stearoyl-CoA desaturase-1 impairs the reparative properties of macrophages and microglia in the brain. *J. Exp. Med.* 217:e20191660. <https://doi.org/10.1084/jem.20191660>

Bosch-Queralt, M., L. Cantuti-Castelvetri, A. Damkou, M. Schifferer, K. Schlepckow, I. Alexopoulos, D. Lütjohann, C. Klose, L. Vaculčiaková, T. Masuda, et al. 2021. Diet-dependent regulation of TGF β impairs reparative innate immune responses after demyelination. *Nat. Metab.* 3: 211–227. <https://doi.org/10.1038/s42255-021-00341-7>

Cantoni, C., B. Bollman, D. Licastro, M. Xie, R. Mikesell, R. Schmidt, C.M. Yuede, D. Galimberti, G. Olivecrona, R.S. Klein, et al. 2015. TREM2 regulates microglial cell activation in response to demyelination in vivo. *Acta Neuropathol.* 129:429–447. <https://doi.org/10.1007/s00401-015-1388-1>

Cantuti-Castelvetri, L., D. Fitzner, M. Bosch-Queralt, M.T. Weil, M. Su, P. Sen, T. Ruhwedel, M. Mitkovski, G. Trendelenburg, D. Lütjohann, et al. 2018. Defective cholesterol clearance limits remyelination in the aged central nervous system. *Science.* 359:684–688. <https://doi.org/10.1126/science.aan4183>

Carman, G.M., and G.S. Han. 2019. Fat-regulating phosphatidic acid phosphatase: a review of its roles and regulation in lipid homeostasis. *J. Lipid Res.* 60:2–6. <https://doi.org/10.1194/jlr.S087452>

Cunha, M.L., M. Su, L. Cantuti-Castelvetri, S.A. Müller, M. Schifferer, M. Djannatian, I. Alexopoulos, F. van der Meer, A. Winkler, T.J. van Ham, et al. 2020. Pro-inflammatory activation following demyelination is required for myelin clearance and oligodendrogenesis. *J. Exp. Med.* 217: e20191390. <https://doi.org/10.1084/jem.20191390>

Deczkowska, A., H. Keren-Shaul, A. Weiner, M. Colonna, M. Schwartz, and I. Amit. 2018. Disease-associated microglia: A universal immune sensor of neurodegeneration. *Cell.* 173:1073–1081. <https://doi.org/10.1016/j.cell.2018.05.003>

Dendrou, C.A., L. Fugger, and M.A. Friese. 2015. Immunopathology of multiple sclerosis. *Nat. Rev. Immunol.* 15:545–558. <https://doi.org/10.1038/nri3871>

Ejsing, C.S., J.L. Sampaio, V. Surendranath, E. Duchoslav, K. Ekroos, R.W. Klemm, K. Simons, and A. Shevchenko. 2009. Global analysis of the yeast lipidome by quantitative shotgun mass spectrometry. *Proc. Natl. Acad. Sci. USA.* 106:2136–2141. <https://doi.org/10.1073/pnas.0811700106>

Evans, R.M., and D.J. Mangelsdorf. 2014. Nuclear receptors, RXR, and the big bang. *Cell.* 157:255–266. <https://doi.org/10.1016/j.cell.2014.03.012>

Feng, B., P.M. Yao, Y. Li, C.M. Devlin, D. Zhang, H.P. Harding, M. Sweeney, J.X. Rong, G. Kuriakose, E.A. Fisher, et al. 2003. The endoplasmic reticulum is the site of cholesterol-induced cytotoxicity in macrophages. *Nat. Cell Biol.* 5:781–792. <https://doi.org/10.1038/ncb1035>

Fitzner, D., J.M. Bader, H. Penkert, C.G. Bergner, M. Su, M.T. Weil, M.A. Surma, M. Mann, C. Klose, and M. Simons. 2020. Cell-type- and brain-region-resolved mouse brain lipidome. *Cell Rep.* 32:108132. <https://doi.org/10.1016/j.celrep.2020.108132>

Franklin, R.J.M., and C. Ffrench-Constant. 2017. Regenerating CNS myelin - from mechanisms to experimental medicines. *Nat. Rev. Neurosci.* 18: 753–769. <https://doi.org/10.1038/nrn.2017.136>

Grajchen, E., J.J.A. Hendriks, and J.F.J. Bogie. 2018. The physiology of foamy phagocytes in multiple sclerosis. *Acta Neuropathol. Commun.* 6:124. <https://doi.org/10.1186/s40478-018-0628-8>

Herzog, R., D. Schwudke, K. Schuhmann, J.L. Sampaio, S.R. Bornstein, M. Schroeder, and A. Shevchenko. 2011. A novel informatics concept for high-throughput shotgun lipidomics based on the molecular fragmentation query language. *Genome Biol.* 12:R8. <https://doi.org/10.1186/gb-2011-12-1-r8>

Ioannou, M.S., J. Jackson, S.H. Sheu, C.L. Chang, A.V. Weigel, H. Liu, H.A. Pasolli, C.S. Xu, S. Pang, D. Matthies, et al. 2019. Neuron-astrocyte metabolic coupling protects against activity-induced fatty acid toxicity. *Cell.* 177:1522–1535.e14. <https://doi.org/10.1016/j.cell.2019.04.001>

Kotter, M.R., W.W. Li, C. Zhao, and R.J. Franklin. 2006. Myelin impairs CNS remyelination by inhibiting oligodendrocyte precursor cell differentiation. *J. Neurosci.* 26:328–332. <https://doi.org/10.1523/JNEUROSCI.2615-05.2006>

Lampron, A., A. Larochelle, N. Laflamme, P. Préfontaine, M.M. Plante, M.G. Sánchez, V.W. Yong, P.K. Stys, M.E. Tremblay, and S. Rivest. 2015. Inefficient clearance of myelin debris by microglia impairs remyelinating processes. *J. Exp. Med.* 212:481–495. <https://doi.org/10.1084/jem.20141656>

Lewcock, J.W., K. Schlepckow, G. Di Paolo, S. Tahirovic, K.M. Monroe, and C. Haass. 2020. Emerging microglia biology defines novel therapeutic approaches for Alzheimer's disease. *Neuron.* 108:801–821. <https://doi.org/10.1016/j.neuron.2020.09.029>

Lin, W., and B. Popko. 2009. Endoplasmic reticulum stress in disorders of myelinating cells. *Nat. Neurosci.* 12:379–385. <https://doi.org/10.1038/nn.2273>

Liu, L., K. Zhang, H. Sandoval, S. Yamamoto, M. Jaiswal, E. Sanz, Z. Li, J. Hui, B.H. Graham, A. Quintana, and H.J. Bellen. 2015. Glial lipid droplets and ROS induced by mitochondrial defects promote neurodegeneration. *Cell.* 160:177–190. <https://doi.org/10.1016/j.cell.2014.12.019>

Lloyd, A.F., and V.E. Miron. 2019. The pro-remyelination properties of microglia in the central nervous system. *Nat. Rev. Neurol.* 15:447–458. <https://doi.org/10.1038/s41582-019-0184-2>

Miron, V.E., A. Boyd, J.W. Zhao, T.J. Yuen, J.M. Ruckh, J.L. Shadrach, P. van Wijngaarden, A.J. Wagers, A. Williams, R.J.M. Franklin, and C. Ffrench-Constant. 2013. M2 microglia and macrophages drive oligodendrocyte differentiation during CNS remyelination. *Nat. Neurosci.* 16:1211–1218. <https://doi.org/10.1038/nn.3469>

Moore, K.J., and I. Tabas. 2011. Macrophages in the pathogenesis of atherosclerosis. *Cell.* 145:341–355. <https://doi.org/10.1016/j.cell.2011.04.005>

Norton, W.T., and S.E. Poduslo. 1973. Myelination in rat brain: method of myelin isolation. *J. Neurochem.* 21:749–757. <https://doi.org/10.1111/j.1471-4159.1973.tb07519.x>

Nugent, A.A., K. Lin, B. van Lengerich, S. Lianoglou, L. Przybyla, S.S. Davis, C. Llapashtica, J. Wang, D.J. Kim, D. Xia, et al. 2020. TREM2 regulates microglial cholesterol metabolism upon chronic phagocytic challenge. *Neuron.* 105:837–854.e9. <https://doi.org/10.1016/j.neuron.2019.12.007>

Ozcan, U., E. Yilmaz, L. Ozcan, M. Furuhashi, E. Vaillancourt, R.O. Smith, C.Z. Görgün, and G.S. Hotamisligil. 2006. Chemical chaperones reduce ER stress and restore glucose homeostasis in a mouse model of type 2 diabetes. *Science.* 313:1137–1140. <https://doi.org/10.1126/science.1128294>

Plemel, J.R., W.Q. Liu, and V.W. Yong. 2017. Remyelination therapies: a new direction and challenge in multiple sclerosis. *Nat. Rev. Drug Discov.* 16: 617–634. <https://doi.org/10.1038/nrd.2017.115>

Poliani, P.L., Y. Wang, E. Fontana, M.L. Robinette, Y. Yamanishi, S. Gilfillan, and M. Colonna. 2015. TREM2 sustains microglial expansion during aging and response to demyelination. *J. Clin. Invest.* 125:2161–2170. <https://doi.org/10.1172/JCI77983>

Reich, D.S., C.F. Lucchinetti, and P.A. Calabresi. 2018. Multiple Sclerosis. *N. Engl. J. Med.* 378:169–180. <https://doi.org/10.1056/NEJMr1401483>

Ulland, T.K., W.M. Song, S.C. Huang, J.D. Ulrich, A. Sergushichev, W.L. Beatty, A.A. Loboda, Y. Zhou, N.J. Cairns, A. Kambal, et al. 2017. TREM2 maintains microglial metabolic fitness in Alzheimer's disease. *Cell.* 170: 649–663.e13. <https://doi.org/10.1016/j.cell.2017.07.023>

Walther, T.C., J. Chung, and R.V. Farese Jr. 2017. Lipid droplet biogenesis. *Annu. Rev. Cell Dev. Biol.* 33:491–510. <https://doi.org/10.1146/annurev-cellbio-100616-060608>

Xu, C., B. Bailly-Maitre, and J.C. Reed. 2005. Endoplasmic reticulum stress: cell life and death decisions. *J. Clin. Invest.* 115:2656–2664. <https://doi.org/10.1172/JCI26373>

Supplemental material

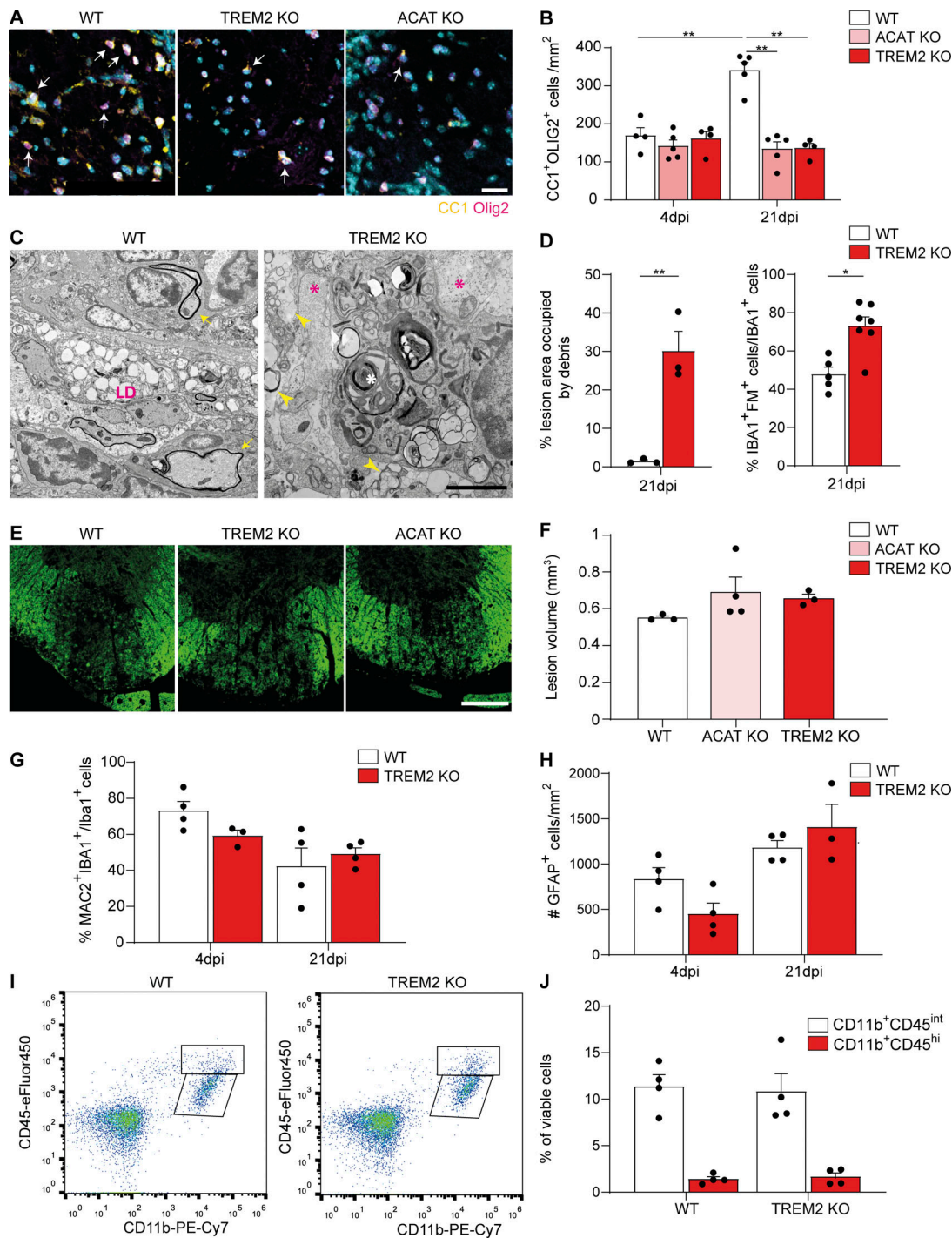


Figure S1. Defective remyelination and myelin clearance in TREM2 KO lesions. (A) Representative images of mature oligodendrocytes labeled for APC (clone CC1, yellow) and OLIG2 (magenta). (B) Relative quantification of the cell density. (C) TEM of WT and TREM2 KO lesions at 21 dpi, showing extracellular and intracellular debris (yellow arrowheads and white asterisk, respectively) in TREM2 KO phagocytes. Lipid droplets (LD) are observed in WT but not in TREM2 KO phagocytes. Remyelinated axons are detected in WT lesions (yellow arrows), while TREM2 KO lesions show naked axons (magenta asterisks). (D) Quantification of the accumulation of extracellular debris expressed as percentage of the lesion occupied by honeycomb-like debris and percentage of the IBA1⁺ cells, which contain debris (labeled by FM) in 21-dpi lesions of WT and TREM2 KO mice. (E and F) Representative images of 4-dpi lesions from WT, TREM2 KO, and ACAT KO mice and relative quantification of the lesion volume. (G) Percentage of IBA1⁺ cells, which are also MAC2⁺ in 4- and 21-dpi lesions of WT and TREM2 KO mice. (H) Quantification of the density of astrocytes (labeled by GFAP) in 4- and 21-dpi lesions of WT and TREM2 KO mice. (I and J) FACS plot showing the distribution of the brain mononuclear-phagocyte populations stained by CD11b (x axis) and CD45 (y axis) in 4-dpi lesions of WT and TREM2 KO mice and relative quantification. Populations of CD11b⁻CD45^{int} microglia and CD11b⁺CD45^{hi} CNS-associated macrophages were gated from viable cells. *n* = 3–5 animals per condition for all the depicted experiments. Scale bars, 10 μm in A, 2 μm in B, and 250 μm in E. Data represent mean ± SEM. P values were calculated with two-way ANOVA followed by Tukey's post hoc test for B, G, and H; with two-tailed unpaired *t* test for D and J; and with one-way ANOVA followed by Tukey's post hoc test for F. *, *P* < 0.05; **, *P* < 0.01.

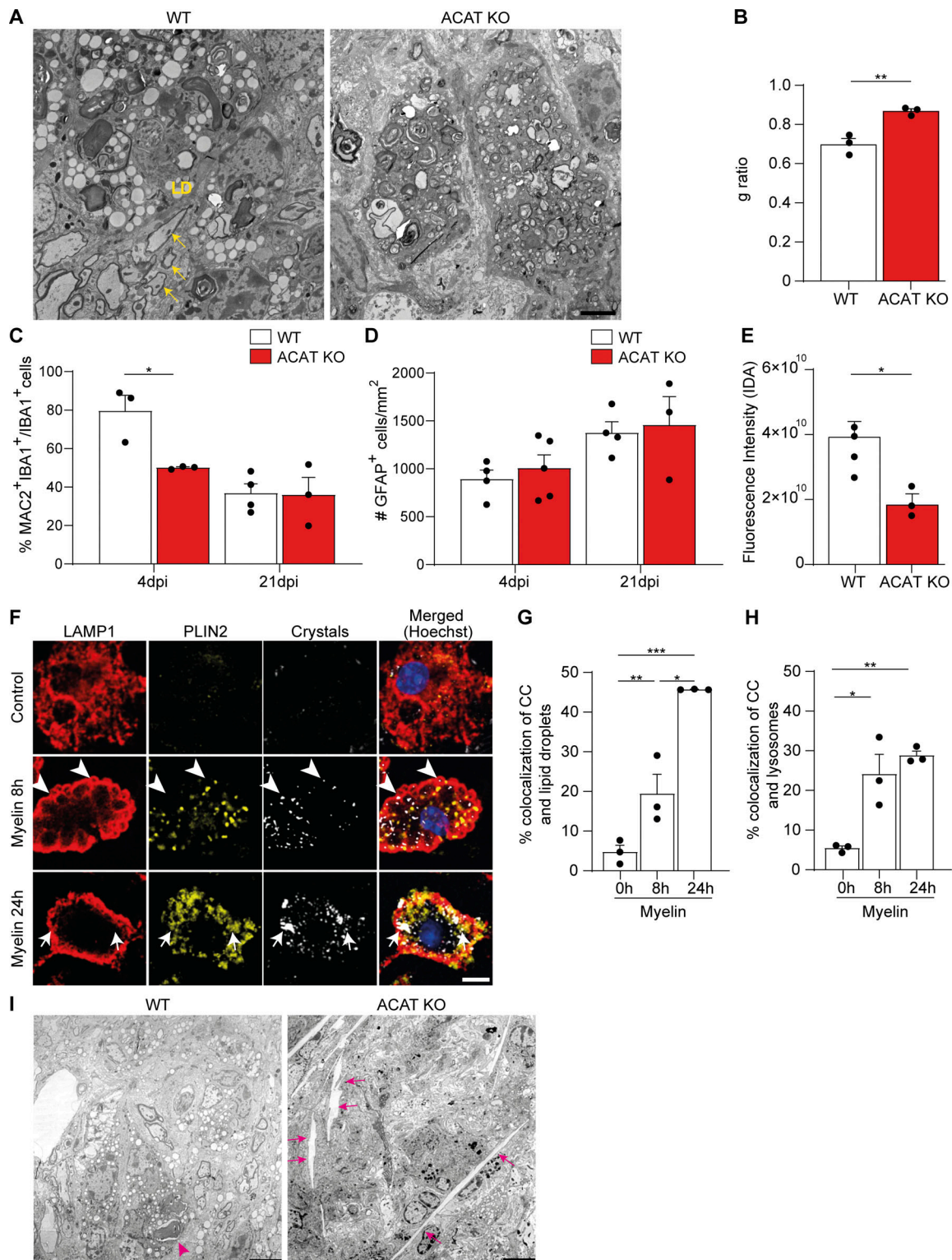


Figure S2. **Defective cholesterol esterification affects remyelination, inflammation, and cholesterol crystal formation.** (A) TEM of 21-dpi lesions of WT and ACAT KO mice showing lipid droplets and remyelinated axons (yellow arrows) in WT but not in KO cells. (B) The g-ratio calculations of 21-dpi lesions of WT and ACAT KO mice. (C and D) Percentage of IBA1⁺ cells, which are also MAC2⁺, and quantification of the density of astrocytes (labeled for GFAP) in 4- and 21-dpi lesions of WT and ACAT KO mice. (E) Quantification of crystal intensity in 21-dpi lesions of WT and ACAT KO mice by confocal reflection microscopy. (F-H) Confocal images of WT microglia and quantification of crystal colocalization with lipid droplets labeled with PLIN2 (yellow) and LAMP1⁺ lysosomes (red). Examples of colocalization with lysosomes and lipid droplets are highlighted by arrowheads and arrows, respectively. (I) Representative TEM pictures of cholesterol crystals in WT and ACAT KO lesions at 21 dpi. WT microglia occasionally showed small crystals (<5 μ m, magenta arrowheads), while large crystals (>15 μ m) were rarely observed in ACAT KO lesions (magenta arrows). The results are representative of three independent experiments. Scale bars, 2 μ m in A, 3 μ m in C, and 5 μ m in I. *, P < 0.05; **, P < 0.01; ***, P < 0.001. CC, cholesterol crystals; IDA, integrated density area.

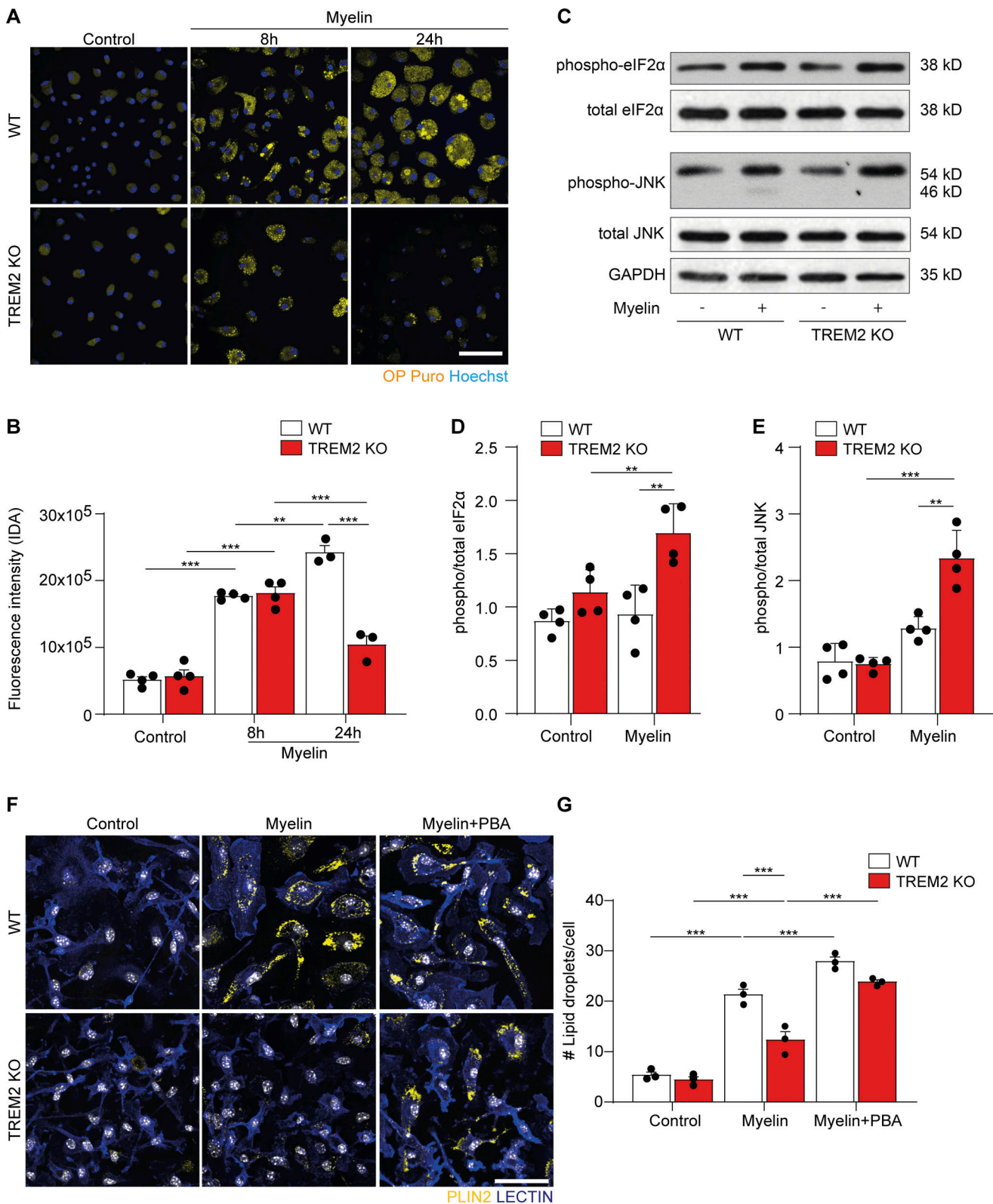


Figure S3. **Myelin phagocytosis causes ER stress in TREM2 KO microglia.** (A) Confocal images of WT and TREM2 KO microglia after treatment with myelin for 8 and 24 h and after incorporation with OP puro (yellow; Hoechst, blue). (B) Quantification of the fluorescence intensity per cell of labeled OP puro. (C-E) Representative Western blot and quantifications of p-eIF2α and total eIF2α, p-JNK and total JNK, and the housekeeping gene GAPDH. (F and G) Representative confocal images and quantification of lipid droplets in WT and TREM2 KO microglia in control conditions and after treatment with myelin for 24 h, with or without 10 μM PBA. Scale bars, 20 μm in A and 25 μm in F. n = 4 biological replicates, where at least 40 cells per condition were measured in each condition. For C, D, and E, n = 4 biological replicates. The results are representative of three independent experiments. Data represent mean ± SEM. P values were calculated using two-way ANOVA (A) with Šidák post hoc correction. **, P < 0.01; ***, P < 0.001. IDA, integrated density area.

PROJECT 2: The “lipodystrophy” brain exhibits enhanced remyelination in a UCP1-independent manner.

The current chapter includes the research article “The “lipodystrophy” brain exhibits enhanced remyelination in a UCP1-independent manner.” To my knowledge, this article is the first study that reports how lipodystrophy as a phenotype affects the regenerative response upon acute CNS injury.

More specifically, in project 2, I investigated how dysregulated peripheral lipid metabolism affects the acute remyelination response. Peripheral lipid metabolism was examined in a murine model of lipodystrophy, where lipid storage in WAT depots is completely abolished. In this model I found that, upon acute CNS demyelination, lesion repair is promoted, and inflammation resolves. Metabolomic analysis indicated amplified levels of BCAAs and several PCs species with polyunsaturated LCFAs in the plasma of lipodystrophic mice. Subsequent proteomic analysis showed BAT metabolic activation via stimulated thermogenesis. However, the activation of thermogenesis via the UCP1-dependent pathway, failed to improve remyelination response. Therefore, I concluded, that, upon demyelinating stimuli, lipodystrophic mice show enhanced remyelination and inflammation resolution, facilitated in a UCP1-independent way.

The author of this thesis is the first author of this article. For details regarding author contributions, please refer to the “Author Contributions” part of this thesis.

The “lipodystrophy” brain exhibits enhanced remyelination in a UCP1-independent manner.

Garyfallia Gouna^{1,2,3}, Agnese Petrera^{4,5}, Cornelia Prehn⁴, Alexander Cecil⁴, Lennart Schlaphoff^{1,2,3}, Julia Scarpa⁴, Michael Witting^{4,6}, Stefanie Hauck^{4,5}, Mikael Simons^{*1,2,3,7,8}

¹Institute of Neuronal Cell Biology, Technical University Munich, 80802 Munich, Germany.

²German Center for Neurodegenerative Diseases (DZNE), 81377 Munich, Germany.

³Graduate School of Systemic Neuroscience (GSN), 82152 Planegg, Germany.

⁴Metabolomics and Proteomics Core, Helmholtz Zentrum München, German Research Center for Environmental Health (GmbH), 85764 Neuherberg, Germany.

⁵German Center for Diabetes Research (DZD), 85764 München-Neuherberg, Germany.

⁶Chair of Analytical Food Chemistry, TUM School of Life Sciences, 85354 Freising-Weihenstephan, Germany.

⁷Munich Cluster of Systems Neurology (SyNergy), 81377 Munich, Germany.

⁸Institute for Stroke and Dementia Research (ISD), 81377 Munich, Germany.

*Correspondence: mikael.simons@dzne.de

Abstract

In inflammatory demyelinating diseases such as multiple sclerosis (MS), the brain initiates an intrinsic response to address acute demyelination challenges, aiming for lesion repair and restoration of normal physiological functions. Nevertheless, this regenerative potential often fails, especially during the chronic phase of the disease. Multiple factors play a pivotal role in shaping the pathophysiology of MS, and recent insights indicate that metabolic disturbances may significantly influence the increased incidence of MS. Specifically, metabolic disorders, including obesity and lipodystrophy, predominantly impact the central node in systemic metabolism, which is adipose tissue. Adipose tissue functions as an endocrine organ and several reports suggest that the dysregulation of adipose tissue metabolism in obesity, directly affects the progression of MS. Whereas there is already an established link between obesity and the progression of MS, the specific impact of lipodystrophy on the regenerative capacities of the central nervous system (CNS) remains poorly defined. Here, we examined the “lipodystrophy” brain under basal conditions, during dietary intervention, and in acute demyelinating challenge. To our knowledge, this is the first study to explore how lipodystrophy affects CNS response to diverse stimuli. We found that lipodystrophic mice exhibited enhanced lesion recovery and resolution of inflammation, after acute demyelinating injury. Metabolomic analysis revealed that a combination of metabolites can potentially contribute to improved lesion repair. Among them, branched-chain amino acids (BCAAs) levels and several phosphatidylcholine (PCs) species with polyunsaturated long-chain fatty acids (LCFAs) were increased in the plasma of lipodystrophic mice. Subsequent proteomic analysis suggested a potential metabolic stimulation of brown

adipose tissue (BAT) via increased thermogenesis. However, upon simultaneous demyelinating injury and activation of UCP1-dependent thermogenesis, wild-type lean and obese mice failed to improve lesion recovery. Therefore, we conclude that, in demyelinating injury, lipodystrophy amplifies the regeneration response in a UCP1-independent manner.

Introduction

Adipose tissue, a multifaceted organ that includes adipocytes, immune cells and endothelial cells, is pivotal at the core of metabolic health. Adipose tissue encompasses all three subtypes; white adipose tissue (WAT), brown adipose tissue (BAT), and beige adipose tissue (BeAT), which all contribute to the regulation of systemic metabolism. Beyond its fundamental capacity as an energy repository and thermal insulation depot, it plays a main role in releasing hormones and metabolites, regulating inflammatory responses and actively participating in heat generation via fatty acid oxidation¹. Adipose tissue is the primarily affected organ in obesity and lipodystrophy diseases. Both diseases show inadequate lipid storage within adipose tissue, either by exhaustion of adipocyte storage capacity in obesity or limited storage capacity from absent or dysfunctional adipocytes in lipodystrophy. As an effect, peripheral organs such as the liver and pancreas, are affected by ectopic lipid accumulation, which is also prominent in peripheral blood flow. While both diseases primarily disturb WAT function, BAT is also compromised, as ectopically accumulates lipid deposition and exhibits reduced fatty acid oxidation². Adipose tissue participates in several metabolic axes in health and disease, such as the adipose tissue-brain axis³.

The interplay between the brain and discrete adipose tissue depots maintains organism homeostasis under metabolic challenges, such as starvation or cold exposure. These external stimuli trigger sympathetic nervous system (SNS) neurons to connect with the different adipose depots, regulating lipolysis in WAT and non-shivering thermogenesis in BAT. In turn, adipose tissue depots communicate to the brain via the sensory afferent pathway and the secretion of several compounds, highly affected in diseases as obesity and lipodystrophy^{1,3,4}. An accumulating body of literature describes the “obese” brain with reduced cognitive functions and grey matter volume and increased neuroinflammation, due to low-grade peripheral inflammation and circulating hormones and metabolites^{5,6}. It has been suggested that the lipid composition of the brain, especially regarding cholesterol metabolism, is independent of the periphery due to the blood-brain barrier (BBB)^{7,8}. However, recent work from our lab and others supported that, the treatment with high-fat and western

diet changes the brain lipid profile of wild-type (Wt) obese mice, in both white and grey matter^{9,10}. Therefore, peripheral lipid metabolism shapes brain lipid signature, influencing factors such as lipid species, the saturation levels of lipids, and the length of lipid acyl chains⁹. All evidence underscores obesity as a risk factor for the deterioration of brain function. Obesity has also been associated with numerous central nervous system (CNS) demyelinating pathologies, such as multiple sclerosis (MS), emphasizing the contribution of a peripheral inflammatory microenvironment in demyelinating lesions¹¹.

Demyelinating lesions are characterized by impaired immune response, increased local inflammation and disrupted myelin integrity^{12,13}. Myelin debris is phagocytosed by microglia, the brain resident immune cells, facilitating the regenerative response and leading to resolution of inflammation. We have previously described that microglial cholesterol esterification in the form of lipid droplets (LD) is necessary for the remyelination process. This highlights the importance of localized lipid metabolism in demyelinating lesions¹⁴. Remarkably, obese mice under western diet (WSD) treatment showed impaired lesion recovery following demyelination, providing additional confirmation of the distinctive characteristics observed in the “obese” brain^{5,9}. While the “obese” brain has been extensively investigated, very little is known about the “lipodystrophy” brain and its impact in basal conditions and on the remyelination response. Here, we addressed this gap in knowledge by using a murine model of congenital generalized lipodystrophy (CGL), under different diet treatments. We aimed to identify how the depletion of peripheral lipid storage affect brain response in basal conditions and upon CNS demyelinating injury. We hypothesized that adipose tissue impaired functions will alter remyelination response, implying that peripheral lipid metabolism contributes to the regenerative process upon demyelinating stimuli.

Results and discussion

Brain phenotype of transgenic aP2-Srebf1c mice under diet treatment in basal conditions

To investigate how the brain responds to the depletion of peripheral lipid storage, we utilized a mouse model that mimics CGL, the aP2-Srebf1c mice. These mice overexpress the human nuclear sterol regulatory element binding protein-1c (SREBP1c), specifically in adipocytes (from now on aP2-Srebf1c mice). Mice carrying the transgene develop fatty liver, enlarged BAT resembling immature WAT phenotype, and noticeably reduced WAT depots (Fig. S1, A and B), as previously characterized¹⁵. Interestingly, the application of hematoxylin and eosin (H&E) staining to BAT from aP2-Srebf1c animals revealed a structure more reminiscent of BeAT, characterized by multi-ocular brown fat-like cells, rather than the typical unilocular

white fat adipocytes (Fig. S1B)¹⁶. Serum analysis revealed that alanine aminotransferase and alkaline phosphatase levels were elevated in the aP2-Srebf1c mice, pointing on liver defects (Fig. S1, C and D). We hypothesized that diet will exacerbate inflammation in the peripheral organs and bloodstream, and this can lead to more prominent effects at the central nervous system (CNS). Thus, we treated both wild-type (Wt) and aP2-Srebf1c transgenic animals with western (WSD) and control diet (CD) and assessed glial cell response in grey and white matter brain regions. At corpus callosum, microglia area coverage (IBA1) was increased in aP2-Srebf1c WSD cohort compared to Wt animals in both diets (Fig. 1, A and B). Reactive astrocytes (GFAP) levels remained unchanged (Fig. 1 A and C) in all cohorts. Previous literature indicates that galectin-3 (MAC2) influences oligodendrocyte progenitor cells (OPC) differentiation and oligodendrocyte maturation¹⁷. In all cohorts, while MAC2 positive cells were mostly colocalized with reactive astrocytes (Fig.1A), their levels remained unaffected across cohorts (Fig. 1, A and D). Oligodendrocytes expressing CAII and CC1 differentiation markers showed no significant differences between cohorts (Fig. 1, F-I). However, a decreased tendency of oligodendrocyte numbers was observed in aP2-Srebf1c WSD cohort (Fig. 1, F and G). At motor cortex, microglia area coverage was increased in aP2-Srebf1c WSD cohort (Fig. S2, A and B), whereas oligodendrocyte maturation remained unaffected (Fig. S2, C-F).

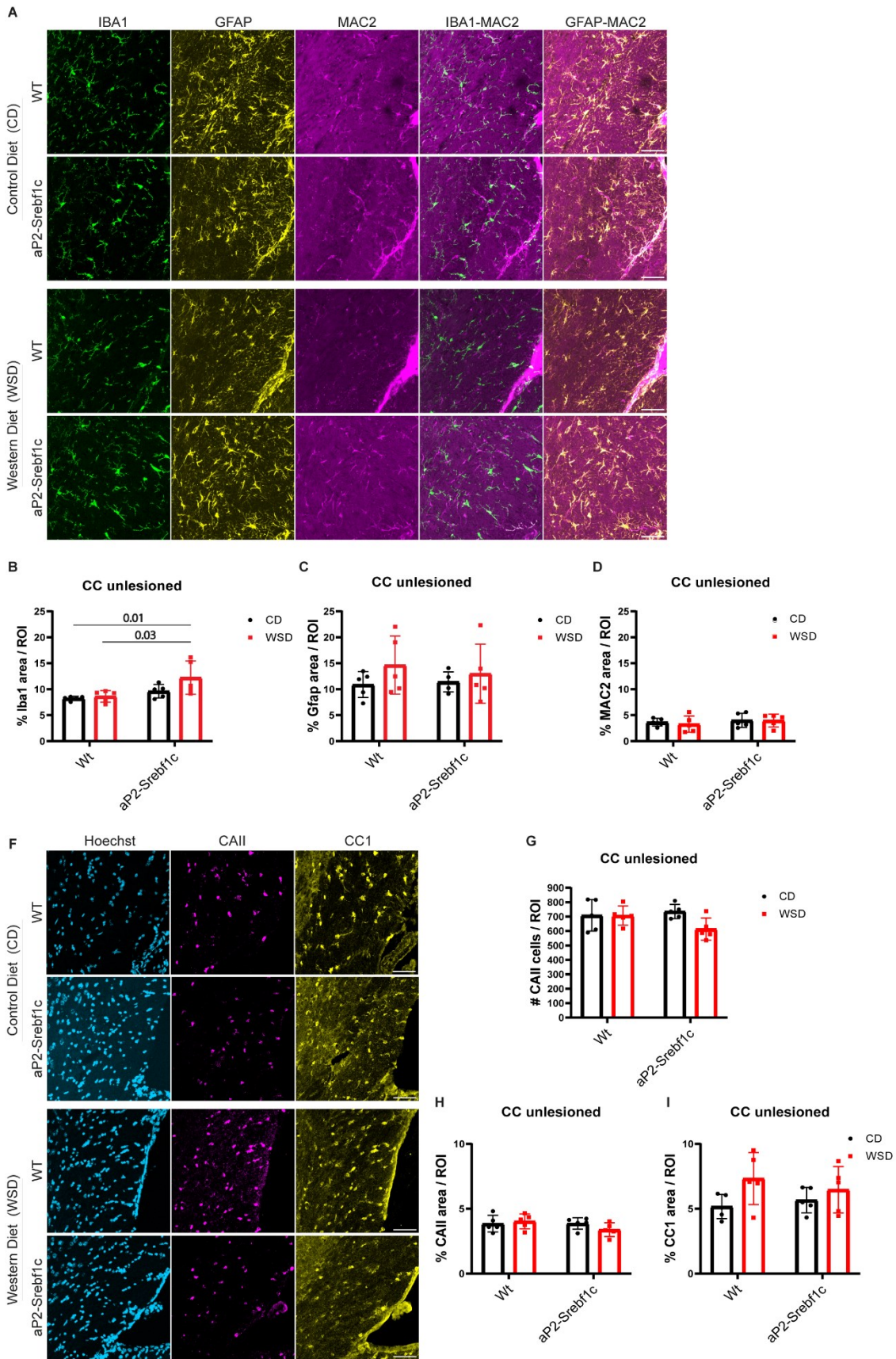


Figure 1 Characterization of aP2-Srebf1c mice in basal conditions: glial cells response in unlesioned corpus callosum. (A) Representative confocal images of unlesioned corpus callosum (CC) from WT and aP2-Srebf1c under Control (CD) and Western (WSD) diets. Tissue is stained for IBA1 (green), GFAP (yellow) and MAC2 (magenta), with subsequent panels show respective colocalizations. Scale bar, 50 μ m. (B-D) Quantification of the percentages of IBA1 positive area (B), GFAP positive area (C) and MAC2 positive area (D) in regions of interest (ROI) in corpus callosum. (F) Representative confocal images of unlesioned CC from WT and aP2-Srebf1c under CD and WSD diets. Tissue is stained for CAII (magenta) and CC1 (yellow). Scale bar, 50 μ m. (G-I) Quantification of the number of the CAII cells (G) and the percentages of CAII positive area (H) and CC1 positive area (I) in ROI in corpus callosum. Data represent mean \pm SD, P-values were calculated using two-way ANOVA with Tukey post-hoc correction. P < 0.05 are numerically depicted in the graph. In the graphs, each dot represent animal (n=5).

Prior research suggests that WSD changes brains lipidome profile, with accumulating lipid droplets (LD) in corpus callosum glial cells and the ventricle wall⁹. To determine how glial cells alter their lipid storage capacity, we assessed LD coverage using perilipin 2 (PLIN2) protein marker. We detected an increased tendency of both microglia and astrocyte percentages colocalizing with PLIN2 in Wt and aP2-Srebf1c WSD animals at corpus callosum. Interestingly, astrocytes tend to contain more PLIN2⁺ LD compared to microglia (Fig. 2, A-C). At the same time, the percentage of PLIN2 area coverage at corpus callosum showed marked increased tendency in Wt and aP2-Srebf1c WSD animals (Fig. 2, A and D). At the ventricle wall, we observed no significant differences in the percentage of PLIN2 area across all cohorts. Together, these results imply that the synergistic effect of both WSD and lipodystrophy phenotype contributes to microglia activation and a potentially altered oligodendrocyte maturation. In addition, glial cells exhibit increased lipid storage capacity, particularly noticeable in astrocytes.

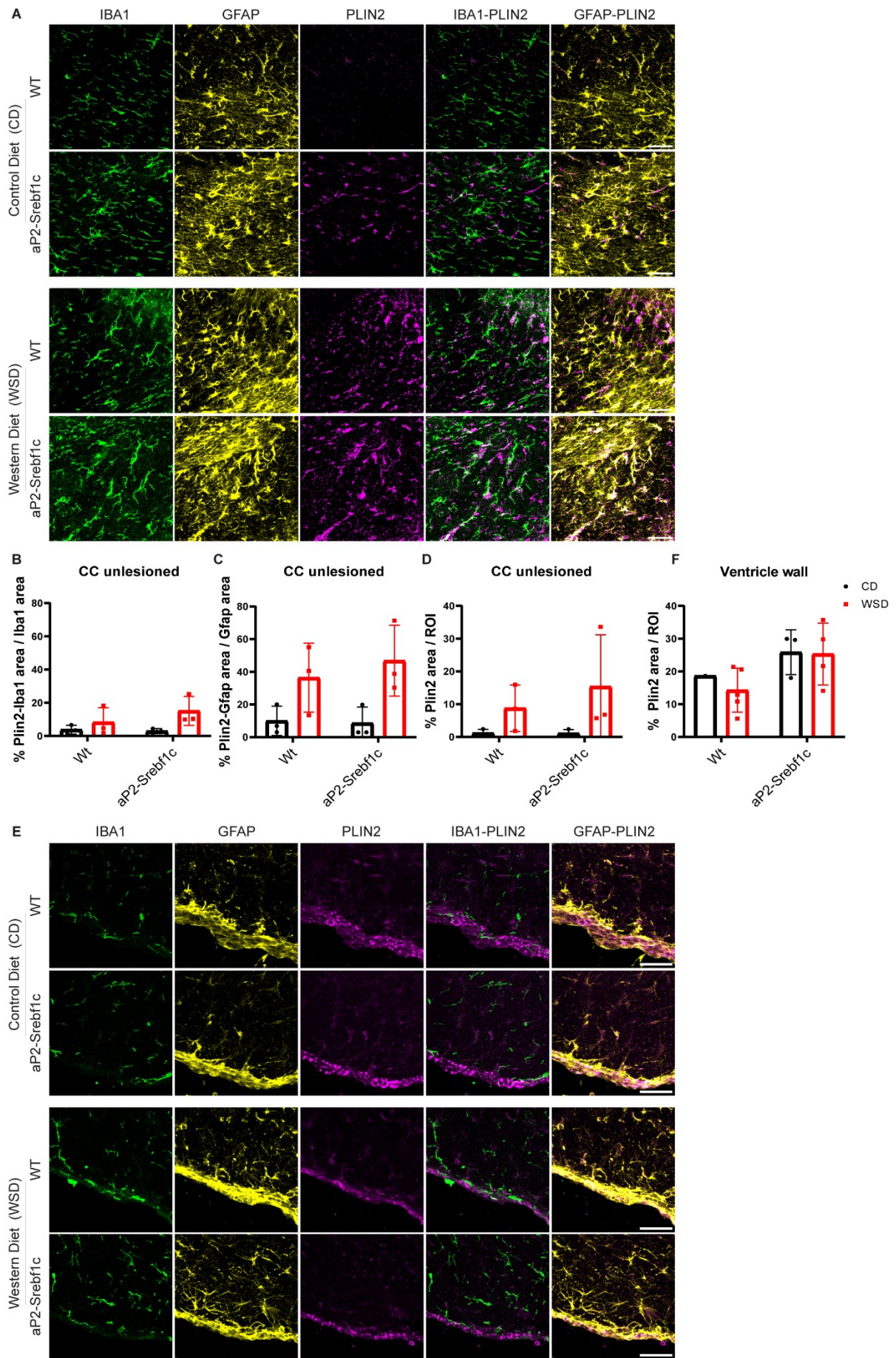


Figure 2 Characterization of aP2-Srebf1c mice in basal conditions: glial cells accumulate lipid droplets (LD) in unlesioned corpus callosum and ventricle wall. (A) Confocal images of unlesioned corpus callosum (CC) from WT and aP2-Srebf1c under CD and WSD. Tissue is stained for IBA1 (green), GFAP (yellow) and PLIN2 (magenta), with subsequent panels show respective colocalizations. Scale bar, 50 μ m. (B-D) Quantification graphs of the percentages of PLIN2-IBA1 double positive area over the total IBA1 positive area (B), PLIN2-GFAP double positive area over the total GFAP positive area (C) and PLIN2 positive area over ROI (D) in corpus callosum. (E) Confocal images of the ventricle wall from WT and aP2-Srebf1c (CD and WSD), after staining for IBA1 (green), GFAP (yellow) and PLIN2 (magenta), with additional colocalization panels. Scale bar, 50 μ m. (F) Quantification of the percentage of PLIN2 positive area over ROI in ventricle wall. Data represent mean \pm SD, P-values were calculated using two-way ANOVA with Tukey post-hoc correction. P > 0.05 are not depicted in the graphs. In the graphs, except for (F), each dot represent animal (n=3-5). In graph (F) n=1-5.

aP2-Srebf1c mice exhibit enhanced remyelination capacity in acute demyelination

To determine whether the altered glial response affects remyelination in aP2-Srebf1c mice, we employed a toxin-induced acute demyelination model. In this model, focal injection of lysolecithin (LLC) initiates demyelination at white matter of corpus callosum or spinal cord within 4 days post-injection (dpi), followed by lesion recovery between 14 and 21 dpi. Microglia orchestrates lesion recovery as they rapidly phagocytose myelin debris in the lesions¹⁸, where there is only a minor influx of monocyte-derived macrophages from the peripheral blood^{19,20}. Using the myelin dye FluoroMyelin (FM) and antibody against IBA1, we assessed lesion recovery and microglia response at 14dpi. aP2-Srebf1c animals fed with CD showed a tendency of smaller lesions, though not significant (Fig. 3, A and B), while the lesion volume occupied by IBA1 positive microglia remained unchanged (Fig. 3, A and C). On the contrary, analysis of aP2-Srebf1c animals fed with WSD revealed significantly smaller lesions (Fig. 3, A and D), supported by smaller volume occupied by IBA1 positive microglia (Fig. 3, A and E). Mature oligodendrocyte (CC1) numbers remained stable in lesions of CD-fed animals (Fig. 3, F,G and I), while they demonstrated increased tendency in lesions of aP2-Srebf1c WSD-fed animals (Fig. 3, F,H and J). Quantification of the all-lineage oligodendrocyte marker, Olig2, showed no substantial difference between cohorts, pointing to unaltered oligodendrocyte capacities (Fig. 3, K and L). These data indicate that aP2-Srebf1c mice exhibit enhanced lesion repair and inflammation resolution, a noteworthy effect observed under WSD treatment conditions.

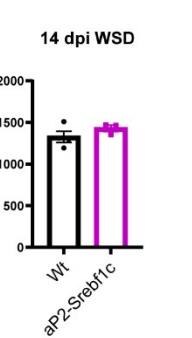
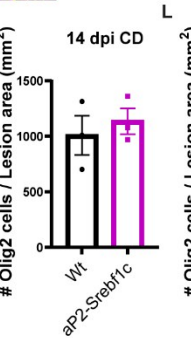
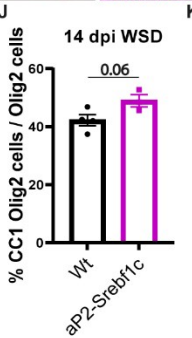
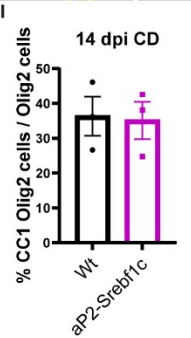
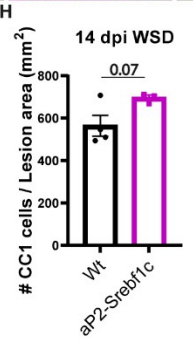
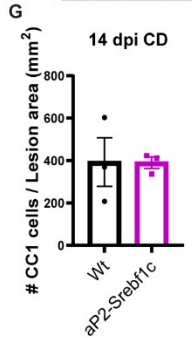
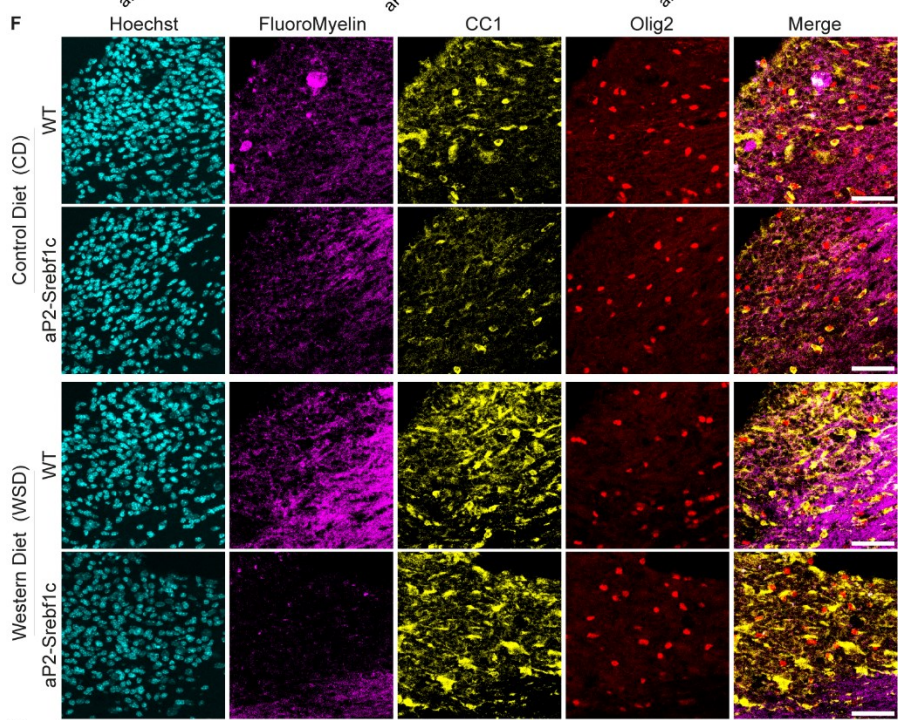
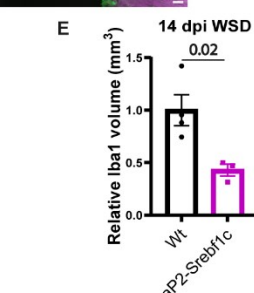
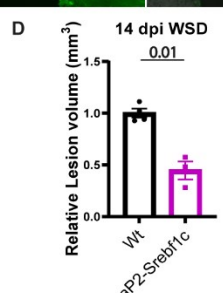
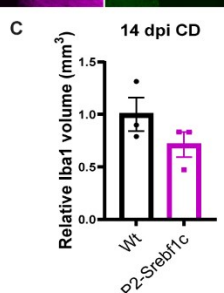
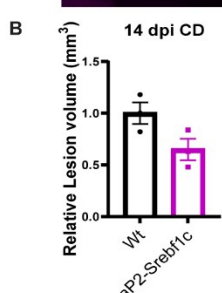
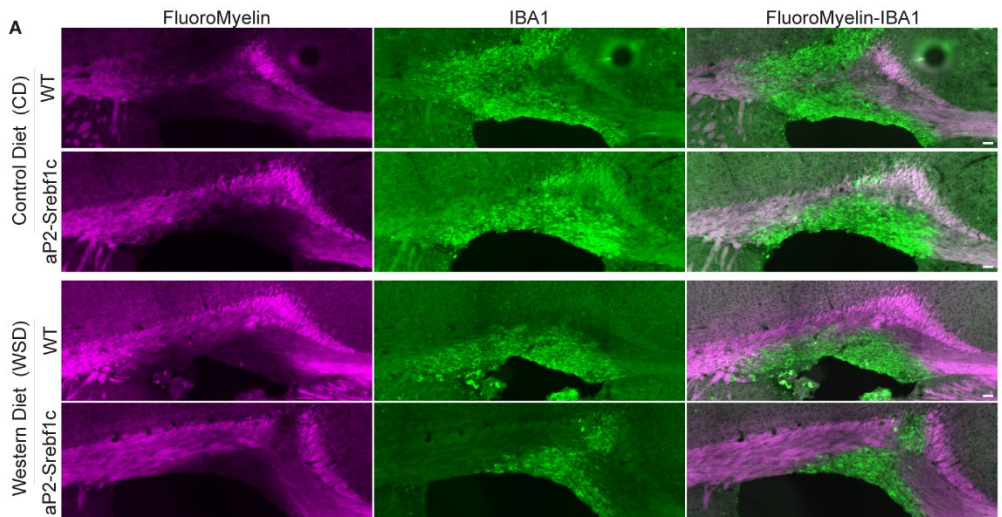


Figure 3 Characterization of aP2-Srebf1c mice in acute demyelination: remyelination is enhanced in transgenic animals under WSD treatment. (A) Confocal images of corpus callosum lesions in 14dpi from WT and aP2-Srebf1c, treated with CD and WSD. Tissue is stained for FluoroMyelin (magenta) and IBA1 (green). Scale bar, 50 μ m. (B-E) Graphs showing relative quantification of lesion volume (B) and IBA1 (C) of 14dpi lesions from CD treated animals and lesion volume (D) and IBA1 (E) of 14dpi lesions from WSD treated animals. (F) Confocal images of corpus callosum lesions in 14dpi from WT and aP2-Srebf1c (CD and WSD). Tissue is stained for Hoechst (cyan), FluoroMyelin (magenta), CC1 (yellow) and Olig2 (red). Scale bar, 50 μ m. (G-L) Quantification of 14dpi corpus callosum lesions between WT and aP2-Srebf1c animals, representing the CC1 positive cell numbers under CD (G) and WSD (H) over the lesion area, the percentages of CC1-Olig2 double positive cells over the total Olig2 positive cell number under CD (I) and WSD (J) and the Olig2 positive cell numbers under CD (K) and WSD (L) over the lesion area. Data represent mean \pm SD, P-values were calculated using two-tailed unpaired t test with Welch's correction. $P \leq 0.07$ are depicted in the graphs. In the graphs, each dot represent animal (n=3-4).

Metabolomic signature of aP2-Srebf1c mice reveals distinctive genotype and diet dependent differences and highlights brown adipose tissue (BAT) metabolism

Glial response of aP2-Srebf1c mice in basal and demyelinating conditions suggested that peripheral signaling can contribute to enhanced remyelination. Thus, we performed targeted metabolomic analysis from plasma from all cohorts, using the Biocrates Absolute/IDQ[®] p180 kit, to identify interesting candidates. We used an additional extra cohort of chow-fed Wt and aP2-Srebf1c mice, to cover all aspects of control diets and their composition, including fiber-content^{21,22}. Absolute/IDQ[®] p180 kit provides quantitative information for metabolites categorized as biogenic amines and amino acids, whereas semi-quantitative information for acylcarnitines, glycerophospholipids, sphingolipids and sugars. More specifically, our analysis included the examination of various sphingomyelin (SM) species from the sphingolipids group and several phosphatidylcholine (PCs) species from the glycerophospholipids group. PCs consist of a glycerol backbone linked to a phosphate-containing headgroup and two fatty acid chains. SM however belong to a group of amphipathic lipids sharing a sphingoid base backbone, which is N-acylated and have only one fatty acid chain attached. Fatty acids, depending on the number of double bonds they form within their carbon atoms, are characterized as saturated (no double bonds) or unsaturated (one or more double bonds)^{23,24}. All metabolites included in the Absolute/IDQ p180 kit have been selected due to their established relevance in metabolic disorders, according to current literature.

Principle component analysis (PCA) showed distinct clustering of all six experimental groups (Fig. 4A). Out of the 188 metabolites examined, 161 metabolites were successfully retained following quality control and normalization steps, with 18 of these demonstrating statistically significant differences (Fig. 4B and Table1). Sphingomyelin species SM C18:0 and SM C18:1 showed significant increase in aP2-Srebf1c under WSD treatment, with SM C18:1 showing the same effect under CD treatment as well (Fig. 4, C and D). Previous literature describes that both species

are increased in the human plasma of patients with diabetes²⁵, validating the aP2-Srebf1c diabetic phenotype. Glycerophospholipid PC ae C42:0, which contains saturated fatty attached moieties, depicted a notable rise in aP2-Srebf1c animals, treated with chow or WSD (Fig. 4E). The annotation “ae” refers to the attached fatty acid moieties and indicates that one of the of moieties is a fatty alcohol which bounds to the glycerol backbone with an ether bond. Metabolomic analysis in previous studies associated PC ae C42:0 with atherosclerosis and heart failure with preserved ejection fraction^{26,27}. Additionally, PCs containing polyunsaturated long-chain fatty acids (LCFAs) were also increased under chow and CD treatment (Fig. S3, A-C), proposing that diet and genotype synergistically affect the saturation levels of the PCs attached fatty moieties. Among the biogenic amines group, we observed elevated levels of key diabetic marker acetylornithine (Ac.Orn) (Fig. 4F)²⁸, while among the acylcarnitines group, hydroxybutyrylcarnitine (C3.DC..C4.OH.) and octadecenoylcarnitine (C18:1) depicted increased levels in aP2-Srebf1c, WSD treated (Fig. 4, G and H). Higher levels of hydroxybutyrylcarnitine indicate ketosis but also a diabetic phenotype^{29,30}, whereas higher C18:1 levels were observed in diet induced obese rats³¹. This identified long chain acylcarnitine (C18:1) can carry oleic acid, a monounsaturated (i.e. one double bond) LCFA, which has been shown to restore the immunosuppressive effects of T-regulatory cells in MS patients, while it also exhibits antioxidant properties in a MS rat model^{32,33}. Nonetheless, our targeted metabolomic analysis does not definitively confirm that octadecenoylcarnitine exclusively transports oleic acid; instead, it pertains to fatty acids characterized by 18 carbon atoms and a single double bond. All together, these data designate a diabetic plasma profile, partially influenced by diet treatment, with a possible anti-inflammatory immune response due to one acylcarnitine species.

Next, we sought to investigate if our defined significant metabolites represent common metabolic pathways. Pathway enrichment analysis using MetaboAnalyst 5.0 software (<https://www.metaboanalyst.ca/MetaboAnalyst/>) highlighted several metabolic pathways (Fig. 4I). Of higher significance and pathway impact, branched-chain amino acids (BCAAs) biosynthesis and degradation were emphasized, confirming our results in individual significant metabolites. BCAAs cluster includes aminoacids leucine, isoleucine and valine (Leu, Ile and Val), which share a similar chemical structure, and are essential substrates of glutamate biosynthesis^{34,35}. Our pathway enrichment analysis also identified phenylalanine (Phe) metabolism-biosynthesis pathways, aminoacyl-tRNA biosynthesis pathway (Val, Leu, Ile and Phe hits), and sphingolipid/glycerophospholipid metabolism pathways, aligning with the previous findings. Interestingly, arachidonic, linoleic and alpha-linolenic acid metabolism pathways were enriched, emphasizing significant regulated glycerophospholipids PC aa C40:5, PC aa C42:4, PC aa C42:5 and PC aa C42:6 in our metabolomic analysis (Fig. 4B). These glycerophospholipids, containing LCFAs, showed significant increase in aP2-Srebf1c animals, under chow treatment, although an increased trend under CD and WSD treatments (Fig. S3, D-F). The annotation

“aa” denotes the attached fatty acid moieties and indicates that both fatty acids bound to the glycerol backbone with ester bonds. All glycerophospholipids above have been identified under the context of obesity and metabolic syndrome^{36,37}. Of note, due to fatty acid remodeling, alpha-linolenic acid induces thermogenic activation of BAT³⁸, while linoleic acid supplementation promotes the biogenesis of beige fat³⁹. Taking a holistic approach, we calculated the sums and ratios of specific metabolite concentrations in the context of metabolic syndrome. This approach reduces both biological and analytical variability and enhances the specificity of the results. BCAA sum showed substantial increase in aP2-Srebf1c animals, treated with chow and CD, and a significant increased trend in aP2-Srebf1c treated with WSD (Fig. 4J). BCAAs degradation in skeletal muscle and uptake from peripheral tissues is inhibited in conditions such as obesity and type 2 diabetes³⁴, although BCAAs supplementation is linked with positive impacts on energy consumption and exhibit anti-obesity effects in rodents⁴⁰. Nevertheless, it was recently reported that BAT induces BCAAs systemic clearance, as they are utilized in BAT mitochondria for thermogenesis⁴¹. Interestingly, a recent study showed that BCAAs levels were decreased in the plasma of relapsing-remitting MS patients, highlighting the association between plasma glutamate concentration and the severity of MS^{35,42}. In fact, in our metabolomic analysis, glutamate levels in the plasma of all cohorts remain unchanged (data not shown). Moreover, under WSD, the ratio of long chain acylcarnitines to free carnitine (CPT-I ratio) was markedly elevated in aP2-Srebf1c animals, revealing an altered activity of carnitine palmitoyltransferase I (CPT-I) (Fig. 4K). CPT-I plays a major role in the process of fatty acid oxidation, mediating the transfer of LCFAs into the mitochondria, where they are used to produce energy. Increased levels of CPT-I ratio have been described in diabetic rats⁴³, further confirming the aP2-Srebf1c diabetic phenotype. Collectively, our plasma metabolomic analysis portrays a metabolic signature, featuring metabolites associated with diabetes, obesity and fatty acid metabolism, while emphasizing the active involvement of BAT metabolism.

Table 1 Significant enriched metabolites in plasma of aP2-Srebf1c animals, under diverse dietary stimuli. Metabolites were identified in targeted metabolomic analysis (see text and Materials and Methods). HMDB: Human Metabolome Database, KEGG: Kyoto Encyclopedia of Genes and Genomes * Concentrations are isotope corrected

Metabolite	Commonly used names	Attached HMDB_ID	Chemical Formula	Attached KEGG_ID
Val	L-Valine	HMDB00883	C5H11NO2	C00183
	L-Valine	HMDB00883	C5H11NO2	C00183
Leu	L-Leucine	HMDB00687	C6H13NO2	C00123
	beta-Leucine	HMDB03640	C6H13NO2	C02486
	D-beta-Leucine	HMDB03640	C6H13NO2	C02486
	L-beta-Leucine	HMDB03640	C6H13NO2	C02486
	D-Leucine	HMDB13773	C6H13NO2	C01570
	L-Leucine	HMDB00687	C6H13NO2	C00123
	D-beta-Leucine	HMDB03640	C6H13NO2	C02486
Phe	L-Phenylalanine	HMDB00159	C9H11NO2	C00079
	L-Phenylalanine	HMDB00159	C9H11NO2	C00079
Ile	L-Isoleucine	HMDB00172	C6H13NO2	C00407
	L-Isoleucine	HMDB00172	C6H13NO2	C00407
	Allo-L-Isoleucine	HMDB00557	C6H13NO2	
C3.DC..C4.OH. *	Malonylcarnitine	HMDB02095	C10H17NO6	
	Hydroxybutyrylcarnitine	HMDB13127	C11H21NO5	
	Malonyl-D-carnitine	HMDB02095	C10H17NO6	
	Malonyl-L-carnitine	HMDB02095	C10H17NO6	
	Hydroxybutyrylcarnitine	HMDB13127	C11H21NO5	
C18.1*	Oleoylcarnitine	HMDB05065	C25H47NO4	
	Elaidic carnitine	HMDB06464	C25H47NO4	
	Elaidic carnitine	HMDB06464	C25H47NO4	
	Oleoylcarnitine	HMDB06464	C25H47NO4	
Ac.Orn	Acetylornithine	HMDB03357	C7H14N2O3	C00437
PC.aa.C40.5*	PC(18:0/22:5(4Z,7Z,10Z,13Z,16Z))	HMDB08055	C48H86NO8P	C00157
	PC(18:0/22:5(7Z,10Z,13Z,16Z,19Z))	HMDB08056	C48H86NO8P	C00157
	PC(18:1(9Z)/22:4(7Z,10Z,13Z,16Z))	HMDB08120	C48H86NO8P	C00157
	PC(18:0/22:5(4Z,7Z,10Z,13Z,16Z))	HMDB08055	C48H86NO8P	C00157
	PC(18:0/22:5(7Z,10Z,13Z,16Z,19Z))	HMDB08056	C48H86NO8P	C00157
	PC(18:1(9Z)/22:4(7Z,10Z,13Z,16Z))	HMDB08120	C48H86NO8P	C00157
PC.aa.C42.4*	PC aa C42:4	HMDB08572	C50H92NO8P	
PC.aa.C42.5*	PC(20:0/22:5(7Z,10Z,13Z,16Z,19Z))	HMDB08287	C50H90NO8P	C00157
	PC(20:0/22:5(7Z,10Z,13Z,16Z,19Z))	HMDB08287	C50H90NO8P	C00157
PC.aa.C42.6*	PC(20:0/22:6(4Z,7Z,10Z,13Z,16Z,19Z))	HMDB08288	C50H88NO8P	C00157
	PC(20:0/22:6(4Z,7Z,10Z,13Z,16Z,19Z))	HMDB08288	C50H88NO8P	C00157
PC.aa.C36.4*	PC ae C36:4	HMDB13435	C44H82NO7P	
PC.aa.C38.5*	PC(o-18:1(9Z)/20:4(8Z,11Z,14Z,17Z))	HMDB13432	C46H84NO7P	
	PC(o-18:1(9Z)/20:4(8Z,11Z,14Z,17Z))	HMDB13432	C46H84NO7P	
PC.aa.C42.0*	PC(o-20:0/22:0)	HMDB13443	C50H102NO7P	
	PC(o-20:0/22:0)	HMDB13443	C50H102NO7P	
PC.aa.C44:3*	PC ae C44:3	HMDB13449	C52H100NO7P	
SM.C18.0*	SM C18:0	HMDB01348	C41H84N2O6P	
SM.C18.1*	C18:1;11Z-enoyl Sphingomyelin	HMDB12100	C41H81N2O6P	C00550
	C18:1;9Z-enoyl Sphingomyelin	HMDB12101	C41H81N2O6P	C00550
SM.C26.0*	SM C26:0	HMDB11698	C49H100N2O6P	

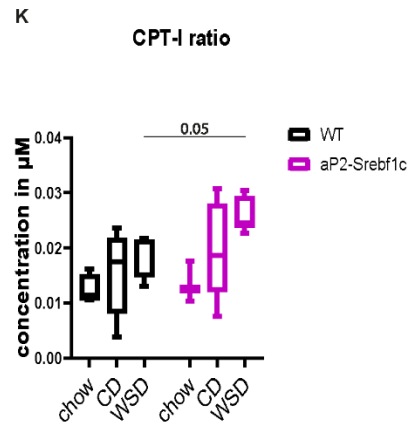
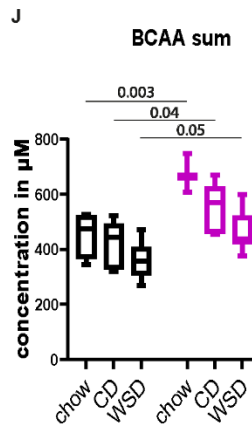
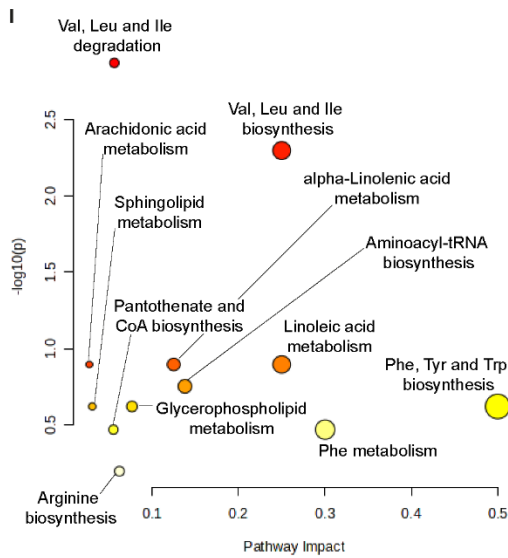
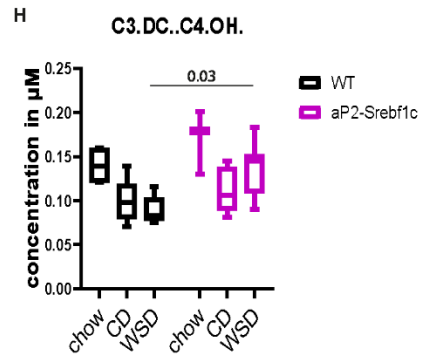
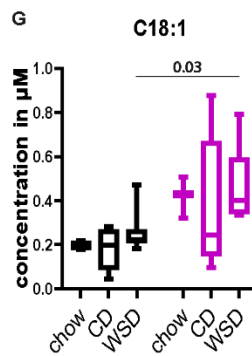
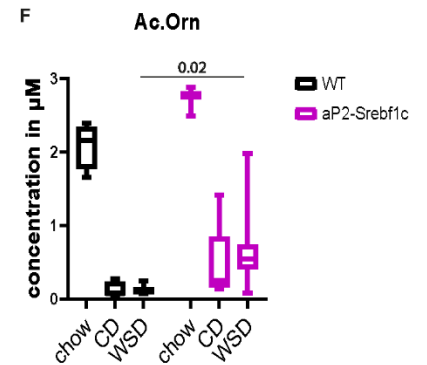
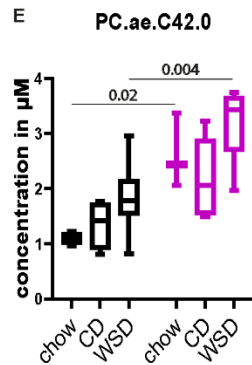
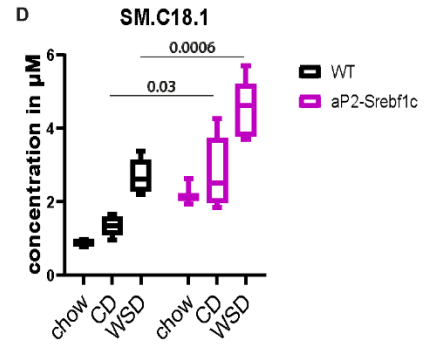
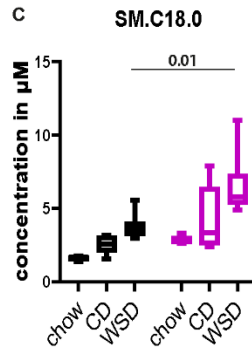
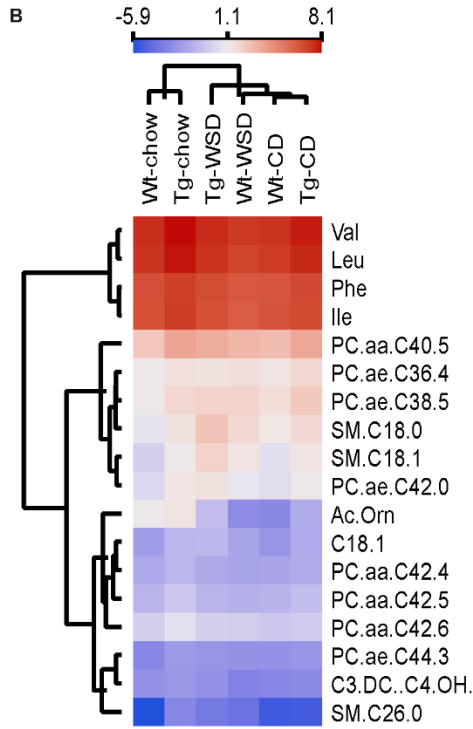
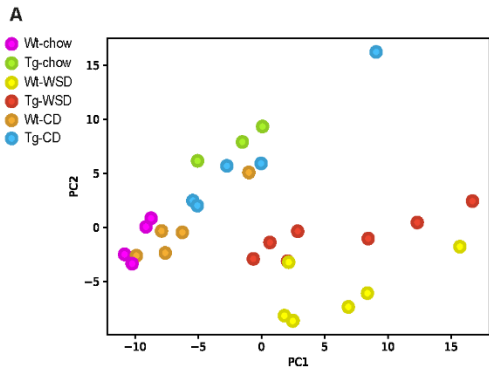


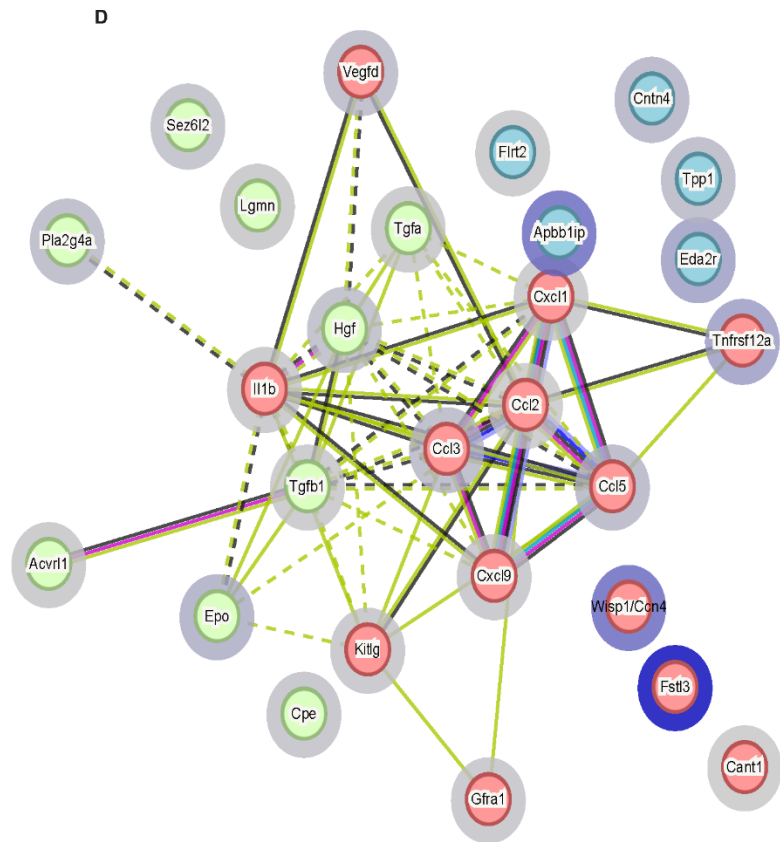
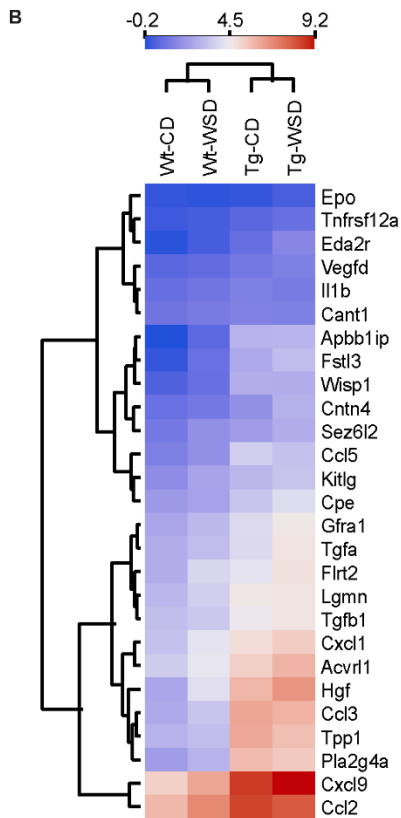
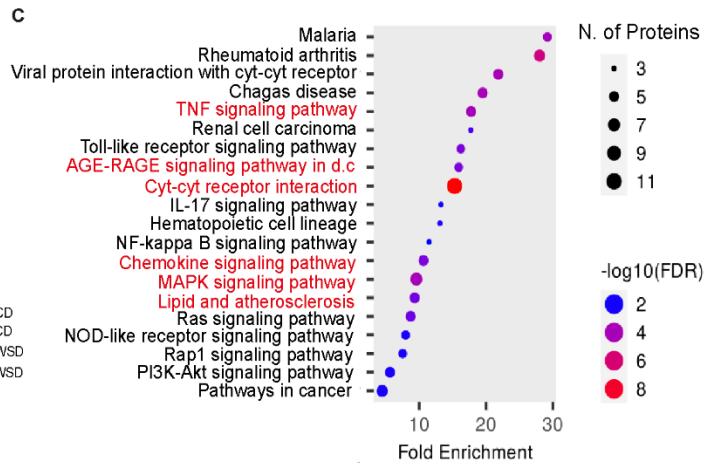
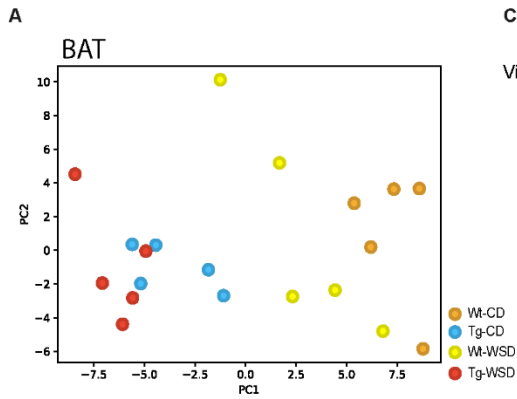
Figure 4 Metabolomic signature of aP2-Srebf1c mice reveals distinctive genotype and diet dependent differences and highlights BAT metabolism. Six groups participated in the metabolomic analysis: regarding the genotype Wild-type (Wt) of aP2-Srebf1c (Tg) and regarding the diet, chow, control diet (CD) and Western diet (WSD). **(A)** Principal component analysis (PCA) of biological replicates for each group, shows clustering among the different groups. The concentration (absolute/relative) values (μM) of all metabolites that pass the quality control test were used as input data. **(B)** Heatmap showing the statistically significant ($P \leq 0.05$, fold ≥ 1.3) metabolites among each group. The mean Log2 concentration (absolute/relative) values (μM) of all significant metabolites were used as input data. **(C-H)** Quantification graphs of selected significant metabolites, further analyzed in the main text. **(I)** Pathway enrichment analysis, using MetaboAnalyst 5.0 software (<https://www.metaboanalyst.ca/MetaboAnalyst/>) showing significant enriched pathways. As input data, all the metabolites depicted at (B) were used. **(J-K)** Significant enriched sum and ratios, derived from the complete analysis of our targeted metabolomic data (explained in details in text and Materials and Methods). Data represent mean \pm SD, P-values were calculated using multivariate analysis with two-way ANOVA followed by Tukey post-hoc correction (normally distributed metabolites) or with Kruskal–Wallis test followed by Wilcoxon post-hoc correction (non-normally distributed metabolites). $P \leq 0.05$ are depicted in the graphs. For this analysis $n=3-7$ animals were used for each group.

Proteomic signature of brown adipose tissue (BAT) in aP2-Srebf1c mice reveal diet independent inflammatory profile

Our plasma metabolomic analysis pinpointed the potential contribution of BAT in the remyelination and glial response of aP2-Srebf1c model, albeit the described WAT-like phenotype¹⁵. Therefore, we addressed BAT role, from Wt and aP2-Srebf1c animals under CD and WSD treatment, by performing targeted proteomic analysis, using OLINK® TARGET 96 Mouse Exploratory panel of 92 protein markers. These markers represent fundamental biological processes, including development, cellular regulation, signal transduction and stress response. In addition, we applied the same markers panel in cerebrospinal fluid (CSF), plasma and brain tissue samples from all four groups, to identify potential periphery-to-CNS protein interplay. PCA clustering failed to distinctively separate the experimental groups in CSF, plasma and brain tissue samples, yielding to no substantial statistical differences (Fig. S4, A-C and data not shown). However, in BAT, PCA analysis revealed distinct genotype-dependent clustering (Fig. 5A), with significant differences in 27 out of the 92 protein markers (Fig. 5B). Among the significant protein hits, pro-inflammatory cytokines and chemokines were upregulated in aP2-Srebf1c independent of diet (Fig. 5B), indicating that adipokine secretion regulates inflammatory response. Pathway enrichment analysis highlighted cytokine and chemokine pathways, such as cytokine to cytokine receptor interaction, chemokine, tumor necrosis factor (TNF) and Toll-like receptor signaling pathways, additionally underlining active inflammation (Fig. 5C). The identification of the AGE-RAGE signaling pathway in the context of diabetic complications further corroborated the diabetic phenotype, with transforming growth factor beta 1 (Tgfb1) to be significantly upregulated, among others. The upregulation of Tgfb1 was further associated with the MAPK signaling pathway, providing additional evidence of an underlying inflammatory response (Fig. 5, B and C). A hierarchical clustering tree analysis of all the significant pathways clusters together cytokine, chemokine and inflammation signaling pathways, whereas MAPK signaling pathway clusters in a branch along with the Ras signaling pathway (Fig. S4D).

Interestingly, lipid and atherosclerosis pathway cluster in close proximity with the highly enriched cytokine pathway, revealing proinflammatory responses as expected from the KEGG pathway database (Fig. S4, D and E). This pathway associates lysosomal enzyme activity with inflammatory response, which is supported from significant upregulation in aP2-Srebf1c BAT of lysosomal enzymes tripeptidyl peptidase 1 (Tpp1) and legumain (Lgmn) (Fig. S4E and 5B).

STRING network analysis clustered significant proteins in three distinct subgroups (red, green, blue), with many associations especially between cytokines and chemokines (Fig. 5D). Red cluster represents the most populated cluster, with five chemokines and interleukin-1 beta (Il1b) cytokine to be closely associated in addition to vascular endothelial growth factor D (Vegfd) and tumor necrosis factor receptor superfamily member 12A (Tnfrsf12a), indicating effects in angiogenesis and endothelial cell proliferation. Previous literature suggests that Vegfd overexpression in murine adipose tissue, led to increased adipose tissue lymphangiogenesis with improved obesity features, but decreased BAT thermogenesis^{44,45}. Soluble KIT ligand (Kitlg) also interacts with chemokines and Il1b in the network, strengthening potential signaling effects. Green cluster includes growth factors hepatocyte growth factor (Hgf) and protransforming growth factor alpha (Tgfa), both associated with Tgfb1 cytokine. Tgfb1 cytokine also strongly associates with activin A receptor like type 1 (Acvr11), demonstrating angiogenesis regulation and endothelial cell differentiation⁴⁶. Prior work showed that, both transforming growth factor b or activin type I receptors positively regulate BAT thermogenesis in brown preadipocytes *in vitro*⁴⁷. Blue cluster, which comprises of five proteins mostly related to cell adhesion and cytoskeleton properties, is disconnected from the remaining network. Additionally, STRING network workflow revealed several significant Gene Ontology (GO) categories related to biological processes, molecular functions, and cellular components (Fig. 5E). Biological processes such as helper T-cell extravasation and regulation of natural killer cell chemotaxis supported the role of proinflammatory response under the context of lipodystrophy. Molecular functions highlighted several chemokine receptors and activin binding ontologies, as well as chemoattractant activity, demonstrating crucial effects in cell-to-cell signaling responses in peripheral inflammation. Noteworthy, extracellular space and region were enriched in cellular component GO analysis, emphasizing proteins role outside of cells and within the broader extracellular environment. This role can be broadly associated with cell-to-cell communication and extracellular signaling pathways. In addition to the secreted adipokines, carboxypeptidase E (Cpe) exhibited an increase in aP2-Srebf1c BAT (Fig. 5B), which further reinforces the process of cellular secretion, as Cpe actively guides prohormones towards the secretory pathway⁴⁸. Taken together, the proteomic profile of BAT demonstrates a pronounced diet independent inflammatory response in aP2-Srebf1c, underscoring the diabetic phenotype and indicating stimulation of BAT thermogenesis and potential cellular secretion.



E

BIOLOGICAL PROCESS (GO)				
GO-term	description	count in network	strength	false discovery rate
GO:0035684	Helper T cell extravasation	2 of 4	2.61	0.0018
GO:2000503	Positive regulation of natural killer cell chemotaxis	2 of 5	2.51	0.0024
GO:2000501	Regulation of natural killer cell chemotaxis	3 of 8	2.48	0.000049
GO:0060754	Positive regulation of mast cell chemotaxis	2 of 7	2.36	0.0038
MOLECULAR FUNCTION (GO)				
GO-term	description	count in network	strength	false discovery rate
GO:0031730	CCR5 chemokine receptor binding	2 of 7	2.36	0.016
GO:0031726	CCR1 chemokine receptor binding	2 of 7	2.36	0.016
GO:0048185	Activin binding	2 of 14	2.06	0.0407
GO:0045236	CXCR chemokine receptor binding	2 of 14	2.06	0.0407
GO:0042056	Chemoattractant activity	4 of 41	1.9	0.00012
CELLULAR COMPONENT (GO)				
GO-term	description	count in network	strength	false discovery rate
GO:0005615	Extracellular space	17 of 1814	0.88	3.49E-09
GO:0005576	Extracellular region	19 of 2609	0.77	3.49E-09

Figure 5 Proteomic signature of brown adipose tissue (BAT) in aP2-Srebf1c mice reveal diet independent inflammatory profile. Four groups participated in the proteomic analysis: regarding the genotype Wild-type (Wt) of aP2-Srebf1c (Tg) and regarding the diet, control diet (CD) and Western diet (WSD). **(A)** Principal component analysis (PCA) of biological replicates (n=5) for each group, shows clustering among the different groups. The NPX values μM of all proteins that pass the quality control test were used as input data. **(B)** Heatmap showing the statistically significant ($P \leq 0.05$, fold ≥ 1.3) proteins among each group. The mean NPX values of all significant proteins were used as input data. **(C)** Pathway enrichment analysis of all significant proteins, analyzed with ShinyGO 0.77 (<http://bioinformatics.sdstate.edu/go/>). **(D)** Functional protein association networks of all significant proteins, analyzed with STRING version 12.0 (<https://string-db.org/>). **(E)** Gene ontology (GO) analysis of significantly enriched proteins, analyzed with STRING version 12.0. As input data for (C-E) analysis, all significant proteins depicted in (B) were used. P-values were calculated using two-way ANOVA with Tukey post-hoc correction. FDR: False Discovery Rate

Increasing UCP1-dependent metabolic rate of brown adipose tissue (BAT) does not influence glial response in demyelinating conditions

The metabolomic and proteomic signature obtained from aP2-Srebf1c lipodystrophy model emphasized the pivotal role of BAT and its thermogenic program. Additionally, our observation that BAT of aP2-Srebf1c animals resembles more of a BeAT structure (Fig. S1C) further supported the potential thermogenic capabilities of BAT within the framework of remyelination. Considering that a substantial number of metabolites and proteins exhibited significant alterations in aP2-Srebf1c animals, our hypothesis was that the collective impact of these compounds, rather than individual components, may influence remyelination and glial response. Hence, we targeted the entire metabolic axis encompassing BAT-CNS within our demyelination model, following a preliminary approach. To investigate the role of BAT metabolic rate in lesion recovery, we treated Wt animals treated with CD or WSD and performed demyelinating lesions at the corpus callosum. At 2dpi, we treated intraperitoneally (i.p.) the animals with CL-316243 (Sigma), a β 3-adrenergic receptor (β 3-AR) agonist or saline, to promote thermogenesis in BAT (Fig. 6A). It has been documented that, the thermogenesis process commences with a central stimulus (exposure to cold or food intake), triggering the release of noradrenaline and subsequent activation of the β 3-AR receptor. This activation sets in motion the cyclic adenosine monophosphate (cAMP)/protein kinase A (PKA) pathway, resulting in the generation of heat and thermogenesis via mitochondrial uncoupling mediated by uncoupling protein 1 (UCP1)⁴⁹. Quantification of mature oligodendrocyte numbers (CC1) in lesions showed no significant variances between saline and CL-316243 treatment. Nevertheless, there was a trend toward increased oligodendrocyte numbers during CL-316243 treatment, which was consistent across both dietary conditions (Fig. 6, B-F). We observed no differences in Olig2 numbers under agonist and diet treatments pointing to unchanged oligodendrocyte capacities (Fig. 6, G and H). Our data imply that glial response in demyelinating conditions does not depend on increased UCP1-dependent metabolic rate of BAT. However, it has been proposed that repeated administration of CL-316243 compromises its metabolic effects of serum glucose, and insulin levels and inhibits liver lipolysis in both lean and high-fat diet treated

mice⁵⁰. Other reports suggest that chronic use of CL-316243 does not desensitize mice in response to thermogenesis effects⁵¹. Optimizing our experimental setup by providing additional controls of BAT thermogenesis features will be our future experiments.

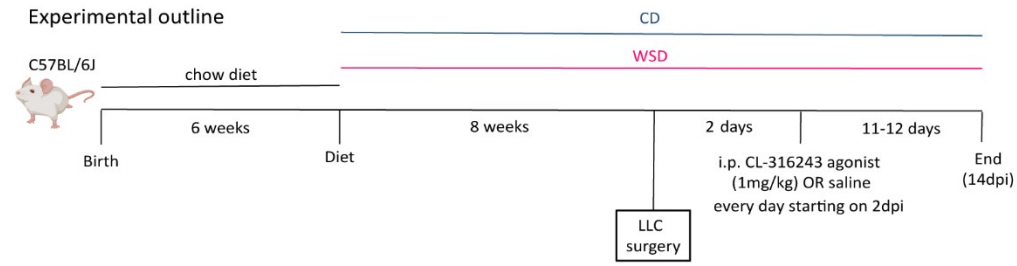
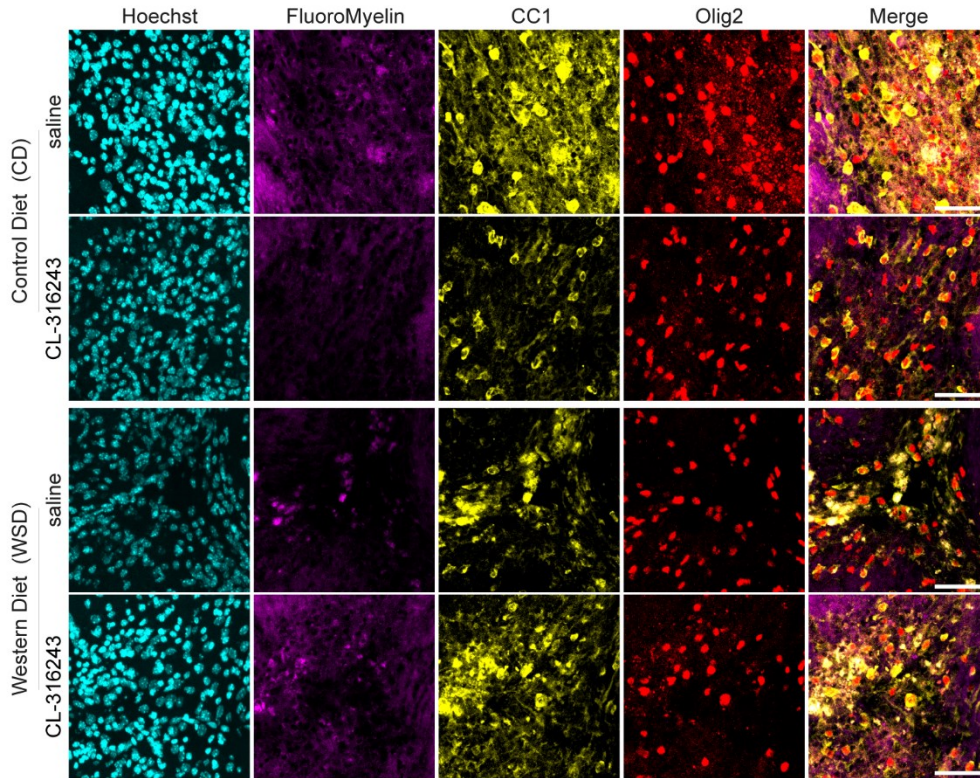
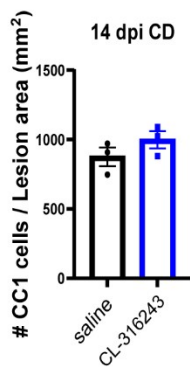
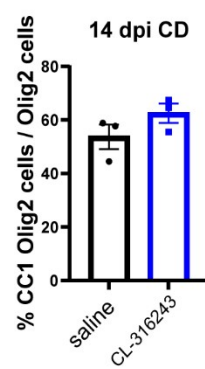
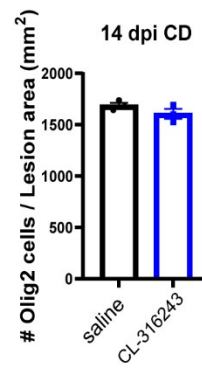
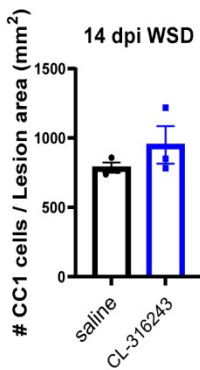
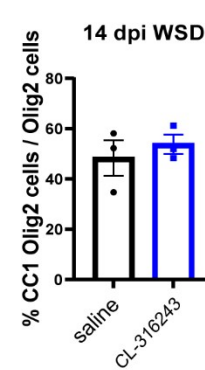
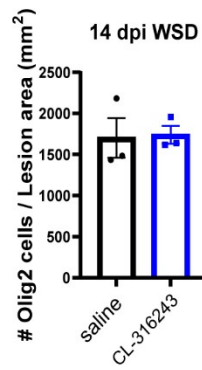
A**B****C****E****G****D****F****H**

Figure 6 Increasing UCP1-dependent metabolic rate of brown adipose tissue (BAT) does not influence glial response in demyelinating conditions. (A) Schematic representation of the diet and agonist administration and timeline. (B) Representative confocal images of corpus callosum lesions in 14dpi from WT lean and obese mice, treated with saline or CL-316243 (1mg/kg) agonist. Tissue is stained for Hoechst (cyan), FluoroMyelin (magenta), CC1 (yellow) and Olig2 (red). Scale bar, 50 μ m. (C-H) Quantification of 14dpi corpus callosum lesions between WT animals treated with saline or CL-316243 agonist, representing the CC1 positive cell numbers under CD (C) and WSD (D) over the lesion area, the percentages of CC1-Olig2 double positive cells over the total Olig2 positive cell number under CD (E) and WSD (F) and the Olig2 positive cell numbers under CD (G) and WSD (H) over the lesion area. Data represent mean \pm SD, P-values were calculated using two-tailed unpaired t test with Welch's correction. P > 0.05 is not depicted in the graphs. In the graphs, each dot represent animal (n=3). LLC: lyssolecithin mouse illustration in (A) was created with Biorender.com.

General discussion and conclusions

The key hallmark of inflammatory demyelinating diseases, such as MS, is the disruption of myelin sheaths, highly influenced by localized glial response. Glial cells orchestrate lesion repair mechanisms, in an effort to restore CNS regular functions⁵². While CNS is isolated anatomically from the periphery via BBB and other barriers⁵³, several axes allow CNS to communicate with peripheral organs, such as adipose tissue. Adipose tissue-brain axis has been widely researched, especially the connection between WAT and the hypothalamus⁵⁴. Upon hypothalamic neuronal stimuli, WAT secrete several compounds and hormones, as leptin, which communicate with the hypothalamic region to regulate food intake and appetite. However, in metabolic disorders like obesity and lipodystrophy, there is a dysregulation in the normal functions of adipose tissue⁴. Although adipose tissue-brain axis has been extensively researched in obesity, there is little knowledge regarding the crosstalk between adipose tissue and the brain in lipodystrophy, especially under demyelinating conditions.

In this study, we characterized the "lipodystrophy" brain in basal and demyelinating conditions and under different diet treatments. We used a murine model of CGL, the aP2-Srebf1c mice¹⁵. Among the different glial types in basal conditions, microglia activation was markedly increased in both cortex and corpus callosum in aP2-Srebf1c mice, treated with WSD, as previously described in obesity⁵⁵. Additionally, in white matter, LD accumulation showed increased tendency upon WSD, in both Wt and aP2-Srebf1c animals, with most LD found in astrocytes, recapitulating prior findings in obesity⁹. Collectively, in unlesioned conditions, our lipodystrophy model exhibits analogous metabolic characteristics to an obesity model, thus corroborating the hypothesis that both obesity and lipodystrophy share common attributes as metabolic disorders. Remarkably, upon demyelinating injury, aP2-Srebf1c lipodystrophic mice showed enhanced lesion recovery, reduced inflammation, and an increased abundance of mature oligodendrocytes in the WSD cohort. These observations differentiate our model from obesity, as previous work from our lab

suggests that obesity impedes the process of remyelination⁹. Adipose tissue is the major organ affected in both diseases, though with distinctive anatomical differences. In obesity, WAT exhibits lipid overload, resulting in decreased thermogenesis capacity in BAT. Conversely, in lipodystrophy, WAT is either absent or atrophied, while BAT takes on characteristics more akin to WAT^{1,15}. In addition, obesity alters adipose tissue secretome, as a consequence of its impaired functionality, which can affect inter organ communication⁵⁶.

To that end, metabolomic analysis of plasma from Wt and aP2-Srebf1c animals, showed distinctive different profile, with several of the identified metabolites being already described in the context of metabolic disorders. One of the most prominently elevated metabolites were the BCAAs. BCAAs are recognized for their neuroprotective properties in traumatic brain injury (TBI)⁵⁷, and diminished levels were observed in the plasma of relapsing-remitting MS patients⁴². BCAA catabolism facilitates the biosynthesis of cholesterol, via the intermediates α -ketoisocaproate (ketoleucine) and the subsequent production of hydroxy- β -methylbutyrate metabolites³⁴. Thus, BCAAs emerge as intriguing candidates for potential involvement in remyelination, given the fact that they can cross the BBB^{34,58}. Moreover, octadecenoylcarnitine (C18:1) was significantly enriched in aP2-Srebf1c-WSD treated, implicating potentially the positive effects of oleic acid as an anti-oxidant and anti-immunosuppressive modulator^{32,33}. Interestingly, several PCs containing polyunsaturated LCFAs were highly enriched in plasma from aP2-Srebf1c animals. PCs species belong to a wider family of glycerophospholipids and they are crucial components of cell membranes²³. A recent plasma lipidomic study documented a notable increase in PCs with polyunsaturated LCFAs in the plasma of CGL patients, regardless of their nutritional state, whether fasting or fat-fed⁵⁹. We also identified one PC species containing saturated LCFAs, to be increased in aP2-Srebf1c WSD treated animals. LCFAs can be synthesized endogenously from other fatty acids primarily in the liver, or obtained from the diet⁶⁰. Depending on the level of saturation, LCFAs can exhibit positive or negative aspects in a plethora of diseases. In the brain, saturated LCFAs are associated with neurotoxic and inflammatory responses, while unsaturated LCFAs are mostly correlated with reduced inflammation and neuroprotective properties in MS models, with few studies reporting contradictory results⁶¹. Polyunsaturated (i.e. two or more double bonds) LCFAs have been described to positively modulate lesion recovery in mice, upon demyelinating injury⁶². Remarkably, many studies describe that circulating lipids in the plasma are required for BAT thermogenesis and that BAT physiologically regulates the plasma lipid pool⁶³.

Along the same lines, our pathway analysis highlighted metabolic pathways implicating in BAT and BeAT increased thermogenesis, due to PCs increased enrichment. PCs act as precursors in the biosynthesis of sphingolipids⁶⁴. In our metabolic analysis three sphingomyelin lipids with 18 and 26 carbon atoms were increased in aP2-Srebf1c mice, with specific species to be diet dependent.

Sphingomyelin (SM) species with more than 30 carbon atoms are increased in the plasma of obese mice, originated from extracellular visceral WAT vesicles, among other sources⁶⁵. Nonetheless, in plasma isolated from GGL patients, one sphingomyelin with 18 carbon atoms was highly enriched⁵⁹, proposing that the absence of functional WAT in lipodystrophy can alter the composition of secreted sphingomyelins in the plasma. Recent literature has reported that in the plasma of MS patients, SM levels and the presence of polyunsaturated fatty acids were reduced. These findings suggest that alterations in plasma SM composition and fatty acid saturation may have an impact on both MS pathophysiology⁶⁶. Thus, elevated levels of PCs and SM with attached polyunsaturated fatty acids (PUFAs) in the plasma of our lipodystrophy model, can have a positive outcome in lesion recovery, as PUFAs can cross the BBB via multiple ways⁶⁰. Plasma ratios of typical metabolic syndrome markers revealed increased levels of CPT-I activity in aP2-Srebf1c, WSD treated mice. CPT-I activity is connected with BAT metabolism, since it increases UCP1 expression, mitochondrial activity and lipolysis in rat brown adipocytes⁶⁷. Nonetheless, a recent study revealed that pharmacological and genetic inhibition of CPT-I led to a reduction in demyelination and inflammation, ultimately contributing to improved lesion recovery in a mouse model of MS⁶⁸. Altogether, our metabolomic data strongly propose altered BCAAs, PCs and SM metabolic signature and the active involvement of BAT metabolism in our lipodystrophy model.

Subsequently, BAT targeted proteomic analysis from aP2-Srebf1c, under CD and WSD treatment revealed a diet independent but highly genotype dependent proteomic profile. As expected, several proinflammatory and chemoattractant factors were upregulated in aP2-Srebf1c animals, consistent with a diabetic profile supported from the GO analysis. Cellular component GO analysis depicted extracellular space and region ontologies, since a plethora of identified proteins are associated with the endolysosomal and secretory pathway, supporting the notion that BAT is an endocrine organ. Notably, aP2-Srebf1c mice demonstrate increased markers of lymphangiogenesis and endothelial cell metabolism. These markers belong to wider protein families, namely vascular endothelial growth factor, transforming growth factor b and activin type I receptors, which have also been documented to regulate BAT thermogenesis, either positively or negatively^{47,56,69}. Since BAT thermogenesis was highlighted from both our metabolomic and proteomic analysis, we investigated the impact of increased UCP1-dependent BAT activity on demyelinating lesions, comparing Wt obese and lean mice. Repeated administration of CL-316243 that targets UCP1 expression, failed to significantly enhance lesion recovery. Still, numbers of mature oligodendrocytes showed an increased trend upon CL-316243 administration. Of note, there are contradictory reports that repeated supplementation of CL-316243 may desensitize β 3-AR receptors and dampen BAT thermogenesis process^{50,51}. Our data suggest that lesion recovery in demyelinating conditions does not rely on amplified, UCP1-dependent, metabolic rate of BAT. In light of these findings, it becomes essential to explore alternative mechanisms driving lesion

recovery in demyelinating conditions, within the framework of adipose tissue-brain communication.

One possibility could be that increased BAT thermogenesis can positively regulate remyelination in an UCP1-independent manner. Intriguingly, recent studies indicate the presence of physiologically relevant thermogenesis in adipocytes, that is UCP1-independent⁷⁰. One compound that has recently been identified at the center of UCP1-independent thermogenesis in adipose tissue is creatine. Creatine role in thermogenesis was initially identified in BeAT, where it stimulates energy expenditure via increased respiration in mitochondria⁷¹. A subsequent study also proposed that BeAT contains both UCP1-positive and UCP1-negative adipocytes and that β 3-AR stimulation does not affect creatine driven thermogenesis⁷². Creatine has also been implicated in cerebral creatine deficiency syndrome (CCDS) and as a pharmacological approach in MS progression. In CCDS mouse model, creatine diet supplementation enhanced remyelination, upon cuprizone induced demyelination, targeting mature oligodendrocytes⁷³. Differentiation and survival of oligodendrocytes are also promoted upon creatine administration in lesions of MS models, suggesting creatine as a potential drug targeting remyelination and oligodendrocyte metabolism^{74,75}. Although creatine biosynthesis occurs primarily in kidney-liver axis⁷⁶, its identification in BeAT further reinforces the adipose tissue-brain crosstalk, within the context of thermogenesis. BeAT adipogenesis is also enhanced by a secreted metabolite, β -hydroxybutyrate (BHB)⁷⁷. BHB levels are increased upon ketogenic diet treatment, which has been found to promote remyelination in the cuprizone model⁷⁸. Besides, a recent study showed that the absence of BeAT shifts microglia towards proinflammatory activation in the context of dietary obesity, emphasizing BeAT role in brain neuroinflammation⁷⁹. All evidence above highlights the importance of BeAT metabolism and BAT non-canonical thermogenesis under the aspects of adipose tissue-brain communication. Interestingly, in our study, histological staining from aP2-Srebf1c animals revealed that BAT resembles more of a BeAT structure, contributing to the hypothesis that BAT altered metabolism may contribute to the remyelination process. Therefore, our future outlook will focus in elucidating the role of UCP1-independent mechanisms in BAT and BeAT and their potential regenerative properties upon demyelinating injury. A limitation of the current study is that we did not monitor adipose tissue metabolic features, in basal, lesion induced and upon β 3-AR agonist stimulation. Metabolic features such as adipose heat production, oxygen consumption and energy balance upon diet treatments, are crucial in studies of metabolic disorders. Our future experiments will include the utilization of metabolic cages and the assessment of adipose tissue thermogenesis markers.

In summary, to our knowledge, this is the first study to provide novel insights of the “lipodystrophy” brain, both in basal conditions and upon demyelinating injury. We showed that adipose tissue-brain axis is primarily affected and can contribute to enhanced lesion recovery. Two noteworthy upregulated metabolite clusters, BCAAs and PCs containing polyunsaturated LCFAs in the periphery may facilitate the

regenerative response via directly crossing BBB. Moreover, PCs with polyunsaturated LCFAs can stimulate the production of sphingolipids or actively modulate BAT and BeAT thermogenesis, thereby providing additional support to the remyelination process. Our results contribute to the evolving understanding of how peripheral lipid metabolism impacts brain response to tissue damage.

Materials and methods

Mice, special diets, and pharmacological treatment

Mice and special diets

All mouse procedures complied with the approval and guidelines from the District Government of Upper Bavaria. aP2-Srebf1c (B6;SjL-Tg(aP2-SREBF1c)9884Reh/J) and Wt C57BL/6J mice were purchased from the Jackson Laboratory and Janvier lab respectively. aP2/Srebf1c, which overexpress human nuclear sterol regulatory element binding protein-1c in adipose tissue under the control of the adipocyte-specific aP2 promoter, were raised according to the suggested breeding scheme and using the recommended PCR primers (genotyping protocol available online). For all working experiments, only male mice were used. All mice were housed in groups of three within Greenline IVC GM500 plastic cages, maintaining a controlled environment at a temperature of $21 \pm 2^\circ\text{C}$, with 40–60% humidity on a 12-hour light/dark cycle. This housing arrangement, along with ad libitum access to food and water, was provided in the pathogen-free animal facility at the German Center for Neurodegenerative Diseases (DZNE-Munich). For the induction of diet-induced obesity, mice were fed with either a control diet (CD88137, Ssniff) or a high-fat Western diet (WD, TD88137, Ssniff) starting at 6 weeks of age and continuing for a duration of 8 to 12 weeks. For the metabolomic analysis, an extra group was added as an additional control, in which mice were fed a standard chow diet.

In vivo pharmacological treatment

For the *in vivo* pharmacological treatment in Wt C57BL/6J mice, the β 3-AR agonist CL-316243 (C5976, Sigma) was administrated intraperitoneally (i.p.) every day at the exact time, starting 2 days after the LLC stereotactical injections and until the mice were sacrificed at 14dpi. Immediately after the i.p. administration, mice were macroscopically monitored for any side effects from the drug administration for 1-2 hours.

LLC induced demyelination

A 1% lysolecithin solution was prepared by combining lysolecithin (L4129, Sigma) with sterile $1\times$ PBS. For enhanced lesion visualization during tissue processing, Monastral blue (274011, Sigma-Aldrich) was added to the lysolecithin solution at a concentration of 0.05% (1ul in 20ul of LLC) just before its intended use. Glass capillaries (504949, World Precision Instruments) were prepared using the P-1000 Next Generation Micropipette Puller (Sutter Instrument) following the already described parameters¹⁴. To induce anesthesia, mice were administered an intraperitoneal injection of an MMF solution comprising 0.5 mg medetomidine/kg (body weight), 5.0 mg midazolam/kg (body weight), and 0.05 mg fentanyl/kg (body weight). Following anesthesia, the head fur was removed, the eyes were covered with Bepanthen cream (1578847, Bayer), and a small incision was made to expose the skull. The mice were

securely positioned in a stereotactic injection apparatus, aligning the ears and snout into their respective holders. The anesthetized animals were maintained on a heating pad set at 37°C, continuously monitoring anesthetic depth by assessing the reflex between the toes and the corneal reflex. A hole was drilled at the designated injection coordinates (from bregma): X, \pm 1.0 mm; Y, -0.1 mm. Then, a glass capillary loaded with the lysolecithin–Monastral blue solution was precisely lowered to Z: -1.40 mm from bregma, and 1 μ L was injected at a controlled rate of 100 nL/minute. Following a two-minute interval post-lysolecithin delivery, the capillary was gently retracted. After the surgical procedure, the animals were administered a 250 μ l injection of 0.9% NaCl (normal saline solution) to compensate for potential blood loss. Subsequently, the mice received an injection of 0.05 mg buprenorphine/kg (body weight), and the incision in the skin was sutured. To terminate anesthesia, subcutaneous injection of AFN solution was administered, consisting of 2.5 mg/kg (body weight) atipamezole, 0.5 mg/kg (body weight) flumazenil and 1.2 mg/kg (body weight) naloxone. Buprenorphine was administered subcutaneously to the animals for a period of 2 days following the surgical procedure.

Antibodies and other reagents

Primary antibodies

Rabbit IBA1 (234 004, 1:500 for IHC; Synaptic Systems), chicken IBA1 (234 009, 1:400; Synaptic Systems), goat IBA1 (ab5076, 1:250; abcam), guinea pig GFAP (173004, 1:500; Synaptic Systems), chicken GFAP (173006, 1:500; Synaptic Systems), rat MAC2 (125402, 1:250; BioLegend), rat CAII (MAB2184, 1:150; Biotechne), mouse APC/CC1 (OP80, 1:100; Merck Calbiochem), rabbit Olig2 (AB9610, 1:250; Millipore), guinea pig PLIN2 (GP40, 1:300; PROGEN) and rabbit PLIN2 (NB110-40877, 1:200; Novus Biologicals).

Secondary fluorescent antibodies

Anti-rabbit 488 (A-32731, 1:1000; Thermofisher), anti-chicken 488 (A-11039, 1:1000, Thermofisher), anti-goat 488 (A-11055, 1:750; Invitrogen), anti-rabbit 555(A-32794, 1:750; Thermofisher), anti-mouse 555 (A-32727, 1:1000; Thermofisher), anti-guinea pig 555 (A-21435, 1:1000; Thermofisher), anti-rat CF633 (20133, 1:500; biotium), anti-rabbit 647 (A-32733, 1:500; Thermofisher), anti-chicken 647 (703-605-155, 1:750; Jackson Immunoresearch), anti-rat 647 (712-605-150, 1:500; Jackson Immunoresearch).

Other reagents

Hoechst 33342 (B2261, 1:2000; Sigma), FluoroMyelin green (F34651, 1:400; Molecular Probes Invitrogen), Prolong™ Gold Antifade mountant (P36930; Invitrogen), Prolong™ Diamond Antifade mountant (P36970; Invitrogen), anti-mouse FAB fragments (715-007-003; Jackson Immunoresearch), saponin (4185.1; Roth), L- α -LLC (L4129; Sigma), Monastral blue (274011; Sigma-Aldrich), CL-316243 (C5976; Sigma), RIPA lysis buffer (20-188; Merck), protease inhibitor tablets (A32955; Pierce™), phenylmethylsulfonyl fluoride-PMSF (10837091001; Sigma).

Immunohistochemistry

Animals were anesthetized with a solution of 10 mg/ml ketamine and 1 mg/ml xylazine administered intraperitoneally. Transcardial perfusion was conducted with 4%

paraformaldehyde (PFA) with a peristaltic pump (Peri-Star PRO, World Precision Instruments). Subsequently, brains were postfixed in 4% PFA for 6-16 hours. Cryoprotection of brain tissue was achieved by immersing it in a 30% sucrose solution in PBS for at least 72 hours. Following freezing on dry ice using Tissue-Tek O.C.T., the tissue was sectioned into 16- μ m coronal (lesioned brains) and sagittal (unlesioned brains) slices using a Leica CM 1900 cryostat and directly mounted on Superfrost Plus slides in a serial manner. The sections were initially dried at 37 °C for 30 minutes, followed by rinsing with PBS 1X and permeabilization for 10 minutes in PBS 1X containing 0.3% Triton X-100. To prevent non-specific binding, sections underwent a 1-hour incubation with a blocking solution (2.5% bovine serum albumin, 2.5% fish gelatin, and 2.5% fetal calf serum in PBS 1X). Primary antibodies, diluted in staining solution (25% of blocking solution in PBS 1X), were then incubated overnight at 4 °C. Subsequently, sections were further incubated with primary antibodies for 1 hour at room temperature, washed with PBS 1X, and then incubated with secondary antibodies (diluted in staining solution) for 1 hour. Following another round of washing with PBS 1X, the sections were incubated with FluoroMyelin in PBS 1X for 20 min, followed with Hoechst in PBS 1X for 10 minutes. Finally, the sections were washed in PBS 1X, rinsed with distilled water and mounted with Prolong Gold or Prolong Diamond. For APC/CC1 and PLIN2 staining, heat-induced (80°C for 20 min) antigen retrieval was performed before blocking, using sodium citrate buffer (10 mM, pH 6). For rabbit PLIN2, the staining solutions were supplemented with 0.05% saponin. For APC/CC1 primary antibody, tissue was incubated with mouse FAB fragments (1:100) in PBS 1X for 1 hour before blocking, to block endogenous immunoglobulins.

Image processing and analysis

All images were acquired utilizing confocal microscopy, employing either a Leica SP5 confocal system with objectives of 20x/0.75 NA (air) and 63x/1.40 NA (oil), or the Zeiss LSM 900 with objectives of 20x/0.8 M27 (air), 40x/1.1 W Korr UV-VIS-IR (water), and 63x/1.2 Imm Korr DIC M27 (oil). Additionally, the navigator function of Zeiss was utilized with a 10x/0.30 M27 (air) objective. Also, the epifluorescence microscopes Zeiss Axio Observer 7 with objective 20x/0.8 M27 (air) and Leica Microsystems DMI6000B with objective 20x/0.75 NA (air) were used. Various fluorophores were stimulated sequentially using specific laser lines: 405 nm for Hoechst, 488 nm for Alexa Fluor 488 (AF488), 561 nm for Alexa Fluor 555 (AF555), and 633 nm for Alexa Fluor 647 (AF647) and CF633. For image analysis, counting tools implemented in Fiji⁸⁰ and Qupath⁸¹ were used. To quantify the lesion and inflammation areas, the demyelinated surface identified by negative FluoroMyelin staining and positive IBA1 staining were measured in serial sections of a lesion, spaced at a known distance. Employing the truncated cone model, the lesion and inflammation volumes were computed using IPython, as previously described⁸².

Sample preparation for metabolomic and proteomic analysis

Animals were anesthetized with a solution of 10 mg/ml ketamine and 1 mg/ml xylazine administered intraperitoneally. For material utilized for metabolomic and proteomic analysis, animals were perfused transcardially with PBS 1x. Prior to perfusion, plasma and CSF were collected, and immediately after perfusion, brain and BAT samples were collected as follows. For plasma isolation, blood was collected directly from the heart using an EDTA-coated 1 mL syringe attached to a 25-G needle, inserted into the left ventricle. The collected blood was

then transferred to an EDTA-coated (<~25 mM) tube and centrifuged at 2,000g for 10 minutes at 4 °C to separate plasma. All available plasma was collected and promptly flash-frozen in liquid nitrogen. To obtain CSF, we used the same capillaries as in LLC stereotactical injections to collect CSF via the cisterna magna, as previously described⁸³, and subsequently flash-freeze it in liquid nitrogen. For brain and BAT tissue collection, the following procedure was followed. Briefly, both brain and BAT tissue samples were homogenized with a Polytron homogenizer (75% amplitude, 15s x 4 for brain; 80% amplitude, 30s x 4 or more times for BAT) in ice-cold RIPA lysis buffer, supplemented with 1 mM PMSF and protease inhibitors (1 tablet per 10ml of lysis buffer). The ratio of tissue to lysis buffer was 1/20-1/50 g/ml. After sonication, the samples were rest on ice for 30min. For brain tissue, the sonicated samples were centrifuged at 30.000rpm for 30 min under vacuum and at 4 °C, using the ultracentrifuge Optima MAX-XP with the 19U TL55 rotor head. For BAT, three consequent rounds of ultracentrifugation were performed: 1st round - 30.000rpm for 1 h, 2nd and 3rd rounds: 30.000rpm for 30 min each. Between every round, the middle layer was collected with a 30G needle and subsequently processed to the next round of ultracentrifugation, as previously described⁸⁴. After the last ultracentrifugation round, supernatants are transferred to clean tubes or plates for future experiments. All frozen samples were kept at -80 °C for future analysis. For the proteomic analysis, the total protein concentration of brain and BAT tissue samples was standardized to 1 µg/µL, using the BCA measurement assay.

Targeted metabolomic analysis

For the quantification of all metabolites in the plasma of mice cohorts, we employed the Biocrates Absolute/DQ[®] p180 Kit, following the procedure outlined in prior documentation⁸⁵⁻⁸⁷. This specialized kit facilitates the quantification of 188 endogenous metabolites spanning six distinct compound categories: amino acids, biogenic amino acids, acylcarnitines, glycerophospholipids, sphingolipids, and hexoses. The methodology employed adheres to FDA guidelines, described in "Guidance for Industry – Bioanalytical Method Validation (May, 2001)". The absolute quantification of amino acids and biogenic amines involved chromatographic separation through liquid chromatography (LC), incorporating isotopically labeled internal standards and calibration curves. For acylcarnitines [Cx:y], sphingomyelins [SM Cx:y], hydroxysphingomyelins [SM (OH) Cx:y], lysophosphatidylcholines [lyso Cx:y], phosphatidylcholines [PC z Cx:y], and the cumulative sum of hexoses [H1], quantification relied on one or more internal standards tailored to each metabolite class. Notably, the variables x and y signify the number of carbon atoms and the number of double bonds, respectively. In the case of phosphatidylcholines, the two lipid side chains can be connected to the glycerophosphatidyl headgroup via either an acyl-acyl ester bond (z = aa) or a mixed acyl-alkyl bond (z = ae). The lipids, acylcarnitines, and hexoses were assessed using FIA-MS/MS (Flow Injection Analysis with Tandem Mass Spectrometry) and produce semi-quantitative concentration results, whereas the amino acids and biogenic amines were quantified through LC-MS/MS (Liquid Chromatography with Tandem Mass Spectrometry) and produce quantitative concentration results. Sample preparation and measurements were executed in accordance with the manufacturer's manual for the p180 kit (UM-P180) and as previously described⁸⁶. All liquid handling procedures were executed using a Hamilton Microlab Star robot. Multiple reaction monitoring (MRM) measurements were carried out utilizing a Sciex API4000 mass spectrometer (Sciex Deutschland GmbH, Darmstadt,

Germany) coupled with an Agilent 1200 series HPLC (Agilent Technologies Deutschland GmbH, Böblingen, Germany), and a HTC PAL autosampler (CTC Analytics, Zwingen, Switzerland). The entire system was controlled by the Analyst software (version 1.4 to 1.6.1). The Met/DQ™ software, an integral component of the Absolute/DQ® p180 kit, was used for the report of the metabolites measurements. For the sums and ratios provided, the Met/DQ™ RatioExplorer by Biocrates was used, following the manual instructions. All metabolite concentrations are presented in μM . Metabolite quality assessment were conducted using also the Met/DQ™ software. This methodology (p180 kit) has undergone comprehensive validation by Biocrates for human plasma samples. This validation encompasses the determination of the limit of detection for both quantitative and semiquantitative metabolites (LOD), the lower and upper limits of quantification (LLOQ and ULOQ, respectively), as well as assessments of linearity, precision, accuracy, reproducibility, and stability. Only the metabolites that passed the quality control were considered for further statistical analysis and biological interpretation.

Targeted Proteomic analysis

For the quantification of proteins, 1 μl from plasma, CSF, brain tissue and BAT lysates were screened using the Olink®Target 96 Mouse Exploratory panel (92 proteins). Olink®Target 96 workflow is using the Proximity Extension Assay (PEA) technology, employing a readout methodology base on real-time quantitative PCR (qPCR), as previously described^{88,89}. Briefly, the PEA operates on a principle where paired antibodies, each linked to DNA oligos, bind to a target protein. This binding initiate hybridization, forming double-stranded DNA that acts as a distinctive barcode for each specific protein. These barcodes are subsequently amplified and quantified through qPCR. All samples from the 4 different biological material passed quality control (data not shown). The Olink® PEA data are presented in NPX values (normalized protein expression levels) that are on a log₂ scale, as previously described⁸⁹. In every PEA measurement, a limit of detection (LOD) is determined using negative controls incorporated in each run. Usually, any measurements falling below this limit are excluded from subsequent analysis. However, Olink® recommends not removing data points below LOD, since certain highly distinctive biomarkers may exhibit low levels in specific analyzed groups and high levels to others. In addition, according to Olink®, incorporating data below the LOD typically does not increase false positives, as there is generally no noteworthy difference between groups below the LOD; these values tend to cluster within a very narrow range. For our analysis, we decided to keep the values detected below LOD, with the prerequisite that all samples should pass the quality control test. Notably, the percentage of significant proteins with more than half values below LOD were less than 12%. Detailed information regarding PEA technology, assay performance and validation data can be accessed directly from the manufacturer (www.olink.com).

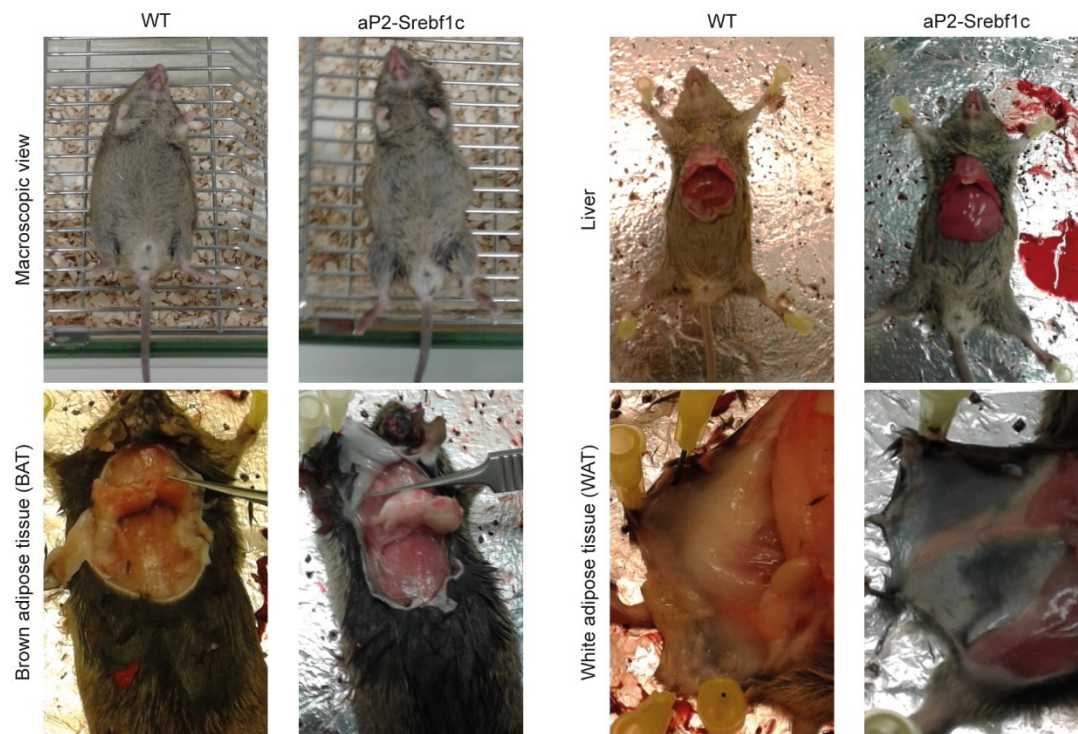
Statistics and software use

All statistical analysis was done in R 4.3.0 and R studio, apart from the proteomic data; NPX values from the proteomic analysis were further statistically analyzed using the free statistical analysis tool provided by Olink®. The bar and box plots were created in GraphPad Prism 9, where all data represent mean \pm SD. P-values were calculated using two-tailed unpaired t test with Welch's correction, two-way ANOVA with Tukey post-hoc correction or Kruskal–Wallis test followed by Wilcoxon post-hoc correction. Each figure legend specify which

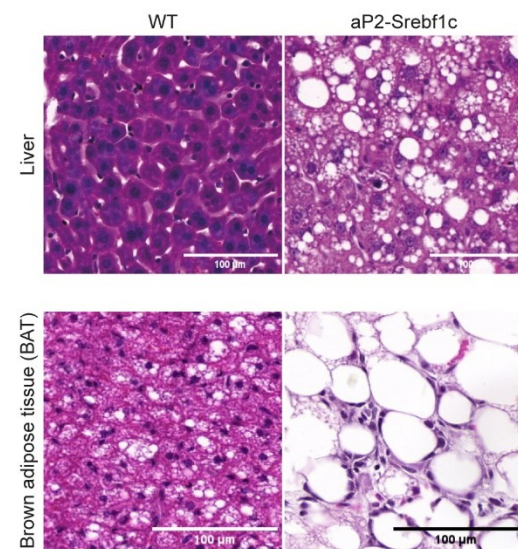
statistical test was used. For the metabolomic analysis, heatmaps and PCA plots were created using the Orange DATA MINING 3.36 software. For the pathway enrichment analysis of significant metabolites, MetaboAnalyst 5.0 software was used⁹⁰. For the proteomic analysis, heatmaps and PCS plots were created using the Orange DATA MINING 3.36 software. The pathway enrichment analysis and tree plot analysis of significant proteins was determined by ShinyGO 0.77⁹¹, while the functional protein association networks and Gene Ontology analysis were determined by STRING version 12.0⁹². The software MetaboAnalyst 5.0, Orange DATA MINING 3.36, ShinyGO 0.77 and STRING version 12.0 are available online for free.

Supplementary Information

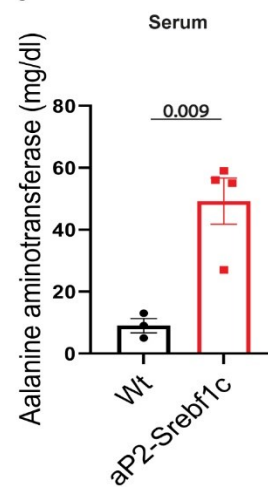
A



B



C



D

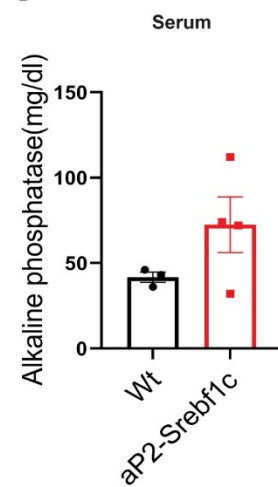


Figure S1 The aP2-Srebf1c murine model resembling congenital generalized lipodystrophy (CGL) disorder.

(A) Macroscopic view of WT and aP2-Srebf1c animals. In the images the liver (upper right) and brown adipose tissue (down left) of aP2-Srebf1c are enlarged, with the brown adipose tissue to resemble white adipose tissue (WAT) morphology. The WAT (down right) of aP2-Srebf1c animals is completely diminished. **(B)** Hematoxylin and eosin (H&E) staining of liver and brown adipose tissue from WT and aP2-Srebf1c animals. Scale bar, 100 μ M. **(C-**

D) Serum levels of alanine aminotransferase (C) and alkaline phosphatase (D) from WT and aP2-Srebf1c animals. Data represent mean \pm SD, P-values were calculated using two-tailed unpaired t test with Welch's correction. $P \leq 0.05$ is depicted in the graphs. For this analysis, n=3-4 animals were used from each group.

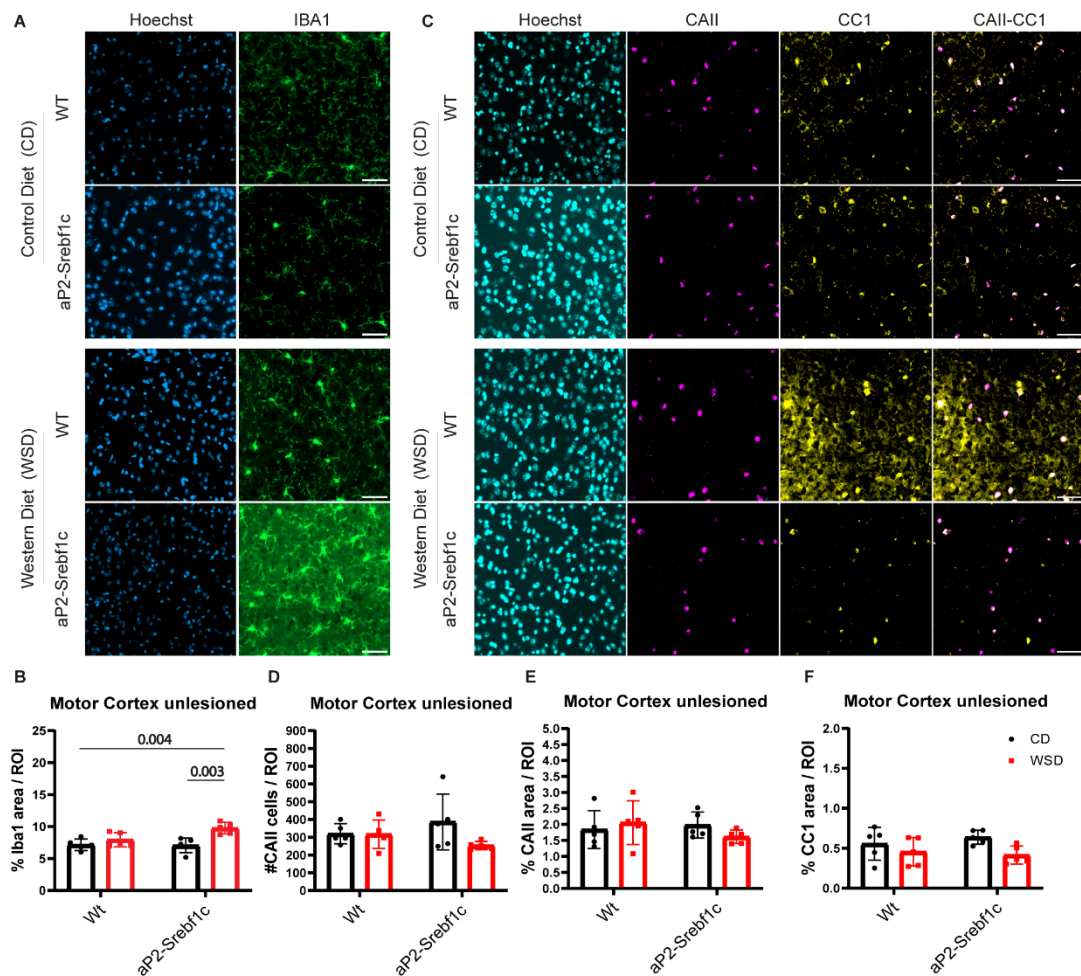


Figure S2 Characterization of aP2-Srebf1c mice in basal conditions: glial cells response in unlesioned motor cortex. (A) Representative confocal images of unlesioned motor cortex from WT and aP2-Srebf1c under Control (CD) and Western (WSD) diets. Tissue is stained for Hoechst (blue) and IBA1 (green). Scale bar, 50 μ m. (B) Quantification of the percentages of IBA1 positive area over regions of interest (ROI) in motor cortex. (C) Confocal images of unlesioned motor cortex from WT and aP2-Srebf1c (CD and WSD). Tissue is stained for Hoechst (cyan), CAII (magenta) and CC1 (yellow). Scale bar, 50 μ m. (D-F) Quantification graphs of the CAII cell numbers (D) and the percentages of CAII positive area (E) and CC1 positive area (F) in ROI in motor cortex. Data represent mean \pm SD, P-values were calculated using two-way ANOVA with Tukey post-hoc correction. $P < 0.05$ are numerically depicted in the graph. In the graphs, each dot represent animal (n=5).

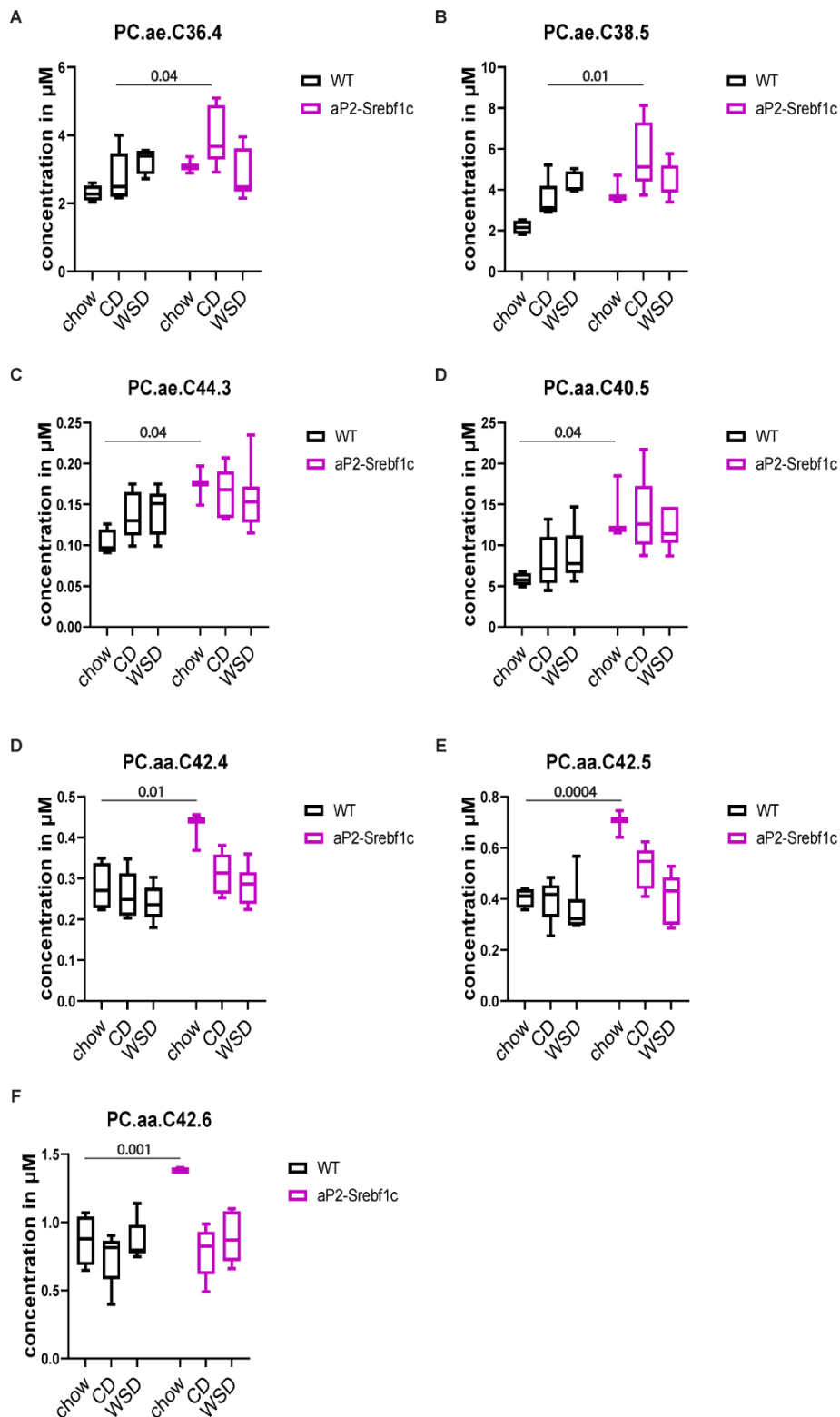


Figure S3 Metabolomic signature of aP2-Srebf1c mice reveals elevated levels of several phosphatidylcholines (PCs) containing long-chain fatty acids (LCFAs) under chow treatment. (A-F) Significant PCs species containing LCFAs in different positions (detailed description in main text and Materials and Methods). Data represent mean \pm SD, P-values were calculated using multivariate analysis with two-way ANOVA followed by Tukey post-hoc correction (normally distributed metabolites) or with Kruskal–Wallis test followed by Wilcoxon post-hoc correction (non-normally distributed metabolites). $P \leq 0.05$ are depicted in the graphs. For this analysis $n=3-7$ animals were used for each group.

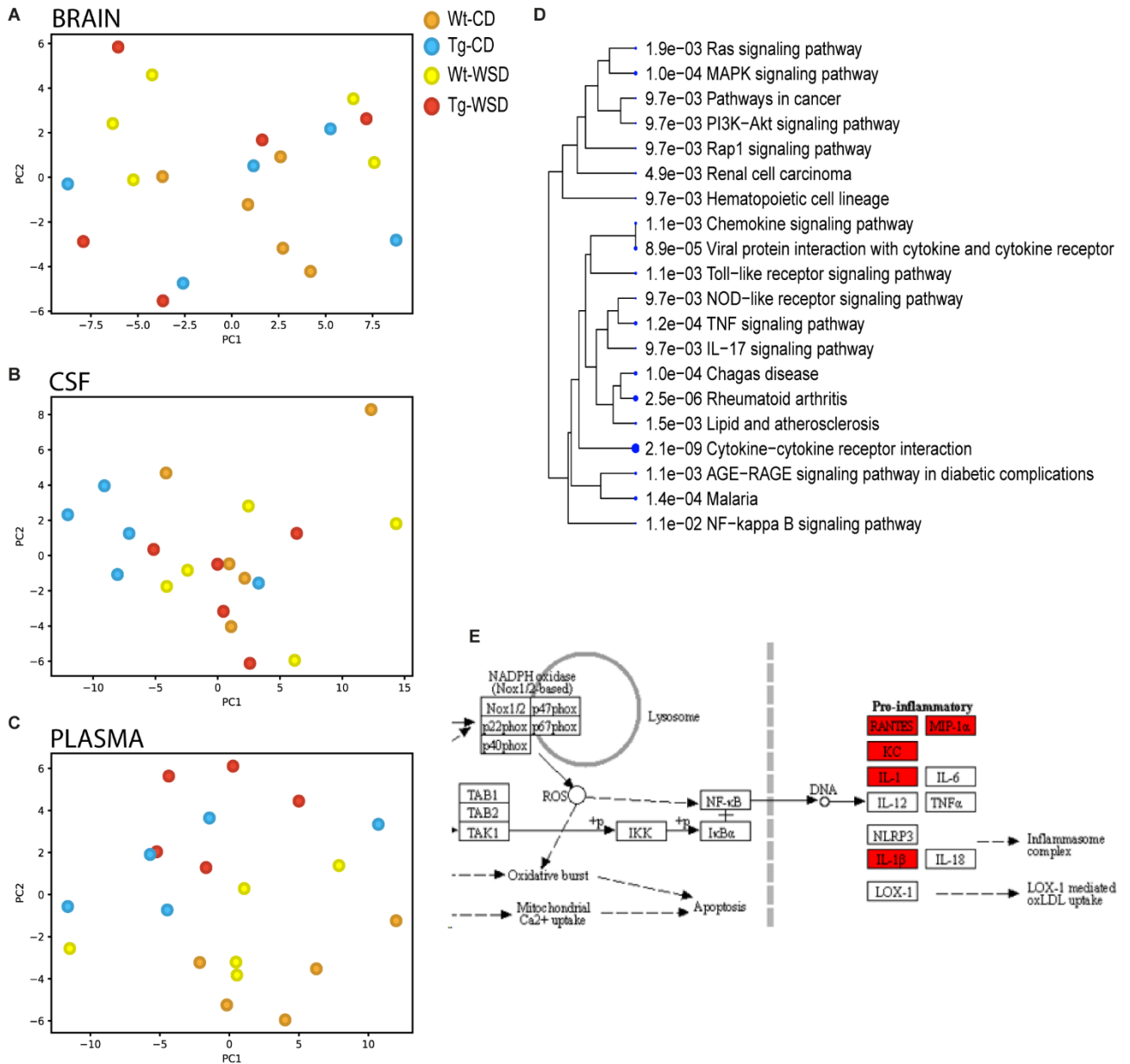


Figure S4 Targeted proteomic analysis of aP2-Srebf1c animals reveal an inflammatory response. Four groups participated in the proteomic analysis: regarding the genotype Wild-type (Wt) of aP2-Srebf1c (Tg) and regarding the diet, control diet (CD) and Western diet (WSD). **(A-C)** Principal component analysis (PCA) of biological replicates (n=5) for each group for brain tissue **(A)**, CSF **(B)** and plasma **(C)** shows not efficient clustering among the different groups. The NPX values μ M of all proteins that pass the quality control test were used as input data. **(D)** Tree plot analysis of all significant proteins, analyzed with ShinyGO 0.77 (<http://bioinformatics.sdstate.edu/go/>). **(E)** Pathway enrichment analysis (KEGG pathway analysis in this panel) of the significant proteins, as they were defined Fig. 5B, using ShinyGO 0.77. Here, the lysosomal pathway is highlighted. Proteins that are marked with a red box are present in our proteomic dataset.

References

- 1 Sakers, A., De Siqueira, M. K., Seale, P. & Villanueva, C. J. Adipose-tissue plasticity in health and disease. **185**, 419-446, doi:10.1016/j.cell.2021.12.016 (2022).
- 2 Rochford, J. J. Mouse Models of Lipodystrophy and Their Significance in Understanding Fat Regulation. *Current Topics in Developmental Biology* **Ch2, Volume 109**, 53-96, doi:10.1016/B978-0-12-397920-9.00005-6 (2014).
- 3 Guilherme, A., Henriques, F., Bedard, A. H. & Czech, M. P. Molecular pathways linking adipose innervation to insulin action in obesity and diabetes mellitus. **15**, 207-225, doi:10.1038/s41574-019-0165-y (2019).
- 4 Caron, A., Lee, S., Elmquist, J. K. & Gautron, L. Leptin and brain–adipose crosstalks. **19**, 153-165, doi:10.1038/nrn.2018.7 (2018).
- 5 Salas-Venegas, V. *et al.* The Obese Brain: Mechanisms of Systemic and Local Inflammation, and Interventions to Reverse the Cognitive Deficit. **16**, doi:10.3389/fnint.2022.798995 (2022).
- 6 Uranga, R. M. & Keller, J. N. The Complex Interactions Between Obesity, Metabolism and the Brain. **13**, doi:10.3389/fnins.2019.00513 (2019).
- 7 Yoon, J. H. *et al.* Brain lipidomics: From functional landscape to clinical significance. **8**, doi:10.1126/sciadv.adc9317 (2022).
- 8 Zhang, J. & Liu, Q. Cholesterol metabolism and homeostasis in the brain. **6**, 254-264, doi:10.1007/s13238-014-0131-3 (2015).
- 9 Bosch-Queralt, M. *et al.* Diet-dependent regulation of TGF β impairs reparative innate immune responses after demyelination. **3**, 211-227, doi:10.1038/s42255-021-00341-7 (2021).
- 10 Sighinolfi, G., Clark, S., Blanc, L., Cota, D. & Rhourri-Frih, B. Mass spectrometry imaging of mice brain lipid profile changes over time under high fat diet. **11**, 19664, doi:10.1038/s41598-021-97201-x (2021).
- 11 Correale, J. & Marrodan, M. Multiple sclerosis and obesity: The role of adipokines. **13**, doi:10.3389/fimmu.2022.1038393 (2022).
- 12 Lassmann, H. Pathogenic Mechanisms Associated With Different Clinical Courses of Multiple Sclerosis. **9**, doi:10.3389/fimmu.2018.03116 (2019).
- 13 Lucchinetti, C. F. *et al.* Inflammatory Cortical Demyelination in Early Multiple Sclerosis. **365**, 2188-2197, doi:10.1056/NEJMoa1100648 (2011).
- 14 Gouna, G. *et al.* TREM2-dependent lipid droplet biogenesis in phagocytes is required for remyelination. **218**, doi:10.1084/jem.20210227 (2021).
- 15 Shimomura, I. *et al.* Insulin resistance and diabetes mellitus in transgenic mice expressing nuclear SREBP-1c in adipose tissue: model for congenital generalized lipodystrophy. **12**, 3182-3194, doi:10.1101/gad.12.20.3182 (1998).
- 16 Wu, J. *et al.* Beige Adipocytes Are a Distinct Type of Thermogenic Fat Cell in Mouse and Human. **150**, 366-376, doi:10.1016/j.cell.2012.05.016 (2012).

- 17 de Jong, C. G. H. M., Gabius, H.-J. & Baron, W. The emerging role of galectins in (re)myelination and its potential for developing new approaches to treat multiple sclerosis. **77**, 1289-1317, doi:10.1007/s00018-019-03327-7 (2020).
- 18 Jeffery, N. D. & Blakemore, W. F. Remyelination of mouse spinal cord axons demyelinated by local injection of lysolecithin. **24**, 775-781, doi:10.1007/BF01191213 (1995).
- 19 Lloyd, A. F. *et al.* Central nervous system regeneration is driven by microglia necroptosis and repopulation. **22**, 1046-1052, doi:10.1038/s41593-019-0418-z (2019).
- 20 Plemel, J. R. *et al.* Microglia response following acute demyelination is heterogeneous and limits infiltrating macrophage dispersion. **6**, doi:10.1126/sciadv.aay6324 (2020).
- 21 González-Blázquez, R. *et al.* Relevance of control diet choice in metabolic studies: impact in glucose homeostasis and vascular function. **10**, 2902, doi:10.1038/s41598-020-59674-0 (2020).
- 22 Pellizzon, M. A. & Ricci, M. R. The common use of improper control diets in diet-induced metabolic disease research confounds data interpretation: the fiber factor. **15**, 3, doi:10.1186/s12986-018-0243-5 (2018).
- 23 van der Veen, J. N. *et al.* The critical role of phosphatidylcholine and phosphatidylethanolamine metabolism in health and disease. **1859**, 1558-1572, doi:10.1016/j.bbamem.2017.04.006 (2017).
- 24 Quinville, B. M., Deschenes, N. M., Ryckman, A. E. & Walia, J. S. A Comprehensive Review: Sphingolipid Metabolism and Implications of Disruption in Sphingolipid Homeostasis. **22**, 5793, doi:10.3390/ijms22115793 (2021).
- 25 Haus, J. M. *et al.* Plasma Ceramides Are Elevated in Obese Subjects With Type 2 Diabetes and Correlate With the Severity of Insulin Resistance. **58**, 337-343, doi:10.2337/db08-1228 (2009).
- 26 Wang, Z. *et al.* Gut flora metabolism of phosphatidylcholine promotes cardiovascular disease. **472**, 57-63, doi:10.1038/nature09922 (2011).
- 27 Zordoky, B. N. *et al.* Metabolomic Fingerprint of Heart Failure with Preserved Ejection Fraction. **10**, e0124844, doi:10.1371/journal.pone.0124844 (2015).
- 28 Li, L. *et al.* Identification of type 2 diabetes subgroups through topological analysis of patient similarity. **7**, doi:10.1126/scitranslmed.aaa9364 (2015).
- 29 Soeters, M. R. *et al.* Characterization of D-3-hydroxybutyrylcarnitine (ketocarnitine): an identified ketosis-induced metabolite. **61**, 966-973, doi:10.1016/j.metabol.2011.11.009 (2012).
- 30 Fikri, A. M. *et al.* Pre-diagnostic biomarkers of type 2 diabetes identified in the UAE's obese national population using targeted metabolomics. **10**, 17616, doi:10.1038/s41598-020-73384-7 (2020).
- 31 Schooneman, M. G., Vaz, F. M., Houten, S. M. & Soeters, M. R. Acylcarnitines. **62**, 1-8, doi:10.2337/db12-0466 (2013).
- 32 Pompura, S. L. *et al.* Oleic acid restores suppressive defects in tissue-resident FOXP3 Tregs from patients with multiple sclerosis. **131**, doi:10.1172/JCI138519 (2021).

- 33 Conde, C. *et al.* The protective effect of extra-virgin olive oil in the experimental model of multiple sclerosis in the rat. **23**, 37-48, doi:10.1080/1028415X.2018.1469281 (2020).
- 34 Holeček, M. Branched-chain amino acids in health and disease: metabolism, alterations in blood plasma, and as supplements. **15**, 33, doi:10.1186/s12986-018-0271-1 (2018).
- 35 Bierhansl, L. *et al.* Thinking outside the box: non-canonical targets in multiple sclerosis. **21**, 578-600, doi:10.1038/s41573-022-00477-5 (2022).
- 36 Boulet, M. M. *et al.* Alterations of plasma metabolite profiles related to adipose tissue distribution and cardiometabolic risk. **309**, E736-E746, doi:10.1152/ajpendo.00231.2015 (2015).
- 37 Payab, M. *et al.* Metabolomics prospect of obesity and metabolic syndrome; a systematic review. **21**, 889-917, doi:10.1007/s40200-021-00917-w (2021).
- 38 You, M., Fan, R., Kim, J., Shin, S.-H. & Chung, S. Alpha-Linolenic Acid-Enriched Butter Promotes Fatty Acid Remodeling and Thermogenic Activation in the Brown Adipose Tissue. **12**, 136, doi:10.3390/nu12010136 (2020).
- 39 Abe, I. *et al.* Lipolysis-derived linoleic acid drives beige fat progenitor cell proliferation. **57**, 2623-2637.e2628, doi:10.1016/j.devcel.2022.11.007 (2022).
- 40 Lynch, C. J. & Adams, S. H. Branched-chain amino acids in metabolic signalling and insulin resistance. **10**, 723-736, doi:10.1038/nrendo.2014.171 (2014).
- 41 Yoneshiro, T. *et al.* BCAA catabolism in brown fat controls energy homeostasis through SLC25A44. **572**, 614-619, doi:10.1038/s41586-019-1503-x (2019).
- 42 Kasakin, M. F. *et al.* Targeted metabolomics approach for identification of relapsing–remitting multiple sclerosis markers and evaluation of diagnostic models. **10**, 1803-1809, doi:10.1039/C9MD00253G (2019).
- 43 Wang, M. *et al.* Carnitine Palmitoyltransferase System: A New Target for Anti-Inflammatory and Anticancer Therapy? **12**, doi:10.3389/fphar.2021.760581 (2021).
- 44 Chakraborty, A. *et al.* Vascular Endothelial Growth Factor–D (VEGF-D) Overexpression and Lymphatic Expansion in Murine Adipose Tissue Improves Metabolism in Obesity. **189**, 924-939, doi:10.1016/j.ajpath.2018.12.008 (2019).
- 45 Phan, T. T. *et al.* Increased adipose tissue lymphatic vessel density inhibits thermogenesis through elevated neurotensin levels. **11**, doi:10.3389/fcell.2023.1100788 (2023).
- 46 Oh, S. P. *et al.* Activin receptor-like kinase 1 modulates transforming growth factor- β 1 signaling in the regulation of angiogenesis. **97**, 2626-2631, doi:10.1073/pnas.97.6.2626 (2000).
- 47 Hashimoto, O. *et al.* Activin E Controls Energy Homeostasis in Both Brown and White Adipose Tissues as a Hepatokine. **25**, 1193-1203, doi:10.1016/j.celrep.2018.10.008 (2018).
- 48 Ji, L., Wu, H.-T., Qin, X.-Y. & Lan, R. Dissecting carboxypeptidase E: properties, functions and pathophysiological roles in disease. **6**, R18-R38, doi:10.1530/EC-17-0020 (2017).
- 49 Gaspar, R. C., Pauli, J. R., Shulman, G. I. & Muñoz, V. R. An update on brown adipose tissue biology: a discussion of recent findings. **320**, 488-495, doi:10.1152/AJPENDO.00310.2020 (2021).

- 50 Medak, K. D., McKie, G. L., Shamshoum, H., Seguin, I. & Wright, D. C. The glucose lowering effects of CL 316,243 dissipate with repeated use and are rescued by cilostamide. **10**, doi:10.14814/phy2.15187 (2022).
- 51 Tournissac, M. *et al.* Repurposing beta-3 adrenergic receptor agonists for Alzheimer's disease: beneficial effects in a mouse model. **13**, 103, doi:10.1186/s13195-021-00842-3 (2021).
- 52 Coutinho Costa, V. G., Araújo, S. E.-S., Alves-Leon, S. V. & Gomes, F. C. A. Central nervous system demyelinating diseases: glial cells at the hub of pathology. **14**, doi:10.3389/fimmu.2023.1135540 (2023).
- 53 Proulx, S. T. & Engelhardt, B. Central nervous system zoning: How brain barriers establish subdivisions for CNS immune privilege and immune surveillance. **292**, 47-67, doi:10.1111/joim.13469 (2022).
- 54 Puente-Ruiz, S. C. & Jais, A. Reciprocal signaling between adipose tissue depots and the central nervous system. **10**, doi:10.3389/fcell.2022.979251 (2022).
- 55 Cope, E. C. *et al.* Microglia Play an Active Role in Obesity-Associated Cognitive Decline. **38**, 8889-8904, doi:10.1523/JNEUROSCI.0789-18.2018 (2018).
- 56 Funcke, J.-B. & Scherer, P. E. Beyond adiponectin and leptin: adipose tissue-derived mediators of inter-organ communication. **60**, 1648-1697, doi:10.1194/jlr.R094060 (2019).
- 57 Dickerman, R. D. *et al.* Branched-Chain Amino Acids Are Neuroprotective Against Traumatic Brain Injury and Enhance Rate of Recovery: Prophylactic Role for Contact Sports and Emergent Use. **3**, 321-332, doi:10.1089/neur.2022.0031 (2022).
- 58 Fernstrom, J. D. Branched-Chain Amino Acids and Brain Function. **135**, 1539S-1546S, doi:10.1093/jn/135.6.1539S (2005).
- 59 Araújo, C. O. D. *et al.* Plasma signatures of Congenital Generalized Lipodystrophy patients identified by untargeted lipidomic profiling are not changed after a fat-containing breakfast meal. **196**, 102584, doi:10.1016/j.plefa.2023.102584 (2023).
- 60 Pifferi, F., Laurent, B. & Plourde, M. Lipid Transport and Metabolism at the Blood-Brain Interface: Implications in Health and Disease. **12**, doi:10.3389/fphys.2021.645646 (2021).
- 61 Bogie, J. F. J., Haidar, M., Kooij, G. & Hendriks, J. J. A. Fatty acid metabolism in the progression and resolution of CNS disorders. **159**, 198-213, doi:10.1016/j.addr.2020.01.004 (2020).
- 62 Penkert, H. *et al.* Proteomic and lipidomic profiling of demyelinating lesions identifies fatty acids as modulators in lesion recovery. **37**, 109898, doi:10.1016/j.celrep.2021.109898 (2021).
- 63 Wade, G., McGahee, A., Ntambi, J. M. & Simcox, J. Lipid Transport in Brown Adipocyte Thermogenesis. **12**, doi:10.3389/fphys.2021.787535 (2021).
- 64 Siddiqui, A. J. *et al.* Therapeutic Role of ELOVL in Neurological Diseases. **8**, 9764-9774, doi:10.1021/acsomega.3c00056 (2023).
- 65 Blandin, A. *et al.* Lipidomic analysis of adipose-derived extracellular vesicles reveals specific EV lipid sorting informative of the obesity metabolic state. **42**, 112169, doi:10.1016/j.celrep.2023.112169 (2023).

- 66 Momchilova, A. *et al.* Sphingolipid Catabolism and Glycerophospholipid Levels Are Altered in Erythrocytes and Plasma from Multiple Sclerosis Patients. **23**, 7592, doi:10.3390/ijms23147592 (2022).
- 67 Calderon-Dominguez, M. *et al.* Carnitine Palmitoyltransferase 1 Increases Lipolysis, UCP1 Protein Expression and Mitochondrial Activity in Brown Adipocytes. **11**, e0159399, doi:10.1371/journal.pone.0159399 (2016).
- 68 Trabjerg, M. S. *et al.* Dysregulation of metabolic pathways by carnitine palmitoyl-transferase 1 plays a key role in central nervous system disorders: experimental evidence based on animal models. **10**, 15583, doi:10.1038/s41598-020-72638-8 (2020).
- 69 Herold, J. & Kalucka, J. Angiogenesis in Adipose Tissue: The Interplay Between Adipose and Endothelial Cells. **11**, doi:10.3389/fphys.2020.624903 (2021).
- 70 Ikeda, K. & Yamada, T. UCP1 Dependent and Independent Thermogenesis in Brown and Beige Adipocytes. **11**, doi:10.3389/fendo.2020.00498 (2020).
- 71 Kazak, L. *et al.* A Creatine-Driven Substrate Cycle Enhances Energy Expenditure and Thermogenesis in Beige Fat. **163**, 643-655, doi:10.1016/j.cell.2015.09.035 (2015).
- 72 Bertholet, A. M. *et al.* Mitochondrial Patch Clamp of Beige Adipocytes Reveals UCP1-Positive and UCP1-Negative Cells Both Exhibiting Futile Creatine Cycling. **25**, 811-822.e814, doi:10.1016/j.cmet.2017.03.002 (2017).
- 73 Rosko, L. M. *et al.* Cerebral Creatine Deficiency Affects the Timing of Oligodendrocyte Myelination. **43**, 1143-1153, doi:10.1523/JNEUROSCI.2120-21.2022 (2023).
- 74 Melchor, G. S., Khan, T., Reger, J. F. & Huang, J. K. Remyelination Pharmacotherapy Investigations Highlight Diverse Mechanisms Underlying Multiple Sclerosis Progression. **2**, 372-386, doi:10.1021/acsptsci.9b00068 (2019).
- 75 Chamberlain, K. A., Chapey, K. S., Nanesco, S. E. & Huang, J. K. Creatine Enhances Mitochondrial-Mediated Oligodendrocyte Survival After Demyelinating Injury. **37**, 1479-1492, doi:10.1523/JNEUROSCI.1941-16.2016 (2017).
- 76 Kazak, L. & Cohen, P. Creatine metabolism: energy homeostasis, immunity and cancer biology. **16**, 421-436, doi:10.1038/s41574-020-0365-5 (2020).
- 77 Wang, W. *et al.* A PRDM16-Driven Metabolic Signal from Adipocytes Regulates Precursor Cell Fate. **30**, 174-189.e175, doi:10.1016/j.cmet.2019.05.005 (2019).
- 78 Stumpf, S. K. *et al.* Ketogenic diet ameliorates axonal defects and promotes myelination in Pelizaeus–Merzbacher disease. **138**, 147-161, doi:10.1007/s00401-019-01985-2 (2019).
- 79 Guo, D.-H. *et al.* Beige adipocytes mediate the neuroprotective and anti-inflammatory effects of subcutaneous fat in obese mice. **12**, 4623, doi:10.1038/s41467-021-24540-8 (2021).
- 80 Schindelin, J. *et al.* Fiji: an open-source platform for biological-image analysis. **9**, 676-682, doi:10.1038/nmeth.2019 (2012).
- 81 Bankhead, P. *et al.* QuPath: Open source software for digital pathology image analysis. **7**, 16878, doi:10.1038/s41598-017-17204-5 (2017).
- 82 Bosch-Queralt, M. *et al.* A fluorescence microscopy-based protocol for volumetric measurement of lysolecithin lesion-associated de- and re-myelination in mouse brain. **3**, 101141, doi:10.1016/j.xpro.2022.101141 (2022).

- 83 Lim, N. K.-H. *et al.* An Improved Method for Collection of Cerebrospinal Fluid from Anesthetized Mice. doi:10.3791/56774 (2018).
- 84 Diaz Marin, R., Crespo-Garcia, S., Wilson, A. M. & Sapieha, P. RELi protocol: Optimization for protein extraction from white, brown and beige adipose tissues. **6**, 918-928, doi:10.1016/j.mex.2019.04.010 (2019).
- 85 Haid, M. *et al.* Long-Term Stability of Human Plasma Metabolites during Storage at -80°C . **17**, 203-211, doi:10.1021/acs.jproteome.7b00518 (2018).
- 86 Zukunft, S. *et al.* High-throughput extraction and quantification method for targeted metabolomics in murine tissues. **14**, 18, doi:10.1007/s11306-017-1312-x (2018).
- 87 Zukunft, S., Sorgenfrei, M., Prehn, C., Möller, G. & Adamski, J. Targeted Metabolomics of Dried Blood Spot Extracts. **76**, 1295-1305, doi:10.1007/s10337-013-2429-3 (2013).
- 88 Petrera, A. *et al.* Multiplatform Approach for Plasma Proteomics: Complementarity of Olink Proximity Extension Assay Technology to Mass Spectrometry-Based Protein Profiling. **20**, 751-762, doi:10.1021/acs.jproteome.0c00641 (2021).
- 89 Assarsson, E. *et al.* Homogenous 96-Plex PEA Immunoassay Exhibiting High Sensitivity, Specificity, and Excellent Scalability. **9**, e95192, doi:10.1371/journal.pone.0095192 (2014).
- 90 Pang, Z. *et al.* MetaboAnalyst 5.0: narrowing the gap between raw spectra and functional insights. **49**, W388-W396, doi:10.1093/nar/gkab382 (2021).
- 91 Ge, S. X., Jung, D. & Yao, R. ShinyGO: a graphical gene-set enrichment tool for animals and plants. **36**, 2628-2629, doi:10.1093/bioinformatics/btz931 (2020).
- 92 Szklarczyk, D. *et al.* The STRING database in 2023: protein–protein association networks and functional enrichment analyses for any sequenced genome of interest. **51**, D638-D646, doi:10.1093/nar/gkac1000 (2023).

DISCUSSION AND FUTURE OUTLOOK

Inflammatory demyelinating diseases are distinguished by both myelin disruption and dysregulated inflammation. Among these conditions, MS is the most prevalent non-traumatic disease impacting young adults. It clinically presents with focal sensory and motor deficits, bladder and bowel dysfunction, ataxia and optic neuritis⁶. MS remains without a cure, but ongoing research focus towards effective treatment options⁷². Current ongoing studies and clinical trials primarily focus on disease-modifying treatments (DMTs), with a particular emphasis on addressing the relapsing-remitting phase of the disease and its associated peripheral inflammatory characteristics. Different DMTs focus on disease aspects such as ameliorating CNS inflammation, disinhibiting and promoting CNS recovery and ultimately providing neural protection⁷³. Nevertheless, an effective treatment for MS, especially for the progressive phase, remains elusive and our understanding of the disease's pathology is still limited.

Demyelination injury in the CNS poses a challenge to tissue remodeling and, ultimately, repair through the process of remyelination. Remyelination, a protective mechanism that naturally occurs also in healthy individuals⁴⁰, aims to restore tissue physiological functions. Tissue repair involves the generation of new myelin sheaths along nerve axons, with these sheaths integrating a multitude of essential myelin lipids. It also requires efficient phagocytosis of myelin debris, with consequent processing of its lipid components. However, under pathological conditions, remyelination can fail, leading to irreversible disabilities⁷.

1. Why remyelination fails?

An extensive body of literature tries to address this question. It has been shown that the location of lesions influences the remyelination process; cortical lesions exhibit more extensive remyelination compared to white matter lesions, whereas cerebellar and periventricular lesions demonstrate lower levels of remyelination in comparison to subcortical lesions⁷⁴⁻⁷⁷. Interestingly, a very recent study highlights the contribution of a specific brain barrier, namely the blood-cerebrospinal fluid barrier (BCSFB), in the dynamics of remyelination. Tonietto et al., through PET imaging from MS patients, showed that periventricular lesions in the white matter displayed diminished capacity for regeneration, suggesting that the anatomical region of the BCSFB can play a role to impaired remyelination⁷⁴. Thus, BCSFB serves as a crucial interface between CNS and the periphery, underscoring how the communication between the periphery and the brain actively impact in the remyelination process. Additionally, the type of lesions also influences the regeneration response. At the onset of the disease, MS lesions initiate as active lesions with elevated phagocytes (macrophage/microglia) presence across the entire lesion area. As inflammation gradually resolves, lesions can transition either to a mixed state (chronic active lesions), characterized by a persistent rim of phagocytes at the lesion border, or to

inactive lesions marked by the absence of phagocytes within the lesion area. Around 40% of lesions, whether active or inactive, showcase evident signs of robust remyelination, while chronic active lesions notably lack substantial remyelination^{26,76}. Therefore, attaining a more profound understanding of remyelination metabolism is of paramount importance.

2. Lipid metabolism and remyelination

Numerous studies in recent years have proposed a robust link between both CNS and systemic changes in lipid metabolism and their significant influence on neurodegenerative diseases, neuroinflammatory as well as neurovascular and neurological disorders^{68,78,79}. In MS, sphingolipid concentrations are reduced, while phospholipid concentrations, especially lysophosphatidylcholine (LPC), are elevated in active lesions. Similarly, LPC levels are increased in the CSF of individuals with MS⁸⁰⁻⁸². Moreover, the contribution of CNS and systemic lipid metabolism in remyelination has been documented through various studies in animal models. Investigating local CNS lipid metabolism, studies using animal models with either inflammatory or toxin-mediated demyelination strategies revealed that oligodendrocytes upregulate genes related to cholesterol and fatty acid synthesis during remyelination^{83,84}. In the same context, oligodendrocytes also rely on lipid sources provided from other CNS cells, such as astrocytes and phagocytes, to mediate an efficient regenerative response^{39,40}. Exploring systemic lipid metabolism in the periphery, prior research from our lab illustrated how obesity and specific lipid supplementation in diet alter the lesion recovery and resolution of inflammation, upon acute demyelinating injury^{85,86}. Bosch-Queralt et al. highlighted the exacerbating effect of obesity on lesion recovery and persistent inflammation⁸⁵. In a separate study, Penkert et al. demonstrated that the supplementation of highly enriched omega 6 (n-6) polyunsaturated fatty acids in the diet sustains inflammation in lesion area⁸⁶. Additionally, Bosch-Queralt et al. also illustrated alterations in the brain lipidomic profile of unlesioned mice, upon diet-induced obesity⁸⁵. These studies highlight the crosstalk between CNS and the periphery. Yet, the question arises: can lipid metabolism serve as the mediator in the intersection between the CNS and the periphery?

The communication channels from the periphery to the CNS are guarded by two critical barriers: the BBB and the BCSFB barriers. These barriers form a protective network, shielding the brain from harmful molecules and immune cells originating in the periphery, thereby maintaining the healthy homeostasis of the brain. However, under neuroinflammation, both BBB and BCSFB undertake functional and morphological changes. These alterations promote the migration of leukocytes from the bloodstream into the CSF and CNS parenchyma, leading to consequent dysfunction of neuronal and glial activity⁸⁷⁻⁸⁹. BBB exhibits compromised integrity in

MS, which is a key hallmark for the early manifestation of the disease. Research indicates that the liver X receptor- α (LXR α), a receptor integral to cholesterol and lipid metabolism, preserves BBB integrity. Experiments involving endothelial cell (EC)-specific knockdown of LXR α demonstrate increased BBB permeability both *in vitro* and *in vivo*, coupled with diminished tight junctions and elevated leukocyte infiltration. Furthermore, mice with EC-specific LXR α deficiency exhibit an amplified disease progression in the experimental autoimmune encephalomyelitis (EAE) model. These findings suggest that targeting LXR α could be a promising avenue for enhancing BBB function, providing potential insights for therapeutic interventions in MS^{80,90}. Recently, the BCSFB has emerged as a noteworthy region implicated in the pathogenesis of MS⁷⁴. Studies have confirmed that the choroid plexus in all ventricles modulates the metabolism of CNS PUFA and oversees the transport of cholesterol, utilizing multiple lipid transporters in the process⁹¹. While all evidence presented has tackled the issue of how lipid metabolism affects remyelination, there remains a gap in our understanding of the molecular mechanisms that intricately connect peripheral and focal lipid metabolism, shaping their synergistic impact on CNS tissue repair.

In this thesis, I addressed this gap; I explored the impact of dysregulated lipid metabolism on the remyelination process in two different projects - one focusing on the “local” CNS perspective (*Project 1*) and the other on the “peripheral” aspect (*Project 2*).

In *Project 1*, I addressed the role of cholesterol metabolism in acute demyelinating lesions in the CNS. I discovered that the esterification of cholesterol and its subsequent integration into the hydrophobic core of LDs, are indispensable mechanisms for an effective regenerative response and resolution of inflammation. LDs, which accumulated into CNS phagocytes, acted as buffering organelles to attenuate lipid toxicity in the cells. Lipid toxicity can arise from the release of free cholesterol during the catabolic breakdown of phagocytosed myelin debris within lysosomes. Since free cholesterol cannot be degraded, it must be directed either for efflux to the extracellular space or for storage within intracellular LDs, to mitigate cholesterol induced cellular stress. Indeed, TREM2 deficient microglia developed ER stress, due to their inability to produce LDs. This resulted in the persistence of the inflammatory response and ultimately, remyelination failure. However, upon ER stress alleviation, TREM2 KO microglia exhibited an increase in the abundance of LDs, which in turn led to the resolution of inflammation (Fig.1).

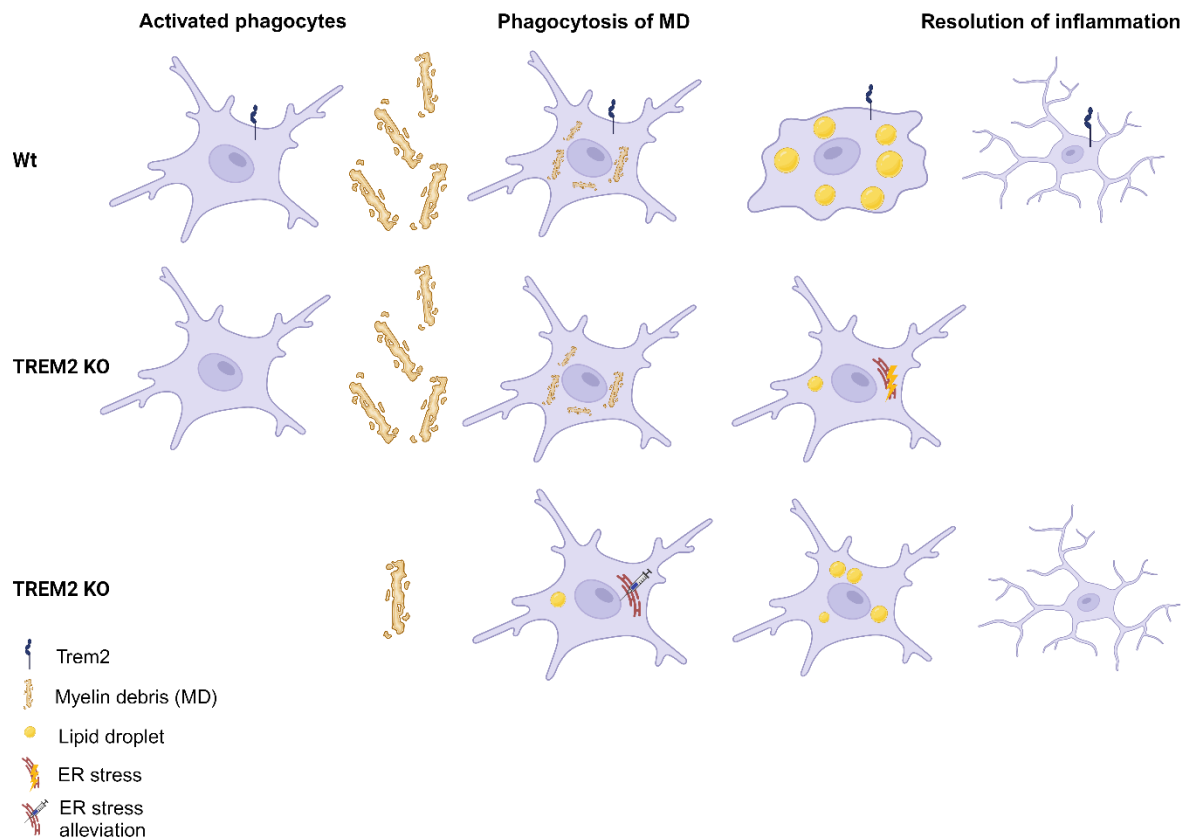


Figure 1 TREM2-dependent lipid droplet biogenesis in phagocytes is required for remyelination. In response to demyelinating stimuli in the CNS, Wt phagocytes expressing TREM2 receptor efficiently engulf myelin debris. Following phagocytosis, they intracellularly process the debris, facilitating the formation of lipid droplets and the subsequent resolution of inflammation (upper lane). Conversely, in TREM2-deficient phagocytes, myelin debris is phagocytosed but the subsequent generation of lipid droplets is impaired, leading to the accumulation of ER stress and an unresolved inflammatory state (middle lane). Pharmacological mitigation of ER stress in TREM2-deficient phagocytes, in-vitro and in-vivo, restore the production of lipid droplets, ultimately resolving inflammation (bottom lane). TREM2: triggering receptor expressed on myeloid cells 2, ER: endoplasmic reticulum, MD: myelin debris. Illustration created with BioRender.com.

These data highlight the significant role of LDs as a buffering mechanism in the lesion repair. Recent research has described that the presence of LDs attenuates remyelination in acute demyelination models^{40,92,93}. Using the cuprizone demyelination model, Loix et al. showed that PLIN2 depletion enhanced remyelination in the acute phase, suggesting that accumulation of LDs mitigates remyelination. However, expression levels of *Soat1* were not altered in PLIN2-deficient mice, indicating that the esterification of cholesterol is unaffected⁹². A growing body of evidence suggests that PLIN2 deficiency enhances the upregulation of perilipin 3 (PLIN3) in cardiomyocytes⁹⁴, hepatocytes⁹⁵ and adrenal cortex⁹⁶, and that PLIN3 is highly expressed in human white matter⁹⁷. PLIN3 belongs to the perilipin family as PLIN2 and is one of the main proteins in LD proteome, which is ubiquitously expressed in all cell types⁹⁸. Thereby, these studies propose a potential

compensatory mechanism for PLIN3 upregulation upon PLIN2 deficiency. Moreover, in acute demyelination state, Berghoff et al. showed that, in cholesterol synthesis deficient mice, accumulation of LDs worsens the regenerative response, without providing any evidence of *Soat1* expression or protein levels⁴⁰. Likewise, Nugent et al. demonstrated that TREM2 depleted microglia accumulate LDs⁹³. Both studies employed the cuprizone-induced demyelination model, which could potentially yield additional implications in cholesterol and TREM2 deficient mice. In this project, I used the SOAT1/ACAT1 deficient mouse model, directly targeting cholesterol esterification. It has been observed that SOAT1, an ER-residing enzyme, utilizes LCFAs as substrates, incorporating them into free cholesterol to generate cholesterol esters within LDs⁹⁹. I observed that SOAT1 depletion completely abolished the accumulation of LDs and lessened remyelination. Importantly, inflammation persisted throughout this process, providing direct evidence that LDs exert a protective buffering mechanism in lesion repair.

In *Project 2*, I addressed how peripheral lipid storage deficiency, in the context of lipodystrophy, impacts the process of regeneration, upon acute demyelination stimuli. To my knowledge, this is the first study that characterizes the “lipodystrophy” brain. Unexpectedly, I observed that lesion repair and resolution of inflammation are enhanced in lipodystrophic mice lacking WAT, displaying an enlarged BAT, with possibly BeAT characteristics, and exhibiting diabetic conditions. Metabolomic analysis of the plasma from lipodystrophic mice revealed an elevation in PCs and SM containing polyunsaturated LCFAs and one acylcarnitine species, which potentially carries oleic acid. Notably, both oleic acid and polyunsaturated LCFAs have been previously associated with promoting lesion recovery and resolution of inflammation^{86,100,101}, highlighting the importance of circulating individual lipid species in the context of improved remyelination. Interestingly, BCAAs levels were also markedly increased in the plasma of lipodystrophic mice. A recent study showed significant decrease of BCAAs levels in the plasma of relapsing-remitting MS patients¹⁰², emphasizing the potential importance of BCAAs in remyelination. In addition, pathway enrichment analysis suggested the potential activation of BAT thermogenesis and the biogenesis of BeAT, as evidenced by the enrichment of pathways central to these processes. Subsequent proteomic analysis from isolated BAT showed that lipodystrophic mice upregulate proinflammatory cytokines and chemokines, secreted molecules and lysosomal proteins. Of note, pathway enrichment analysis from BAT also indicated pathways correlated to BAT thermogenesis mechanism, due to the increased abundance of markers associated with endothelial cell metabolism and lymphangiogenesis. However, pharmacological activation of UCP1-dependent BAT thermogenesis in demyelinating lesioned Wt mice failed to improve lesion recovery or inflammation.

The findings from *Project 2* propose that the absence of WAT ameliorates lesion repair and improves remyelination capacity. This discovery was unexpected, as our initial hypothesis posited that the lipodystrophy model would resemble the impact of

obesity on the regeneration response, as previously described by our lab⁸⁵. The lipodystrophy model is distinguished by an enlarged BAT, which the original study suggested resembles a WAT phenotype¹⁰³. BAT has been a subject of debate within the scientific community, initially considered completely absent from adults. Nonetheless, research over the last 15 years has conclusively established both the existence and metabolic significance of BAT in human adults^{104,105}. Recent research has been dedicated to exploring whether the metabolic activation of BAT can improve obesity phenotype. This highlights that concomitant BAT stimulation and WAT depletion, achieved through controlled cold exposure or thermogenesis-induced diets, show promising preliminary results. Also, pilot studies investigate the potential beneficial effects of either transplanting BAT or promoting the formation of BeAT depots within WAT to address obesity^{105,106}. In my study, I hypothesize that lipodystrophic BAT has the potential to adopt a BeAT phenotype, since H&E staining showed multilocular adipocytes, which closely resemble beige adipocytes. This finding, in combination with our metabolomic and proteomic data pointing out enriched thermogenesis pathways, led us to investigate the impact of UCP1-dependent activation of thermogenesis in lesion repair. The negative outcome of this tactic prompt us to follow a different line for our forthcoming experiments, which will focus on exploring the UCP1-independent thermogenesis pathways and investigating the involvement of BAT and BeAT metabolism in the remyelination process.

Both projects of my thesis emphasized on the impact of abnormal lipid metabolism in lesion recovery and resolution of inflammation in acute demyelination. I approached this topic from a dual perspective, including adipose tissue and CNS lipid metabolism properties. In the CNS pathology, lipid incorporation into LDs has been described to have either a protective or detrimental effect, which is highly dependable on the disease characteristics¹⁰⁷. In my thesis we challenged this notion, exploring how lipid storage affects the regenerative response. A molecular link between my two projects is the function of TREM2, a lipid receptor that is expressed on myeloid cells and in the CNS microglia¹⁰⁸. In *Project 1* I directly addressed how TREM2 total absence affect the remyelination capacity. I found that, TREM2 dependent biogenesis of LDs is a prerequisite for resolution of inflammation, highlighting the significance of lipid storage in the CNS, upon demyelinating injury. Interestingly, a recent study identified TREM2 as the main lipid receptor that govern lipid-associated macrophages (LAM) metabolism in the adipose tissue, within the context of obesity. LAM is also strongly correlated with increased lysosomal metabolism, highlighting the central role of lipid processing and signaling in the immune response¹⁰⁹. It is tempting to speculate that lipid processing, either focally in the adipose tissue or systemically via their secretion in the periphery, impact severely lesion recovery upon acute demyelination. It has been documented that circulating polyunsaturated LCFAs cross the brain barriers (BBB or BCSFB) and maintain CNS homeostatic lipid composition⁹¹, further enhancing our hypothesis. Another interesting finding from *Project 2* is the upregulation of BCAAs in the plasma of lipodystrophic mice. It is known that BCAAs

also cross the BBB through specific transporters¹¹⁰. This provides an additional potential explanation for the enhanced lesion recovery observed in lipodystrophic mice, further underscoring the importance of peripheral metabolism and its impact on the CNS response to injury. Undoubtedly, the data presented in my thesis, along with seminal work conducted by other researchers, emphasize the prominent role of lipid metabolism. This focus aims to elucidate the molecular mechanisms restricting effective regeneration capacity and seeks to identify targets for enhancing the efficiency or remyelination.

3. Limitations and Future perspectives

In this study, I aim to actively contribute to the scientific comprehension of the molecular mechanisms governing demyelination and the consequent remyelination response through lipid metabolism. Our collective objective is to improve treatment options in MS. Nevertheless, it is crucial to acknowledge that my experimental approach is bound to certain fundamental limitations, nicely described in a very recent review (Fig. 2)⁷⁶.

For the study of demyelination-remyelination, two commonly models are employed; the lysolecithin and cuprizone models. In both instances, demyelination is triggered by toxins, resulting in lesions that closely resemble the monofocal and monophasic nature, observed in active MS lesions. At the peak of demyelination in both models, there is a complete loss of mature oligodendrocytes, and subsequent remyelination occurs over the span of some weeks. In contrast, demyelination in MS is initiated by the activation of immune system, resulting in a spectrum of lesions, including active, chronic active (mixed state) and inactive lesions. Notably, in MS active lesions, a proportion of mature oligodendrocytes manages to survive and the process of remyelination can extend over months to years, representing a continuous and dynamic repair mechanism^{76,111}.

In addition, the inflammatory response differs markedly between animal models and human MS. In animal models, the demyelination state encompasses a brief pro-inflammatory phase, with a focus on phagocytes engulfing myelin debris and consequent recruitment of immune cells. The remyelination state is characterized by the removal of the demyelinating stimuli, leading to extensive regeneration and resolution of inflammation, facilitated by a more protective lesion environment and the function of immune cells. Consequently, animal models illustrate a relatively high intrinsic capacity for lesion repair. By contrast, in human MS, a plethora of lesions persevere throughout lifetime, featuring simultaneous ongoing proinflammation and reparatory stimuli. A longitudinal imaging study in MS patients showed repeated demyelinating and remyelinating waves, indicating a low intrinsic remyelinating capacity^{112,113}. Finally, the effect of aging in the process of remyelination in human MS remains unknown, whereas, in animal models, this aspect has been investigated (Fig. 2)⁷⁶.

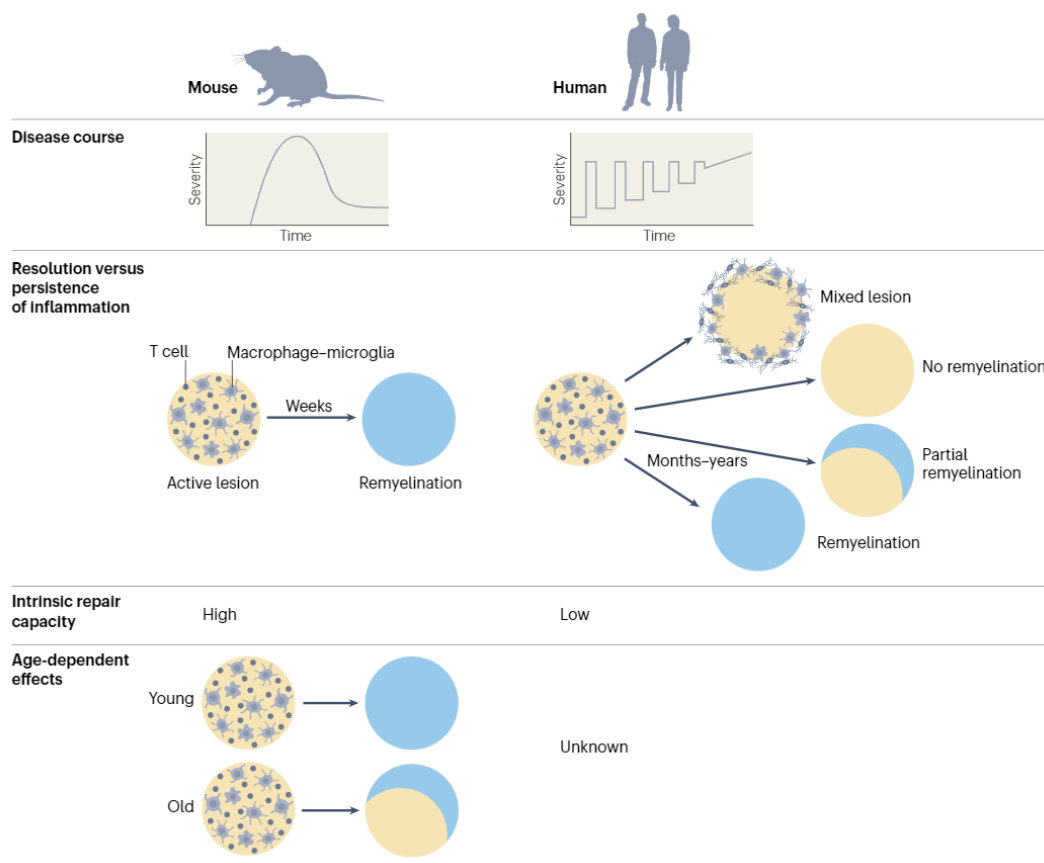


Figure 2 Disease manifestation in animal models of MS compared to the human phenotype. The MS disease course consists of a chronic and diverse phenotype, while commonly used animal models, such as lysolecithin or cuprizone models, exhibit a monophasic nature. In both animal models of demyelination, inflammation subsides and the regenerative response occurs extensively and rapidly, following the cessation of demyelinating trigger. This process indicates a robust intrinsic repair mechanism of oligodendrocytes. The lesion outcome in demyelinating murine models is closely resembling only one type of MS lesions, the active lesions. Conversely, in MS patients, the lesions outcome can vary, with active lesions transforming into chronic active lesions (mixed state), remaining completely demyelinated, despite inflammation resolution or displaying multiple degrees of regeneration. In addition, just a minority of lesions in MS patients exhibit significant remyelination, suggesting a defective intrinsic repair mechanism in human oligodendrocytes may prompt this outcome. In young murine models, OPCs substantially proliferate, migrate and differentiate into mOLGs, leading in effective regenerative response. However, regeneration capacity declines in aged mice. The impact of age on remyelination in individuals with MS has yet to be studied. Data source: Reproduced with permission from Springer Nature; Klotz, Antel and Kuhlmann, Inflammation in multiple sclerosis: consequences for remyelination and disease progression., *Nat. Rev. Neurol.*, Volume 19, 311, 2023, Springer Nature⁷⁶.

Considering all the factors mentioned above, the future outlook should prioritize the utilization of improved experimental models to ensure successful translation of findings from animals to meaningful outcomes in humans. One avenue for enhancement involves refining animal models to specifically target the clinical implications of successful remyelination, with a focus on ameliorating the disease

phenotype in humans - potentially slowing down, stabilizing or even improve it. Also, the use of human induced pluripotent stem cells (iPSC), either in single, co-cultures or in organoids with different cell types of human origin, represents another promising approach. Nevertheless, the challenge lies in the fact that these cultures do not constitute a whole organism. Ideally, both cell culture and animal models should facilitate highly reproducible, standardized and rapid screening of drug candidates. They should also accurately mirror crucial facets of remyelination in the presence of inflammatory conditions. Such a holistic approach is vital for progressing our comprehension and expanding treatment options for demyelinating disorders⁷⁶.

Over the past ten years, a variety of novel technologies have contributed to a deeper comprehension of the underlying mechanisms behind MS. Among these, a widely utilized method is single-cell RNA (scRNA) sequencing, which has proven instrumental in analyzing gene expression in glial and neuronal cells⁷⁶. Interestingly, one recent study performed scRNA sequencing of postmortem brains from MS patients. This study identified multiple oligodendrocyte subclusters, with certain subclusters exhibiting lower representation in MS tissue, while others displayed increase prevalence. Notably, analogous alterations were identified in normal-appearing white matter, challenging the notion that MS is solely characterized focal demyelination and highlighting its more diffuse nature¹¹⁴. While scRNA has a limitation in spatial resolution, this gap is addressed by a complementary technique known as spatial transcriptomics. Spatial transcriptomics involves mapping messenger RNA (mRNA) expression profiles in individual cells or cell clusters to specific tissue regions. Such precision proves particularly beneficial in diseases like MS, characterized by diverse cell populations⁷⁶. Thus, it becomes apparent that emerging methodological techniques make it possible to investigate tissue from MS patients and are opening pathways to a more comprehensive understanding of the metabolic nature in MS lesions. The next crucial step is to address lipid metabolism and precisely target the impact of individual lipids and lipid storage within remyelinating lesions, utilizing these new techniques.

The evolution of spatial transcriptomics, coupled with cutting-edge electron microscopy techniques, has paved the way for better characterization of the comprehensive omic profile of these lesions. Indeed, in our recent method study, we employed spatial transcriptomics in combination with correlated electron microscopy to meticulously characterize remyelinating lesions. As anticipated, our findings reveal that the center of the remyelinating lesion is populated by foamy microglia, lipid-loaded¹¹⁵, indicating that new techniques will elucidate the lipidic profile of the remyelinating regions. Yet, a compelling prospect lies in monitoring the trajectory by which peripheral lipid metabolism or distinct lipids from the periphery intricately traverse into the brain, directly influencing the remyelination process. The emerging fields of spatial lipidomics and spatial single cell metabolomics can shed light on the lipid signature of remyelinating lesions^{116,117}. Lipidomics focuses on examining the lipidome, which comprises the entirety of chemically diverse lipid species in a

biological system¹¹⁸. The integration of spatial omic technology has proven revolutionary in the field of lipidomics, since it is essential to understand the distinct lipid composition in cells or cell clusters from MS patients in comparison to those from healthy donors. This approach enables the interpretation of potential differences under the scope of biological significance.

Moreover, the utilization of targeted lipid-probes, specifically designed not to disrupt endogenous cellular functions, *in vitro* or *in vivo* can provide valuable insights into the origin of these lipids. Recently, probes were developed using the “click-cage” structure technique. These structures are designed to be coupled with specific lipids and provide the capability to attach to targeted organelles through click chemistry. Currently, the click-caged lipid probes are used in *in vitro* experimental settings¹¹⁹. Employing this innovative approach, we can evaluate the distinct lipid composition of specific organelles, such as lipid droplets, in different pathological conditions. Notably, these lipid probes can also facilitate the significance of signaling events between different intracellular organelles¹¹⁹. In addition, there is potential to trace the origins of specific lipids and monitor their pathways within the body. Are they originating from the periphery crossing the BBB and actively contributing to the lesion repair? Alternatively, could these lipids be influencing peripheral organs to secrete other potentially significant molecules that enhance the regenerative response? Future directions can focus on effectively monitoring these probes in *in vivo* experiments, utilizing the recent advancements in two-photon¹²⁰ and three-photon¹²¹ microscopy live imaging. These approaches enable us to dynamically observe the movement of lipids within the brain and intracellularly in specific cells in real-time. Certainly, recent advancements in lipid research can be valuable tools for actively illustrating the complex intercommunication between periphery and the CNS, particularly concerning the process of remyelination.

In conclusion, lipid metabolism has already been proved to contribute in many pathophysiological conditions, highlighting the role of lipids. The term “lipids” made its appearance in the scientific community a mere century ago, when Gabriel Bertrand introduced “lipids” in his paper “Projet de reforme de la nomenclature de chimie biologique”¹²². However, only recently and with the assistance of new technological methods we are able to understand, evaluate and appreciate the importance of lipids in health and disease. Given that the brain is the second most lipid enriched organ in the human body⁶¹, it highlights the significance of lipids in neurodegenerative and neuroinflammatory diseases. Lipids, functioning as structural components and as signaling molecules or forming storage organelles, contribute to every facet of homeostatic health. Thus, it is evident that the future direction should prioritize a deeper exploration of lipid metabolism. This exploration should seek to comprehend why irregular lipid metabolism exerts a pivotal influence in the pathophysiology of demyelinating diseases and how alleviating lipid dysregulation can contribute to the development of more efficient treatments. In this regard, lipids take center stage, demanding in-depth investigation and recognition for their paramount importance.

REFERENCES

- 1 Wallin, M. T. *et al.* Global, regional, and national burden of multiple sclerosis 1990–2016: a systematic analysis for the Global Burden of Disease Study 2016. **18**, 269-285, doi:10.1016/S1474-4422(18)30443-5 (2019).
- 2 Walton, C. *et al.* Rising prevalence of multiple sclerosis worldwide: Insights from the Atlas of MS, third edition. **26**, 1816-1821, doi:10.1177/1352458520970841 (2020).
- 3 Bebo, B. *et al.* The Economic Burden of Multiple Sclerosis in the United States. **98**, e1810-e1817, doi:10.1212/WNL.0000000000200150 (2022).
- 4 Kobelt, G., Thompson, A., Berg, J., Gannedahl, M. & Eriksson, J. New insights into the burden and costs of multiple sclerosis in Europe. **23**, 1123-1136, doi:10.1177/1352458517694432 (2017).
- 5 Eshaghi, A., Young, A.L., Wijeratne, P.A. *et al.* Identifying multiple sclerosis subtypes using unsupervised machine learning and MRI data. *Nat Commun* **12**, 2078 (2021). <https://doi.org/10.1038/s41467-021-22265-2>
- 6 Coutinho Costa, V. G., Araújo, S. E.-S., Alves-Leon, S. V. & Gomes, F. C. A. Central nervous system demyelinating diseases: glial cells at the hub of pathology. **14**, doi:10.3389/fimmu.2023.1135540 (2023).
- 7 Franklin, R. J. M. & ffrench-Constant, C. Regenerating CNS myelin — from mechanisms to experimental medicines. **18**, 753-769, doi:10.1038/nrn.2017.136 (2017).
- 8 SMITH, K. J., BLAKEMORE, W. F. & MCDONALD, W. I. Central remyelination restores secure conduction. **280**, 395-396, doi:10.1038/280395a0 (1979).
- 9 ffrench-Constant, C. & Raff, M. C. Proliferating bipotential glial progenitor cells in adult rat optic nerve. **319**, 499-502, doi:10.1038/319499a0 (1986).
- 10 Lachapelle, F. *et al.* Transplantation of CNS Fragments into the Brain of Shiverer Mutant Mice: Extensive Myelination by Implanted Oligodendrocytes. **6**, 325-334, doi:10.1159/000112359 (1983).
- 11 Duncan, I. D. *et al.* The adult oligodendrocyte can participate in remyelination. **115**, doi:10.1073/pnas.1808064115 (2018).
- 12 Mezydło, A. *et al.* Remyelination by surviving oligodendrocytes is inefficient in the inflamed mammalian cortex. **111**, 1748-1759.e1748, doi:10.1016/j.neuron.2023.03.031 (2023).
- 13 Kotter, M. R., Li, W.-W., Zhao, C. & Franklin, R. J. M. Myelin Impairs CNS Remyelination by Inhibiting Oligodendrocyte Precursor Cell Differentiation. **26**, 328-332, doi:10.1523/JNEUROSCI.2615-05.2006 (2006).
- 14 Lloyd, A. F. & Miron, V. E. The pro-remyelination properties of microglia in the central nervous system. **15**, 447-458, doi:10.1038/s41582-019-0184-2 (2019).
- 15 Keren-Shaul, H. *et al.* A Unique Microglia Type Associated with Restricting Development of Alzheimer’s Disease. **169**, 1276-1290.e1217, doi:10.1016/j.cell.2017.05.018 (2017).
- 16 Krasemann, S. *et al.* The TREM2-APOE Pathway Drives the Transcriptional Phenotype of Dysfunctional Microglia in Neurodegenerative Diseases. **47**, 566-581.e569, doi:10.1016/j.immuni.2017.08.008 (2017).

- 17 Skripuletz, T. *et al.* Astrocytes regulate myelin clearance through recruitment of microglia during cuprizone-induced demyelination. **136**, 147-167, doi:10.1093/brain/aws262 (2013).
- 18 Rawji, K. S., Gonzalez Martinez, G. A., Sharma, A. & Franklin, R. J. M. The Role of Astrocytes in Remyelination. **43**, 596-607, doi:10.1016/j.tins.2020.05.006 (2020).
- 19 BLAKEMORE, W. F. Pattern of remyelination in the CNS. **249**, 577-578, doi:10.1038/249577a0 (1974).
- 20 Duncan, I. D., Marik, R. L., Broman, A. T. & Heidari, M. Thin myelin sheaths as the hallmark of remyelination persist over time and preserve axon function. **114**, doi:10.1073/pnas.1714183114 (2017).
- 21 Poitelon, Y., Kopec, A. M. & Belin, S. Myelin Fat Facts: An Overview of Lipids and Fatty Acid Metabolism. **9**, 812, doi:10.3390/cells9040812 (2020).
- 22 Grassi, S. *et al.* Lipid rafts and neurodegeneration: structural and functional roles in physiologic aging and neurodegenerative diseases. **61**, 636-654, doi:10.1194/jlr.TR119000427 (2020).
- 23 Howie, D., Bokum, A. T., Necula, A. S., Cobbold, S. P. & Waldmann, H. The role of lipid metabolism in T lymphocyte differentiation and survival. **8**, 322986, doi:10.3389/FIMMU.2017.01949/BIBTEX (2018).
- 24 Pineda-Torra, I., Siddique, S., Waddington, K. E., Farrell, R. & Jury, E. C. Disrupted Lipid Metabolism in Multiple Sclerosis: A Role for Liver X Receptors? **12**, doi:10.3389/fendo.2021.639757 (2021).
- 25 Dendrou, C. A., Fugger, L. & Friese, M. A. Immunopathology of multiple sclerosis. **15**, 545-558, doi:10.1038/nri3871 (2015).
- 26 Stadelmann, C., Timmler, S., Barrantes-Freer, A. & Simons, M. Myelin in the Central Nervous System: Structure, Function, and Pathology. **99**, 1381-1431, doi:10.1152/physrev.00031.2018 (2019).
- 27 Luo, L. & Liu, M. Adipose tissue in control of metabolism. **231**, R77-R99, doi:10.1530/JOE-16-0211 (2016).
- 28 Tracey, T. J., Kirk, S. E., Steyn, F. J. & Ngo, S. T. The role of lipids in the central nervous system and their pathological implications in amyotrophic lateral sclerosis. **112**, 69-81, doi:10.1016/j.semcd.2020.08.012 (2021).
- 29 Kister, A. & Kister, I. Overview of myelin, major myelin lipids, and myelin-associated proteins. **10**, doi:10.3389/fchem.2022.1041961 (2023).
- 30 Barnes-Vélez, J. A., Aksoy Yasar, F. B. & Hu, J. Myelin lipid metabolism and its role in myelination and myelin maintenance. **4**, 100360, doi:10.1016/j.xinn.2022.100360 (2023).
- 31 Korade, Z. & Kenworthy, A. K. Lipid rafts, cholesterol, and the brain. **55**, 1265-1273, doi:10.1016/j.neuropharm.2008.02.019 (2008).
- 32 Saher, G., Quintes, S. & Nave, K.-A. Cholesterol: A Novel Regulatory Role in Myelin Formation. **17**, 79-93, doi:10.1177/1073858410373835 (2011).
- 33 Berghoff, S. A., Spieth, L. & Saher, G. Local cholesterol metabolism orchestrates remyelination. **45**, 272-283, doi:10.1016/j.tins.2022.01.001 (2022).

- 34 Björkhem, I., Leoni, V. & Meaney, S. Genetic connections between neurological disorders and cholesterol metabolism. **51**, 2489-2503, doi:10.1194/jlr.R006338 (2010).
- 35 Dietschy, J. M. Central nervous system: cholesterol turnover, brain development and neurodegeneration. **390**, 287-293, doi:10.1515/BC.2009.035 (2009).
- 36 Saher, G. *et al.* High cholesterol level is essential for myelin membrane growth. **8**, 468-475, doi:10.1038/nn1426 (2005).
- 37 Wang, H. & Eckel, R. H. What are lipoproteins doing in the brain? **25**, 8-14, doi:10.1016/j.tem.2013.10.003 (2014).
- 38 Camargo, N. *et al.* Oligodendroglial myelination requires astrocyte-derived lipids. **15**, e1002605, doi:10.1371/journal.pbio.1002605 (2017).
- 39 Molina-Gonzalez, I. *et al.* Astrocyte-oligodendrocyte interaction regulates central nervous system regeneration. **14**, 3372, doi:10.1038/s41467-023-39046-8 (2023).
- 40 Berghoff, S. A. *et al.* Microglia facilitate repair of demyelinated lesions via post-squalene sterol synthesis. **24**, 47-60, doi:10.1038/s41593-020-00757-6 (2021).
- 41 Berghoff, S. A. *et al.* Neuronal cholesterol synthesis is essential for repair of chronically demyelinated lesions in mice. **37**, 109889, doi:10.1016/j.celrep.2021.109889 (2021).
- 42 Greaves, D. R. & Gordon, S. Thematic review series: The Immune System and Atherogenesis. Recent insights into the biology of macrophage scavenger receptors. **46**, 11-20, doi:10.1194/jlr.R400011-JLR200 (2005).
- 43 Grajchen, E., Hendriks, J. J. A. & Bogie, J. F. J. The physiology of foamy phagocytes in multiple sclerosis. **6**, 124, doi:10.1186/s40478-018-0628-8 (2018).
- 44 Wang, X. *et al.* Macrophages in spinal cord injury: Phenotypic and functional change from exposure to myelin debris. **63**, 635-651, doi:10.1002/glia.22774 (2015).
- 45 Sun, X. *et al.* Myelin Activates FAK/Akt/NF-κB Pathways and Provokes CR3-Dependent Inflammatory Response in Murine System. **5**, e9380, doi:10.1371/journal.pone.0009380 (2010).
- 46 Kroner, A. *et al.* TNF and Increased Intracellular Iron Alter Macrophage Polarization to a Detrimental M1 Phenotype in the Injured Spinal Cord. **83**, 1098-1116, doi:10.1016/j.neuron.2014.07.027 (2014).
- 47 Bogie, J. F. J. *et al.* Myelin-Derived Lipids Modulate Macrophage Activity by Liver X Receptor Activation. **7**, e44998, doi:10.1371/journal.pone.0044998 (2012).
- 48 Bogie, J. F. *et al.* Myelin alters the inflammatory phenotype of macrophages by activating PPARs. **1**, 43, doi:10.1186/2051-5960-1-43 (2013).
- 49 Mailleux, J. *et al.* Active liver X receptor signaling in phagocytes in multiple sclerosis lesions. **24**, 279-289, doi:10.1177/1352458517696595 (2018).
- 50 Cantuti-Castelvetri, L. *et al.* Defective cholesterol clearance limits remyelination in the aged central nervous system. **359**, 684-688, doi:10.1126/science.aan4183 (2018).
- 51 Farese, R. V. & Walther, T. C. Lipid Droplets Finally Get a Little R-E-S-P-E-C-T. **139**, 855-860, doi:10.1016/j.cell.2009.11.005 (2009).

- 52 Coleman, R. A. The “discovery” of lipid droplets: A brief history of organelles hidden in plain sight. **1865**, 158762, doi:10.1016/j.bbalip.2020.158762 (2020).
- 53 Olzmann, J. A. & Carvalho, P. Dynamics and functions of lipid droplets. **20**, 137-155, doi:10.1038/s41580-018-0085-z (2019).
- 54 Singh, R. *et al.* Autophagy regulates lipid metabolism. **458**, 1131-1135, doi:10.1038/nature07976 (2009).
- 55 Kaushik, S. & Cuervo, A. M. Degradation of lipid droplet-associated proteins by chaperone-mediated autophagy facilitates lipolysis. **17**, 759-770, doi:10.1038/ncb3166 (2015).
- 56 Walther, T. C., Chung, J. & Farese, R. V. Lipid Droplet Biogenesis. **33**, 491-510, doi:10.1146/annurev-cellbio-100616-060608 (2017).
- 57 Zadoorian, A., Du, X. & Yang, H. Lipid droplet biogenesis and functions in health and disease. **19**, 443-459, doi:10.1038/s41574-023-00845-0 (2023).
- 58 Walther, T. C. & Farese, R. V. Lipid Droplets and Cellular Lipid Metabolism. **81**, 687-714, doi:10.1146/annurev-biochem-061009-102430 (2012).
- 59 Missaglia, S., Coleman, R., Mordente, A. & Tavian, D. Neutral Lipid Storage Diseases as Cellular Model to Study Lipid Droplet Function. **8**, 187, doi:10.3390/cells8020187 (2019).
- 60 Onal, G., Kutlu, O., Gozuacik, D. & Dokmeci Emre, S. Lipid Droplets in Health and Disease. **16**, 128, doi:10.1186/s12944-017-0521-7 (2017).
- 61 Ralhan, I., Chang, C.-L., Lippincott-Schwartz, J. & Ioannou, M. S. Lipid droplets in the nervous system. **220**, doi:10.1083/jcb.202102136 (2021).
- 62 Farmer, B. C., Walsh, A. E., Kluemper, J. C. & Johnson, L. A. Lipid Droplets in Neurodegenerative Disorders. **14**, doi:10.3389/fnins.2020.00742 (2020).
- 63 Kunjathoor, V. V., Tseng, A. A., Medeiros, L. A., Khan, T. & Moore, K. J. β -Amyloid promotes accumulation of lipid peroxides by inhibiting CD36-mediated clearance of oxidized lipoproteins. **1**, 23, doi:10.1186/1742-2094-1-23 (2004).
- 64 Ioannou, M. S. *et al.* Neuron-Astrocyte Metabolic Coupling Protects against Activity-Induced Fatty Acid Toxicity. **177**, 1522-1535.e1514, doi:10.1016/j.cell.2019.04.001 (2019).
- 65 Rambold, Angelika S., Cohen, S. & Lippincott-Schwartz, J. Fatty Acid Trafficking in Starved Cells: Regulation by Lipid Droplet Lipolysis, Autophagy, and Mitochondrial Fusion Dynamics. **32**, 678-692, doi:10.1016/j.devcel.2015.01.029 (2015).
- 66 Liu, L. *et al.* Glial Lipid Droplets and ROS Induced by Mitochondrial Defects Promote Neurodegeneration. **160**, 177-190, doi:10.1016/j.cell.2014.12.019 (2015).
- 67 Zwick, R. K., Guerrero-Juarez, C. F., Horsley, V. & Plikus, M. V. Anatomical, Physiological, and Functional Diversity of Adipose Tissue. **27**, 68-83, doi:10.1016/j.cmet.2017.12.002 (2018).
- 68 Versini, M., Jeandel, P.-Y., Rosenthal, E. & Shoenfeld, Y. Obesity in autoimmune diseases: Not a passive bystander. **13**, 981-1000, doi:10.1016/j.autrev.2014.07.001 (2014).
- 69 Caron, A., Lee, S., Elmquist, J. K. & Gautron, L. Leptin and brain–adipose crosstalks. **19**, 153-165, doi:10.1038/nrn.2018.7 (2018).

- 70 Guilherme, A., Henriques, F., Bedard, A. H. & Czech, M. P. Molecular pathways linking adipose innervation to insulin action in obesity and diabetes mellitus. **15**, 207-225, doi:10.1038/s41574-019-0165-y (2019).
- 71 Correale, J. & Marrodan, M. Multiple sclerosis and obesity: The role of adipokines. **13**, doi:10.3389/fimmu.2022.1038393 (2022).
- 72 Dobson, R. & Giovannoni, G. Multiple sclerosis – a review. **26**, 27-40, doi:10.1111/ene.13819 (2019).
- 73 Oh, J. & Bar-Or, A. Emerging therapies to target CNS pathophysiology in multiple sclerosis. **18**, 466-475, doi:10.1038/s41582-022-00675-0 (2022).
- 74 Tonietto, M. *et al.* Periventricular remyelination failure in multiple sclerosis: a substrate for neurodegeneration. **146**, 182-194, doi:10.1093/brain/awac334 (2023).
- 75 Lazzarotto, A. *et al.* Clinically relevant profiles of myelin content changes in patients with multiple sclerosis: A multimodal and multicompartiment imaging study. **28**, 1881-1890, doi:10.1177/13524585221096975 (2022).
- 76 Klotz, L., Antel, J. & Kuhlmann, T. Inflammation in multiple sclerosis: consequences for remyelination and disease progression. **19**, 305-320, doi:10.1038/s41582-023-00801-6 (2023).
- 77 Albert, M., Antel, J., Brück, W. & Stadelmann, C. Extensive Cortical Remyelination in Patients with Chronic Multiple Sclerosis. **17**, 129-138, doi:10.1111/j.1750-3639.2006.00043.x (2007).
- 78 Cheng, A., Jia, W., Kawahata, I. & Fukunaga, K. A novel fatty acid-binding protein 5 and 7 inhibitor ameliorates oligodendrocyte injury in multiple sclerosis mouse models. **72**, 103582, doi:10.1016/j.ebiom.2021.103582 (2021).
- 79 Parimisetty, A. *et al.* Secret talk between adipose tissue and central nervous system via secreted factors—an emerging frontier in the neurodegenerative research. **13**, 67, doi:10.1186/s12974-016-0530-x (2016).
- 80 Bierhansl, L. *et al.* Thinking outside the box: non-canonical targets in multiple sclerosis. **21**, 578-600, doi:10.1038/s41573-022-00477-5 (2022).
- 81 Noguerras, L. *et al.* Lipid profile of cerebrospinal fluid in multiple sclerosis patients: a potential tool for diagnosis. **9**, 11313, doi:10.1038/s41598-019-47906-x (2019).
- 82 Pieragostino, D. *et al.* An integrated metabolomics approach for the research of new cerebrospinal fluid biomarkers of multiple sclerosis. **11**, 1563-1572, doi:10.1039/C4MB00700J (2015).
- 83 Dimas, P. *et al.* CNS myelination and remyelination depend on fatty acid synthesis by oligodendrocytes. **8**, doi:10.7554/eLife.44702 (2019).
- 84 Voskuhl, R. R. *et al.* Gene expression in oligodendrocytes during remyelination reveals cholesterol homeostasis as a therapeutic target in multiple sclerosis. **116**, 10130-10139, doi:10.1073/pnas.1821306116 (2019).
- 85 Bosch-Queralt, M. *et al.* Diet-dependent regulation of TGF β impairs reparative innate immune responses after demyelination. **3**, 211-227, doi:10.1038/s42255-021-00341-7 (2021).

- 86 Penkert, H. *et al.* Proteomic and lipidomic profiling of demyelinating lesions identifies fatty acids as modulators in lesion recovery. **37**, 109898, doi:10.1016/j.celrep.2021.109898 (2021).
- 87 Angelini, G., Bani, A., Constantin, G. & Rossi, B. The interplay between T helper cells and brain barriers in the pathogenesis of multiple sclerosis. **17**, doi:10.3389/fncel.2023.1101379 (2023).
- 88 Solár, P., Zamani, A., Kubíčková, L., Dubový, P. & Joukal, M. Choroid plexus and the blood–cerebrospinal fluid barrier in disease. **17**, 35, doi:10.1186/s12987-020-00196-2 (2020).
- 89 Takata, F., Nakagawa, S., Matsumoto, J. & Dohgu, S. Blood-Brain Barrier Dysfunction Amplifies the Development of Neuroinflammation: Understanding of Cellular Events in Brain Microvascular Endothelial Cells for Prevention and Treatment of BBB Dysfunction. **15**, doi:10.3389/fncel.2021.661838 (2021).
- 90 Wouters, E. *et al.* Liver X Receptor Alpha Is Important in Maintaining Blood-Brain Barrier Function. **10**, doi:10.3389/fimmu.2019.01811 (2019).
- 91 Pifferi, F., Laurent, B. & Plourde, M. Lipid Transport and Metabolism at the Blood-Brain Interface: Implications in Health and Disease. **12**, doi:10.3389/fphys.2021.645646 (2021).
- 92 Loix, M. *et al.* Perilipin-2 limits remyelination by preventing lipid droplet degradation. **79**, 515, doi:10.1007/s00018-022-04547-0 (2022).
- 93 Nugent, A. A. *et al.* TREM2 Regulates Microglial Cholesterol Metabolism upon Chronic Phagocytic Challenge. **105**, 837-854.e839, doi:10.1016/j.neuron.2019.12.007 (2020).
- 94 Mardani, I. *et al.* Plin2-deficiency reduces lipophagy and results in increased lipid accumulation in the heart. **9**, 6909, doi:10.1038/s41598-019-43335-y (2019).
- 95 Lassen, S., Grüttner, C., Nguyen-Dinh, V. & Herker, E. Perilipin-2 is critical for efficient lipoprotein and hepatitis C virus particle production. doi:10.1242/jcs.217042 (2018).
- 96 Li, Y. *et al.* Plin2 deletion increases cholesteryl ester lipid droplet content and disturbs cholesterol balance in adrenal cortex. **62**, 100048, doi:10.1016/j.jlcr.2021.100048 (2021).
- 97 Conte, M. *et al.* Expression pattern of perilipins in human brain during aging and in Alzheimer's disease. **48**, doi:10.1111/nan.12756 (2022).
- 98 Sztalryd, C. & Brasaemle, D. L. The perilipin family of lipid droplet proteins: Gatekeepers of intracellular lipolysis. **1862**, 1221-1232, doi:10.1016/j.bbalip.2017.07.009 (2017).
- 99 Pol, A., Gross, S. P. & Parton, R. G. Biogenesis of the multifunctional lipid droplet: Lipids, proteins, and sites. **204**, 635-646, doi:10.1083/jcb.201311051 (2014).
- 100 Conde, C. *et al.* The protective effect of extra-virgin olive oil in the experimental model of multiple sclerosis in the rat. **23**, 37-48, doi:10.1080/1028415X.2018.1469281 (2020).
- 101 Pompura, S. L. *et al.* Oleic acid restores suppressive defects in tissue-resident FOXP3 Tregs from patients with multiple sclerosis. **131**, doi:10.1172/JCI138519 (2021).
- 102 Kasakin, M. F. *et al.* Targeted metabolomics approach for identification of relapsing–remitting multiple sclerosis markers and evaluation of diagnostic models. **10**, 1803-1809, doi:10.1039/C9MD00253G (2019).

- 103 Shimomura, I. *et al.* Insulin resistance and diabetes mellitus in transgenic mice expressing nuclear SREBP-1c in adipose tissue: model for congenital generalized lipodystrophy. **12**, 3182-3194, doi:10.1101/gad.12.20.3182 (1998).
- 104 Hachemi, I. & U-Din, M. Brown Adipose Tissue: Activation and Metabolism in Humans. **38**, 214-222, doi:10.3803/EnM.2023.1659 (2023).
- 105 Till, A., Fries, C. & Fenske, W. K. Brain-to-BAT - and Back?: Crosstalk between the Central Nervous System and Thermogenic Adipose Tissue in Development and Therapy of Obesity. **12**, 1646, doi:10.3390/brainsci12121646 (2022).
- 106 Cheng, L. *et al.* Brown and beige adipose tissue: a novel therapeutic strategy for obesity and type 2 diabetes mellitus. **10**, 48-65, doi:10.1080/21623945.2020.1870060 (2021).
- 107 Islimye, E., Girard, V. & Gould, A. P. Functions of Stress-Induced Lipid Droplets in the Nervous System. **10**, doi:10.3389/fcell.2022.863907 (2022).
- 108 Gratuze, M., Leyns, C. E. G. & Holtzman, D. M. New insights into the role of TREM2 in Alzheimer's disease. **13**, 66, doi:10.1186/s13024-018-0298-9 (2018).
- 109 Jaitin, D. A. *et al.* Lipid-Associated Macrophages Control Metabolic Homeostasis in a Trem2-Dependent Manner. **178**, 686-698.e614, doi:10.1016/j.cell.2019.05.054 (2019).
- 110 Zaragoza, R. Transport of Amino Acids Across the Blood-Brain Barrier. **11**, doi:10.3389/fphys.2020.00973 (2020).
- 111 Heß, K. *et al.* Lesion stage-dependent causes for impaired remyelination in MS. **140**, 359-375, doi:10.1007/s00401-020-02189-9 (2020).
- 112 Bogie, J. F. J., Stinissen, P. & Hendriks, J. J. A. Macrophage subsets and microglia in multiple sclerosis. **128**, 191-213, doi:10.1007/s00401-014-1310-2 (2014).
- 113 Brown, R. A., Narayanan, S. & Arnold, D. L. Imaging of repeated episodes of demyelination and remyelination in multiple sclerosis. **6**, 20-25, doi:10.1016/j.nicl.2014.06.009 (2014).
- 114 Jäkel, S. *et al.* Altered human oligodendrocyte heterogeneity in multiple sclerosis. **566**, 543-547, doi:10.1038/s41586-019-0903-2 (2019).
- 115 Androvic, P. *et al.* Spatial Transcriptomics-correlated Electron Microscopy maps transcriptional and ultrastructural responses to brain injury. **14**, 4115, doi:10.1038/s41467-023-39447-9 (2023).
- 116 Ma, X. & Fernández, F. M. Advances in mass spectrometry imaging for spatial cancer metabolomics. doi:10.1002/mas.21804 (2022).
- 117 Saunders, K. D. G., Lewis, H.-M., Beste, D. J., Cexus, O. & Bailey, M. J. Spatial single cell metabolomics: Current challenges and future developments. **75**, 102327, doi:10.1016/j.cbpa.2023.102327 (2023).
- 118 Lydic, T. A. & Goo, Y. H. Lipidomics unveils the complexity of the lipidome in metabolic diseases. **7**, doi:10.1186/s40169-018-0182-9 (2018).
- 119 Iglesias-Artola, J. M. & Nadler, A. The Road to Quantitative Lipid Biochemistry in Living Cells. **56**, 810-820, doi:10.1021/acs.accounts.2c00804 (2023).
- 120 Helmchen, F. & Denk, W. Deep tissue two-photon microscopy. **2**, 932-940, doi:10.1038/nmeth818 (2005).

- 121 Xiao, Y., Deng, P., Zhao, Y., Yang, S. & Li, B. Three-photon excited fluorescence imaging in neuroscience: From principles to applications. **17**, doi:10.3389/fnins.2023.1085682 (2023).
- 122 Gidez, L. I. The lore of lipids. **25**, 1430-1436, doi:10.1016/S0022-2275(20)34415-1 (1984).

LIST OF FIGURES

Introduction

- Figure 1 The remyelination process orchestrates the response of oligodendrocytes and microglia/macrophages towards regeneration.
- Figure 2 Foam cells in remyelination respond in three phases.
- Figure 3 What triggers lipid droplet (LD) formation in the CNS?

Project 1: Trem2-dependent lipid droplet biogenesis in phagocytes is required for remyelination.

- Figure 1 TREM2 is required for lipid droplet biogenesis and remyelination.
- Figure 2 TREM2 is required for innate immune cell resolution and foam cell formation.
- Figure 3 Cholesterol esterification and lipid droplet formation are defective in myelin-treated TREM2 KO microglia.
- Figure 4 Cholesterol esterification is necessary for remyelination.
- Figure 5 ER stress and protein synthesis defects in TREM2 KO demyelinating lesions.
- Figure S1 Defective remyelination and myelin clearance in TREM2 KO lesions.
- Figure S2 Defective cholesterol esterification affects remyelination, inflammation, and cholesterol crystal formation.
- Figure S3 Myelin phagocytosis causes ER stress in TREM2 KO microglia.

Project 2: The “lipodystrophy” brain exhibits enhanced remyelination in a UCP1-independent manner.

- Figure 1 Characterization of aP2-Srebf1c mice in basal conditions: glial cells response in unlesioned corpus callosum.
- Figure 2 Characterization of aP2-Srebf1c mice in basal conditions: glial cells accumulate lipid droplets (LD) in unlesioned corpus callosum and ventricle wall.
- Figure 3 Characterization of aP2-Srebf1c mice in acute demyelination: remyelination is enhanced in transgenic animals under WSD treatment.

- Figure 4 Metabolomic signature of aP2-Srebf1c mice reveals distinctive genotype and diet dependent differences and highlights BAT metabolism.
- Figure 5 Proteomic signature of brown adipose tissue (BAT) in aP2-Srebf1c mice reveal diet independent inflammatory profile.
- Figure 6 Increasing UCP1-dependent metabolic rate of brown adipose tissue (BAT) does not influence glial response in demyelinating conditions.
- Figure S1 The aP2-Srebf1c murine model resembling congenital generalized lipodystrophy (CGL) disorder.
- Figure S2 Characterization of aP2-Srebf1c mice in basal conditions: glial cells response in unlesioned motor cortex.
- Figure S3 Metabolomic signature of aP2-Srebf1c mice reveals elevated levels of several phosphatidylcholines (PCs) containing long-chain fatty acids (LCFAs) under chow treatment.
- Figure S4 Targeted proteomic analysis of aP2-Srebf1c animals reveal an inflammatory response.

Discussion

- Figure 1 TREM2-dependent lipid droplet biogenesis in phagocytes is required for remyelination.
- Figure 2 Disease manifestation in animal models of MS compared to the human phenotype.

LIST OF TABLES

Project 2: The “lipodystrophy” brain exhibits enhanced remyelination in a UCP1-independent manner.

- Table 1 Significant enriched metabolites in plasma of aP2-Srebf1c animals, under diverse dietary stimuli.

LIST OF ABBREVIATIONS

ABCA1	ATP-binding cassette transporter A member 1
ABCG1	ATP-binding cassette transporter G member 1
Ac.Orn	acetylorntithine
Acvr11	activin A receptor like type 1
AD	Alzheimer's disease
AFN	atipamezole/flumazenil/naloxone
AGE-RAGE	advanced glycation end products- receptor for advanced glycation end products
aOPCs	adult oligodendrocyte precursor cells
Apbb1ip	amyloid beta A4 precursor protein-binding family B member 1-interacting protein
APC; clone CC1	adenomatous polyposis coli
Apoe	apolipoprotein E
ARG1	arginase 1
BAT	brown adipose tissue
BBB	blood-brain barrier
BCAAs	branched-chain amino acids
BCSFB	blood-cerebrospinal fluid barrier
BeAT	beige adipose tissue
BHB	β -hydroxybutyrate
C18:1	octadecenoylcarnitine
C3.DC..C4.OH.	hydroxybutyrylcarnitine
cAMP/ PKA	cyclic adenosine monophosphate/protein kinase A pathway
Cant1	soluble calcium-activated nucleotidase 1
CCDS	cerebral creatine deficiency syndrome
CIS	clinically isolated syndrome
Ccl2	C-C motif chemokine 2

Ccl3	C-C motif chemokine 3
Ccl5	C-C motif chemokine 5
CD	control diet
CD206	mannose receptor
CE	cholesterol esters
Cer	ceramide
CGL	congenital generalized lipodystrophy
Chol	cholesterol
CL	cardiolipin
CNS	central nervous system
Cntn4	contactin-4
Cpe	carboxypeptidase E
CPT-I	ratio of long chain acylcarnitines to free carnitine
CSF	cerebrospinal fluid
Cxcl1	growth-regulated alpha protein
Cxcl9	C-X-C motif chemokine 9
DAG	diacylglycerol
DAM	disease-associated microglia
DAP12	TYRO protein tyrosine kinase-binding protein
DMTs	disease-modifying treatments
dpi	days post-injection
Eda2r	tumor necrosis factor receptor superfamily member 27
eIF2α	translation initiation factor 2 α
Epo	erythropoietin
ER	endoplasmic reticulum
FFAs	free fatty acids
Flrt2	leucine-rich repeat transmembrane protein FLRT2
FM	fluoroMyelin

Fstl3	follistatin-related protein 3
GFAP	glial fibrillary acidic protein
Gfra1	GDNF family receptor alpha-1
GO	gene ontology
H&E	hematoxylin and eosin
HexCer	hexosylceramide
Hgf	hepatocyte growth factor
HMDB	Human Metabolome Database,
IBA1	allograft inflammatory factor 1
IFNγ	interferon-gamma
IGF1	insulin-like growth factor 1
IHC	immunohistochemistry
IL10	interleukin 10
Il1b	interleukin-1 beta
IL1RA	interleukin-1 receptor antagonist
IL-1β	interleukin 1 beta
IL-6	interleukin 6
Ile	isoleucine
ITAM	immunoreceptor tyrosine-based activation motif
KC	C-X-C motif chemokine ligand 1 (synonym of Cxcl1)
KEGG	Kyoto Encyclopedia of Genes and Genomes
Kitlg	soluble KIT ligand
LAM	lipid-associated macrophages
LAMP1	lysosome-associated membrane glycoprotein 1
LCFAs	long-chain fatty acids
LD	lipid droplet
Leu	leucine
Lgals3 or MAC2	galectin-3

Lgmn	legumain
LLC	lysolecithin
LPC	lysophosphatidylcholine,
LPE	lysophosphatidylethanolamine
LPE O	ether-linked lyso-phosphatidyl-ethanolamine
LPG	lysophosphatidylglycerol
LPI	lysophosphatidylinositol
LPS	lysophosphatidylserine
LXR	liver X receptor
MAPK	mitogen-activated protein kinase
MBP	myelin basic protein
mRNA	messenger RNA (Ribonucleic acid)
MIP-1a	macrophage inflammatory protein-1 alpha (synonym of Ccl3)
MMF	medetomidine/midazolam/fentanyl
MMPs	metalloproteinases
mOLGs	mature oligodendrocytes
MRI	magnetic resonance imaging
MS	multiple sclerosis
NLRP3	NOD-, LRR- and pyrin domain-containing protein 3
NO	nitric oxide
Olig2	oligodendrocyte transcription factor 2
OP puro	O-propargyl-puromycin
OPCs	oligodendrocyte precursor cells
PA	phosphatidic acid
PBA	4-phenyl butyric acid
PC	phosphatidylcholine
PC aa C40:5	phosphatidylcholine diacyl C40:5
PC aa C42:4	phosphatidylcholine diacyl C42:4

PC aa C42:5	phosphatidylcholine diacyl C42:5
PC aa C42:6	phosphatidylcholine diacyl C42:6
PC.ae.C36.4	phosphatidylcholine acyl-alkyl C36:4
PC.ae.C38.5	phosphatidylcholine acyl-alkyl C38:5
PC.ae.C42.0	phosphatidylcholine acyl-alkyl C42:0
PC.ae.C44:3	phosphatidylcholine acyl-alkyl C44:3
PC O	ether-linked Phosphatidylcholine
PCA	principle component analysis
PCs	phosphatidylcholine
PE	phosphatidylethanolamine
PE O	ether-linked phosphatidyl-ethanolamine
p-eIF2α	phosphorylated eIF2 α
PFA	paraformaldehyde
PG	phosphatidylglycerol
PGES	prostaglandin E synthase
Phe	phenylalanine
PI	phosphatidylinositol
p-JNK	phospho-Jun N-terminal kinase
Pla2g4a	cytosolic phospholipase A2
PLIN2	perilipin 2
PLIN3	perilipin 3
PPAR	proliferator-activated receptor
PPMS	primary-progressive MS
PS	phosphatidylserine
PUFAs	polyunsaturated fatty acids
RANTES	regulated on activation, normal T cell expressed and secreted (synonym of Ccl5)
Ras	Rat sarcoma

ROS	reactive oxygen species
RRMS	relapsing-remitting MS
RT-PCR	real-time polymerase chain reaction
scRNA	single-cell RNA (Ribonucleic acid)
Sez6l2	seizure 6-like protein 2
SM C18.0	sphingomyelin C18:0
SM C26.0	sphingomyelin C26:0
SM	sphingomyelin
SM C18.1	sphingomyelin C18:1
SNS	sympathetic nervous system
soat1/Acat	acyl-CoA:cholesterol acyltransferase
SREBP1c	sterol regulatory element binding protein-1c
SPMS	secondary progressive MS
TAG	triglycerides (synonym to TGs)
TEM	transmission electron microscopy
Tgfa	protransforming growth factor alpha
Tgfb1	transforming growth factor beta 1
TGs	triglycerides
TNF	tumor necrosis factor
Tnfrsf12a	tumor necrosis factor receptor superfamily member 12A
TNF-α	tumor necrosis factor-alpha
Tpp1	tripeptidyl peptidase 1
TREM2 KO	TREM2-deficient mice
TREM2	triggering receptor expressed on myeloid cells 2
UCP1	uncoupling protein 1
Val	valine
Vegfd	vascular endothelial growth factor D
WAT	white adipose tissue

Wisp1	WNT1-inducible-signaling pathway protein 1
WSD	western diet
Wt	wild-type
β3-AR	β3-adrenergic receptor

LIST OF PUBLICATIONS

Tiwari, V., Prajapati, B., Asare, Y., Damkou, A., Ji, H., Liu, L., Naser, N., **Gouna, G.**, Leszczyńska, K., Mieczkowski, J., Dichgans, M., Wang, Q., Kawaguchi, R., Shi, Z., Swarup, V., Geschwind, D.H., Prinz, M., Gokce, O., Simons, M. Innate immune training restores pro-reparative myeloid functions for remyelination in the aged central nervous system. *Immunity* (resubmitted 11/2023 – in final revisions, after the second submission)

Androvic, P.*, Schifferer, M.*, Perez Anderson, K., Cantuti-Castelvetri, L., Jiang, H., Ji, H., Liu, L., **Gouna, G.**, Berghoff, S.A., Besson-Girard, S., Knoferle, J., Simons, M. & Gokce, O. (2023). Spatial Transcriptomics-correlated Electron Microscopy maps transcriptional and ultrastructural responses to brain injury. *Nature Communications* <https://doi.org/10.1038/s41467-023-39447-9>

Mathioudakis, L.*, Dimovasili, C.*, Bourbouli, M., Latsoudis, H., Kokosali, E., **Gouna, G.**, Vogiatzi, E., Basta, M., Kapetanaki, S., Panagiotakis, S., Kanterakis, A., Boumpas, D., Lionis, C., Plaitakis, A., Simos, P., Vgontzas, A., Kafetzopoulos, D., Zaganas, I. (2022). Study of Alzheimer's disease- and frontotemporal dementia-associated genes in the Cretan Aging Cohort. *Neurobiology of Aging*. <https://doi.org/10.1016/j.neurobiolaging.2022.07.002>

Gouna, G., Klose, C., Bosch-Queralt, M., Liu, L., Gokce, O., Schifferer, M., Cantuti-Castelvetri, L.* Simons, M.* (2021). TREM2-dependent lipid droplet biogenesis in phagocytes is required for remyelination. *The Journal of Experimental Medicine*, 218(10), e20210227. <https://doi.org/10.1084/jem.20210227>

Safaiyan, S., Besson-Girard, S., Kaya, T., Cantuti-Castelvetri, L., Liu, L., Ji, H., Schifferer, M., **Gouna, G.**, Usifo, F., Kannaiyan, N., Fitzner, D., Xiang, X., Rossner, M.J., Brendel, M., Gokce, O.* & Simons, M.* (2021). White matter aging drives microglial diversity. *Neuron*, 109(7), 1100–1117.e10. <https://doi.org/10.1016/j.neuron.2021.01.027>

Basta, M., Koutentaki, E., Vgontzas, A., Zaganas, I., Vogiatzi, E., **Gouna, G.**, Bourbouli, M., Panagiotakis, S., Kapetanaki, S., Fernandez-Mendoza, J., Simos, P. (2020). Objective Daytime Napping is Associated with Disease Severity and Inflammation in Patients with Mild to Moderate Dementia. *Journal of Alzheimer's disease: JAD*, 74(3), 803–815. <https://doi.org/10.3233/JAD-190483>

* Equal contribution

COPYRIGHT OF FIGURES TAKEN FROM PUBLICATIONS

Bellow you can find all copyright licenses at the following order:

A. Introduction: Figure 1

Rights and permissions for Franklin and ffrench-Constant, Regenerating CNS myelin - from mechanisms to experimental medicines., Nat. Rev. Neurosci., Volume 18, 756, 2017, Springer Nature

B. Introduction: Figure 2

Rights and permissions for Grajchen et al., The physiology of foamy phagocytes in multiple sclerosis., Acta Neuropathol. Commun., page 7, 2018, 6:124

C. Introduction: Figure 3

Rights and permissions for Lipid droplets in the nervous system, Ralhan et al., J. Cell. Biol. 2021 Vol. 220 No. 7 e20210213660, year of copyright 2023; permission conveyed through Copyright Clearance Center, Inc.

D. Project 1: Trem2-dependent lipid droplet biogenesis in phagocytes is required for remyelination.

Rights and permissions for TREM2-dependent lipid droplet biogenesis in phagocytes is required for remyelination, Gouna et al., J. Exp. Med. 2021 Vol. 218 No. 10 e20210227 year of copyright 2023; permission conveyed through Copyright Clearance Center, Inc.

E. Discussion: Figure 1

Biorender.com rights and permissions

F. Discussion: Figure 2

Rights and permissions for Klotz, Antel and Kuhlmann, Inflammation in multiple sclerosis: consequences for remyelination and disease progression., Nat. Rev. Neurol., Volume 19, 311, 2023, Springer Nature

SPRINGER NATURE LICENSE TERMS AND CONDITIONS

Nov 14, 2023

This Agreement between Garyfallia Gouna ("You") and Springer Nature ("Springer Nature") consists of your license details and the terms and conditions provided by Springer Nature and Copyright Clearance Center.

License Number	5667760718786
License date	Nov 14, 2023
Licensed Content Publisher	Springer Nature
Licensed Content Publication	Nature Reviews Neuroscience
Licensed Content Title	Regenerating CNS myelin — from mechanisms to experimental medicines
Licensed Content Author	Robin J. M. Franklin et al
Licensed Content Date	Nov 16, 2017
Type of Use	Thesis/Dissertation
Requestor type	academic/university or research institute
Format	print and electronic
Portion	figures/tables/illustrations
Number of figures/tables/illustrations	1
Would you like a high resolution image with your order?	no
Will you be translating?	no
Circulation/distribution	1 - 29
Author of this Springer Nature content	no
Title of new work	Lipid Metabolism in Remyelination: Does a Hidden Dialogue Exist Between the Central Nervous System and the Periphery?
Institution name	LMU - DZNE
Expected presentation date	Nov 2023
Portions	Figure 2(a) (i do not need the b part of the figure2, just the illustration)
Requestor Location	Garyfallia Gouna Feodor Lynen straÙe 17 Munich, 81377 Germany Attn: Garyfallia Gouna
Total	0.00 EUR

Terms and Conditions

Springer Nature Customer Service Centre GmbH Terms and Conditions

The following terms and conditions ("Terms and Conditions") together with the terms specified in your [RightsLink] constitute the License ("License") between you as Licensee and Springer Nature Customer Service Centre GmbH as Licensor. By clicking 'accept' and completing the transaction for your use of the material ("Licensed Material"), you confirm your acceptance of and obligation to be bound by these Terms and Conditions.

1. Grant and Scope of License

1. 1. The Licensor grants you a personal, non-exclusive, non-transferable, non-sublicensable, revocable, world-wide License to reproduce, distribute, communicate to the public, make available, broadcast, electronically transmit or create derivative works using the Licensed Material for the purpose(s) specified in your RightsLink Licence Details only. Licenses are granted for the specific use requested in the order and for no other use, subject to these Terms and Conditions. You acknowledge and agree that the rights granted to you under this License do not include the right to modify, edit, translate, include in collective works, or create derivative works of the Licensed Material in whole or in part unless expressly stated in your RightsLink Licence Details. You may use the Licensed Material only as permitted under this Agreement and will not reproduce, distribute, display, perform, or otherwise use or exploit any Licensed Material in any way, in whole or in part, except as expressly permitted by this License.

1. 2. You may only use the Licensed Content in the manner and to the extent permitted by these Terms and Conditions, by your RightsLink Licence Details and by any applicable laws.

1. 3. A separate license may be required for any additional use of the Licensed Material, e.g. where a license has been purchased for print use only, separate permission must be obtained for electronic re-use. Similarly, a License is only valid in the language selected and does not apply for editions in other languages unless additional translation rights have been granted separately in the License.

1. 4. Any content within the Licensed Material that is owned by third parties is expressly excluded from the License.

1. 5. Rights for additional reuses such as custom editions, computer/mobile applications, film or TV reuses and/or any other derivative rights requests require additional permission and may be subject to an additional fee. Please apply to journalpermissions@springernature.com or bookpermissions@springernature.com for these rights.

2. Reservation of Rights

Licensor reserves all rights not expressly granted to you under this License. You acknowledge and agree that nothing in this License limits or restricts Licensor's rights in or use of the Licensed Material in any way. Neither this License, nor any act, omission, or statement by Licensor or you, conveys any ownership right to you in any Licensed Material, or to any element or portion thereof. As between Licensor and you, Licensor owns and retains all right, title, and interest in and to the Licensed Material subject to the license granted in Section 1.1. Your permission to use the Licensed Material is expressly conditioned on you not impairing Licensor's or the applicable copyright owner's rights in the Licensed Material in any way.

3. Restrictions on use

3. 1. Minor editing privileges are allowed for adaptations for stylistic purposes or formatting purposes provided such alterations do not alter the original meaning or intention of the Licensed Material and the new figure(s) are still accurate and representative of the Licensed Material. Any other changes including but not limited to, cropping, adapting, and/or omitting material that affect the meaning, intention or moral rights of the author(s) are strictly prohibited.

3. 2. You must not use any Licensed Material as part of any design or trademark.

3. 3. Licensed Material may be used in Open Access Publications (OAP), but any such reuse must include a clear acknowledgment of this permission visible at the same time as the figures/tables/illustration or abstract and which must indicate that the Licensed Material is not part of the governing OA license but has been reproduced with permission. This may be indicated according to any standard referencing system but must include at a minimum 'Book/Journal title, Author, Journal Name (if applicable), Volume (if applicable), Publisher, Year, reproduced with permission from SNCSC'.

4. STM Permission Guidelines

4. 1. An alternative scope of license may apply to signatories of the STM Permissions Guidelines ("STM PG") as amended from time to time and made available at <https://www.stm-assoc.org/intellectual-property/permissions/permissions-guidelines/>.

4. 2. For content reuse requests that qualify for permission under the STM PG, and which may be updated from time to time, the STM PG supersede the terms and conditions contained in this License.

4. 3. If a License has been granted under the STM PG, but the STM PG no longer apply at the time of publication, further permission must be sought from the Rightsholder. Contact journalpermissions@springernature.com or

bookpermissions@springernature.com for these rights.

5. Duration of License

5. 1. Unless otherwise indicated on your License, a License is valid from the date of purchase ("License Date") until the end of the relevant period in the below table:

Reuse in a medical communications project	Reuse up to distribution or time period indicated in License
Reuse in a dissertation/thesis	Lifetime of thesis
Reuse in a journal/magazine	Lifetime of journal/magazine
Reuse in a book/textbook	Lifetime of edition
Reuse on a website	1 year unless otherwise specified in the License
Reuse in a presentation/slide kit/poster	Lifetime of presentation/slide kit/poster. Note: publication whether electronic or in print of presentation/slide kit/poster may require further permission.
Reuse in conference proceedings	Lifetime of conference proceedings
Reuse in an annual report	Lifetime of annual report
Reuse in training/CME materials	Reuse up to distribution or time period indicated in License
Reuse in newsmedia	Lifetime of newsmedia
Reuse in coursepack/classroom materials	Reuse up to distribution and/or time period indicated in license

6. Acknowledgement

6. 1. The Licensor's permission must be acknowledged next to the Licensed Material in print. In electronic form, this acknowledgement must be visible at the same time as the figures/tables/illustrations or abstract and must be hyperlinked to the journal/book's homepage.

6. 2. Acknowledgement may be provided according to any standard referencing system and at a minimum should include "Author, Article/Book Title, Journal name/Book imprint, volume, page number, year, Springer Nature".

7. Reuse in a dissertation or thesis

7. 1. Where 'reuse in a dissertation/thesis' has been selected, the following terms apply: Print rights of the Version of Record are provided for; electronic rights for use only on institutional repository as defined by the Sherpa guideline (www.sherpa.ac.uk/romeo/) and only up to what is required by the awarding institution.

7. 2. For theses published under an ISBN or ISSN, separate permission is required. Please contact journalpermissions@springernature.com or bookpermissions@springernature.com for these rights.

7. 3. Authors must properly cite the published manuscript in their thesis according to current citation standards and include the following acknowledgement: '*Reproduced with permission from Springer Nature*'.

8. License Fee

You must pay the fee set forth in the License Agreement (the "License Fees"). All amounts payable by you under this License are exclusive of any sales, use, withholding, value added or similar taxes, government fees or levies or other assessments. Collection and/or remittance of such taxes to the relevant tax authority shall be the responsibility of the party who has the legal obligation to do so.

9. Warranty

9. 1. The Licensor warrants that it has, to the best of its knowledge, the rights to license reuse of the Licensed Material. **You are solely responsible for ensuring that the material you wish to license is original to the Licensor and does not carry the copyright of another entity or third party (as credited in the published version).** If the credit

line on any part of the Licensed Material indicates that it was reprinted or adapted with permission from another source, then you should seek additional permission from that source to reuse the material.

9. 2. EXCEPT FOR THE EXPRESS WARRANTY STATED HEREIN AND TO THE EXTENT PERMITTED BY APPLICABLE LAW, LICENSOR PROVIDES THE LICENSED MATERIAL "AS IS" AND MAKES NO OTHER REPRESENTATION OR WARRANTY. LICENSOR EXPRESSLY DISCLAIMS ANY LIABILITY FOR ANY CLAIM ARISING FROM OR OUT OF THE CONTENT, INCLUDING BUT NOT LIMITED TO ANY ERRORS, INACCURACIES, OMISSIONS, OR DEFECTS CONTAINED THEREIN, AND ANY IMPLIED OR EXPRESS WARRANTY AS TO MERCHANTABILITY OR FITNESS FOR A PARTICULAR PURPOSE. IN NO EVENT SHALL LICENSOR BE LIABLE TO YOU OR ANY OTHER PARTY OR ANY OTHER PERSON OR FOR ANY SPECIAL, CONSEQUENTIAL, INCIDENTAL, INDIRECT, PUNITIVE, OR EXEMPLARY DAMAGES, HOWEVER CAUSED, ARISING OUT OF OR IN CONNECTION WITH THE DOWNLOADING, VIEWING OR USE OF THE LICENSED MATERIAL REGARDLESS OF THE FORM OF ACTION, WHETHER FOR BREACH OF CONTRACT, BREACH OF WARRANTY, TORT, NEGLIGENCE, INFRINGEMENT OR OTHERWISE (INCLUDING, WITHOUT LIMITATION, DAMAGES BASED ON LOSS OF PROFITS, DATA, FILES, USE, BUSINESS OPPORTUNITY OR CLAIMS OF THIRD PARTIES), AND WHETHER OR NOT THE PARTY HAS BEEN ADVISED OF THE POSSIBILITY OF SUCH DAMAGES. THIS LIMITATION APPLIES NOTWITHSTANDING ANY FAILURE OF ESSENTIAL PURPOSE OF ANY LIMITED REMEDY PROVIDED HEREIN.

10. Termination and Cancellation

10. 1. The License and all rights granted hereunder will continue until the end of the applicable period shown in Clause 5.1 above. Thereafter, this license will be terminated and all rights granted hereunder will cease.

10. 2. Licensor reserves the right to terminate the License in the event that payment is not received in full or if you breach the terms of this License.

11. General

11. 1. The License and the rights and obligations of the parties hereto shall be construed, interpreted and determined in accordance with the laws of the Federal Republic of Germany without reference to the stipulations of the CISG (United Nations Convention on Contracts for the International Sale of Goods) or to Germany's choice-of-law principle.

11. 2. The parties acknowledge and agree that any controversies and disputes arising out of this License shall be decided exclusively by the courts of or having jurisdiction for Heidelberg, Germany, as far as legally permissible.

11. 3. This License is solely for Licensor's and Licensee's benefit. It is not for the benefit of any other person or entity.

Questions? For questions on Copyright Clearance Center accounts or website issues please contact springernaturesupport@copyright.com or +1-855-239-3415 (toll free in the US) or +1-978-646-2777. For questions on Springer Nature licensing please visit <https://www.springernature.com/gp/partners/rights-permissions-third-party-distribution>

Other Conditions:

Version 1.4 - Dec 2022

Questions? E-mail us at customer-care@copyright.com.



RightsLink

The physiology of foamy phagocytes in multiple sclerosis

Author: Elien Grajchen et al

Publication: Acta Neuropathologica Communications

Publisher: Springer Nature

Date: Nov 19, 2018

Copyright © 2018, The Author(s).

Creative Commons

This is an open access article distributed under the terms of the [Creative Commons CC BY](#) license, which permits unrestricted use, distribution, and reproduction in any medium, provided the original work is properly cited.

You are not required to obtain permission to reuse this article.

CC0 applies for supplementary material related to this article and attribution is not required.

© 2023 Copyright - All Rights Reserved | [Copyright Clearance Center, Inc.](#) | [Privacy statement](#) | [Data Security and Privacy](#)
| [For California Residents](#) | [Terms and Conditions](#) Comments? We would like to hear from you. E-mail us at customercare@copyright.com



Marketplace

This is a License Agreement between Garyfallia Gouna ("User") and Copyright Clearance Center, Inc. ("CCC") on behalf of the Rightsholder identified in the order details below. The license consists of the order details, the Marketplace Permissions General Terms and Conditions below, and any Rightsholder Terms and Conditions which are included below.

All payments must be made in full to CCC in accordance with the Marketplace Permissions General Terms and Conditions below.

Order Date	09-Nov-2023	Type of Use	Republish in a thesis/dissertation
Order License ID	1415077-1	Publisher	ROCKEFELLER UNIVERSITY PRESS
ISSN	0021-9525	Portion	Image/photo/illustration

LICENSED CONTENT

Publication Title	The Journal of cell biology	Country	United States of America
Article Title	Lipid droplets in the nervous system	Rightsholder	Rockefeller University Press
Author/Editor	ROCKEFELLER INSTITUTE., AMERICAN SOCIETY FOR CELL BIOLOGY.	Publication Type	Journal
Date	01/01/1962	Issue	7
Language	English	Volume	220

REQUEST DETAILS

Portion Type	Image/photo/illustration	Distribution	Worldwide
Number of Images / Photos / Illustrations	1	Translation	Original language of publication
Format (select all that apply)	Print, Electronic	Copies for the Disabled?	No
Who Will Republish the Content?	Academic institution	Minor Editing Privileges?	No
Duration of Use	Life of current edition	Incidental Promotional Use?	No
Lifetime Unit Quantity	Up to 499	Currency	EUR
Rights Requested	Main product, any product related to main product, and other compilations/derivative products		

NEW WORK DETAILS

Title	Lipid Metabolism in Remyelination: Does a Hidden Dialogue Exist Between the Central Nervous System and the Periphery?	Institution Name	LMU - DZNE
		Expected Presentation Date	2023-11-09

Instructor Name Garyfallia Gouna

ADDITIONAL DETAILS

Order Reference Number	N/A	The Requesting Person / Organization to Appear on the License	Garyfallia Gouna
------------------------	-----	---	------------------

REQUESTED CONTENT DETAILS

Title, Description or Numeric Reference of the Portion(s)	Figure 2.	Title of the Article / Chapter the Portion Is From	Lipid droplets in the nervous system
Editor of Portion(s)	Ralhan, Isha; Chang, Chi-Lun; Lippincott-Schwartz, Jennifer; Ioannou, Maria S.	Author of Portion(s)	Ralhan, Isha; Chang, Chi-Lun; Lippincott-Schwartz, Jennifer; Ioannou, Maria S.
Volume / Edition	220	Issue, if Republishing an Article From a Serial	7
Page or Page Range of Portion	3 of 18	Publication Date of Portion	2021-07-05

Marketplace Permissions General Terms and Conditions

The following terms and conditions (“General Terms”), together with any applicable Publisher Terms and Conditions, govern User’s use of Works pursuant to the Licenses granted by Copyright Clearance Center, Inc. (“CCC”) on behalf of the applicable Rightsholders of such Works through CCC’s applicable Marketplace transactional licensing services (each, a “Service”).

1) **Definitions.** For purposes of these General Terms, the following definitions apply:

“License” is the licensed use the User obtains via the Marketplace platform in a particular licensing transaction, as set forth in the Order Confirmation.

“Order Confirmation” is the confirmation CCC provides to the User at the conclusion of each Marketplace transaction. “Order Confirmation Terms” are additional terms set forth on specific Order Confirmations not set forth in the General Terms that can include terms applicable to a particular CCC transactional licensing service and/or any Rightsholder-specific terms.

“Rightsholder(s)” are the holders of copyright rights in the Works for which a User obtains licenses via the Marketplace platform, which are displayed on specific Order Confirmations.

“Terms” means the terms and conditions set forth in these General Terms and any additional Order Confirmation Terms collectively.

“User” or “you” is the person or entity making the use granted under the relevant License. Where the person accepting the Terms on behalf of a User is a freelancer or other third party who the User authorized to accept the General Terms on the User’s behalf, such person shall be deemed jointly a User for purposes of such Terms.

“Work(s)” are the copyright protected works described in relevant Order Confirmations.

2) **Description of Service.** CCC’s Marketplace enables Users to obtain Licenses to use one or more Works in accordance with all relevant Terms. CCC grants Licenses as an agent on behalf of the copyright rightsholder identified in the relevant Order Confirmation.

3) **Applicability of Terms.** The Terms govern User’s use of Works in connection with the relevant License. In the event of any conflict between General Terms and Order Confirmation Terms, the latter shall govern. User acknowledges that Rightsholders have complete discretion whether to grant any permission, and whether to place any limitations on any grant, and that CCC has no right to supersede or to modify any such discretionary act by a Rightsholder.

4) **Representations; Acceptance.** By using the Service, User represents and warrants that User has been duly authorized by the User to accept, and hereby does accept, all Terms.

5) **Scope of License; Limitations and Obligations.** All Works and all rights therein, including copyright rights, remain the sole and exclusive property of the Rightsholder. The License provides only those rights expressly set forth in the terms and conveys no other rights in any Works

6) **General Payment Terms.** User may pay at time of checkout by credit card or choose to be invoiced. If the User chooses to be invoiced, the User shall: (i) remit payments in the manner identified on specific invoices, (ii) unless otherwise specifically stated in an Order Confirmation or separate written agreement, Users shall remit payments upon receipt of the relevant invoice from CCC, either by delivery or notification of availability of the invoice via the Marketplace platform, and (iii) if the User does not pay the invoice within 30 days of receipt, the User may incur a service charge of 1.5% per month or the maximum rate allowed by applicable law, whichever is less. While User may exercise the rights in the License immediately upon receiving the Order Confirmation, the License is automatically revoked and is null and void, as if it had never been issued, if CCC does not receive complete payment on a timely basis.

7) **General Limits on Use.** Unless otherwise provided in the Order Confirmation, any grant of rights to User (i) involves only the rights set forth in the Terms and does not include subsequent or additional uses, (ii) is non-exclusive and non-transferable, and (iii) is subject to any and all limitations and restrictions (such as, but not limited to, limitations on duration of use or circulation) included in the Terms. Upon completion of the licensed use as set forth in the Order Confirmation, User shall either secure a new permission for further use of the Work(s) or immediately cease any new use of the Work(s) and shall render inaccessible (such as by deleting or by removing or severing links or other locators) any further copies of the Work. User may only make alterations to the Work if and as expressly set forth in the Order Confirmation. No Work may be used in any way that is unlawful, including without limitation if such use would violate applicable sanctions laws or regulations, would be defamatory, violate the rights of third parties (including such third parties' rights of copyright, privacy, publicity, or other tangible or intangible property), or is otherwise illegal, sexually explicit, or obscene. In addition, User may not conjoin a Work with any other material that may result in damage to the reputation of the Rightsholder. Any unlawful use will render any licenses hereunder null and void. User agrees to inform CCC if it becomes aware of any infringement of any rights in a Work and to cooperate with any reasonable request of CCC or the Rightsholder in connection therewith.

8) **Third Party Materials.** In the event that the material for which a License is sought includes third party materials (such as photographs, illustrations, graphs, inserts and similar materials) that are identified in such material as having been used by permission (or a similar indicator), User is responsible for identifying, and seeking separate licenses (under this Service, if available, or otherwise) for any of such third party materials; without a separate license, User may not use such third party materials via the License.

9) **Copyright Notice.** Use of proper copyright notice for a Work is required as a condition of any License granted under the Service. Unless otherwise provided in the Order Confirmation, a proper copyright notice will read substantially as follows: "Used with permission of [Rightsholder's name], from [Work's title, author, volume, edition number and year of copyright]; permission conveyed through Copyright Clearance Center, Inc." Such notice must be provided in a reasonably legible font size and must be placed either on a cover page or in another location that any person, upon gaining access to the material which is the subject of a permission, shall see, or in the case of republication Licenses, immediately adjacent to the Work as used (for example, as part of a by-line or footnote) or in the place where substantially all other credits or notices for the new work containing the republished Work are located. Failure to include the required notice results in loss to the Rightsholder and CCC, and the User shall be liable to pay liquidated damages for each such failure equal to twice the use fee specified in the Order Confirmation, in addition to the use fee itself and any other fees and charges specified.

10) **Indemnity.** User hereby indemnifies and agrees to defend the Rightsholder and CCC, and their respective employees and directors, against all claims, liability, damages, costs, and expenses, including legal fees and expenses, arising out of any use of a Work beyond the scope of the rights granted herein and in the Order Confirmation, or any use of a Work which has been altered in any unauthorized way by User, including claims of defamation or infringement of rights of copyright, publicity, privacy, or other tangible or intangible property.

11) **Limitation of Liability.** UNDER NO CIRCUMSTANCES WILL CCC OR THE RIGHTSHOLDER BE LIABLE FOR ANY DIRECT, INDIRECT, CONSEQUENTIAL, OR INCIDENTAL DAMAGES (INCLUDING WITHOUT LIMITATION DAMAGES FOR LOSS OF BUSINESS PROFITS OR INFORMATION, OR FOR BUSINESS INTERRUPTION) ARISING OUT OF THE USE OR INABILITY TO USE A WORK, EVEN IF ONE OR BOTH OF THEM HAS BEEN ADVISED OF THE POSSIBILITY OF SUCH DAMAGES. In any event, the total liability of the Rightsholder and CCC (including their respective employees and directors) shall not exceed the total

amount actually paid by User for the relevant License. User assumes full liability for the actions and omissions of its principals, employees, agents, affiliates, successors, and assigns.

12) **Limited Warranties.** THE WORK(S) AND RIGHT(S) ARE PROVIDED "AS IS." CCC HAS THE RIGHT TO GRANT TO USER THE RIGHTS GRANTED IN THE ORDER CONFIRMATION DOCUMENT. CCC AND THE RIGHTSHOLDER DISCLAIM ALL OTHER WARRANTIES RELATING TO THE WORK(S) AND RIGHT(S), EITHER EXPRESS OR IMPLIED, INCLUDING WITHOUT LIMITATION IMPLIED WARRANTIES OF MERCHANTABILITY OR FITNESS FOR A PARTICULAR PURPOSE. ADDITIONAL RIGHTS MAY BE REQUIRED TO USE ILLUSTRATIONS, GRAPHS, PHOTOGRAPHS, ABSTRACTS, INSERTS, OR OTHER PORTIONS OF THE WORK (AS OPPOSED TO THE ENTIRE WORK) IN A MANNER CONTEMPLATED BY USER; USER UNDERSTANDS AND AGREES THAT NEITHER CCC NOR THE RIGHTSHOLDER MAY HAVE SUCH ADDITIONAL RIGHTS TO GRANT.

13) **Effect of Breach.** Any failure by User to pay any amount when due, or any use by User of a Work beyond the scope of the License set forth in the Order Confirmation and/or the Terms, shall be a material breach of such License. Any breach not cured within 10 days of written notice thereof shall result in immediate termination of such License without further notice. Any unauthorized (but licensable) use of a Work that is terminated immediately upon notice thereof may be liquidated by payment of the Rightsholder's ordinary license price therefor; any unauthorized (and unlicensable) use that is not terminated immediately for any reason (including, for example, because materials containing the Work cannot reasonably be recalled) will be subject to all remedies available at law or in equity, but in no event to a payment of less than three times the Rightsholder's ordinary license price for the most closely analogous licensable use plus Rightsholder's and/or CCC's costs and expenses incurred in collecting such payment.

14) **Additional Terms for Specific Products and Services.** If a User is making one of the uses described in this Section 14, the additional terms and conditions apply:

a) **Print Uses of Academic Course Content and Materials (photocopies for academic coursepacks or classroom handouts).** For photocopies for academic coursepacks or classroom handouts the following additional terms apply:

i) The copies and anthologies created under this License may be made and assembled by faculty members individually or at their request by on-campus bookstores or copy centers, or by off-campus copy shops and other similar entities.

ii) No License granted shall in any way: (i) include any right by User to create a substantively non-identical copy of the Work or to edit or in any other way modify the Work (except by means of deleting material immediately preceding or following the entire portion of the Work copied) (ii) permit "publishing ventures" where any particular anthology would be systematically marketed at multiple institutions.

iii) Subject to any Publisher Terms (and notwithstanding any apparent contradiction in the Order Confirmation arising from data provided by User), any use authorized under the academic pay-per-use service is limited as follows:

A) any License granted shall apply to only one class (bearing a unique identifier as assigned by the institution, and thereby including all sections or other subparts of the class) at one institution;

B) use is limited to not more than 25% of the text of a book or of the items in a published collection of essays, poems or articles;

C) use is limited to no more than the greater of (a) 25% of the text of an issue of a journal or other periodical or (b) two articles from such an issue;

D) no User may sell or distribute any particular anthology, whether photocopied or electronic, at more than one institution of learning;

E) in the case of a photocopy permission, no materials may be entered into electronic memory by User except in order to produce an identical copy of a Work before or during the academic term (or analogous period) as to which any particular permission is granted. In the event that User shall choose to retain materials that are the subject of a photocopy permission in electronic memory for purposes of producing identical copies more than one day after such retention (but still within the scope of any permission granted), User must notify CCC of such fact in the applicable permission request and such retention shall constitute one copy actually sold for purposes of calculating permission fees due; and

F) any permission granted shall expire at the end of the class. No permission granted shall in any way include any right by User to create a substantively non-identical copy of the Work or to edit or in any other way

modify the Work (except by means of deleting material immediately preceding or following the entire portion of the Work copied).

iv) Books and Records; Right to Audit. As to each permission granted under the academic pay-per-use Service, User shall maintain for at least four full calendar years books and records sufficient for CCC to determine the numbers of copies made by User under such permission. CCC and any representatives it may designate shall have the right to audit such books and records at any time during User's ordinary business hours, upon two days' prior notice. If any such audit shall determine that User shall have underpaid for, or underreported, any photocopies sold or by three percent (3%) or more, then User shall bear all the costs of any such audit; otherwise, CCC shall bear the costs of any such audit. Any amount determined by such audit to have been underpaid by User shall immediately be paid to CCC by User, together with interest thereon at the rate of 10% per annum from the date such amount was originally due. The provisions of this paragraph shall survive the termination of this License for any reason.

b) **Digital Pay-Per-Uses of Academic Course Content and Materials (e-coursepacks, electronic reserves, learning management systems, academic institution intranets).** For uses in e-coursepacks, posts in electronic reserves, posts in learning management systems, or posts on academic institution intranets, the following additional terms apply:

i) The pay-per-uses subject to this Section 14(b) include:

A) **Posting e-reserves, course management systems, e-coursepacks for text-based content**, which grants authorizations to import requested material in electronic format, and allows electronic access to this material to members of a designated college or university class, under the direction of an instructor designated by the college or university, accessible only under appropriate electronic controls (e.g., password);

B) **Posting e-reserves, course management systems, e-coursepacks for material consisting of photographs or other still images not embedded in text**, which grants not only the authorizations described in Section 14(b)(i)(A) above, but also the following authorization: to include the requested material in course materials for use consistent with Section 14(b)(i)(A) above, including any necessary resizing, reformatting or modification of the resolution of such requested material (provided that such modification does not alter the underlying editorial content or meaning of the requested material, and provided that the resulting modified content is used solely within the scope of, and in a manner consistent with, the particular authorization described in the Order Confirmation and the Terms), but not including any other form of manipulation, alteration or editing of the requested material;

C) **Posting e-reserves, course management systems, e-coursepacks or other academic distribution for audiovisual content**, which grants not only the authorizations described in Section 14(b)(i)(A) above, but also the following authorizations: (i) to include the requested material in course materials for use consistent with Section 14(b)(i)(A) above; (ii) to display and perform the requested material to such members of such class in the physical classroom or remotely by means of streaming media or other video formats; and (iii) to "clip" or reformat the requested material for purposes of time or content management or ease of delivery, provided that such "clipping" or reformatting does not alter the underlying editorial content or meaning of the requested material and that the resulting material is used solely within the scope of, and in a manner consistent with, the particular authorization described in the Order Confirmation and the Terms. Unless expressly set forth in the relevant Order Confirmation, the License does not authorize any other form of manipulation, alteration or editing of the requested material.

ii) Unless expressly set forth in the relevant Order Confirmation, no License granted shall in any way: (i) include any right by User to create a substantively non-identical copy of the Work or to edit or in any other way modify the Work (except by means of deleting material immediately preceding or following the entire portion of the Work copied or, in the case of Works subject to Sections 14(b)(1)(B) or (C) above, as described in such Sections) (ii) permit "publishing ventures" where any particular course materials would be systematically marketed at multiple institutions.

iii) Subject to any further limitations determined in the Rightsholder Terms (and notwithstanding any apparent contradiction in the Order Confirmation arising from data provided by User), any use authorized under the electronic course content pay-per-use service is limited as follows:

A) any License granted shall apply to only one class (bearing a unique identifier as assigned by the institution, and thereby including all sections or other subparts of the class) at one institution;

B) use is limited to not more than 25% of the text of a book or of the items in a published collection of essays, poems or articles;

C) use is limited to not more than the greater of (a) 25% of the text of an issue of a journal or other periodical or (b) two articles from such an issue;

D) no User may sell or distribute any particular materials, whether photocopied or electronic, at more than one institution of learning;

E) electronic access to material which is the subject of an electronic-use permission must be limited by means of electronic password, student identification or other control permitting access solely to students and instructors in the class;

F) User must ensure (through use of an electronic cover page or other appropriate means) that any person, upon gaining electronic access to the material, which is the subject of a permission, shall see:

- o a proper copyright notice, identifying the Rightsholder in whose name CCC has granted permission,
- o a statement to the effect that such copy was made pursuant to permission,
- o a statement identifying the class to which the material applies and notifying the reader that the material has been made available electronically solely for use in the class, and
- o a statement to the effect that the material may not be further distributed to any person outside the class, whether by copying or by transmission and whether electronically or in paper form, and User must also ensure that such cover page or other means will print out in the event that the person accessing the material chooses to print out the material or any part thereof.

G) any permission granted shall expire at the end of the class and, absent some other form of authorization, User is thereupon required to delete the applicable material from any electronic storage or to block electronic access to the applicable material.

iv) Uses of separate portions of a Work, even if they are to be included in the same course material or the same university or college class, require separate permissions under the electronic course content pay-per-use Service. Unless otherwise provided in the Order Confirmation, any grant of rights to User is limited to use completed no later than the end of the academic term (or analogous period) as to which any particular permission is granted.

v) Books and Records; Right to Audit. As to each permission granted under the electronic course content Service, User shall maintain for at least four full calendar years books and records sufficient for CCC to determine the numbers of copies made by User under such permission. CCC and any representatives it may designate shall have the right to audit such books and records at any time during User's ordinary business hours, upon two days' prior notice. If any such audit shall determine that User shall have underpaid for, or underreported, any electronic copies used by three percent (3%) or more, then User shall bear all the costs of any such audit; otherwise, CCC shall bear the costs of any such audit. Any amount determined by such audit to have been underpaid by User shall immediately be paid to CCC by User, together with interest thereon at the rate of 10% per annum from the date such amount was originally due. The provisions of this paragraph shall survive the termination of this license for any reason.

c) ***Pay-Per-Use Permissions for Certain Reproductions (Academic photocopies for library reserves and interlibrary loan reporting) (Non-academic internal/external business uses and commercial document delivery).*** The License expressly excludes the uses listed in Section (c)(i)-(v) below (which must be subject to separate license from the applicable Rightsholder) for: academic photocopies for library reserves and interlibrary loan reporting; and non-academic internal/external business uses and commercial document delivery.

i) electronic storage of any reproduction (whether in plain-text, PDF, or any other format) other than on a transitory basis;

ii) the input of Works or reproductions thereof into any computerized database;

iii) reproduction of an entire Work (cover-to-cover copying) except where the Work is a single article;

iv) reproduction for resale to anyone other than a specific customer of User;

v) republication in any different form. Please obtain authorizations for these uses through other CCC services or directly from the rightsholder.

Any license granted is further limited as set forth in any restrictions included in the Order Confirmation and/or in these Terms.

d) **Electronic Reproductions in Online Environments (Non-Academic-email, intranet, internet and extranet).** For “electronic reproductions”, which generally includes e-mail use (including instant messaging or other electronic transmission to a defined group of recipients) or posting on an intranet, extranet or Intranet site (including any display or performance incidental thereto), the following additional terms apply:

i) Unless otherwise set forth in the Order Confirmation, the License is limited to use completed within 30 days for any use on the Internet, 60 days for any use on an intranet or extranet and one year for any other use, all as measured from the “republication date” as identified in the Order Confirmation, if any, and otherwise from the date of the Order Confirmation.

ii) User may not make or permit any alterations to the Work, unless expressly set forth in the Order Confirmation (after request by User and approval by Rightsholder); provided, however, that a Work consisting of photographs or other still images not embedded in text may, if necessary, be resized, reformatted or have its resolution modified without additional express permission, and a Work consisting of audiovisual content may, if necessary, be “clipped” or reformatted for purposes of time or content management or ease of delivery (provided that any such resizing, reformatting, resolution modification or “clipping” does not alter the underlying editorial content or meaning of the Work used, and that the resulting material is used solely within the scope of, and in a manner consistent with, the particular License described in the Order Confirmation and the Terms.

15) Miscellaneous.

a) User acknowledges that CCC may, from time to time, make changes or additions to the Service or to the Terms, and that Rightsholder may make changes or additions to the Rightsholder Terms. Such updated Terms will replace the prior terms and conditions in the order workflow and shall be effective as to any subsequent Licenses but shall not apply to Licenses already granted and paid for under a prior set of terms.

b) Use of User-related information collected through the Service is governed by CCC’s privacy policy, available online at www.copyright.com/about/privacy-policy/.

c) The License is personal to User. Therefore, User may not assign or transfer to any other person (whether a natural person or an organization of any kind) the License or any rights granted thereunder; provided, however, that, where applicable, User may assign such License in its entirety on written notice to CCC in the event of a transfer of all or substantially all of User’s rights in any new material which includes the Work(s) licensed under this Service.

d) No amendment or waiver of any Terms is binding unless set forth in writing and signed by the appropriate parties, including, where applicable, the Rightsholder. The Rightsholder and CCC hereby object to any terms contained in any writing prepared by or on behalf of the User or its principals, employees, agents or affiliates and purporting to govern or otherwise relate to the License described in the Order Confirmation, which terms are in any way inconsistent with any Terms set forth in the Order Confirmation, and/or in CCC’s standard operating procedures, whether such writing is prepared prior to, simultaneously with or subsequent to the Order Confirmation, and whether such writing appears on a copy of the Order Confirmation or in a separate instrument.

e) The License described in the Order Confirmation shall be governed by and construed under the law of the State of New York, USA, without regard to the principles thereof of conflicts of law. Any case, controversy, suit, action, or proceeding arising out of, in connection with, or related to such License shall be brought, at CCC’s sole discretion, in any federal or state court located in the County of New York, State of New York, USA, or in any federal or state court whose geographical jurisdiction covers the location of the Rightsholder set forth in the Order Confirmation. The parties expressly submit to the personal jurisdiction and venue of each such federal or state court.

Last updated October 2022



Marketplace

This is a License Agreement between Garyfallia Gouna ("User") and Copyright Clearance Center, Inc. ("CCC") on behalf of the Rightsholder identified in the order details below. The license consists of the order details, the Marketplace Permissions General Terms and Conditions below, and any Rightsholder Terms and Conditions which are included below.

All payments must be made in full to CCC in accordance with the Marketplace Permissions General Terms and Conditions below.

Order Date	09-Nov-2023	Type of Use	Republish in a thesis/dissertation
Order License ID	1415082-1	Publisher	ROCKEFELLER UNIVERSITY PRESS,
ISSN	0022-1007	Portion	Chapter/article

LICENSED CONTENT

Publication Title	The Journal of experimental medicine	Country	United States of America
Article Title	TREM2-dependent lipid droplet biogenesis in phagocytes is required for remyelination.	Rightsholder	Rockefeller University Press
Author/Editor	ROCKEFELLER UNIVERSITY., ROCKEFELLER INSTITUTE., ROCKEFELLER INSTITUTE FOR MEDICAL RESEARCH.	Publication Type	Journal
Date	01/01/1896	Issue	10
Language	English	Volume	218

REQUEST DETAILS

Portion Type	Chapter/article	Rights Requested	Main product, any product related to main product, and other compilations/derivative products
Page Range(s)	1-12, S1, S2, S3, S4	Distribution	Worldwide
Total Number of Pages	16	Translation	Original language of publication
Format (select all that apply)	Print, Electronic	Copies for the Disabled?	No
Who Will Republish the Content?	Author of requested content	Minor Editing Privileges?	No
Duration of Use	Life of current edition	Incidental Promotional Use?	No
Lifetime Unit Quantity	Up to 499	Currency	EUR

NEW WORK DETAILS

Title	Lipid Metabolism in Remyelination: Does a Hidden Dialogue Exist Between the Central Nervous System and the Periphery?	Institution Name	LMU - DZNE
		Expected Presentation Date	2023-11-09
Instructor Name	Garyfallia Gouna		

ADDITIONAL DETAILS

Order Reference Number	N/A	The Requesting Person / Organization to Appear on the License	Garyfallia Gouna
-------------------------------	-----	--	------------------

REQUESTED CONTENT DETAILS

Title, Description or Numeric Reference of the Portion(s)	The entire article, with supplementary figures and references	Title of the Article / Chapter the Portion Is From	TREM2-dependent lipid droplet biogenesis in phagocytes is required for remyelination.
Editor of Portion(s)	Gouna, Garyfallia; Klose, Christian; Bosch-Queralt, Mar; Liu, Lu; Gokce, Ozgun; Schifferer, Martina; Cantuti-Castelvetri, Ludovico; Simons, Mikael	Author of Portion(s)	Gouna, Garyfallia; Klose, Christian; Bosch-Queralt, Mar; Liu, Lu; Gokce, Ozgun; Schifferer, Martina; Cantuti-Castelvetri, Ludovico; Simons, Mikael
Volume / Edition	218	Issue, if Republishing an Article From a Serial	10
Page or Page Range of Portion	1-16 (The entire article)	Publication Date of Portion	2021-10-04

Marketplace Permissions General Terms and Conditions

The following terms and conditions ("General Terms"), together with any applicable Publisher Terms and Conditions, govern User's use of Works pursuant to the Licenses granted by Copyright Clearance Center, Inc. ("CCC") on behalf of the applicable Rightsholders of such Works through CCC's applicable Marketplace transactional licensing services (each, a "Service").

1) **Definitions.** For purposes of these General Terms, the following definitions apply:

"License" is the licensed use the User obtains via the Marketplace platform in a particular licensing transaction, as set forth in the Order Confirmation.

"Order Confirmation" is the confirmation CCC provides to the User at the conclusion of each Marketplace transaction. "Order Confirmation Terms" are additional terms set forth on specific Order Confirmations not set forth in the General Terms that can include terms applicable to a particular CCC transactional licensing service and/or any Rightsholder-specific terms.

"Rightsholder(s)" are the holders of copyright rights in the Works for which a User obtains licenses via the Marketplace platform, which are displayed on specific Order Confirmations.

"Terms" means the terms and conditions set forth in these General Terms and any additional Order Confirmation Terms collectively.

"User" or "you" is the person or entity making the use granted under the relevant License. Where the person accepting the Terms on behalf of a User is a freelancer or other third party who the User authorized to accept the General Terms on the

User's behalf, such person shall be deemed jointly a User for purposes of such Terms.

"Work(s)" are the copyright protected works described in relevant Order Confirmations.

2) **Description of Service.** CCC's Marketplace enables Users to obtain Licenses to use one or more Works in accordance with all relevant Terms. CCC grants Licenses as an agent on behalf of the copyright rightsholder identified in the relevant Order Confirmation.

3) **Applicability of Terms.** The Terms govern User's use of Works in connection with the relevant License. In the event of any conflict between General Terms and Order Confirmation Terms, the latter shall govern. User acknowledges that Rightsholders have complete discretion whether to grant any permission, and whether to place any limitations on any grant, and that CCC has no right to supersede or to modify any such discretionary act by a Rightsholder.

4) **Representations; Acceptance.** By using the Service, User represents and warrants that User has been duly authorized by the User to accept, and hereby does accept, all Terms.

5) **Scope of License; Limitations and Obligations.** All Works and all rights therein, including copyright rights, remain the sole and exclusive property of the Rightsholder. The License provides only those rights expressly set forth in the terms and conveys no other rights in any Works

6) **General Payment Terms.** User may pay at time of checkout by credit card or choose to be invoiced. If the User chooses to be invoiced, the User shall: (i) remit payments in the manner identified on specific invoices, (ii) unless otherwise specifically stated in an Order Confirmation or separate written agreement, Users shall remit payments upon receipt of the relevant invoice from CCC, either by delivery or notification of availability of the invoice via the Marketplace platform, and (iii) if the User does not pay the invoice within 30 days of receipt, the User may incur a service charge of 1.5% per month or the maximum rate allowed by applicable law, whichever is less. While User may exercise the rights in the License immediately upon receiving the Order Confirmation, the License is automatically revoked and is null and void, as if it had never been issued, if CCC does not receive complete payment on a timely basis.

7) **General Limits on Use.** Unless otherwise provided in the Order Confirmation, any grant of rights to User (i) involves only the rights set forth in the Terms and does not include subsequent or additional uses, (ii) is non-exclusive and non-transferable, and (iii) is subject to any and all limitations and restrictions (such as, but not limited to, limitations on duration of use or circulation) included in the Terms. Upon completion of the licensed use as set forth in the Order Confirmation, User shall either secure a new permission for further use of the Work(s) or immediately cease any new use of the Work(s) and shall render inaccessible (such as by deleting or by removing or severing links or other locators) any further copies of the Work. User may only make alterations to the Work if and as expressly set forth in the Order Confirmation. No Work may be used in any way that is unlawful, including without limitation if such use would violate applicable sanctions laws or regulations, would be defamatory, violate the rights of third parties (including such third parties' rights of copyright, privacy, publicity, or other tangible or intangible property), or is otherwise illegal, sexually explicit, or obscene. In addition, User may not conjoin a Work with any other material that may result in damage to the reputation of the Rightsholder. Any unlawful use will render any licenses hereunder null and void. User agrees to inform CCC if it becomes aware of any infringement of any rights in a Work and to cooperate with any reasonable request of CCC or the Rightsholder in connection therewith.

8) **Third Party Materials.** In the event that the material for which a License is sought includes third party materials (such as photographs, illustrations, graphs, inserts and similar materials) that are identified in such material as having been used by permission (or a similar indicator), User is responsible for identifying, and seeking separate licenses (under this Service, if available, or otherwise) for any of such third party materials; without a separate license, User may not use such third party materials via the License.

9) **Copyright Notice.** Use of proper copyright notice for a Work is required as a condition of any License granted under the Service. Unless otherwise provided in the Order Confirmation, a proper copyright notice will read substantially as follows: "Used with permission of [Rightsholder's name], from [Work's title, author, volume, edition number and year of copyright]; permission conveyed through Copyright Clearance Center, Inc." Such notice must be provided in a reasonably legible font size and must be placed either on a cover page or in another location that any person, upon gaining access to the material which is the subject of a permission, shall see, or in the case of republication Licenses, immediately adjacent to the Work as used (for example, as part of a by-line or footnote) or in the place where substantially all other credits or notices for the new work containing the republished Work are located. Failure to include the required notice results in loss to the Rightsholder and CCC, and the User shall be liable to pay liquidated damages for each such failure equal to

twice the use fee specified in the Order Confirmation, in addition to the use fee itself and any other fees and charges specified.

10) **Indemnity.** User hereby indemnifies and agrees to defend the Rightsholder and CCC, and their respective employees and directors, against all claims, liability, damages, costs, and expenses, including legal fees and expenses, arising out of any use of a Work beyond the scope of the rights granted herein and in the Order Confirmation, or any use of a Work which has been altered in any unauthorized way by User, including claims of defamation or infringement of rights of copyright, publicity, privacy, or other tangible or intangible property.

11) **Limitation of Liability.** UNDER NO CIRCUMSTANCES WILL CCC OR THE RIGHTSHOLDER BE LIABLE FOR ANY DIRECT, INDIRECT, CONSEQUENTIAL, OR INCIDENTAL DAMAGES (INCLUDING WITHOUT LIMITATION DAMAGES FOR LOSS OF BUSINESS PROFITS OR INFORMATION, OR FOR BUSINESS INTERRUPTION) ARISING OUT OF THE USE OR INABILITY TO USE A WORK, EVEN IF ONE OR BOTH OF THEM HAS BEEN ADVISED OF THE POSSIBILITY OF SUCH DAMAGES. In any event, the total liability of the Rightsholder and CCC (including their respective employees and directors) shall not exceed the total amount actually paid by User for the relevant License. User assumes full liability for the actions and omissions of its principals, employees, agents, affiliates, successors, and assigns.

12) **Limited Warranties.** THE WORK(S) AND RIGHT(S) ARE PROVIDED "AS IS." CCC HAS THE RIGHT TO GRANT TO USER THE RIGHTS GRANTED IN THE ORDER CONFIRMATION DOCUMENT. CCC AND THE RIGHTSHOLDER DISCLAIM ALL OTHER WARRANTIES RELATING TO THE WORK(S) AND RIGHT(S), EITHER EXPRESS OR IMPLIED, INCLUDING WITHOUT LIMITATION IMPLIED WARRANTIES OF MERCHANTABILITY OR FITNESS FOR A PARTICULAR PURPOSE. ADDITIONAL RIGHTS MAY BE REQUIRED TO USE ILLUSTRATIONS, GRAPHS, PHOTOGRAPHS, ABSTRACTS, INSERTS, OR OTHER PORTIONS OF THE WORK (AS OPPOSED TO THE ENTIRE WORK) IN A MANNER CONTEMPLATED BY USER; USER UNDERSTANDS AND AGREES THAT NEITHER CCC NOR THE RIGHTSHOLDER MAY HAVE SUCH ADDITIONAL RIGHTS TO GRANT.

13) **Effect of Breach.** Any failure by User to pay any amount when due, or any use by User of a Work beyond the scope of the License set forth in the Order Confirmation and/or the Terms, shall be a material breach of such License. Any breach not cured within 10 days of written notice thereof shall result in immediate termination of such License without further notice. Any unauthorized (but licensable) use of a Work that is terminated immediately upon notice thereof may be liquidated by payment of the Rightsholder's ordinary license price therefor; any unauthorized (and unlicensable) use that is not terminated immediately for any reason (including, for example, because materials containing the Work cannot reasonably be recalled) will be subject to all remedies available at law or in equity, but in no event to a payment of less than three times the Rightsholder's ordinary license price for the most closely analogous licensable use plus Rightsholder's and/or CCC's costs and expenses incurred in collecting such payment.

14) **Additional Terms for Specific Products and Services.** If a User is making one of the uses described in this Section 14, the additional terms and conditions apply:

a) ***Print Uses of Academic Course Content and Materials (photocopies for academic coursepacks or classroom handouts).*** For photocopies for academic coursepacks or classroom handouts the following additional terms apply:

i) The copies and anthologies created under this License may be made and assembled by faculty members individually or at their request by on-campus bookstores or copy centers, or by off-campus copy shops and other similar entities.

ii) No License granted shall in any way: (i) include any right by User to create a substantively non-identical copy of the Work or to edit or in any other way modify the Work (except by means of deleting material immediately preceding or following the entire portion of the Work copied) (ii) permit "publishing ventures" where any particular anthology would be systematically marketed at multiple institutions.

iii) Subject to any Publisher Terms (and notwithstanding any apparent contradiction in the Order Confirmation arising from data provided by User), any use authorized under the academic pay-per-use service is limited as follows:

A) any License granted shall apply to only one class (bearing a unique identifier as assigned by the institution, and thereby including all sections or other subparts of the class) at one institution;

B) use is limited to not more than 25% of the text of a book or of the items in a published collection of essays, poems or articles;

C) use is limited to no more than the greater of (a) 25% of the text of an issue of a journal or other periodical or (b) two articles from such an issue;

D) no User may sell or distribute any particular anthology, whether photocopied or electronic, at more than one institution of learning;

E) in the case of a photocopy permission, no materials may be entered into electronic memory by User except in order to produce an identical copy of a Work before or during the academic term (or analogous period) as to which any particular permission is granted. In the event that User shall choose to retain materials that are the subject of a photocopy permission in electronic memory for purposes of producing identical copies more than one day after such retention (but still within the scope of any permission granted), User must notify CCC of such fact in the applicable permission request and such retention shall constitute one copy actually sold for purposes of calculating permission fees due; and

F) any permission granted shall expire at the end of the class. No permission granted shall in any way include any right by User to create a substantively non-identical copy of the Work or to edit or in any other way modify the Work (except by means of deleting material immediately preceding or following the entire portion of the Work copied).

iv) Books and Records; Right to Audit. As to each permission granted under the academic pay-per-use Service, User shall maintain for at least four full calendar years books and records sufficient for CCC to determine the numbers of copies made by User under such permission. CCC and any representatives it may designate shall have the right to audit such books and records at any time during User's ordinary business hours, upon two days' prior notice. If any such audit shall determine that User shall have underpaid for, or underreported, any photocopies sold or by three percent (3%) or more, then User shall bear all the costs of any such audit; otherwise, CCC shall bear the costs of any such audit. Any amount determined by such audit to have been underpaid by User shall immediately be paid to CCC by User, together with interest thereon at the rate of 10% per annum from the date such amount was originally due. The provisions of this paragraph shall survive the termination of this License for any reason.

b) **Digital Pay-Per-Uses of Academic Course Content and Materials (e-coursepacks, electronic reserves, learning management systems, academic institution intranets).** For uses in e-coursepacks, posts in electronic reserves, posts in learning management systems, or posts on academic institution intranets, the following additional terms apply:

i) The pay-per-uses subject to this Section 14(b) include:

A) **Posting e-reserves, course management systems, e-coursepacks for text-based content**, which grants authorizations to import requested material in electronic format, and allows electronic access to this material to members of a designated college or university class, under the direction of an instructor designated by the college or university, accessible only under appropriate electronic controls (e.g., password);

B) **Posting e-reserves, course management systems, e-coursepacks for material consisting of photographs or other still images not embedded in text**, which grants not only the authorizations described in Section 14(b)(i)(A) above, but also the following authorization: to include the requested material in course materials for use consistent with Section 14(b)(i)(A) above, including any necessary resizing, reformatting or modification of the resolution of such requested material (provided that such modification does not alter the underlying editorial content or meaning of the requested material, and provided that the resulting modified content is used solely within the scope of, and in a manner consistent with, the particular authorization described in the Order Confirmation and the Terms), but not including any other form of manipulation, alteration or editing of the requested material;

C) **Posting e-reserves, course management systems, e-coursepacks or other academic distribution for audiovisual content**, which grants not only the authorizations described in Section 14(b)(i)(A) above, but also the following authorizations: (i) to include the requested material in course materials for use consistent with Section 14(b)(i)(A) above; (ii) to display and perform the requested material to such members of such class in the physical classroom or remotely by means of streaming media or other video formats; and (iii) to "clip" or reformat the requested material for purposes of time or content management or ease of delivery, provided that such "clipping" or reformatting does not alter the underlying editorial content or meaning of the requested material and that the resulting material is used solely within the scope of, and in a manner consistent with, the particular authorization described in the Order Confirmation and the Terms. Unless

expressly set forth in the relevant Order Confirmation, the License does not authorize any other form of manipulation, alteration or editing of the requested material.

ii) Unless expressly set forth in the relevant Order Confirmation, no License granted shall in any way: (i) include any right by User to create a substantively non-identical copy of the Work or to edit or in any other way modify the Work (except by means of deleting material immediately preceding or following the entire portion of the Work copied or, in the case of Works subject to Sections 14(b)(1)(B) or (C) above, as described in such Sections) (ii) permit “publishing ventures” where any particular course materials would be systematically marketed at multiple institutions.

iii) Subject to any further limitations determined in the Rightsholder Terms (and notwithstanding any apparent contradiction in the Order Confirmation arising from data provided by User), any use authorized under the electronic course content pay-per-use service is limited as follows:

A) any License granted shall apply to only one class (bearing a unique identifier as assigned by the institution, and thereby including all sections or other subparts of the class) at one institution;

B) use is limited to not more than 25% of the text of a book or of the items in a published collection of essays, poems or articles;

C) use is limited to not more than the greater of (a) 25% of the text of an issue of a journal or other periodical or (b) two articles from such an issue;

D) no User may sell or distribute any particular materials, whether photocopied or electronic, at more than one institution of learning;

E) electronic access to material which is the subject of an electronic-use permission must be limited by means of electronic password, student identification or other control permitting access solely to students and instructors in the class;

F) User must ensure (through use of an electronic cover page or other appropriate means) that any person, upon gaining electronic access to the material, which is the subject of a permission, shall see:

- a proper copyright notice, identifying the Rightsholder in whose name CCC has granted permission,
- a statement to the effect that such copy was made pursuant to permission,
- a statement identifying the class to which the material applies and notifying the reader that the material has been made available electronically solely for use in the class, and
- a statement to the effect that the material may not be further distributed to any person outside the class, whether by copying or by transmission and whether electronically or in paper form, and User must also ensure that such cover page or other means will print out in the event that the person accessing the material chooses to print out the material or any part thereof.

G) any permission granted shall expire at the end of the class and, absent some other form of authorization, User is thereupon required to delete the applicable material from any electronic storage or to block electronic access to the applicable material.

iv) Uses of separate portions of a Work, even if they are to be included in the same course material or the same university or college class, require separate permissions under the electronic course content pay-per-use Service. Unless otherwise provided in the Order Confirmation, any grant of rights to User is limited to use completed no later than the end of the academic term (or analogous period) as to which any particular permission is granted.

v) Books and Records; Right to Audit. As to each permission granted under the electronic course content Service, User shall maintain for at least four full calendar years books and records sufficient for CCC to determine the numbers of copies made by User under such permission. CCC and any representatives it may designate shall have the right to audit such books and records at any time during User’s ordinary business hours, upon two days’ prior notice. If any such audit shall determine that User shall have underpaid for, or underreported, any electronic copies used by three percent (3%) or more, then User shall bear all the costs of any such audit; otherwise, CCC shall bear the costs of any such audit. Any amount determined by such audit to have been underpaid by User

shall immediately be paid to CCC by User, together with interest thereon at the rate of 10% per annum from the date such amount was originally due. The provisions of this paragraph shall survive the termination of this license for any reason.

c) ***Pay-Per-Use Permissions for Certain Reproductions (Academic photocopies for library reserves and interlibrary loan reporting) (Non-academic internal/external business uses and commercial document delivery)***. The License expressly excludes the uses listed in Section (c)(i)-(v) below (which must be subject to separate license from the applicable Rightsholder) for: academic photocopies for library reserves and interlibrary loan reporting; and non-academic internal/external business uses and commercial document delivery.

i) electronic storage of any reproduction (whether in plain-text, PDF, or any other format) other than on a transitory basis;

ii) the input of Works or reproductions thereof into any computerized database;

iii) reproduction of an entire Work (cover-to-cover copying) except where the Work is a single article;

iv) reproduction for resale to anyone other than a specific customer of User;

v) republication in any different form. Please obtain authorizations for these uses through other CCC services or directly from the rightsholder.

Any license granted is further limited as set forth in any restrictions included in the Order Confirmation and/or in these Terms.

d) ***Electronic Reproductions in Online Environments (Non-Academic-email, intranet, internet and extranet)***. For “electronic reproductions”, which generally includes e-mail use (including instant messaging or other electronic transmission to a defined group of recipients) or posting on an intranet, extranet or Intranet site (including any display or performance incidental thereto), the following additional terms apply:

i) Unless otherwise set forth in the Order Confirmation, the License is limited to use completed within 30 days for any use on the Internet, 60 days for any use on an intranet or extranet and one year for any other use, all as measured from the “republication date” as identified in the Order Confirmation, if any, and otherwise from the date of the Order Confirmation.

ii) User may not make or permit any alterations to the Work, unless expressly set forth in the Order Confirmation (after request by User and approval by Rightsholder); provided, however, that a Work consisting of photographs or other still images not embedded in text may, if necessary, be resized, reformatted or have its resolution modified without additional express permission, and a Work consisting of audiovisual content may, if necessary, be “clipped” or reformatted for purposes of time or content management or ease of delivery (provided that any such resizing, reformatting, resolution modification or “clipping” does not alter the underlying editorial content or meaning of the Work used, and that the resulting material is used solely within the scope of, and in a manner consistent with, the particular License described in the Order Confirmation and the Terms.

15) Miscellaneous.

a) User acknowledges that CCC may, from time to time, make changes or additions to the Service or to the Terms, and that Rightsholder may make changes or additions to the Rightsholder Terms. Such updated Terms will replace the prior terms and conditions in the order workflow and shall be effective as to any subsequent Licenses but shall not apply to Licenses already granted and paid for under a prior set of terms.

b) Use of User-related information collected through the Service is governed by CCC’s privacy policy, available online at www.copyright.com/about/privacy-policy/.

c) The License is personal to User. Therefore, User may not assign or transfer to any other person (whether a natural person or an organization of any kind) the License or any rights granted thereunder; provided, however, that, where applicable, User may assign such License in its entirety on written notice to CCC in the event of a transfer of all or substantially all of User’s rights in any new material which includes the Work(s) licensed under this Service.

d) No amendment or waiver of any Terms is binding unless set forth in writing and signed by the appropriate parties, including, where applicable, the Rightsholder. The Rightsholder and CCC hereby object to any terms contained in any writing prepared by or on behalf of the User or its principals, employees, agents or affiliates and purporting to govern

or otherwise relate to the License described in the Order Confirmation, which terms are in any way inconsistent with any Terms set forth in the Order Confirmation, and/or in CCC's standard operating procedures, whether such writing is prepared prior to, simultaneously with or subsequent to the Order Confirmation, and whether such writing appears on a copy of the Order Confirmation or in a separate instrument.

e) The License described in the Order Confirmation shall be governed by and construed under the law of the State of New York, USA, without regard to the principles thereof of conflicts of law. Any case, controversy, suit, action, or proceeding arising out of, in connection with, or related to such License shall be brought, at CCC's sole discretion, in any federal or state court located in the County of New York, State of New York, USA, or in any federal or state court whose geographical jurisdiction covers the location of the Rightsholder set forth in the Order Confirmation. The parties expressly submit to the personal jurisdiction and venue of each such federal or state court.

Last updated October 2022

Gallery

BioRender
Templates

Learning
Hub

Get a Free
BioRender T-
Shirt

NEW



Garyfallia Gouna

General

 Profile

 Groups

 Rewards

Admin

Plan & Billing

Plan & Billing

Your Plan DZNE'S Plan

- ✓ Create unlimited figures
- ✓ Publish in journals and for commercial purposes
- ✓ No watermark
- ✓ High-resolution export and transp
- ✓ Create multiple canvases with Sli
- ✓ ...and more!
- ✓ **Publishing rights:** You may publish in journals and for other academic purposes.
[Learn more about publishing rights](#)

Help

SPRINGER NATURE LICENSE TERMS AND CONDITIONS

Nov 14, 2023

This Agreement between Garyfallia Gouna ("You") and Springer Nature ("Springer Nature") consists of your license details and the terms and conditions provided by Springer Nature and Copyright Clearance Center.

License Number	5667751426135
License date	Nov 14, 2023
Licensed Content Publisher	Springer Nature
Licensed Content Publication	Nature Reviews Neurology
Licensed Content Title	Inflammation in multiple sclerosis: consequences for remyelination and disease progression
Licensed Content Author	Luisa Klotz et al
Licensed Content Date	Apr 14, 2023
Type of Use	Thesis/Dissertation
Requestor type	academic/university or research institute
Format	print and electronic
Portion	figures/tables/illustrations
Number of figures/tables/illustrations	1
Would you like a high resolution image with your order?	no
Will you be translating?	no
Circulation/distribution	1 - 29
Author of this Springer Nature content	no
Title of new work	Lipid Metabolism in Remyelination: Does a Hidden Dialogue Exist Between the Central Nervous System and the Periphery?
Institution name	LMU - DZNE
Expected presentation date	Nov 2023
Portions	Figure 1
Requestor Location	Garyfallia Gouna Feodor Lynen Straße 17 Munich, 81377 Germany Attn: Garyfallia Gouna
Total	0.00 EUR

Terms and Conditions

Springer Nature Customer Service Centre GmbH Terms and Conditions

The following terms and conditions ("Terms and Conditions") together with the terms specified in your [RightsLink] constitute the License ("License") between you as Licensee and Springer Nature Customer Service Centre GmbH as Licensor. By clicking 'accept' and completing the transaction for your use of the material ("Licensed Material"), you confirm your acceptance of and obligation to be bound by these Terms and Conditions.

1. Grant and Scope of License

1. 1. The Licensor grants you a personal, non-exclusive, non-transferable, non-sublicensable, revocable, world-wide License to reproduce, distribute, communicate to the public, make available, broadcast, electronically transmit or create derivative works using the Licensed Material for the purpose(s) specified in your RightsLink Licence Details only. Licenses are granted for the specific use requested in the order and for no other use, subject to these Terms and Conditions. You acknowledge and agree that the rights granted to you under this License do not include the right to modify, edit, translate, include in collective works, or create derivative works of the Licensed Material in whole or in part unless expressly stated in your RightsLink Licence Details. You may use the Licensed Material only as permitted under this Agreement and will not reproduce, distribute, display, perform, or otherwise use or exploit any Licensed Material in any way, in whole or in part, except as expressly permitted by this License.

1. 2. You may only use the Licensed Content in the manner and to the extent permitted by these Terms and Conditions, by your RightsLink Licence Details and by any applicable laws.

1. 3. A separate license may be required for any additional use of the Licensed Material, e.g. where a license has been purchased for print use only, separate permission must be obtained for electronic re-use. Similarly, a License is only valid in the language selected and does not apply for editions in other languages unless additional translation rights have been granted separately in the License.

1. 4. Any content within the Licensed Material that is owned by third parties is expressly excluded from the License.

1. 5. Rights for additional reuses such as custom editions, computer/mobile applications, film or TV reuses and/or any other derivative rights requests require additional permission and may be subject to an additional fee. Please apply to journalpermissions@springernature.com or bookpermissions@springernature.com for these rights.

2. Reservation of Rights

Licensor reserves all rights not expressly granted to you under this License. You acknowledge and agree that nothing in this License limits or restricts Licensor's rights in or use of the Licensed Material in any way. Neither this License, nor any act, omission, or statement by Licensor or you, conveys any ownership right to you in any Licensed Material, or to any element or portion thereof. As between Licensor and you, Licensor owns and retains all right, title, and interest in and to the Licensed Material subject to the license granted in Section 1.1. Your permission to use the Licensed Material is expressly conditioned on you not impairing Licensor's or the applicable copyright owner's rights in the Licensed Material in any way.

3. Restrictions on use

3. 1. Minor editing privileges are allowed for adaptations for stylistic purposes or formatting purposes provided such alterations do not alter the original meaning or intention of the Licensed Material and the new figure(s) are still accurate and representative of the Licensed Material. Any other changes including but not limited to, cropping, adapting, and/or omitting material that affect the meaning, intention or moral rights of the author(s) are strictly prohibited.

3. 2. You must not use any Licensed Material as part of any design or trademark.

3. 3. Licensed Material may be used in Open Access Publications (OAP), but any such reuse must include a clear acknowledgment of this permission visible at the same time as the figures/tables/illustration or abstract and which must indicate that the Licensed Material is not part of the governing OA license but has been reproduced with permission. This may be indicated according to any standard referencing system but must include at a minimum 'Book/Journal title, Author, Journal Name (if applicable), Volume (if applicable), Publisher, Year, reproduced with permission from SNCSC'.

4. STM Permission Guidelines

4. 1. An alternative scope of license may apply to signatories of the STM Permissions Guidelines ("STM PG") as amended from time to time and made available at <https://www.stm-assoc.org/intellectual-property/permissions/permissions-guidelines/>.

4. 2. For content reuse requests that qualify for permission under the STM PG, and which may be updated from time to time, the STM PG supersede the terms and conditions contained in this License.

4. 3. If a License has been granted under the STM PG, but the STM PG no longer apply at the time of publication, further permission must be sought from the Rightsholder. Contact journalpermissions@springernature.com or

bookpermissions@springernature.com for these rights.

5. Duration of License

5. 1. Unless otherwise indicated on your License, a License is valid from the date of purchase ("License Date") until the end of the relevant period in the below table:

Reuse in a medical communications project	Reuse up to distribution or time period indicated in License
Reuse in a dissertation/thesis	Lifetime of thesis
Reuse in a journal/magazine	Lifetime of journal/magazine
Reuse in a book/textbook	Lifetime of edition
Reuse on a website	1 year unless otherwise specified in the License
Reuse in a presentation/slide kit/poster	Lifetime of presentation/slide kit/poster. Note: publication whether electronic or in print of presentation/slide kit/poster may require further permission.
Reuse in conference proceedings	Lifetime of conference proceedings
Reuse in an annual report	Lifetime of annual report
Reuse in training/CME materials	Reuse up to distribution or time period indicated in License
Reuse in newsmedia	Lifetime of newsmedia
Reuse in coursepack/classroom materials	Reuse up to distribution and/or time period indicated in license

6. Acknowledgement

6. 1. The Licensor's permission must be acknowledged next to the Licensed Material in print. In electronic form, this acknowledgement must be visible at the same time as the figures/tables/illustrations or abstract and must be hyperlinked to the journal/book's homepage.

6. 2. Acknowledgement may be provided according to any standard referencing system and at a minimum should include "Author, Article/Book Title, Journal name/Book imprint, volume, page number, year, Springer Nature".

7. Reuse in a dissertation or thesis

7. 1. Where 'reuse in a dissertation/thesis' has been selected, the following terms apply: Print rights of the Version of Record are provided for; electronic rights for use only on institutional repository as defined by the Sherpa guideline (www.sherpa.ac.uk/romeo/) and only up to what is required by the awarding institution.

7. 2. For theses published under an ISBN or ISSN, separate permission is required. Please contact journalpermissions@springernature.com or bookpermissions@springernature.com for these rights.

7. 3. Authors must properly cite the published manuscript in their thesis according to current citation standards and include the following acknowledgement: '*Reproduced with permission from Springer Nature*'.

8. License Fee

You must pay the fee set forth in the License Agreement (the "License Fees"). All amounts payable by you under this License are exclusive of any sales, use, withholding, value added or similar taxes, government fees or levies or other assessments. Collection and/or remittance of such taxes to the relevant tax authority shall be the responsibility of the party who has the legal obligation to do so.

9. Warranty

9. 1. The Licensor warrants that it has, to the best of its knowledge, the rights to license reuse of the Licensed Material. **You are solely responsible for ensuring that the material you wish to license is original to the Licensor and does not carry the copyright of another entity or third party (as credited in the published version).** If the credit

line on any part of the Licensed Material indicates that it was reprinted or adapted with permission from another source, then you should seek additional permission from that source to reuse the material.

9. 2. EXCEPT FOR THE EXPRESS WARRANTY STATED HEREIN AND TO THE EXTENT PERMITTED BY APPLICABLE LAW, LICENSOR PROVIDES THE LICENSED MATERIAL "AS IS" AND MAKES NO OTHER REPRESENTATION OR WARRANTY. LICENSOR EXPRESSLY DISCLAIMS ANY LIABILITY FOR ANY CLAIM ARISING FROM OR OUT OF THE CONTENT, INCLUDING BUT NOT LIMITED TO ANY ERRORS, INACCURACIES, OMISSIONS, OR DEFECTS CONTAINED THEREIN, AND ANY IMPLIED OR EXPRESS WARRANTY AS TO MERCHANTABILITY OR FITNESS FOR A PARTICULAR PURPOSE. IN NO EVENT SHALL LICENSOR BE LIABLE TO YOU OR ANY OTHER PARTY OR ANY OTHER PERSON OR FOR ANY SPECIAL, CONSEQUENTIAL, INCIDENTAL, INDIRECT, PUNITIVE, OR EXEMPLARY DAMAGES, HOWEVER CAUSED, ARISING OUT OF OR IN CONNECTION WITH THE DOWNLOADING, VIEWING OR USE OF THE LICENSED MATERIAL REGARDLESS OF THE FORM OF ACTION, WHETHER FOR BREACH OF CONTRACT, BREACH OF WARRANTY, TORT, NEGLIGENCE, INFRINGEMENT OR OTHERWISE (INCLUDING, WITHOUT LIMITATION, DAMAGES BASED ON LOSS OF PROFITS, DATA, FILES, USE, BUSINESS OPPORTUNITY OR CLAIMS OF THIRD PARTIES), AND WHETHER OR NOT THE PARTY HAS BEEN ADVISED OF THE POSSIBILITY OF SUCH DAMAGES. THIS LIMITATION APPLIES NOTWITHSTANDING ANY FAILURE OF ESSENTIAL PURPOSE OF ANY LIMITED REMEDY PROVIDED HEREIN.

10. Termination and Cancellation

10. 1. The License and all rights granted hereunder will continue until the end of the applicable period shown in Clause 5.1 above. Thereafter, this license will be terminated and all rights granted hereunder will cease.

10. 2. Licensor reserves the right to terminate the License in the event that payment is not received in full or if you breach the terms of this License.

11. General

11. 1. The License and the rights and obligations of the parties hereto shall be construed, interpreted and determined in accordance with the laws of the Federal Republic of Germany without reference to the stipulations of the CISG (United Nations Convention on Contracts for the International Sale of Goods) or to Germany's choice-of-law principle.

11. 2. The parties acknowledge and agree that any controversies and disputes arising out of this License shall be decided exclusively by the courts of or having jurisdiction for Heidelberg, Germany, as far as legally permissible.

11. 3. This License is solely for Licensor's and Licensee's benefit. It is not for the benefit of any other person or entity.

Questions? For questions on Copyright Clearance Center accounts or website issues please contact springernaturesupport@copyright.com or +1-855-239-3415 (toll free in the US) or +1-978-646-2777. For questions on Springer Nature licensing please visit <https://www.springernature.com/gp/partners/rights-permissions-third-party-distribution>

Other Conditions:

Version 1.4 - Dec 2022

Questions? E-mail us at customer@copyright.com.

ACKNOWLEDGEMENTS

I would like to thank my supervisor Prof. Dr. Mikael Simons for the opportunity to join his research team for my doctoral studies. I would also like to thank both Prof. Dr. Mikael Simons and Dr. Ludovico Cantuti-Castervetri for their scientific guidance and fruitful discussions. Moreover, I would like to thank Prof. Dr. Martin Kerschensteiner and Prof. Dr. Dieter Edbauer for their scientific input into my projects in their role as thesis advisor committee.

I would like to thank the "Graduate School of Systemic Neurosciences - GSN". I am happy I joined this amazing scientific community for my doctoral studies and being part of this great program. Thank you for the beautiful social community you have created and for all your help and the support system during my studies. Also, extra thank you for all your support during the writing of this thesis when I was panicking and you calmed me down. Thank you.

I would like to also thank everyone at the animal, genomic and EM facilities for their valuable help. Without you, these projects would not have existed. Special thanks to Martina, Georg and Conny. Georg and Conny, thank you for all the laughs we shared in our small area office.

Writing these words, the feelings are bittersweet, because I know the circle for my doctoral studies and living in Munich has closed. I feel both sad and excited, as I know I leave behind many people that supported me during this great adventure. So, I would like to pay tribute to specific people, without who, my life in the lab would not be that good. We are all working for so many hours, that we are "work" family, so I will use DeepL and goole translator to express all I want to say.

Ludo, grazie per tutto, per esserci stato fin dal primo giorno, per essere stato un grande supervisore per tutti questi anni e per avermi guidato scientificamente. Grazie per tutte le discussioni che abbiamo avuto, quelle belle e quelle brutte, e grazie per avermi accettato per quello che sono. Senza di voi, credo che non sarei diventato il ricercatore e la persona che sono oggi. Grazie per tutto. Il koala che hai lasciato verrà a Edimburgo con me.

Lili, obrigada por veres o que eu estava a passar e por me ajudares a reencontrarme quando me sentia completamente perdida. Obrigada por seres esta pessoa maravilhosa, um ser humano gentil, és realmente a luz do sol em forma humana e estou feliz por ser tua amiga. O íman da ovelhinha branca e o teu casaco de laboratório que deixaste para trás também viajarão para Edimburgo.

Jianping, 建平, 谢谢你对我的支持, 谢谢你接受了真实的我。我知道我们一开始有分歧, 但你是一个非常善良的人, 我很感激能和你称兄道弟。

Swathi, स्वाति, वह ढुलब बननेके िलए धवुवाद िजसनेमुझेतब शांत िकिया जब मॆडरी डई और असहाय महसूस कर रही थी। सभी गहन वाताणुलापों के िलए और आप जैसेढुलब हॆवैसेहोनेके िलए धवुवाद, आप एक दयालुआढा हॆजो इस दुिनिया मँबँत दुलणुभ है। इसके अलावा, मॆनेू िडयो वन मँ एक साथ हमारी जैज नृ क्ाओंका आनंद िलिया। मॆयेशः कभी नहींभूलूंगी "तूतेरा कर!" और "जो हैसो है।"

Vini, विनी, आपके सभी समर्थन और मदद के लिए धन्यवाद। एक अद्भुत इंसान होने के लिए धन्यवाद। मुझे जीएसएन दुनिया से परिचित कराने के लिए धन्यवाद। गहरी बातचीत के लिए और मुझे यह दिखाने के लिए भी धन्यवाद कि शांति से अपनी भावनाओं को व्यक्त करना ही आगे बढ़ने का तरीका है।

Martin, danke, dass du auch gesehen hast, dass ich in einer dunklen Lage war und deine Hilfe angeboten hast. Ich schätze jedes Gespräch, das wir hatten, die guten und die schlechten. Dankeschön.

Simona, grazie per tutta la tua energia positiva e per essere stata sincera con me. Sono felice di averti conosciuto e mi sono divertita ogni giorno andando alla Mensa e lamentandomi del cibo. Grazie anche per la bellissima Lunga Notte del Museo e per l'ambasciata italiana dove ho sperimentato cosa significa l'ospitalità italiana.

Lena, ich danke dir für all die Gespräche, die wir in Göttingen und München geführt haben und dafür, dass du mir den besten Eiskaffee der Welt angeboten hast. Ich bin froh, dass ich dich kennengelernt und mit dir gearbeitet habe. Danke, dass du immer da warst, wenn ich in Not war.

Öge ya da daha doğrusu Tuana, U2'nin alt katında bana bir sigara ikram ettiğin ve korkularımı ve düşüncelerimi dinlediğin tüm günler için teşekkür ederim. Bana güvendiğin ve hem işle ilgili hem de ilgisiz konularda bana yardımcı olduğun için teşekkür ederim. Orada olduğun için ve olduğun kişi için teşekkür ederim.

Stefan und Lennart, ich danke euch für all die wissenschaftlichen und nicht-wissenschaftlichen Gespräche, die wir geführt haben. Danke für deine Unterstützung in all diesen Jahren.

Seiji, 誠司、長い間、いろいろとお世話になりました。人として感謝していますし、出会えてよかったと思っています。

Ivana, hvala i tebi na pomoći i podršci u laboratoriji i van nje i na cigaretama i svim razgovorima koje smo vodili.

Taisiia, Таїсія, дякую тобі за те, що ти була доброю душею в лабораторії. Також мені сподобався наш єдиний урок танців, який ми провели разом.

I would also want to thank Minou, Agata, Jana, Yan, Laura, Ruoqing and Janos for creating a nice atmosphere in the lab and for all your help.

Last but not least, I would like to thank all the people I consider as my family in this world.

Andreia, não há palavras para descrever o que sinto por ti. Vocês são a minha família de eleição e tenho muita sorte por vos ter conhecido, por ter vivido convosco e por ser mais do que amiga de vocês. Obrigada por todos os dias e noites naquele GT que partilhámos, por me teres ensinado tantas coisas, és um ser humano raro, o teu coração é tão bondoso e és uma pessoa tão adorável. Obrigada por me aceites como eu sou, por me veres com todos os meus defeitos e escolheres ficar por perto. A minha vida é muito melhor agora que vos posso chamar família.

Akrivi and Christie, words cannot describe how I feel about you. Thank you for being there from the very beginning, back in Greece, in Crete where our paths met. You are my chosen family, I am such a better person because of you. Thank you for the last 7 years, all the things we experienced together, all your support and laughs and tears and drinks and cigarettes and deep existential conversations. You are kind spirits on this earth and I am so thankful I can call you family. To many more years together, celebrating life with laughs and love.

Στον μπαμπά μου Παναγιώτη, τη μαμά μου Σταυρούλα, τον αδερφό μου Νίκο και στην σκύλα μας Έλλη. Σας ευχαριστώ για όλα. Ευχαριστώ για όλη τη στήριξη και βοήθεια όταν ήθελα να τα παρατήσω όλα. Σας ευχαριστώ που με κάνατε όλα όσα είμαι σήμερα. Σας αγαπάω πάρα πολύ και ας μην το λέω συχνά. Φιλιά.

AUTHOR CONTRIBUTIONS

For Project 1 (published paper): “TREM2-dependent lipid droplet biogenesis in phagocytes is required for remyelination.” 2021, *The Journal of Experimental Medicine*, 218(10), e20210227. <https://doi.org/10.1084/jem.20210227>

Gouna, G., Klose, C., Bosch-Queralt, M., Liu, L., Gokce, O., Schifferer, M., Cantuti-Castelvetri, L.* Simons, M.*

L. Cantuti-Castelvetri and M. Simons conceived the project and designed experiments. L. Cantuti-Castelvetri, **G. Gouna**, M. Bosch-Queralt, M. Schifferer, C. Klose, O. Gokce, and L. Liu carried out experiments and analyzed the data. L. Cantuti-Castelvetri performed all stereotactical injections at the spinal cord. **G. Gouna** did formal analysis, investigation and validation of the data. M. Bosch-Queralt did data curation, investigation and methodology. C. Klose performed the lipidomic analysis. L. Liu performed the FACS sorting experiment. O. Gokce supervised the FACS sorting experiment. M. Schifferer obtained the EM images. L. Cantuti-Castelvetri and **G. Gouna** visualized the data. L. Cantuti-Castelvetri and M. Simons wrote the manuscript (original draft). **G. Gouna**, L. Cantuti-Castelvetri and M. Simons reviewed and edited the manuscript with input from all authors. L. Cantuti-Castelvetri and M. Simons supervised the project. *Equal contribution

My contribution to this publication in detail:

For this publication, I was responsible for all the breedings for TREM2 and SOAT1 lines, doing genotyping. I was monitoring the mice after stereotactical injections. I quantified all the EM images in all time points in TREM2 and SOAT1 KO animals. I performed all the immunohistochemistry experiments, from perfusing the mice, cutting the tissue at the cryostat, immunostaining, imaging and quantification analysis for all tissue from TREM2 and SOAT1 KO animals. I performed the *in vitro* experiments with primary microglia and subsequent treatments (myelin debris, pharmacological treatment) used for immunocytochemistry and Western blot analysis. I immunostained, imaged and quantified all the *in vitro* experiments and performed Western Blot experiment, visualization and quantified the protein concentration. I performed the *in vivo* pharmacological treatment in the TREM2 KO mice and processed all the tissue from perfusing the mice, cutting at the cryostat, immunostainings, imaging and quantifying the data. I visualized and interpreted all the data. I reviewed and edited the original draft of the manuscript. The following figures include all the data I contributed to this publication: Figure 1 (A-C), Figure 2, Figure 3 (A-E), Figure 4, Figure 5 (A-B, E-I), Figure S1 (A-F), Figure S2 (A-B, E), Figure S3 (A-B, F-G).

For Project 2 (unpublished): “The “lipodystrophy” brain exhibits enhanced remyelination in a UCP1-independent manner.”

Gouna, G., Petrera, A., Prehn, C., Cecil, A., Schlaphoff, L., Scarpa, J., Witting, M., Hauck, S., Simons, M.

G. Gouna and M. Simons conceived the project and designed experiments. **G. Gouna**, carried out experiments, analyzed and interpreted the data. A. Petrera performed the targeted proteomic analysis. C. Prehn performed the sample preparation and mass spectrometric measurements for the targeted metabolomic analysis. Cecil, A. performed basic statistics and bioinformatics of quality control tests for the targeted metabolomic analysis. L. Schlaphoff assisted in the plasma and CSF collection. J. Scarpa assisted in the targeted metabolomic analysis. M. Witting is supervising the metabolomic facility. S. Hauck is the head of the Helmholtz proteomic and metabolomic facility. **G. Gouna** made additional bioinformatic and enrichment analyses and quantified the metabolomic and proteomic data. **G. Gouna** visualized the data. **G. Gouna** wrote the original draft of the manuscript. **G. Gouna** and M. Simons reviewed and edited the manuscript. M. Simons supervised the project.

My contribution to this project (unpublished) in detail:

For this project, I conceived the project and designed experiments. I was responsible for all the breedings for aP2-Srebf1c line, doing genotyping and performing diet treatments. I performed all stereotactical injections at the corpus callosum of both aP2-Srebf1c and wild-type mice and monitored the mice after surgery. I performed all after-surgery processing of the mice for all procedures; I perfused the mice, cut the tissue at the cryostat, and performed immunohistochemistry with subsequent imaging and quantifying the results. For the wild-type mice, I carried out the *in vivo* pharmacological treatment. For the targeted proteomic and metabolomic analysis, I initially prepared all samples according to the instructions from the facilities. After I received the data from both facilities, I performed statistical analysis of all values and additional quantification. For both metabolomic and proteomic data I performed additional analysis of the significant results using pathway enrichment methodologies. I visualized all the data and interpreting the data. I wrote the original draft of the manuscript. I additionally reviewed and edited the manuscript. The following figures include all the data I contributed to this publication: Figures 1-6 and Figures S1-S4. In fact, all figures contain all the data I contributed to this project. For Table 1, I extracted some information for the significant metabolites from the provided general table from the metabolomic facility.

München / Munich

21/11/2023

(Datum / Date)

(Unterschrift / Signature)

(Unterschrift / Signature)

CURRICULUM VITAE

GARYFALLIA GOUNA

Deutsches Zentrum für Neurodegenerative Erkrankungen e. V. (DZNE),
Feodor-Lynen-Straße 17, DE 81377, Munich, Germany,

Phone:

E-Mail:

ORCID: <https://orcid.org/0000-0002-4644-8252>

• EDUCATION

- 09/2016 – 12/2018: Master of Science (MSc) in “Molecular basis of Human Disease”**
Faculty of Medicine, School of Health Sciences, University of Crete (UoC), Greece
• **Master thesis:** “Dissecting the role of lipid metabolism and the nature of autophagosomal cargo in CNS” GPA: Excellent (9.73/10)
- 09/2006 – 03/2015: Ptychion (BSc) in Biology**
Faculty of Biology, School of Science, National and Kapodistrian University of Athens (UoA)
• **Bachelor thesis:** “Association of bone morphogenetic protein 6 polymorphism rs267192 to patients with sickle beta thalassemia” GPA: Good (6.3/10)

• RESEARCH EXPERIENCE & CURRENT POSITION

- 10/2019 – ongoing: PhD student**
• **Project:** “Lipid Metabolism in Remyelination: Does a Hidden Dialogue Exist Between the Central Nervous System and the Periphery?”
Graduate School of Systemic Neurosciences (GSN), Ludwig-Maximilians-Universität München (LMU), Germany
Supervisor: Mikael Simons, MD, Professor
- 01/2019 – 09/2019: Research internship under the ERASMUS+ program**
• **Project:** “Investigating the role of cholesterol esterification in demyelinating conditions”
AG Mikael Simons Molecular Neurobiology laboratory, Deutsches Zentrum für Neurodegenerative Erkrankungen e. V. (DZNE), Munich, Germany
Supervisor: Mikael Simons, MD, Professor and Ludovico Cantuti-Castelvetri, PhD
- 05/2015 – 11/2016: Research assistant**
• **Project:** “Next-Generation Sequencing genetic analysis in patients with neurological and other disorders”.
Neurology Laboratory, Faculty of Medicine, School of Health Sciences, University of Crete (UoC), Greece
Supervisor: Ioannis Zaganas, PhD, MD, Assistant Professor

• FELLOWSHIPS AND AWARDS

- 12/2022** **Best paper Award** for an outstanding scientific publication on neurodegenerative diseases. Deutsches Zentrum für Neurodegenerative Erkrankungen e. V. (DZNE), DZNE – Stiftung, Munich, Germany
- 09-10/2022** **Travel grant** for the participation at the 3rd EpiLipidNET General Action meeting 2022 – Portugal, SyNergy - Munich Cluster for Systems Neurology, Germany
- 09/2022** **Best Poster Award** at the 3rd EpiLipidNET General Action meeting - Portugal
Lipotype GmbH, Germany
- 01/2019 – 09/2019** **Erasmus+ 2018-2019 scholarship (practical internship) by European Commission.** Faculty of Medicine, School of Health Sciences, University of Crete (UoC), Greece
- 01/2018 – 12/2018** **MSc studentship by ERC StG 2016 - The role of autophagy in Synaptic Plasticity–NEUROPHAGY, Program Coordinator Dr. Vassiliki Nikolettou.** Institute of Molecular Biology and Biotechnology of the Foundation for Research and Technology Hellas (IMBB-FORTH)

• PUBLICATIONS

Tiwari, V., Prajapati, B., Asare, Y., Damkou, A., Ji, H., **Gouna, G.**, et al. Innate immune training restores pro-reparative myeloid functions for remyelination in the aged central nervous system. *Immunity* (resubmitted 11/2023 – in final revisions, after the second submission)

Androvic, P., Schifferer, M., Perez Anderson, K., Cantuti-Castelvetri, L., Jiang, H., Ji, H., Liu, L., **Gouna, G.**, et al (2023). Spatial Transcriptomics-correlated Electron Microscopy maps transcriptional and ultrastructural responses to brain injury. *Nature Communications* <https://doi.org/10.1038/s41467-023-39447-9> IF: 16.6

Mathioudakis, L., Dimovasili, C., Bourbouli, M., Latsoudis, H., Kokosali, E., **Gouna, G.**, et al (2022). Study of Alzheimer’s disease- and frontotemporal dementia-associated genes in the Cretan Aging Cohort. *Neurobiology of Aging*. <https://doi.org/10.1016/j.neurobiolaging.2022.07.002> IF: 5.133

Gouna, G. et al (2021). TREM2-dependent lipid droplet biogenesis in phagocytes is required for remyelination. *The Journal of experimental medicine*, 218(10), e20210227. <https://doi.org/10.1084/jem.20210227> IF: 17.579

Safaiyan, S., Besson-Girard, S., Kaya, T., Cantuti-Castelvetri, L., Liu, L., Ji, H., Schifferer, M., **Gouna, G.**, et al (2021). White matter aging drives microglial diversity. *Neuron*, 109(7), 1100–1117.e10. <https://doi.org/10.1016/j.neuron.2021.01.027> IF: 18.688

Basta, M., Koutentaki, E., Vgontzas, A., Zaganas, I., Vogiatzi, E., **Gouna, G.** et al (2020). Objective Daytime Napping is Associated with Disease Severity and Inflammation in Patients with Mild to Moderate Dementia. *Journal of Alzheimer's disease: JAD*, 74(3), 803–815. <https://doi.org/10.3233/JAD-190483> IF: 4.160

- **SELECTED COURSES & TRAINING**

- 10/2017 – 10/2018:** E-learning course in “Medical Genetics”
Lifelong Learning Center, University of Ioannina (UoI LLC), Greece
- **Practical internship** at Genesis-Genoma Lab, **GPA:** Excellent (89/100)

LABORATORY SKILLS

- Felasa accreditation (27/07/2018 - Felasa ID: 051/15_08_2018)
- Stereotactical injections (brain) in mice
- Primary and Cell line cultures, Western blot, Immunocytochemistry, Immunohistochemistry, Immunoprecipitation, Real time PCR (qPCR), Enzyme-Linked Immunosorbent Assay (ELISA), Autophagosome/Myelin isolation, Ingenuity Variant Analysis (IVA)
- Main applications: MS Office Suite, Libre Office Suite, Adobe Photoshop CS2, Adobe Illustrator CS2, GraphPad Prism 6, ImageJ-Fiji, IMARIS, R language, R Studio

- **SUPERVISION OF GRADUATE STUDENTS**

- 2020 – 2022** 2 Master Students, Biomedical Neuroscience, MSc, Technische Universität München (TUM)

- **MEMBERSHIPS OF SCIENTIFIC SOCIETIES**

- 2022 – ongoing** Member, Research Network “CA19105 - Pan-European Network in Lipidomics and EpiLipidomics (EpiLipidNET)” <https://www.epilipid.net/>